MODELLING AND PREVENTING THE DEVELOPMENT OF CHRONIC COMMUNICATING HYDROCEPHALUS

By

HANNAH FLORENCE BOTFIELD

A thesis submitted to the University of Birmingham for the degree of Doctor of Philosophy

School of Clinical and Experimental Medicine

College of Medical and Dental Sciences

The University of Birmingham

October 2013

Abstract

Introduction: In post-haemorrhagic communicating hydrocephalus, cerebrospinal fluid flow and drainage is obstructed by subarachnoid fibrosis in which the potent fibrogenic cytokine transforming growth factor-β1 has been aetiologically implicated. Here, the hypothesis that the transforming growth factor-β antagonist Decorin has therapeutic potential for (1) reducing fibrosis and the development of hydrocephalus and (2) degrading fibrosis and resolving established hydrocephalus, was tested using a rat model of juvenile communicating hydrocephalus.

Methods: In the acute study, hydrocephalus was induced by a single basal cistern injection of kaolin in 3-week-old rats, immediately followed by 3 or 14 days of continuous intraventricular infusion of either human recombinant Decorin or phosphate-buffered saline (vehicle). In the chronic study, hydrocephalus was allowed to develop for 7 days before continuous intraventricular infusion of either human recombinant Decorin or phosphate-buffered saline for a further 14 days. Ventricular expansion was measured by magnetic resonance imaging. Inflammation, fibrosis, Decorin, transforming growth factor-β/Smad2/3 activation and hydrocephalic brain pathology were evaluated by immunohistochemistry and basic histology.

Results: In the acute study continuous Decorin infusion prevented the development of hydrocephalus by blocking transforming growth factor-β-induced subarachnoid fibrosis and protected against hydrocephalic brain damage. In the chronic study

Decorin had no impact on hydrocephalus, TGF-β1 levels or subarachnoid fibrosis, however the efficiency of Decorin infusion was in disrepute.

Conclusion: The results suggest that Decorin is a potential clinical therapeutic for the prevention of juvenile post-haemorrhagic communicating hydrocephalus.

Acknowledgements

Firstly I would like to thank my supervisors Ann Logan and Ana Maria Gonzalez. Ann provided me with continued intellectual input, encouragement, support and guidance throughout my PhD and Ana has been indispensable as my mentor. Ana gave up countless hours helping me with my work and gave me lots of technical support as well as being my emotional rock. I would also like to thank Pat McAllister for being my knight in shining armour, for welcoming me and looking after me in Utah, training me in *in vivo* techniques and giving me advice in matters of hydrocephalus. Without their help, completing my PhD would have been an impossible task.

I would like to thank the molecular neuroscience group (that includes you Andy Thewles) for all their technical and intellectual support, and making my time at work enjoyable. In particular, thanks to Lisa Hill for keeping me sane during my PhD, listening to me rant and giving me faith even when things went wrong. I hope I can return the favour!

I would also like to thank my funding body Biotechnology and Biological Sciences Research Council, BMSU staff for looking after my animals, Peter Nightingale for his help with statistics and the staff at the University of Utah in the MRI department for all their help.

Finally I would like to thank my family and Adam for their continued love and support through all the highs and lows of my PhD.

Contents

List of Figures

List of Abbreviations

ABC – avidin biotin complex

APS – ammonium persulfate

ALK - activin receptor-like kinase

BCP – basal cerebral peduncle

BSA – bovine serum albumin

BV – blood vessel

CBF – cerebral blood flow

CP – choroid plexus

CSF – cerebrospinal fluid

CSPG – chondroitin sulphate proteoglycan

CNS – central nervous system

CTGF – connective tissue growth factor

DAB - 3, 3’-diaminobenzidine

DAPI - 4',6-diamidino-2-phenylindole

DMEM - Dulbecco’s modified eagle medium

DNA – deoxyribose nucleic acid

E - ependyma

ECL - enhanced chemiluminescence

ECM – extracellular matrix

EGFR – epidermal growth factor receptor

ELISA – enzyme-linked immunosorbent assay

EMT – epithelial to mesenchymal transition

Erk - extracellular signal related kinase

FBS – foetal bovine serum

FGF-2 – basic fibroblast growth factor

GFAP – glial fibrillary acidic protein

HRP – horseradish peroxidase

H&E – haematoxylin and eosin

ICC - immunocytochemistry

ICP – intracranial pressure

IF – immunofluorescence staining

IP – immunoperoxidase staining

IVH – intraventricular haemorrhage

JNK - c-jun amino terminal kinase

LV – lateral ventricle

MAPKs - mitogen activated protein kinases

MMP – matrix metalloproteinase

MRI – magnetic resonance imaging

OB – occipital bone

OCT – optimum cutting temperature

PAGE – polyacrylemide gel electrophoresis

PBS – phosphate buffered saline

PCR – polymerase chain reaction

Pen-strep - penicillin-streptomycin

PFA - paraformaldehyde

pSmad2/3 – phosphorylated Smad2/3

PVDF – polyvinylidene fluoride

RECA-1 – rat endothelial cell marker

RhoA – Ras homolog gene family, member A

ROI – region of interest

RTK – receptor tyrosine kinase

SAH – subarachnoid haemorrhage

SAS – subarachnoid space

SDS - sodium dodecyl sulphate

SEM – standard error of the mean

SH - sternohyoid muscle

SM - sternomastoid muscle

TGF-β1 – transforming growth factor 1

TGF-β2 – transforming growth factor 2

TIMP – tissue inhibitors of metalloproteinases

WB – western blot

3N – oculomotor nerve

3V – third ventricle

4V – fourth ventricle

Chapter 1

General Introduction

1.1. Introduction to hydrocephalus

Hydrocephalus is a complicated and poorly understood condition that can affect any age, from foetal development through to adulthood. It is described as a pathophysiological condition caused by a disturbance in cerebrospinal fluid (CSF) dynamics and characterised by ventricular enlargement (Oi, 2010; **Fig. 1.1)**. In the United States paediatric hydrocephalus accounts for 3% of all paediatric hospital charges which in 2003, amounted to $2 billion dollars (Simon *et al.,* 2008). Congenital hydrocephalus can be a consequence of myelomeningocele, aquaduct stenosis and cranioencephalic malformations (such as Dandy-Walker malformation). Acquired hydrocephalus can be idiopathic (normal pressure hydrocephalus) or caused by infection, trauma, haemorrhage and tumours (Massimi *et al.,* 2009). Currently hydrocephalus is managed by implanting an intraventricular shunt to drain CSF however this treats the symptoms and not the cause of the condition.

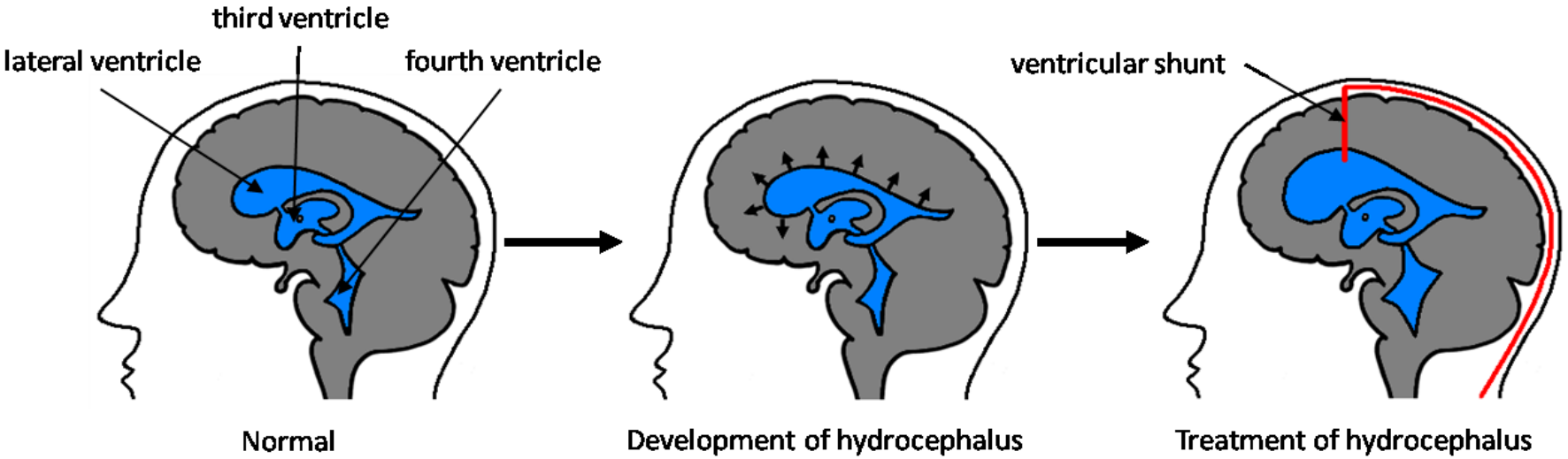

Figure 1.1. Diagram representing the development of hydrocephalus. Hydrocephalus is the enlargement of the brain ventricles and is treated by implantation of a ventricular shunt to drain cerebrospinal fluid.

1.2. Cerebrospinal fluid dynamics

CSF is produced by the choroid plexus and circulates from the lateral ventricles, through the third and fourth ventricles and into the subarachnoid space where it is drained into the venous sinuses and lymphatics **(Fig. 1.2)**. CSF has both mechanical and biochemical functions that help to protect the brain and allow normal brain function. CSF gives the brain buoyancy which reduces tension on the lower portion of the brain, and acts as a fluid 'cushion' to protect the brain from physical impact on the skull (Redzic and Segal, 2004). CSF also regulates intracranial pressure (ICP) in conjunction with changes in cerebral blood flow, removes toxic metabolic waste and moves nutrients, neurotransmitters and hormones around the brain (Di Terlizzi and Platt, 2006)

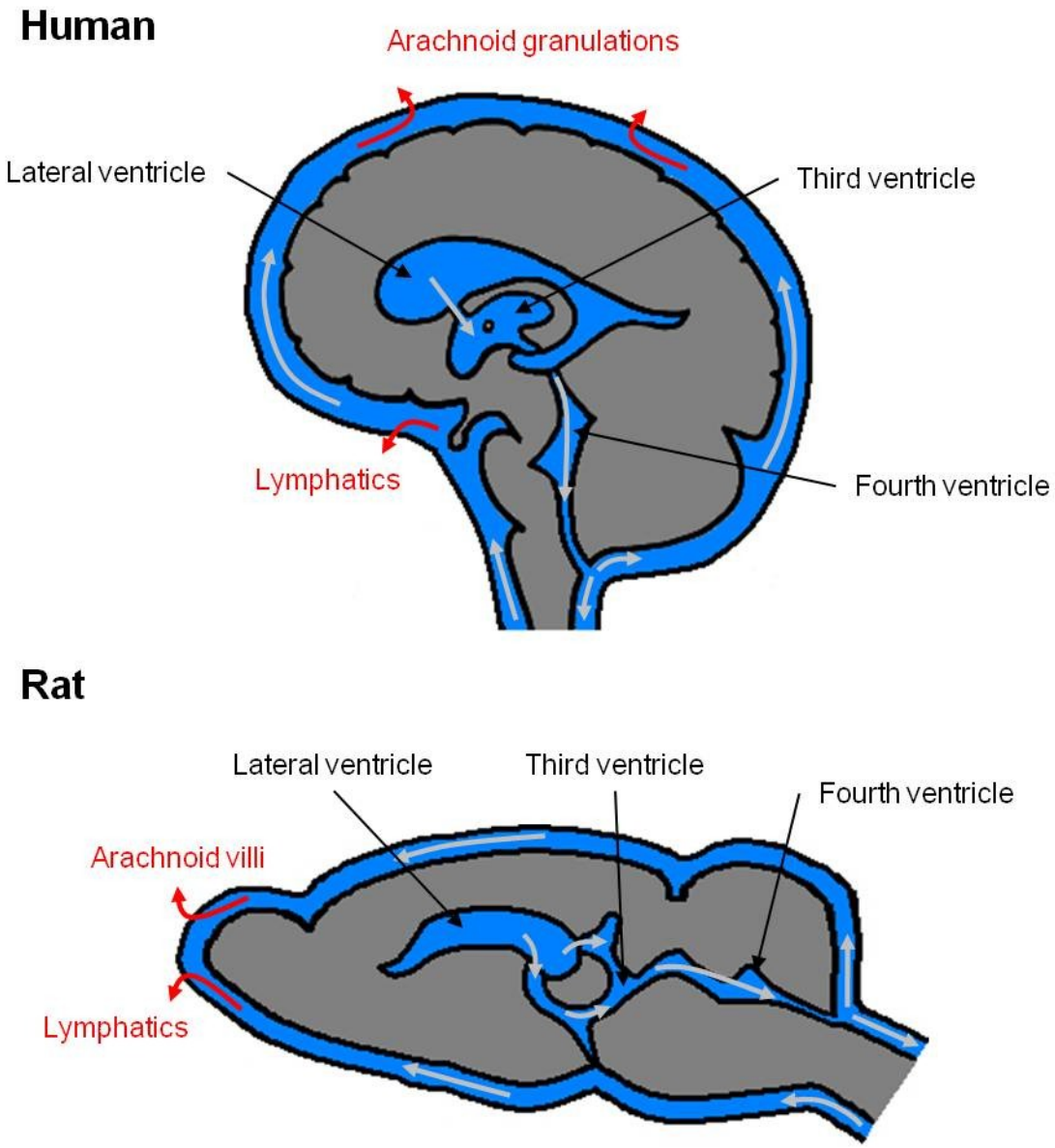

Figure 1.2. Diagram representing CSF dynamics in the human and rat brain. CSF is produced by the choroid plexus and flows from the lateral ventricles, through the third and fourth ventricle and into the subarachnoid space, where it is absorbed through the arachnoid villi/granulations into the blood stream or through the lymphatic circulation.

1.2.1. The choroid plexus and cerebrospinal fluid formation

The choroid plexus is a structure found in the lateral, third and fourth ventricles and is an extension of the ependymal epithelium. The choroid plexus consists of a single layer of epithelial cells joined by tight junctions over a network of fenestrated capillaries (Redzic and Segal, 2004). The choroid plexus epithelium is polarised, has numerous mitochondria, microvilli and long cilia on the apical surface and infoldings on the basal surface **(Fig. 1.3)**. These morphological features allow the choroid plexus to function as secreting epithelium (Strazielle and Ghersi-Egea, 2000).

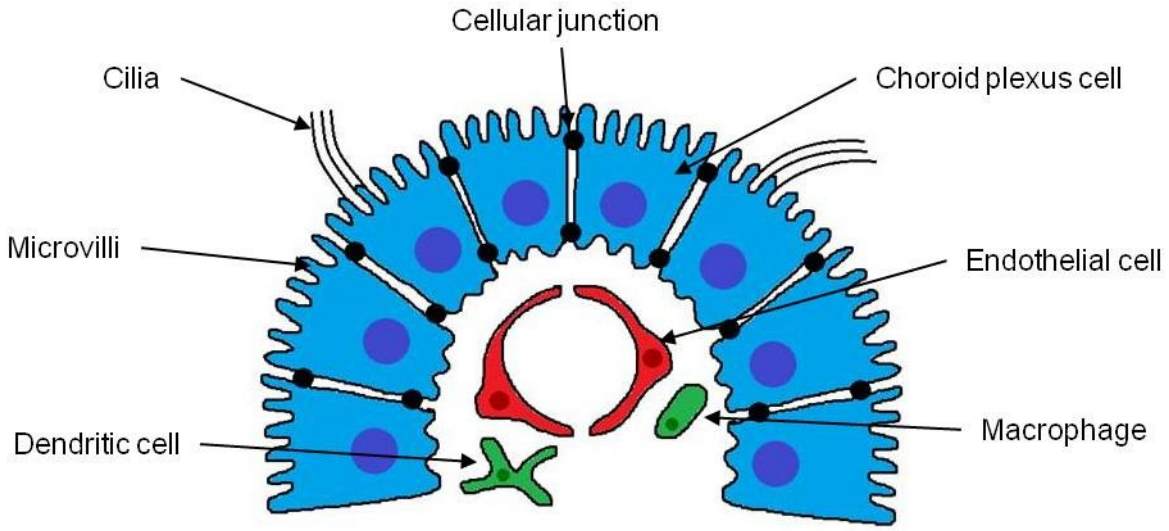

Figure 1.3. Diagram of the choroid plexus. The choroid plexus is composed of a layer of epithelial cells, fenestrated capillaries, dendritic cells and macrophages. The epithelial cells are specialised and have microvilli and cilia on the apical membrane, infoldings on the basal membrane and are joined by cellular junctions.

CSF formation occurs in 2 stages: First, the hydrostatic pressure causes passive filtration of fluid from the blood through the fenestrated endothelium into the choroidal interstitial fluid; then ions are transported actively from the choroidal interstitial fluid across the choroid plexus epithelium and into the CSF. This generates an osmotic gradient causing the transcellular movement of water from the interstitial fluid into the CSF through aquaporin 1 channels on the epithelial cells (Sakka *et al*., 2011).

The first stage of active secretion is the conversion of H_2O and CO_2 to HCO_3^- and H^+ catalysed by the enzyme carbonic anhydrase. The ion exchangers on the basal membrane then exchange H^+ for Na^+ and HCO_3^- for Cl^-. On the apical surface the Na^+/K^+ATPase actively pumps $2K^+$ in and $3Na^+$ out and the $Cl^-Na^+K^+$ cotransporter, driven by the accumulation of Cl^-, moves $2Cl^-$, Na^+ and K^+ ions out. HCO_3^- and K^+ also passively move out of the cells on the apical membrane through HCO_3^- and K^+ channels respectively on the apical surface. The net movement of Na^+, Cl^- and HCO_3^- from the epithelial basal membrane into the CSF generates an osmotic gradient causing the movement of water in the same direction **(Fig. 1.4;** Speake *et al*., 2001; Redzic and Segal, 2004).

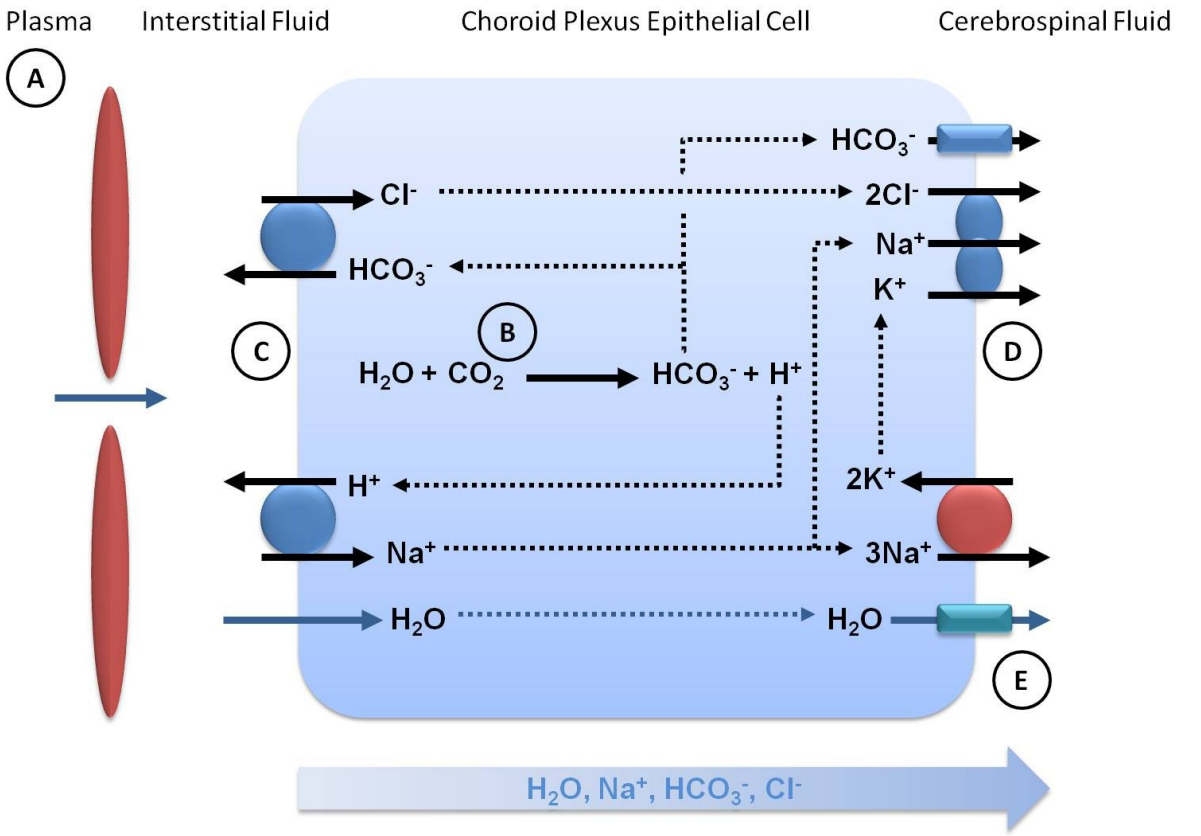

Figure 1.4. Diagram representing the formation of CSF. (A) Fluid diffuses out of the blood vessels into the interstitial fluid. **(B)** The carbonic anhydrase enzyme catalyses the conversion of H_2O and CO_2 to HCO_3^- and H^+. **(C)** At the basolateral membrane ion exchangers substitute H^+ and HCO_3^- for Na^+ and Cl^- respectively. **(D)** On the apical surface the Na^+/K^+ATPase actively pumps $2K^+$ in and $3Na^+$ out and the $Cl^-Na^+K^+$ cotransporter, driven by the accumulation of Cl^-, moves $2Cl^-$, Na^+ and K^+ ions out. HCO_3^- and K^+ also passively move out of the cells. **(E)** The net movement of Na^+, Cl^- and HCO_3^- generates an osmotic gradient causing the movement of water in the same direction.

The production of CSF is regulated by neurogenic and endocrine mechanisms. The choroid plexus is innervated by sympathetic and cholinergic nerve fibres and although there are variations among species, it is believed that sympathetic innervation reduces CSF secretion while cholinergic innervation increases CSF secretion (Nilsson *et al*., 1992). CSF formation requires high cerebral blood flow and therefore vasoactive molecules may also influence the rate of CSF formation (Szmydynger-Chodobska *et al*., 1994). The vasoactive intestinal polypeptide, peptide histidine isoleucine and Neuropeptide Y are all found in nerve fibres in the choroid plexus. Results from various studies suggest that they may be involved in modulating the sympathetic adrenergic response. Moreover, receptors and binding sites for serotonin, atrial natriuretic peptide, endothelin 1 and angiotensin II have also been discovered on the choroid plexus epithelial cell membrane suggesting that these neuropeptides may also play a role in CSF production (Nilsson *et al*., 1992). Vasopressin is the most widely investigated peptide and it has been shown that at high levels (levels only observed after severe haemorrhage) it reduces cerebral blood flow and in turn decreases CSF production (Chodobski and Szmydynger-Chodobska, 2001). This suggests that even though these neuropeptides can significantly reduce cerebral blood flow this does not always result in reduced CSF production.

1.3. Ependyma

The ventricles are lined by a layer of cells known as the ependyma. Ependymal cells are low columnar to cuboidal epithelial cells with the apical surface covered with cilia and microvilli and a basement membrane at the basal surface.

Ependymal cells are joined to one another mainly by gap junctions and sometimes tight junctions (Del Bigio, 2010). The cilia beat in a coordinated fashion in the same direction causing the constant flow of CSF through the ventricular system (Meunier *et al*., 2013) while the microvilli play a role in the exchange of molecules with the CSF. The ependyma is the interface between the CSF and the brain parenchyma, and allows diffusion of fluid and molecules between the interstitial fluid and the CSF (Abbott, 2004), therefore contributing to the extrachoroidal production of CSF (Curl and Pollay, 1968). The ependyma is also the source of multiple growth factors including basic fibroblast growth factor (FGF-2), hence the ependyma may provide trophic support to the neural progenitor cells in the underlying subventricular zone, or by releasing growth factors into the CSF to get to other regions of the brain (Hayamizu *et al*., 2001; Johanson *et al*., 2011). In addition, the ependyma is the first line of defence against infection by acting as a physical barrier and responding to inflammatory cytokines through toll like receptors and complement molecules, although the ependyma does act to reduce intraventricular inflammation (Neal and Gasque, 2013).

1.4. The meninges and subarachnoid space

The meninges are composed of three layers; the pia mater, the arachnoid mater and the dura mater **(Fig. 1.5)**. The meninges function is to protect the brain, maintain the blood brain barrier and the blood CSF barrier and are involved in the absorption and drainage of CSF. The pia mater is composed of a single continuous layer of flattened cells connected by desmosomes and gap junctions (Adeeb *et al*., 2013b). The pia mater covers the brain and lines the subarachnoid space through

which CSF flows. The pia mater is attached to the brain via the extracellular basement membrane, the glial limitans, and also covers the small blood vessels that enter the subarachnoid space from the brain (Siegenthaler et al,, 2013). The inner reticular cell layer of the arachnoid mater transverses the subarachnoid space and forms arachnoid trabeculae composed of a web of collagenous fibres covered by arachnoid trabecular cells (fibroblasts). The trabeculae form a network of extracellular channels allowing the flow of CSF through the subarachnoid space (Vandenabeele *et al*., 1996). The outer arachnoid layer lines the subarachnoid space and is composed of multiple layers of tightly packed arachnoid barrier cells. The cells lie on a basal lamina and are characterised by their flat shape, lack of extracellular space and collagen fibres between them and the presence of desmosomes and tight junctions. These arachnoid barrier cells are responsible for CSF absorption and form the barrier between CSF and blood. (Adeeb *et al*., 2013b; Siegenthaler et al., 2013). The outer layer of the meninges is the dura mater which attaches to the skull bone and is composed of fibroblasts, collagen and elastic fibrils. The inner dural border cell layer contains flattened fibroblastic cells forming cellular junctions between the arachnoid barrier cells, and is characterised by little extracellular spaces and the lack of extracellular collagen fibres. The middle dura layer is the meningeal layer and is flexible as it contains many fibroblasts that lie in a collagen matrix. The outer layer has fewer fibroblasts compared to the meningeal layer but more collagen and elastic fibres, making it a strong and durable layer that forms the periosteal lining that adheres to the skull bone (Adeeb, 2012; Mack *et al*., 2009).

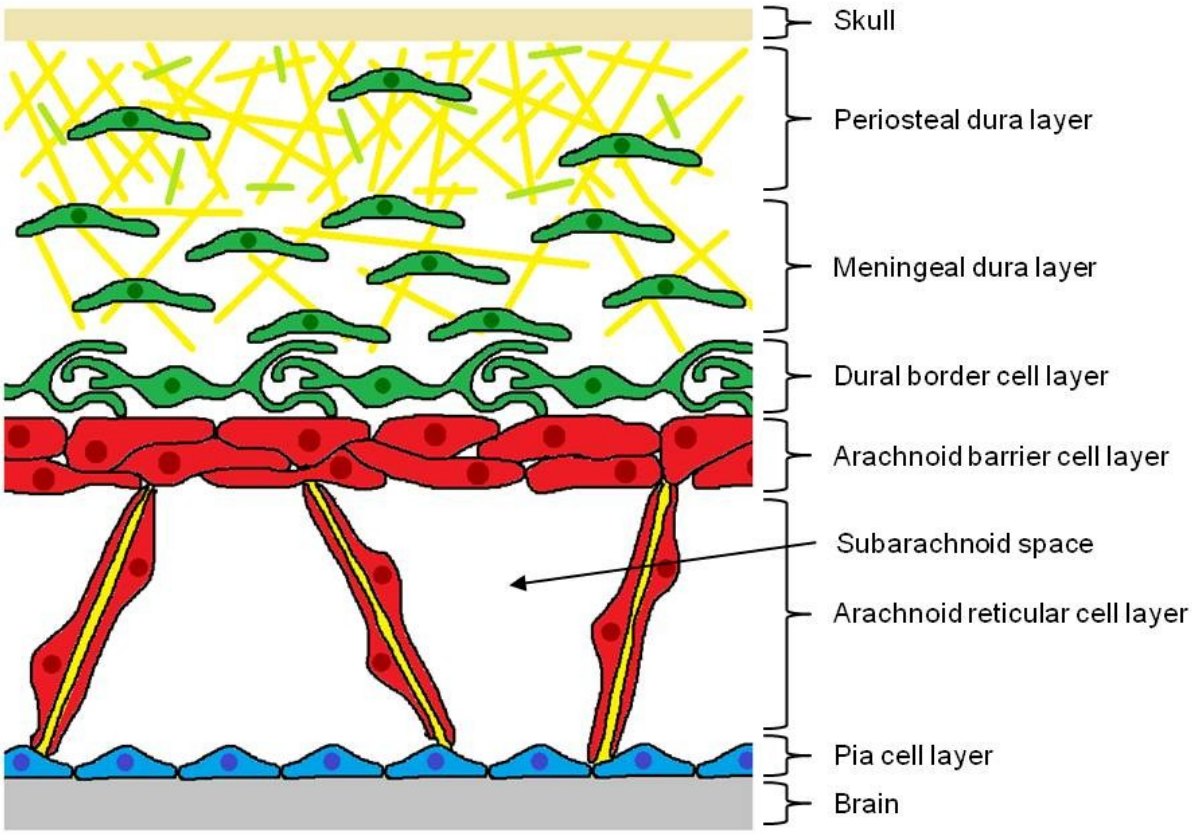

Figure 1.5. Diagram of the meninges. The meninges is composed of three layers; the pia mater, the arachnoid mater and the dura mater. The pia mater covers the brain and lines the subarachnoid space through which CSF flows. The arachnoid mater transverses and lines the subarachnoid space forming a CSF-blood barrier. The outer layer is the dura mater which attaches to the skull bone and is composed of fibroblasts, collagen and elastic fibrils.

1.4.1. Arachnoid granulations, lymphatics and the absorption of cerebrospinal fluid

Arachnoid granulations and villi are located in the lateral lacunae of the superior sagittal sinus and over the cerebral cortices. Only arachnoid villi are present in infants and therefore it is speculated that arachnoid granulations develop from villi and with age increase in complexity (Jayatilaka, 1969; Pollay, 2010). Human arachnoid granulations have four components; a central core, an arachnoid cell layer, a cap cell cluster and a thin fibrous capsule (Kida *et al*., 1988; **Fig. 1.6)**. The central core is an extension of the subarachnoid space protruding into the lumen and contains collagen trabeculae and arachnoid trabecular cells. Lining the core is the arachnoid barrier cell layer which continues from the arachnoid mater. This single layer of cells forms multiple layers of arachnoid barrier cells at the apical portion called the cap cell cluster. Covering the arachnoid cells is the thin fibrous capsule that is composed of vascular endothelial cells, and fibroblasts and connective tissue from the dura mater. This fibrous capsule does not cover the apical portion of the granulation and therefore the cap cell cluster is in direct contact with the blood vessel lumen (Upton and Weller, 1985; Kida *et al*., 1988; Kapoor *et al*., 2008). Jayatilaka (1969) has suggested that humans have two types of arachnoid granulations: type 1, with the structure outlined above and type 2, with a layer of endothelial cells covering the cap cell cluster. Type 1 granulations appear to be specific for humans as other mammals only have type 2 granulations. In contrast Ohta *et al* (2002) has suggested that humans only have type 2 granulations. In the rat, Jayatilaka (1969) has not observed arachnoid villi or granulations whereas Kida *et al* (1993) detected arachnoid villi in the superior and inferior sagittal sinus. Due to the differing opinions

on the structure of arachnoid granulations there are two proposed mechanisms of CSF drainage; first, through extracellular cisterns and second, by active transport through endothelial cells via pinocytic vesicles and vacuoles (Pollay, 2010).

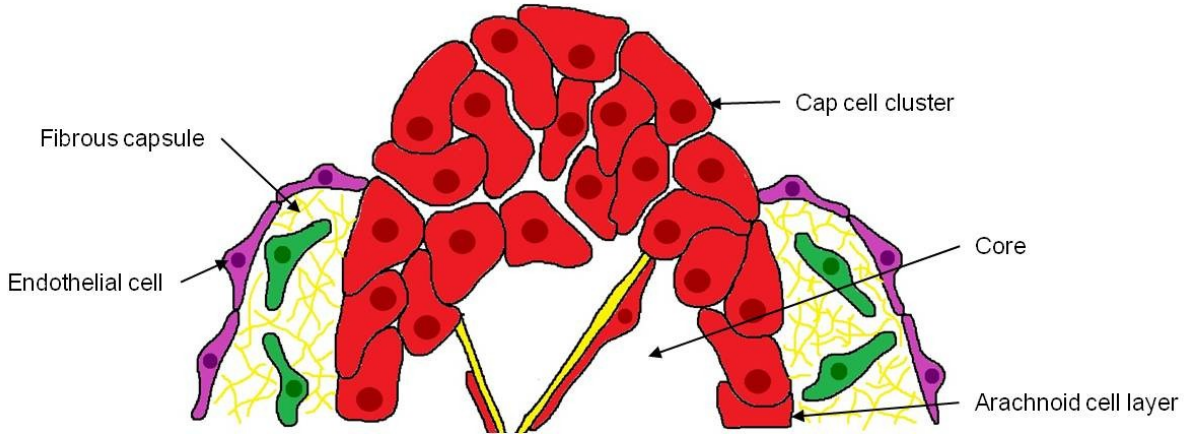

Figure 1.6. Diagram of the arachnoid granulations. Arachnoid granulations are composed of 4 main parts; the core, the arachnoid cell layer, the cap cell cluster and the fibrous capsule. CSF drains through the arachnoid granulations into the blood vessels.

More recently, studies have revealed the importance of the lymphatic system in CSF drainage. Boulton *et al* (1999) have demonstrated the equal contribution of lymphatic vessels and arachnoid villi to CSF drainage after injecting human serum albumin into the lateral ventricles of rats (although the authors recognise that this experimental approach may lead to an underestimation of lymphatic drainage). Injections of Indian ink (Walter *et al*., 2006) and Microfil® (Johnston *et al*., 2004) into the subarachnoid space have demonstrated that the respective compounds are present discontinuously around the olfactory nerves in the cribriform plate and nasal mucosa. These compounds were also observed in the lymphatic network of the nasal mucosa and in the cervical lymph nodes. Walter *et al* (2006) have hypothesised that there is no direct communication between the subarachnoid space and the lymphatic system and suggested that the meninges fuse together at the cribriform plate. This implies that CSF is drained through channels between the epineurial and perineurial layers around the olfactory nerves and then diffuses into lymphatic vessels of the nasal mucosa. Therefore in some mammals where arachnoid granulations are absent or the arachnoid villi are not prominent, lymphatic drainage may be the major route of CSF drainage, and the arachnoid villi may only contribute under high intracranial pressure (Nagra *et al*., 2008).

1.5. Glial cells

1.5.1. Astrocytes

Astrocytes are ten times more abundant than neurones in the brain. There are two main subtypes; protoplasmic astrocytes have finely branched processes that envelop synapses and are located in grey matter, and fibrous astrocytes have long

fibre-like processes that make contacts with nodes of ranvier and so are mainly found in white matter (Sofroniew and Vinters, 2010).

During neural development astrocytes have an integral role in the guidance of developing axons by forming boundaries and in mediating synapse formation and elimination (Sofroniew and Vinters, 2010; Allen, 2013). Although the involvement of astrocytes in the functional part of the blood brain barrier is unresolved, astrocytes are involved in the development and maintenance of the blood brain barrier (Ballabh *et al.,* 2004). In addition, in the adult brain astrocytes are involved in maintaining brain homeostasis. Astrocytes maintain extracellular K^+ levels by removing K^+ from the extracellular space after neuronal depolarisation through the actions of Ca^{+2} channels, Ca^{+2} activated K^+ channels, Na^+/K^+-ATPase transporter and K^+ spatial buffering (Allen, 2013). One of the most important roles of astrocytes is the recycling of glutamate. Astrocytes take up glutamate which is subsequently converted to the inactive glutamine by the enzyme glutamine synthetase. Glutamine is then released and taken up by neurones and converted back to glutamate by the enzyme glutaminase (Kimelberg and Nedergaard, 2010). Astrocytic processes make contacts with both synapses and blood vessels hence they are involved in neurovascular coupling; the relationship between neuronal activity and cerebral blood flow (Longden *et al.*, 2011). Neural activity leads to an increase in intracellular Ca^{+2} in astrocytes, inducing in turn the release of vasoactive molecules, resulting in the increase in blood vessel diameter and subsequent increase in blood flow (Zonta and Carmignoto, 2002).

Reactive astrogliosis is the most prominent cellular response to all forms of CNS injury and is regulated by specific signalling pathways which can lead to gain

and loss of functions through altered gene and protein expression. Mild to moderate astrogliosis causes hypertrophy of the cell body and processes which, if the trigger is removed, resolves and the astrocytes return to their original state. The initial hypertrophy is associated with an increase in GFAP, vimentin, and nestin expression which is in turn associated with increased stiffness of astrocytes (Lu *et al*., 2010). Hypertrophy of astrocytes does not only transpire adjacent to the injury but occurs throughout the brain. In severe astrogliosis the astrocytes also proliferate rapidly causing overlapping of cell processes and the formation of a glial scar which can persist even after the trigger has disappeared (Sofroniew, 2009). There are many molecules released by all cell types in the CNS (neurones, oligodendrocytes, microglia, endothelial cells, pericytes and other astrocytes) that can mediate different aspects of reactive gliosis. These include growth factors, cytokines, neurotransmitters and reactive oxygen species to name a few (Sofroniew and Vinters, 2010). Often reactive astrogliosis is beneficial as it is neuroprotective and promotes neuronal survival, it prevents the infiltration of inflammatory cells into uninjured tissue via the glial scar, it facilitates tissue and blood brain barrier repair by promoting ECM production and helps to clear debris by inducing microglia (Bush *et al*., 1999; Faulkner *et al*., 2004; Myer *et al*., 2006). However the same roles reactive astrocytes conduct that are beneficial can result in detrimental effects if astrogliosis is prolonged. Reactive astrogliosis can produce high levels of pro-inflammatory cytokines which exacerbate inflammation after injury. It can also damage neurones by producing high levels of reactive oxygen species and glutamate and be inhibitory to axonal growth by promoting the production of ECM and growth inhibitory proteoglycans (Sofroniew and Vinters, 2010).

1.5.2. Microglia

Microglial cells have finely branched processes with a small elongated nucleus (Aguzzi *et al*., 2013). In the normal brain microglial cells are referred to as 'resting' microglia, a controversial term as it implies that they are in a quiescent state which is far from the truth. Although their soma remains fairly stationary, their processes are constantly moving, new processes are continually formed and old processes are withdrawn. This suggests that these cells are constantly monitoring and surveying their surrounding area, removing debris in the close vicinity, thus making them primed to respond to injury immediately. Therefore, microglial cells are the primary immune response in the central nervous system. Similar to astrocytes, microglia appear to occupy a specific area that does not overlap with other microglia and their processes are in contact with neurones, astrocytes and blood vessels (Nimmerjahn *et al.,* 2005; Kettenmann *et al*., 2011).

When microglia become activated their processes are shortened, thickened and they take on a more amoeboid morphology (Aguzzi *et al.*, 2013). As microglia are primed to react immediately, microglia activation often occurs before other cells react to injury in the brain (kreutzberg, 1996) and only microglia in the immediate vicinity will become activated (Nimmerjahn *et al.,* 2005). During activation, microglial cells migrate to the injury site, secrete pro-inflammatory cytokines and increase adhesion to invading inflammatory cells. If there is no further damage then the microglia will return to their resting state. However if there is neuronal cell death the microglia will proliferate and phagocytose pathogens and cellular debris and also form a protective barrier around the injury site to protect healthy neurones (Nimmerjahn *et al*., 2005; Raivich *et al*., 1999).

1.6. Post-haemorrhagic hydrocephalus

There are two types of hydrocephalus that develop after a haemorrhage; acute non-communicating hydrocephalus and chronic communicating hydrocephalus. Communication is dependent upon the CSF being able to flow freely between the lateral ventricles and the subarachnoid space (Rekate, 2008; Oi, 2010). Non-communicating hydrocephalus usually develops within the first 24 hours after a bleed due to blood clots obstructing the ventricular system. On the other hand communicating hydrocephalus develops later (around 2 weeks) as a result of obstruction at the site of CSF absorption, most likely due to the development of subarachnoid fibrosis (Bederson and AANS Publications Committee., 1997; Strahle *et al*., 2012).

1.6.1. Subarachnoid haemorrhage

Subarachnoid haemorrhage (SAH) is a bleed in the subarachnoid space between the pia and the arachnoid mater. It is most commonly caused by a ruptured cerebral aneurysm but can also occur as a consequence of a traumatic injury (Bederson and AANS Publications Committee., 1997). Latest statistics illustrate that worldwide, SAH affects around 9 in 100,000 people every year and is associated with a high morbidity and mortality rate (de Rooij *et al*., 2007). The symptoms of SAH are sudden onset severe headache which can be accompanied by loss of consciousness and/or signs of meningism such as vomiting and neck stiffness (Ferro *et al.,* 2008; Kumar and Friedman, 2011). The existence of an aneurysm is confirmed by intra-arterial angiography (Ferro *et al.*, 2008) and the presence of subarachnoid haematic

densities on early CT scans indicates SAH. If the CT scan is performed later on a lumbar puncture is necessary to confirm the diagnosis.

SAH is generally treated by either neurosurgical clipping or endovascular coiling to stabilise the patient before additional medical management to prevent further complications such as rebleeding, delayed ischaemia, vasospasm, and hydrocephalus (Al-Shahi *et al*., 2006). The risk of developing hydrocephalus is associated with a higher grade of SAH (based on the Fisher SAH Scale) and the presence of intraventricular blood (Wang *et al*., 2012).

1.6.2. Intraventricular haemorrhage

Intraventricular haemorrhage (IVH) commonly develops as a result of a bleed in the germinal matrix entering the ventricles and can affect 20% of premature or very low birth weight infants (Merhar, 2012). These infants are more at risk because the capillaries in the germinal matrix are not fully developed and are very delicate. When combined with the respiratory problems commonly seen in preterm infants which cause fluctuations in cerebral blood flow, it leads to haemorrhage and bleeding into the ventricles (Ballabh, 2010). The clinical presentation of IVH varies from no signs to changes in haematocrit levels, unconsciousness, abnormal eye movements and altered mobility and seizures. IVH can be diagnosed using cranial ultrasound and the severity of IVH ranges from mild haemorrhage in the germinal matrix to an intraventricular haemorrhage that fills more than 50% of the ventricles with dilation of the ventricles (Martin, 2011). IVH is the second leading cause of hydrocephalus in infants and the incidence has remained fairly constant in the last 20 years, accounting for around 20% of cases (Massimi *et al.,* 2009).

1.6.3. Treatment of Hydrocephalus

Non-communicating hydrocephalus developing after SAH is treated by placement of an external ventricular drain within the ventricle before surgery is carried out on the aneurysm (Kumar and Friedman, 2011). Communicating hydrocephalus affects around 20% of surviving SAH patients (Vale *et al*., 1997), with the main symptoms being urinary incontinence, gait disturbances and cognitive impairment and requires implantation of a permanent ventricular shunt (Edwards *et al*., 2004).

Treatment for post IVH-hydrocephalus in premature infants is more complex as ventriculo-peritoneal shunt cannot be implanted until the infant weighs 2kg (very low birth weight infants weigh less than 1.5kg). Initially, the development of hydrocephalus is controlled by performing repeated lumbar punctures or ventricular taps, however both procedures are associated with an increased risk of infection. Alternatively, a ventricular access device can be implanted to facilitate repeat ventricular taps. Later on, an external ventricular drain can then be implanted although there is still a risk of up to 50% infection with this technique (Brouwer, 2011).

Drug treatments have also been trialled to reduce the need for shunt implantation. Acetazolamide and furosemide have been shown to reduce CSF production by inhibiting the carbonic anhydrase enzyme and the Na^+-K^+-Cl^- symporter respectively. Unfortunately a large randomised trial into the use of these drugs in post haemorrhagic ventricular dilatation in infants demonstrated that they did not have a beneficial effect, and even caused an increase in the number of initial

shunt placements. Moreover, an increased neurological morbidity was observed (anonymous, 1998).

Streptokinase, urokinase or tissue plasminogen activator are fibrinolytics and have been given intraventricularly to breakdown blood clots to restore normal CSF flow. Similarly, these drugs did not show beneficial effects and carried an increased risk of haemorrhage (Whitelaw and Odd, 2007). Antifibrolytic therapy has been further investigated in DRIFT (drainage, irrigation and fibrinolytic therapy) aiming to remove blood, iron, inflammatory and profibrotic molecules before hydrocephalus is established but the increased risk of secondary IVH outweighed the benefits (Whitelaw *et al*., 2007).

Consequently the only current standard of care for post-haemorrhagic hydrocephalus is the implantation of a ventriculo-peritoneal shunt. Unfortunately shunt failure is still a large problem in the management of hydrocephalus (Bergsneider *et al*., 2006) because of risk of further intracerebral haemorrhage, infection and general lack of shunt longevity (O'Kelly *et al*., 2009). Infants with IVH tend to be very young and so the risk of shunt malfunction is much higher. Their incompetent immune system favours infection and the shunts are more easily blocked by blood clots from the haemorrhage (Shooman *et al*., 2009). In the United States there were around 39,000 admissions in 2003 surrounding paediatric hydrocephalus. Half of these admissions were due to shunt related issues but surprising the admission for shunt complications was much higher than the admission for the initial shunt placement (Simon *et al.,* 2008). A recent study in Australia indicates that 75% of expenditure for hydrocephalus is due to complications or failure to treat hydrocephalus (Pham *et al*., 2013).

Other complications of shunt malfunction include impaired cognitive development, reduced IQ, prolonged hospital visits, more surgeries and an increased risk of mortality (Kandasamy *et al*., 2011). However, even without the complications mentioned above, after shunt treatment there is still residual morbidity and hydrocephalic children suffer with motor deficits, visual or auditory deficits, epilepsy and severe behavioural disorders affecting social integration (Hoppe-Hirsch *et al.,* 1998). Consequently there is a need for research into developing novel preventative therapies, especially as this type of hydrocephalus develops after a specific insult and therefore there is the potential for preventing it.

1.7. Murine models of haemorrhage and hydrocephalus

1.7.1. Subarachnoid haemorrhage models

There are two main experimental murine models of SAH used by researchers in the field. The first model is the blood injection model, where blood is removed from the tail and injected into either the prechiasmatic cistern (Prunell *et al*., 2002; Tait *et al*., 2010) or the cisterna magna (Solomon *et al*., 1985; Sajanti *et al*., 1999; Gul *et al*., 2010). The second model is the endovascular perforation model where a sharpened suture is advanced along the internal carotid artery to perforate the bifurcation of the anterior and middle cerebral arteries (Park *et al*., 2008; Suzuki *et al*., 2010). The endovascular perforation model, although more severe, more closely resembles human SAH. This model demonstrates a greater reduction in cerebral blood flow, a greater increase in ICP and more neuronal death but consequently has a higher mortality rate (Jeon *et al*., 2009; Lee *et al*., 2009). All the models show other features observed in human SAH, including vasospasm and cerebral ischaemia (Jeon *et al*.,

2009). They also show an increase in collagen synthesis and deposition in the meninges which can lead to chronic fibrosis (Sajanti *et al*., 1999). This high collagen deposition is also observed in post mortem tissue from SAH patients (Motohashi *et al*., 1995) and patients with SAH appear to have greater levels of collagen propeptides in their CSF (Sajanti and Majamaa, 1999).

There are only a limited number of studies assessing the underlying aetiology of post-haemorrhagic hydrocephalus in adult SAH murine models. One of the pitfalls of the blood injection technique is that large amounts of blood cannot be injected as it results in an increased risk of mortality. However the quantity of blood injected is a critical variable, as a thick collection of subarachnoid blood is associated with the development of post-haemorrhagic hydrocephalus (Graff-Radford *et al*., 1989; Dorai *et al*., 2003). To overcome this problem some investigators have conducted double injections, where the first injection of blood is followed 2 days later by a second injection to increase the maximum amount of blood administered (Carpenter *et al*., 2001; Gules *et al*., 2002). However a possible concern may be that the double injection technique models rebleeding, a separate complication of SAH that is not associated with an increased risk of developing post-SAH communicating hydrocephalus. SAH models develop extensive fibrosis in the subarachnoid space over 4 weeks but enlargement of the ventricles is harder to come by (Sajanti *et al*., 1999). Recently Chu *et al*. (2011) reported the induction of hydrocephalus in 21 out of 50 rats after a double injection of blood (800µl in total) into the cisterna magna. These results are interesting as previous studies conducting a double injection with a total of 800µl of blood have not reported enlarged ventricles (Takata *et al*., 2008).

1.7.2. Intraventricular haemorrhage models

Unfortunately only a small number of studies have been conducted into IVH taking into account that the presence of IVH in SAH patients is one of the factors associated with the development of shunt dependent hydrocephalus (Graff-Radford *et al*., 1989, Dorai *et al*., 2003). Lodhia *et al* (2006) has demonstrated that an injection of blood into the lateral ventricles in adult rats results in a peak ventricular dilatation at two days which is still observed at 8 weeks although to a lesser degree. The initial peak corresponds to the acute non-communicating hydrocephalus that develops due to blood clots causing an obstruction. Cherian *et al* (2004) has generated a model of neonatal IVH by administering 2 injections (1 in each lateral ventricle on consecutive days) of 80µl citrated blood. The mortality rate with this procedure was over 20% and hydrocephalus was induced in 65% of rats. Interestingly 50% of the control rats which received two injections of artificial CSF also developed hydrocephalus.

1.7.3. Biological Molecules that Induce Hydrocephalus

1.7.3.1. Growth Factors

The general consensus is that the formation of chronic subarachnoid fibrosis contributes to the development of post-haemorrhagic hydrocephalus by blocking CSF drainage and therefore the pro-fibrotic molecules released during a haemorrhage could be used to induce experimental hydrocephalus.

Transforming Growth Factor (TGF)-βs are a family of multifunctional cytokines that are released from activated platelets (TGF-βs will be discussed in depth in section 1.9). Transgenic mice that specifically overexpress TGF-β1 in astrocytes

(Galbreath *et al*., 1995; Wyss-Coray *et al*.,1995) develop communicating hydrocephalus within 7-20 days after birth with an increase in the deposition of ECM in the meninges (Wyss-Coray *et al*., 1995). Moreover several studies have shown that a single intrathecal injection of human recombinant TGF-β1 into neonatal mice induces hydrocephalus within 6 weeks (Kanaji *et al.*, 1997; Tada *et al.*, 1994). These animals also show the appearance of subarachnoid fibrosis, proliferation of meningeal cells and subsequent disturbed CSF flow (Moinuddin and Tada, 2000). In these mice, hydrocephalus could be prevented by injecting a TGF-β1 antibody (Kanaji *et al.*, 1997). Interestingly this last experiment was replicated in adult rats and, even though they developed meningeal fibrosis, they did not develop enlarged ventricles (Nakazato *et al.*, 2002). All together these studies clearly suggest a role for TGF-β1 in the development of hydrocephalus.

Fibroblast growth factor 2 (FGF-2; also known as basic fibroblast growth factor) is produced by glia and neurones throughout the brain and is also present in ependymal and blood vessel basement membranes (Logan *et al.*, 1992; Matsuyama *et al.*, 1992). It is a potent mitogenic, fibrogenic and angiogenic agent which also regulates motility, adhesion, differentiation, cell survival and apoptosis (Greenwood *et al.*, 2008). Continual infusion of FGF-2 into the lateral ventricle of rats for 12 days induced communicating hydrocephalus with increased deposits of collagen in close proximity to arachnoid villi in the superior sagittal sinus. FGF-2 infusion also caused a reduction in CSF production and an increase in resistance to CSF absorption (Johanson *et al*., 1999). Although FGF-2 has also induced hydrocephalus in mice (Ohmiya *et al.*, 2001) and marmosets (Pearce *et al.*, 1996), a link between FGF-2 and the development of hydrocephalus in humans has not been established.

The development of hydrocephalus is most likely to be multifactorial, involving multiple molecular pathways, and thus combinations of growth factors may be involved in inducing hydrocephalus. Other growth factors that are released by activated platelets that may play a role in the development of post-haemorrhagic hydrocephalus are platelet derived growth factor (PDGF) and epidermal growth factor (EGF; Rendu and Brohard-Bohn, 2001). Both PDGF and EGF promote the proliferation of meningeal cells *in vitro* (Motohashi *et al.*, 1995b) and therefore could contribute to the development of chronic fibrosis and obstruct CSF drainage.

1.7.3.2. β1-Integrins

It has been suggested that meningeal fibrosis may not completely explain the pathology of hydrocephalus since it has been demonstrated that hydrodynamic factors also play an important role in the regulation of interstitial fluid and CSF volume (Oreskovic and Klarica, 2011). β1-integrins mediate cell-extracellular matrix adhesion and act as mechanoreceptors by actively conveying force transmission which allows cells to alter interstitial pressure (Wiig *et al.*, 2003). For example, β-integrin receptors may allow connective tissue cells to exert tension on collagen and fibril networks preventing the connective tissue from expanding (Wiig *et al.*, 2003). Nagra *et al* (2009) have shown that 2 weeks after injection of β1-integrin antibodies into the lateral ventricle of rats, the majority of animals developed hydrocephalus and they could detect changes in pressure between the parenchyma and the ventricles. Although it is not well understood how β1-integrin antibodies induce hydrocephalus this approach opens many avenues for investigation. It highlights the fact that modulating specific proteins can affect pressure gradients and that molecular

pathways could be targeted to develop a treatment for hydrocephalus. β1-integrins may also have relevance to post-SAH hydrocephalus as integrins are involved in blood clotting, in the aggregation of blood platelets and extravasation of white blood cells (Wiig *et al.*, 2003).

1.7.4. Inflammatory Molecules

Inflammation is an important aspect in the development of hydrocephalus. Lysophosphatidylcholine (LPC) is a lipid associated with inflammatory disorders, as it has multiple effects on cells involved in inflammation. For example, it acts as a chemo-attractant, regulates proliferation and induces the expression of growth factors in a variety of immune and endothelial cells (Kim *et al.*, 2007; Okajima *et al.*, 1998). LPC injection into the internal capsule causes an inflammatory response which spreads from the parenchyma into the ventricles, leading to the development of communicating hydrocephalus (Tourdias *et al.*, 2009).

Neuraminidase catalyses the removal of terminal sialic acid residues from many different glycoconjugates and is usually found in bacteria and viruses where it plays a role in pathogenesis (Gaskell *et al.*, 1995). Grondona *et al* (1996) administered neuraminidase into the lateral ventricle of rats as sialoglycoproteins are involved in the adhesion of ependymal cells. In these studies, neuraminidase caused the ependymal cells to die and detach, except in regions sealed by tight junctions such as the choroid plexus and the subcommissural organ. Hydrocephalus developed after 4 days as a result of obliteration of the cerebral aqueduct (Grondona *et al.*, 1996), and therefore was classed as non-communicating hydrocephalus. Defects in adhesion and in cilia function appeared to be related to the development

of hydrocephalus (Del Bigio, 2010). These models emphasise the importance of inflammation and the integrity of the ependyma in the development of hydrocephalus.

1.7.5. Non-Biological Molecules that Induce Hydrocephalus

1.7.5.1. Dextran

Since the exchange of fluid and solutes between the parenchyma and the ventricles plays an important role in CSF dynamics (Oreskovic and Klarica, 2011), changes in CSF osmolarity could potentially unbalance this exchange and lead to ventricular enlargement and hydrocephalus. Krishnamurphy *et al* (2009) have demonstrated that continuous infusion of a hyperosmotic solution of Dextran (10kD) into the lateral ventricle of rats causes ventricular enlargement that appears to be more pronounced than with FGF-2 treatment. Dextran causes no blockage or fibrosis therefore it would be interesting to see whether the ventricular enlargement resolved once infusion was stopped, or if the dextran was exchanged for a hypo-osmotic solution.

1.7.5.2. Kaolin

The kaolin model of hydrocephalus is the best characterised and most widely used. Kaolin, an aluminum silicate, induces an inflammatory response with the concomitant deposition of collagen and dense fibrosis in areas of the subarachnoid space close to the injection site (Hatta *et al.*, 2006; Nakagawa *et al.*, 1985).

Kaolin is usually injected into the cisterna magna where it induces inflammation generally at the site of the foramina of Luschka, and ultimately produces an obstructive type of hydrocephalus, in most instances, between the

ventricular system and the subarachnoid space (Irigoin *et al.*, 1990; Kondziella *et al.*, 2002; Nagra *et al.*, 2008; Nakagawa *et al.*, 1985). However, a study by Lopes *et al* (2009) in mice showed development of extraventricular hydrocephalus after injection into the cisterna magna and surmised that the hydrocephalus was of the communicating form with the obstruction at the site of CSF absorption. More recently the injection of kaolin has been attempted in the basal cisterns (Li *et al.*, 2008; Nagra *et al.*, 2010; Wagshul *et al.*, 2009) and the cerebral convexities (Li *et al.*, 2008). In both cases communicating hydrocephalus was generated with kaolin deposits in the basal cisterns and no obstruction at the foramina of Luschka (Li *et al.*, 2008). The pathophysiology of hydrocephalus develops due to of a variety of different insults; gradual stretching and compression of brain tissue, chronic cerebral ischaemia, accumulation of toxic metabolic waste products and alterations in neurotransmitter systems (Braun *et al.*, 1998; Del Bigio, 2000). The kaolin injection model successfully replicates the development and the pathophysiological consequence of acquired hydrocephalus.

1.8. Pathological consequences of experimental hydrocephalus

The pathology of hydrocephalus has been thoroughly investigated and the majority of data has been gathered using the kaolin model of hydrocephalus (discussed in section 1.7.5.2).

1.8.1. Ventricular enlargement

The pathology of hydrocephalus is closely associated with the age of onset of hydrocephalus, its duration and the rate at which the ventricles expand (Del Bigio,

2004). The rate of ventricular expansion varies between studies, possibly due to the diversity of concentrations and volumes of kaolin injected. Kondziella *et al* (2002) have demonstrated that the ventricles continue to enlarge for up to 8 weeks post kaolin injection, with the most significant change taking place between the 4th and 6th weeks. Conversely, Tashiro *et al* (1997a) have described the enlargement of ventricles as an initial rapid increase followed by a slow but steady progression. Braun *et al* (1998) suggestion of 3 types of hydrocephalus; progressive, declining and stable, better reflects the variety of hydrocephalus observed in the kaolin model and in human hydrocephalus.

1.8.2. Intracranial pressure

In the acute stages of hydrocephalus the enlargement of ventricles is closely associated with an increase in ICP. However, between 4 and 6 weeks the raised ICP returns to normal levels without a reduction in ventricular enlargement (Egawa *et al.,* 2002; Kondziella *et al*., 2002). In addition, at this point CSF outflow resistance decreases which could all be a consequence of alternative CSF pathways opening (Kondziella *et al*., 2009) such as compensatory spinal mechanisms (Voelz *et al*., 2007).

1.8.3. Cerebral blood flow, blood vessels and oxidative metabolism

In the initial stages of hydrocephalus, cerebral blood flow (CBF) is reduced throughout the brain, with levels reaching the ischaemic threshold in the periventricular white matter. However 8 weeks after the induction of hydrocephalus, CBF is restored to normal levels. The reduction in CBF is most likely due to

compression of blood vessels associated with the increase in ICP rather than the enlargement of the ventricles (Klinge *et al*., 2003). Hydrocephalus also causes functional damage to the sympathetic nervous system which could result in a reduction in CBF through incomplete adrenergic denervation of the cerebral blood vessels (Caner *et al*., 1991). In addition to affecting CBF, hydrocephalus also causes a reduction in the number and diameter of capillaries in white and grey matter (Oka *et al*., 1985), and the vessels become spastic with corrugation of their endothelium and lamina elastica (Caner *et al*., 1993).

Alterations in CBF resulting in ischaemia will affect oxidative metabolism. A number of investigators (Braun *et al*., 1999, Kondziella *et al*., 2009) have shown that hydrocephalic rats have increased levels of lactate in their CSF, which is also abundant in the brain parenchyma when hydrocephalus is fatal. Greater lactate concentrations are an indication of cerebral ischaemia as it indicates impairment in energy metabolism (Braun *et al*., 1997, Braun *et al*., 1998). In the acute stages, the increase in lactate concentration and lactate dehydrogenase activity shows the conversion to anaerobic glycolysis (Hidaka *et al*., 1997) whereas in the chronic stages of hydrocephalus energy metabolism shifts back to being aerobic (Sogabe *et al*., 1989, Matsumae *et al*., 1990), possibly due to the normalisation of CBF.

1.8.4. Cerebrospinal fluid dynamics

Multiple studies have shown that kaolin-induced hydrocephalus leads to an increase in CSF outflow resistance (Brinker *et al*., 1998; Luedemann *et al*., 2002; Nagra *et al*., 2010) which is consistent with human hydrocephalus. In this model there is also a reduction in lymphatic CSF absorption mainly through the cribriform

plate (Nagra *et al*., 2008; Nagra *et al*., 2010) and other CSF outflow pathways, such as the spinal perineural CSF outflow pathways, may also be recruited (Luedemann *et al*., 2002). The arachnoid villi may be involved although they are not considered important in CSF absorption under normal conditions in rats (Nagra *et al*., 2008). There are also changes in the pulsatile CSF flow through the cerebral aqueduct depending on the extent of ventriculomegaly. Severe ventricular enlargement appears to be associated with persistent elevated pulsations, whereas mild ventricular enlargement is associated with mildly elevated pulsations (Wagshul *et al*., 2009). The kaolin model has also been shown to have a reduction in the CSF formation rate (Hochwald *et al*., 1981; Nakamura and Hochwald, 1983, Caner *et al*., 1991), most likely a compensatory mechanism which has been suggested to be related to an increase in ICP leading to a decrease in choroid plexus epithelial function (Knuckey *et al*., 1993).

1.8.5. Behavioural and biochemical changes

There are a number of behavioural changes observed with the development of hydrocephalus and these tend to be related to disturbances in various neurotransmitter systems in different areas of the brain. A number of studies have assessed the behavioural changes observed after kaolin injection and development of hydrocephalus. A reduction in weight and a loss of appetite appear to be very common, with some animals losing as much as 30% of their body weight (Nakamura and Hochwald, 1983; Lopes *et al*., 2009). Other areas affected by hydrocephalus include motor activity; the hydrocephalic animals had decreased activity and locomotion (Kuchiwaki *et al*., 1994; Del Bigio, 2000; Klinge *et al*., 2003), reduced

coordination and a body tremor (Tashiro *et al*., 1997b; Hwang *et al*., 2009). Hydrocephalic rats also have varying degrees of impairment in spatial memory depending on the severity of ventriculomegaly (Egawa *et al*., 2002; Okii *et al*., 2007) and learning ability (Shim *et al*., 2003).

In the basal ganglia, a structure associated with the control of voluntary movements, the dopaminergic, GABAergic and cholinergic systems are all functionally damaged in hydrocephalic animals (Tashiro *et al*., 1997b). The noradrenergic system in the striatum (Miyake *et al*., 1992) and in the locus ceruleus, which is involved in cognition, has been shown to undergo functional injury (Tashiro and Drake, 1998). The noradrenergic system is also affected by incomplete denervation of the cerebral vessels caused by functional damage to the perivascular sympathetic nerve plexus (Caner *et al*., 1991). In the medial septum and hippocampus there is a reduction in the number of cholinergic neurones which may contribute to impairments in learning and memory processes (Shim *et al*., 2003). These changes to neurotransmitter systems are not permanent and can be reversed by shunting. Tashiro and Drake (1998) have demonstrated the importance of early shunt implantation, as shunting at 2 weeks appears to reverse the functional injury seen in the cholinergic, dopaminergic and noradrenergic systems. However, shunting after 2 weeks does not seem to improve function.

1.8.6. Ependyma and oedema

The loss of ependymal cells lining the ventricle appears to be a prominent pathological feature of hydrocephalus and is associated with ventricular enlargement (Go and Molenaar, 1983). In the acute stages of hydrocephalus the ependyma

becomes flattened with a reduction in cilia, followed by focal ependymal loss and eventually widespread denudation (Bruni *et al*., 1985). Stretching of the ependyma can also lead to the opening of intercellular channels allowing CSF to access the underlying parenchyma (Gopinath *et al*., 1979). Investigations in congenital animal models have demonstrated that in the HTx rat (Kiefer *et al*., 1998) and in the Hy3 mouse (Lawson and Raimondi, 1973) ventricular enlargement causes ependymal loss whereas in the hyh mouse, ependymal denudation occurs before enlargement of the ventricles (Jimenez *et al*., 2001). Transgenic mice with ciliopathies also develop hydrocephalus due to mutations in cilia causing impaired CSF flow and abnormal CSF production (Banizs *et al*., 2005).

Impairment of ventricular fluid flow, CSF outflow resistance and increased ICP cause a reduction in CSF production by the choroid plexus (Knuckey *et al*., 1993) and an increase in CSF uptake through the transependymal route (Braun *et al*., 1998). Enlargement of the ventricles causes compression of the brain parenchyma, particularity the grey matter which in turn reduces the total water content and impairs fluid diffusion (Massicotte *et al*., 2000). As white matter has a wider interstitial space and fluid moves through the intercellular spaces between ependymal, interstitial oedema develops in the brain parenchyma (Gopinath *et al*., 1979). The lack of fluid movement leads to the accumulation of toxic waste products that can affect neurotransmitter homeostasis (Del Bigio, 2004), impairment of oxidative metabolism and activation of anaerobic glycolysis (Kawamata *et al*., 2003). However, it has been show that oedema is only temporary as it subsides once ICP and CSF outflow resistance have normalised (Braun *et al*., 1997; Braun *et al*., 1998; Kondziella *et al*., 2009).

1.8.7. Periventricular white matter

Thinning of the corpus callosum is a hallmark of hydrocephalus and has been observed in both humans and hydrocephalus models. Enlargement of the ventricles causes stretching of the periventricular white matter which damages axons and myelin (Del Bigio, 2004). Increased free calcium and activity of calcium dependent proteolytic enzyme Calpain I suggests a role for calcium activated proteolysis in axonal damage (Del Bigio, 2000). It has also been shown a decrease in phospholipids and cholesterol (Higashi *et al*., 1986) which could be related to myelin damage and gliosis (Kondziella *et al*., 2008). Axonal degeneration was shown by silver staining in the sensorimotor cortex, corpus callosum, neostratium and hippocampus (Ding *et al*., 2001a). Even though there appears to be functional damage to neurones there is little evidence for neuronal cell death during hydrocephalus (Ding *et al*., 2001b, a).

1.8.8. The glial response to hydrocephalus

In hydrocephalus there is an ongoing reactive glial response which depends upon the severity of ventricular enlargement. Increases in both GFAP (a marker of astrocytes) and Iba-1 (a marker of microglia) are observed in the parietal cortex (Deren *et al*., 2010; Xu *et al*., 2012). Astroglial cells also proliferate around the ventricles and form a layer of reactive gliosis where there is a loss of ependymal cells (Del Bigio, 2004).

Astrocyte metabolism also appears to be disturbed in hydrocephalic rats in the acute phase of hydrocephalus. These changes in metabolism have been determined by less glutamine reaching glutamatergic neurones (Kondziella *et al*., 2003), an

increase in glial glutamate dehydrogenase activity (Klinge *et al*., 2002) and decreased glutamate levels in the cortex, hippocampus and thalamus (Kondziella *et al*., 2009). Due to the interplay between glia and neurones, this has a large impact on energy metabolism and signalling (Kondziella *et al*., 2008).

1.8.9. Kaolin and other neurodegenerative diseases

Hydrocephalus has been associated with a number of other neurological conditions. Kaolin injected into aged rats (12 months old) to model normal pressure hydrocephalus (NPH) results in accumulation of β-amyloid due to disruption of its clearance (Klinge *et al*., 2006) and an increase in hyperphosphorylated tau (Silverberg *et al*., 2010). These are pathological changes also seen in patients with Alzheimer's disease, further clarifying the link between the symptoms of NPH and Alzheimer's disease. Hydrocephalus patients have also been seen to have Parkinsonism-like symptoms. When the kaolin injection is combined with 6-hydroxydopamine treatment, an animal model of Parkinson's disease, the Parkinsonism-like symptoms develop earlier and are more severe (Oi *et al*., 2004).

1.8.10. Adults vs. neonates

There are a few studies that have compared the development of hydrocephalus in neonates and adult rats/mice. The general consensus is that neonatal animals tend to develop a more severe form of hydrocephalus which is accompanied by brain distortion and greater ventriculomegaly. Nevertheless, neonates appear to survive longer in comparison to adult animals (Del Bigio, 2000; Del Bigio and Enno, 2008; Lopes *et al*., 2009). The severe form seen in neonates is

more likely to lead to oligodendrocyte cell death, axonal damage but also proliferation of cells (Del Bigio and Zhang, 1998) whereas the less severe adult form appears to cause global white matter ischaemia (Del Bigio, 2000). Neonates have expandable skulls thus allowing for greater ventricular enlargement which could explain the differences in the severity of hydrocephalus (Nagra *et al*., 2008). There are also differences in cerebral metabolism which suggests that adult rats are more tolerant to hydrocephalus compared with neonatal rats (Kondziella *et al*., 2002). Balasubramaniam and Del Bigio (2002) have further highlighted the differences between the two age groups by comparing the gene profiles of neonatal and adult rats after kaolin-induced hydrocephalus. Neonatal rats appear to have altered expression in neural genes relating to neuronal morphology and synapses, in oligodendrocyte and myelin genes relating to axonal damage and in neurotrophic factors. These all indicate alterations in genes contributing to neuronal survival, development and protection. This was not seen in adult rats and could be a feature of the plasticity of neonatal hydrocephalic brains (Kondziella *et al*., 2002, Del Bigio and Enno, 2008).

1.9. Fibrosis

1.9.1. Wound healing and fibrosis

The wound healing response is similar in all tissues irrespective of the stimuli. This could be an infection, autoimmune reaction, toxin or mechanical injury. The stimulus causes epithelial and endothelial cell damage and apoptosis resulting in the initiation of the coagulation cascade and activation of platelets. Damaged epithelial/endothelial cells and activated platelets release chemo-attractant

molecules, and blood vessels become more permeable resulting in the recruitment and infiltration of monocytes and neutrophils (Wynn and Ramalingam, 2012). Neutrophils are attracted within hours of the injury followed by monocytes that mature into macrophages to phagocytose cellular debris (Stramer *et al*., 2007). Phagocytosis of dead cells cause the release of pro-inflammatory cytokines that promote inflammatory cell recruitment, however phagocytosis can also be anti-fibrotic as it clears apoptotic myofibroblasts and reduces pro-fibrotic stimuli (Wynn and Barron, 2010). Inflammatory cells also produce toxic molecules that damage the surrounding tissue and exacerbate the response (Wynn, 2008). In wound healing there is a close link between inflammation and fibrosis. Embryonic wounds do not scar as the inflammatory response is not yet established whereas adult wounds produce a lot of scar tissue and produce a robust inflammatory response as inflammation is critical for preventing infection (Stramer *et al*., 2007).

The pro-fibrotic cytokines produced by inflammatory cells activate fibroblasts, also termed myofibroblasts. Myofibroblasts not only originate from local mesenchymal cells but also from epithelial to mesenchymal transition (EMT), endothelial to mesenchymal transition (EndMT) and from fibrocytes derived from bone marrow stem cells. EMT often occurs after epithelial cell stress caused by injury. EMT is induced by cytokines often associated with fibrosis and requires proteolytic digestion of the basement membrane. It results in the loss of epithelial characteristics including polarity, cell junctions and intermediate filaments and the conversion to a more motile phenotype with the rearrangement of actin cytoskeleton and development of migratory podia (Kalluri and Neilson, 2003). Myofibroblasts are an integral part of wound healing. They contain actin microfilaments that form a local

adhesion with fibronectin in the extracellular matrix, so when myofibroblasts contract there is also contraction of the ECM. Contraction is stabilised by the deposition of ECM and the formation of granulation tissue. In normal healing wounds, the wound contracts so that the edges meet, epithelial cells repopulate the tissue and the myofibroblasts become apoptotic and are removed by phagocytosis (Gabbiani *et al.*, 2003; Porter, 2007).

If the inflammatory response is persistent or recurrent it leads to the simultaneous occurrence of inflammation, tissue modelling and repair leading to fibrosis (Wynn. 2008). Fibrosis is the excessive accumulation of ECM molecules such as collagen, fibronectin and laminin.

1.9.2. Fibrosis and hydrocephalus

It is well recognised that post-haemorrhagic communicating hydrocephalus is caused by blockage of CSF absorption pathways by proliferation of leptomeningeal cells and fibrosis at the site of arachnoid granulations (Motohashi *et al.*, 1995a; Massicotte and Del Bigio, 1999), and narrowing of the subarachnoid space by fibrosis leading to a disturbance in CSF flow. Collagen deposition is observed in the subarachnoid space of experimental hydrocephalus models (Suzuki *et al.*, 1977; Sajanti *et al.*, 1999; Moinuddin and Tada, 2000; Slobodian *et al.*, 2007) and has been associated with an increase in collagen turnover measured by prolyl 4-hydroxylase activity (Sajanti *et al.*, 1999), carboxyterminal propeptide of type I procollagen (Heep *et al.*, 2002) and aminoterminal propeptide of type III procollagen levels in the CSF (Sajanti and Majamaa, 1999; Sajanti *et al.*, 2000, 2001)

1.10. TGF-β1

TGF-βs are multifunctional cytokines involved in proliferation, adhesion, motility, apoptosis and differentiation. TGF-β signalling is cell type and context dependent and therefore produces a wide range of contradictory effects.

1.10.1. TGF-β1 signalling pathway

TGF-β initiates intracellular signalling by binding to TGF-β receptor II (RII) causing it to complex with TGF-β receptor I (RI). TGF-βRII activates TGF-βRI by phosphorylation allowing it to bind to the receptor activated smads; Smad2 and Smad3. TGF-βRI then phosphorylates Smad2/3 at the carboxyl terminus causing them to be released, thus allowing them to form a complex with Smad4 that translocates to the nucleus (Wells, 2000; Lan, 2011; **Fig. 1.7)**. Smads have a low affinity for DNA and thus require the cooperation transcription factors including both co-repressors and coactivators to regulate gene transcription (Schilling *et al*, 2008).

In addition to TGF-β signalling through the Smad pathway it has also been demonstrated that TGF-β signals through various other pathways mediated by mitogen activated protein kinases (MAPKs) and Rho GTPases (Zhang, 2010). TGF-β activation of the MAPKs; extracellular signal related kinase (Erk), c-jun amino terminal kinase (JNK) and p38, can affect cell growth, apoptosis, ECM production and EMT transition (Hartsough and Mulder, 1997; Hocevar *et al*., 1999; Yu *et al*., 2002). TGF-β signalling through the RhoA, a Rho-like GTPase, is involved in EMT and regulates stress fibre acquisition and the conversion to a more fibroblastic morphology (Bhowmick *et al*., 2001).

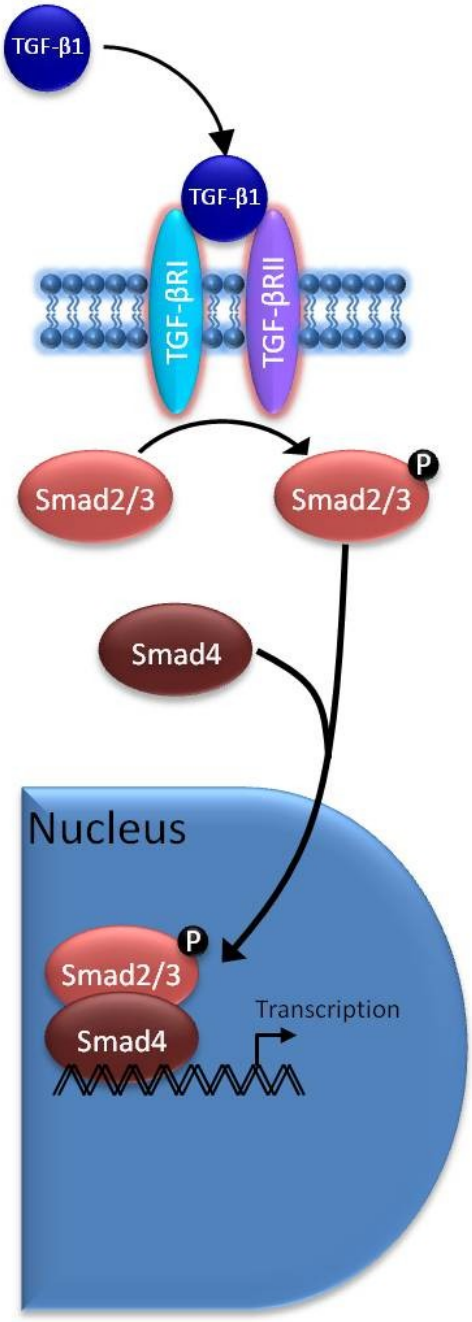

Figure 1.7. The TGF-β/Smad signalling pathway. TGF-β binds to its receptors, TGF-β receptor I (TGF-βR1) and receptor II (TGF-βRII). This leads to activation of the receptors and subsequent phosphorylation of the receptor activated the Smads; Smad2 and Smad3. Phosphorylated Smad2/3 then forms a complex with Smad4 and translocates to the nucleus where it facilitates the transcription of TGF-β related genes.

1.10.2. Regulation of TGF-β signalling

The tightly regulated TGF-β signalling pathway allows for the various different responses to TGF-β. The first site of regulation is at the point of synthesis. TGF-β is produced as an inactive form bound to the latency associated protein (LAP). In order to become active TGF-β has to be dissociated from LAP before it can bind to TGF-βRII, and is cleaved by proteases such as plasmin, thrombospondin 1, integrin αVβ6 and free radicals. This process allows for its temporal and spatial control. For example, during inflammation an increase in integrin β6 causes an increase in the activation of TGF-β (Munger *et al.*, 1999).

Signalling can also be altered by recruiting different types of TGF-β RI. In endothelial cells, the recruitment of the activin receptor-like kinase (ALK)-5 leads to the activation of the Smad2/3 pathway and causes inhibition of proliferation and migration, and so TGF-β is anti-angiogenic. On the other hand the recruitment of ALK-1 which requires higher concentrations of TGF-β, activates the Smad1/5/8 pathway leading to proliferation and migration, resulting in TGF-β being angiogenic. This paradoxical activity demonstrates how slight changes in the TGF-β signalling can have opposing effects (Goumans *et al.,* 2002).

Other signalling pathways can influence the smad pathway, for example MAPK can phosphorylate smad2/3 in a different area to the carboxyl terminus leading to impaired nuclear accumulation (Kretzschmar *et al.,* 1999). The Smad-signalling pathway is essential for inducing endogenous cytokine production and also activation of ECM gene expression by TGF-β and therefore is important in the induction of fibrosis (Verrecchia and Mauviel, 2002). However the induction of ECM genes also requires the cooperation of other pathways. This is demonstrated with the

induction of connective tissue growth factor (CTGF) by TGF-β which requires both smad and ras/mek/erk signalling (Chen *et al.*, 2002). The MAPK pathways can produce transcription factors that cooperate with the smads to affect gene transcription (Zhang, 2009). Having different pathways cooperating together, producing transcription factors that can be synergistic with other pathways allows for a greater specificity of gene regulation (Schilling *et al.*, 2008).

1.10.3. TGF-β and wound healing

TGF-β1 is involved in all processes of wound healing including inflammation, EMT and fibrosis and has demonstrated both anti- and pro- inflammatory and fibrotic effects. Consequently due to its key roles in various aspects of fibrosis, excessive TGF-β signalling has been implicated in fibrotic disorders in the kidney, liver, lung, skin and systemic conditions (reviewed in Bottinger, 2008).

TGF-β is chemo-attractive for a multitude of inflammatory cells including monocytes, macrophages, neutrophils and mast cells. The monocytes that are recruited to the site of injury are also activated by TGF-β causing them to produce key inflammatory cytokines in addition to inducing its own expression (Wahl *et al*., 1989). Once monocytes mature into macrophages they lessen the response to TGF-β1 due to the downregulation of receptors (Wahl *et al*., 1987). However these cells do continue to produce TGF-β1 which in turn influences other cell types such as fibroblasts. The anti-inflammatory actions of TGF-β1 also relates to its influence on T cells. TGF-β1 is able to inhibit natural killer and cytotoxic T cells while promoting regulatory T cell and effector 17 T cell differentiation (Yang *et al*., 2010). In addition regulatory T cells produce TGF-β1 to mediate immune suppression (Taylor, 2009).

TGF-β1 is chemotactic for fibroblasts, induces EMT and also plays a key role in the differentiation of fibroblasts into myofibroblasts (Kalluri *et al*., 2003; Bottinger, 2010). TGF-β1 is also involved in inducing the production of extracellular matrix proteins such as collagen and fibronectin, and affects matrix degradation by reducing the expression of proteases such as matrix metalloproteinases (MMPs), and increasing the expression of protease inhibitors including tissue inhibitors of metalloproteinases (TIMPs; Verrecchia and Mauviel, 2002).

1.10.4. TGF-β and the brain

There are low levels of TGF-β1 in the CSF and brain parenchyma of healthy humans (Mogi *et al*., 1995; Krupinski *et al*., 1996; Flood *et al*., 2001) and rats (Unsicker *et al*., 1991). After central nervous system injury, TGF-β1 levels are increased around the lesion site, particularity in astrocytes (Logan *et al*., 1992). TGF-β1 prevents astrocytes from proliferating and alternatively induces hypertrophy and migration of astrocytes, encouraging them to produce ECM (Unsicker *et al*., 1991; Morganti-Kossmann *et al.,* 1992). In response to pro-inflammatory molecules microglial cells produce TGF-β1. In turn TGF-β1 affects microglial cells by reducing their activation, suppressing the release of pro-inflammatory cytokines, reducing their proliferation and also inducing apoptosis (Bottner *et al.,* 2000; Lui *et al*., 2011).

1.10.5. TGF-β and hydrocephalus

Several lines of evidence implicate TGF-β1 in the development of post-haemorrhagic hydrocephalus. Patients with SAH who go on to develop post-haemorrhagic hydrocephalus have higher levels of TGF-β1 and β2 in their CSF

compared to those patients with SAH who don't develop hydrocephalus (Kitazawa and Tada, 1994; Flood *et al*., 2001; Douglas *et al*., 2009). The hypothesis is that in SAH, blood enters the subarachnoid space and TGF-β1 is released by activated platelets (Assoian *et al*., 1983) into the CSF. TGF-β1 then induces its own expression in cells of the meninges and choroid plexus, resulting in a second increase in TGF-β1 in CSF (Flood *et al*., 2001). It promotes the growth and proliferation of cells such as leptomeningeal cells and increases their production and deposition of extracellular matrix which ultimately obstructs CSF absorption sites leading to the development of hydrocephalus (Motohashi *et al*., 1995; Massicotte and Del Bigio, 1999).

Experimental studies in models of hydrocephalus have also implicated TGF-β1 in the development of hydrocephalus. Overexpression of TGF-β1 specifically in the CNS of transgenic mice (Galbreath *et al*., 1995; Wyss-Coray, *et al*.,1995) and an intrathecal injection of human recombinant TGF-β1 into neonatal mice (Tada *et al*., 1994; Kanaji *et al*., 1997), lead to the development of hydrocephalus. The latter model also showed increased fibrosis and proliferation of meningeal cells resulting in disturbed CSF flow (Moinuddin and Tada, 2000) and the hydrocephalus could be prevented by injecting a TGF-β1 antibody (Kanaji *et al*., 1997). In a kaolin induced mouse model of hydrocephalus most macrophages in the subarachnoid space and the choroid plexus were TGF-β1 positive (Hatta *et al*., 2006). These studies together suggest a role for TGF-β1 in the development of hydrocephalus, possibly due to its effects on promoting fibrosis.

1.11. Decorin

Decorin is a small leucine rich chondroitin-dermatan sulphate proteoglycan (CSPG). As the name suggests Decorin is composed of a protein core that contains leucine rich repeats and has a glycosaminoglycan side chain of either chondroitin sulphate or dermatan sulphate. Decorin's curved shaped is attributed to the leucine rich repeats. Proteins that contain leucine rich repeats appear to be involved in protein-protein interactions (Kobe and Deisenhofer, 1995). Initially, Decorin's role was first associated with the organisation of collagen fibril formation and maintenance during development and repair due to its binding properties to fibrillar collagens such as type I, II, V, VI and XIV. Decorin is found in tissues rich in these collagens such as the heart and lungs (Brown and Vogel, 1989; Hocking *et al.*, 1998). From knockout studies it has been demonstrated that a lack of Decorin causes abnormal formation of the collagen fibril network in the skin with collagen fibrils of different shapes and sizes leading to reduced strength (Danielson *et al*., 1997). Since then Decorin has been shown to bind to a variety of different bioactive molecules all of which allows it to influence diverse cellular functions including protein synthesis, cell proliferation and inflammation. When considering the actions of Decorin it is important to realise that due to its diverse interactions it may lead to different responses in different situations (e.g. normal tissue vs. cancerous tissue).

1.11.1. Decorin and TGF-β

Yamaguchi *et al*. (1990) first demonstrated that Decorin binds to TGF-β and sequesters it into the ECM thus preventing it from interacting with its receptors **(Fig. 1.8)**. Although in some particular circumstances Decorin binding to TGF-β enhances

growth factor activity (Takeuchi *et al*., 1994), inhibition of TGF-β activity after Decorin binding is more widely reported. TGF-β has also been demonstrated to induce Decorin expression (Border *et al.,* 1990) therefore it is hypothesised that it acts as a negative-feedback regulator of TGF-β activity. However, in fibroblasts from the skin (Breuer *et al*, 1990; Kahari *et al*, 1991), lung (Romaris *et al*, 1991), cornea (Brown *et al*, 1999), arterial smooth muscle cells (Schonherr *et al*., 1993) and human endothelial cells (Nelmarkka *et al*., 1997), TGF-β1 either had no impact or reduced Decorin expression. Therefore, in wound healing, the lack of Decorin expression could lead to aberrant TGF-β signalling and the formation of fibrosis. Increased levels of TGF-β1 and reduction in Decorin expression have been demonstrated in fibroblasts from hypertrophic scar tissue (Scott *et al.*, 1998), myofibroblasts from liver fibrogenesis (Meyer *et al.,* 1992) and bleomycin induced pulmonary fibrosis (Westergren-Thorsson *et al.,*1993).

The antagonistic activity of Decorin has implicated it as an anti-fibrotic agent. In skin wounds, inhibition of TGF-β1 by Decorin leads to inhibition of fibroblast proliferation and reduction in collagen synthesis (Zhang *et al*., 2007). Also Decorin is able to delay wound contraction which is thought to be beneficial in reducing scar and promoting regeneration (Shafritz *et al*., 1994). Decorin reduces fibrosis in cardiac allografts causing reduced allograft rejection, and reduces hypertension induced cardiac fibrosis leading to improved cardiac function (Faust *et al*., 2009; Yan *et al*., 2009). There is also evidence that Decorin may be involved in reversing cardiac remodelling through its inhibition of TGF-β1 (Jahanyar *et al*., 2007). In models of pulmonary fibrosis increasing Decorin levels suppresses TGF-β1 inhibition of lung morphogenesis (Zhao *et al*., 1999), reduces neutrophil infiltration (Giri *et al*, 1997)

and reduces the fibrogenic response (Kolb *et al*., 2001). In models of renal fibrosis including glomerulonephritis (Noble *et al*., 1992; Border *et al*., 1992), and in diabetic nephropathy (Wu *et al*., 2007), Decorin suppresses TGF-β1 induced ECM deposition. Decorin reduces scarring in eye pathologies including glaucoma and proliferative vitreoretinopathy (Grisanti *et al*., 2005; Nassar *et al*., 2011). Decorin also has beneficial effects after muscle injury by promoting the differentiation of myoblasts into myotubes instead of myofibroblasts thus reducing fibrous scar formation in addition to promoting muscle regeneration by inhibiting TGF-β and myostatin (Li *et al*., 2004, 2007).

TGF-β is also involved in inflammation and EMT and inhibition of TGF-β by Decorin has been shown to reduce the number of OX42/ED1 positive microglia (Engel *et al*., 1999), to increase activation of macrophages (Comalada *et al*., 2003) and to prevent the transformation of fibroblasts into myofibroblasts (Mohan *et al*., 2010). Accordingly, in CNS lesions, Decorin reduces the deposition of chondroitin sulphate proteoglycans, fibronectin and laminin, and suppresses astrocytic, microglial and macrophage reactions in and around the wound (Logan *et al*., 1999a; Davies *et al*., 2004). Similarly, immuno-neutralisation of TGF-β2 suppresses inflammation and scarring in brain lesions (Logan *et al*., 1999b). All together, these findings suggest that Decorin could be a potential therapeutic for inhibiting TGF-β-induced post-haemorrhagic fibrosis.

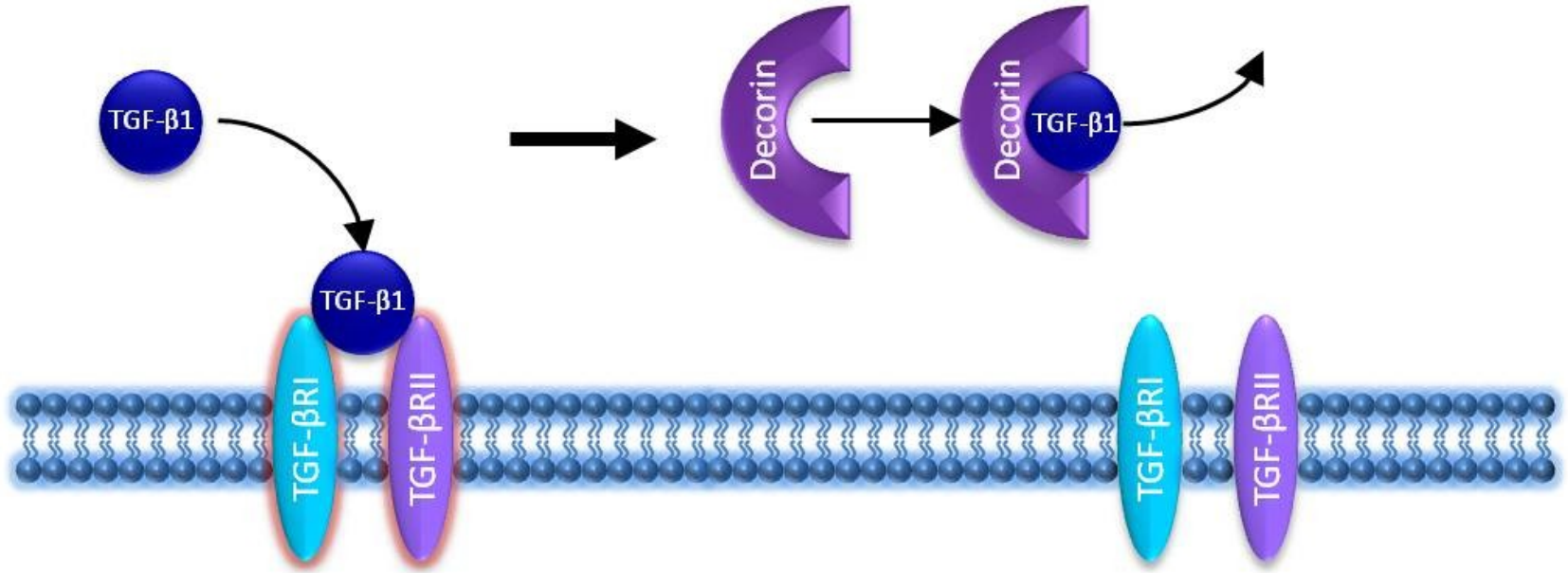

Figure 1.8. Inhibition of TGF-β1 by Decorin. Decorin Binds to TGF-β1, sequestering it into the extracellular matrix so that it is unable to bind to its receptors; TGF-β receptor I (TGF-βR1) and receptor II (TGF-βRII).

1.11.2. Decorin and the tyrosine kinase receptors

Decorin's involvement in signalling through the receptor tyrosine kinases (RTKs) was first identified when it was observed that Decorin arrested cell growth in squamous carcinoma cells through its affects on epidermal growth factor receptor (EGFR; De Luca *et al*., 1996).

The EGF pathway is involved in cell proliferation, survival, angiogenesis, adhesion, migration/invasion and differentiation and therefore Decorin has been implicated as an anti-tumour agent. It has been shown that Decorin binds directly to the EGFR causing dimerisation of the receptor and activation of its signalling pathway (Moscatello *et al.*, 1998, Iozzo *et al.*, 1999). However this is only transient and is rapidly followed by internalisation of EGFR by caveolar mediated endocytosis and subsequent degradation by lysosomes (Csordás *et al.*, 2000; Zhu *et al.*, 2005). Inhibiting the EGF pathway leads to production of the cyclin dependent kinase inhibitor p21 that leads to growth arrest at the G1 phase of the cell cycle (Moscatello *et al*., 1998).

Decorin also affects other members of the Erb family including ErbB2 and ErbB2. In breast carcinoma cells that lack EGFR but overexpress ErbB2, Decorin first causes transient activation of ErbB2 followed by its prolonged downregulation resulting in growth suppression and reduced metastasis (Reed *et al.*, 2005; Goldoni *et al.*, 2008). The initial activation also signals through the RhoA pathway to induce thrombospondin-1 which results in Decorin inhibiting tumour angiogenesis in breast carcinoma cells (Neill *et al.*, 2013). PCR array data also demonstrates that in carcinoma cells Decorin upregulates anti-angiogenic genes and downregulates pro-angiogenic genes (Neill *et*

al., 2012). However, in osteosarcoma cells that overexpress continually phosphorylated EGFR Decorin had no effect on growth suppression (Zafiropoulos *et al.*, 2008).

The hepatocyte growth factor receptor known as the met receptor is involved in tumour transformation, invasion and metastasis (Goldoni *et al*., 2009). In squamous and breast carcinoma cells Decorin binds to the Met receptor causing an initial activation followed by internal degradation of Met through E3 ubiquitin Ligase C. This causes attenuation of β-catenin levels leading to degradation of Myc, which was shown to reduce cell growth and suppress migration (Goldoni *et al.*, 2009; Buraschi *et al.*, 2010). Also by inhibiting the Met receptor, Decorin causes a reduction in VEGF and HIF1α, increased TIMP-1 and suppression of MMP2 and 9 leading to suppression of tumour angiogenesis (Neill *et al.*, 2012).

There is not extensive research into Decorin's effects on TKRs in normal tissue. A study by Santra *et al*. (2008) investigating the effects of Decorin on mouse cerebral endothelial cells demonstrated the activation of EGFR signalling through ERK1/2 and PI3K pathways lead to an increase in VEGF. This in turn increased the protein levels of plasminogen and plasmin and reduced the activity of MMP2 and 9 thus leading to the promotion of angiogenesis. The results from this study appear to be contradictory to its effects in tumour environments.

1.11.3. Other effects of Decorin

Decorin acts as a cell adhesion modulator and is able to inhibit cell attachment *in vitro* by binding to fibronectin (Bidanset *et al*., 1992) and thrombospondin (Winnemoller *et al*., 1992). Decorin is able to increase the inhibition of thrombin by heparin sulphate II

and therefore could affect the coagulation of blood (Whinna *et al*., 1993). It also binds to C1q, inhibiting the C1 complex which is part of the classical complement pathway, and could consequently affect the innate immune response (Krumdieck *et al*., 1992).

1.12. Hypothesis and aims

1.12.1. Hypothesis

Post-haemorrhagic hydrocephalus develops due to inflammation-induced fibrosis in the subarachnoid space that obstructs CSF drainage. The inflammatory cytokine TGF-β1 plays a significant role in the development of fibrosis through promoting ECM deposition, as well as preventing the degradation of fibrosis through inhibition of proteases. Several lines of evidence implicate TGF-β1 in the development of post-haemorrhagic hydrocephalus, including: (i) CSF levels of TGF-β1 are higher in post-haemorrhagic hydrocephalus patients compared with the levels recorded in patients with both non-haemorrhagic hydrocephalus and haemorrhage without hydrocephalus (Kitazawa and Tada, 1994; Whitelaw *et al*., 1999; Flood *et al*., 2001; Douglas *et al*., 2009); (ii) ventriculomegaly is positively correlated with the intensity of TGF-β1 immunostaining in experimental neonatal post-haemorrhagic hydrocephalus (Cherian *et al*., 2004); and (iii) hydrocephalus develops both in transgenic mice overexpressing TGF-β1 in astrocytes (Galbreath *et al*., 1995) and after intrathecal injection of human recombinant TGF-β1 (Tada *et al*., 1994; Kanaji *et al*., 1997).

Therefore, it was hypothesised that if post-haemorrhagic communicating hydrocephalus is caused by TGF-β-induced subarachnoid fibrosis, then Decorin, a TGF-

β antagonist, would be beneficial as a therapeutic agent by preventing the development of subarachnoid fibrosis and subsequently the development of hydrocephalus, and, by degrading subarachnoid fibrosis leading to the resolution of established hydrocephalus.

1.12.2. Aims

a) To generate an *in vitro* model of rat meningeal fibroblasts to assess the effects of human recombinant Decorin on TGF-β1-induced meningeal fibrogenesis.
b) To develop a reliable *in vivo* rat model of communicating hydrocephalus and determine the changes in endogenous TGF-β1 in the model.
c) To assess the ability of human recombinant Decorin to prevent subarachnoid fibrosis and the development of hydrocephalus in the model of communicating hydrocephalus developed in b).
d) To assess the ability of human recombinant Decorin to degrade subarachnoid fibrosis and resolve established hydrocephalus.

Chapter 2

Materials and Methods

Unless otherwise stated reagents were obtained from Sigma-Aldrich, Poole, UK.

2.1. In Vitro methods (Chapter 3)

2.1.1. Isolation and culture of rat meningeal fibroblasts

Adult Sprague Dawley rats (weight ~ 200g) were killed in a rising CO_2 chamber and the heads removed and put on ice. The top of the skull was carefully removed and the meninges peeled off the top of the brain and the base of the skull once the brain was removed. Meningeal tissue was placed in Dulbecco's modified eagle medium (DMEM; Life Technologies, Paisley, UK) on ice and unwanted brain tissue or bone fragments were removed. The meningeal tissue was cut into $1mm^2$ pieces, transferred to a mini petri dish with DMEM supplemented with 100U/ml (1%) penicillin-streptomycin (pen-strep; Life Technologies), containing dispase I (2.5U/ml; Life Technologies) and collagenase (200U/ml), and incubated for 2 hours at 37°C in a humidified 5% CO_2 chamber. The reaction was stopped by adding Complete Medium (DMEM, 1% pen-strep and 10% foetal bovine serum; FBS) and the tissue was gently triturated. The meningeal tissue was transferred to a 15ml falcon tube (Sarstedt, Leicester, UK) and centrifuged for 5 minutes at 1,500 rpm. After removing the supernatant the cells were resuspended in Complete Medium and seeded in 2 wells of a 6 well tissue culture plate (BD Biosciences, Oxford, UK).

2.1.2. Passaging of cells

When the meningeal cell culture had reached confluency the cells were washed in sterile 10mM phosphate buffered saline pH 7.4 (PBS) and incubated in 2% Trypsin-EDTA (Life Technologies) at 37°C in a humidified 5% CO_2 chamber for 5 minutes or until the cells had detached. Complete Medium was then added and the cell suspension was transferred to a 15ml falcon tube and centrifuged for 5 minutes at 1,200 rpm. After removing the supernatant the cells were resuspended in Complete Medium and seeded in 25, 75 or 175 cm^2 vented flasks (Sarstedt).

2.1.3. TGF-β1 and Decorin bioassay

Rat meningeal fibroblasts were seeded onto 6 well tissue culture plates in Complete Medium at a density of 80,000-100,000 cells per well, and incubated at 37^0C in a humidified 5% CO_2 chamber for 48 hours. The medium was then removed and replaced with serum free medium (DMEM, 1% pen-strep) and incubated for a further 24 hours. The cells were treated with 10, 25 or 50ng/ml human recombinant TGF-β1 (PeproTech Inc, NJ, USA) and/or 20µg/ml non-cGMP (current good manufacturing practice) purified Decorin (Galacorin™, Catalent, Pharma Solutions, NJ, USA), and incubated for 48 hours. The cells were then washed in PBS, scraped from the dish and centrifuged for 5 minutes at 1,500 rpm. The supernatant was removed, the cell pellet incubated on ice for 30 minutes with ice-cold lysis buffer (20mM Tris-HCl pH 7.4, 150mM NaCl, 1mM EDTA, 0.5mM EGTA, 0.1% NP-40) containing 5µg/ml protease inhibitor cocktail, and then centrifuged for 30 minutes at 13,000 rpm at 4°C. The supernatant was removed and stored at -80°C.

2.2. Western blot (Chapter 3)

2.2.1. Principles

Western blotting is used to identify specific proteins based on their molecular weight characteristics and using the specificity of antigen-antibody interactions. It is a semi-quantitative technique that allows differences in protein levels and isoforms to be identified between treatment groups. An electric current is used to separate proteins captured in a gel, with separation based on their size/charge, the separated proteins in the gel are then transferred to a nitrocellulose or polyvinylidene fluoride (PVDF) membrane ready for detection. The membrane is incubated with a primary antibody which binds to the specific protein of interest. A secondary antibody linked to horseradish peroxidase (HRP) binds to the primary antibody. The HRP catalyses the oxidation of luminol emitting light, as it decays. This reaction can then be caught on photographic film **(Fig. 2.1)**. The intensity of the light emitted is proportional to the amount of protein present in the band of interest.

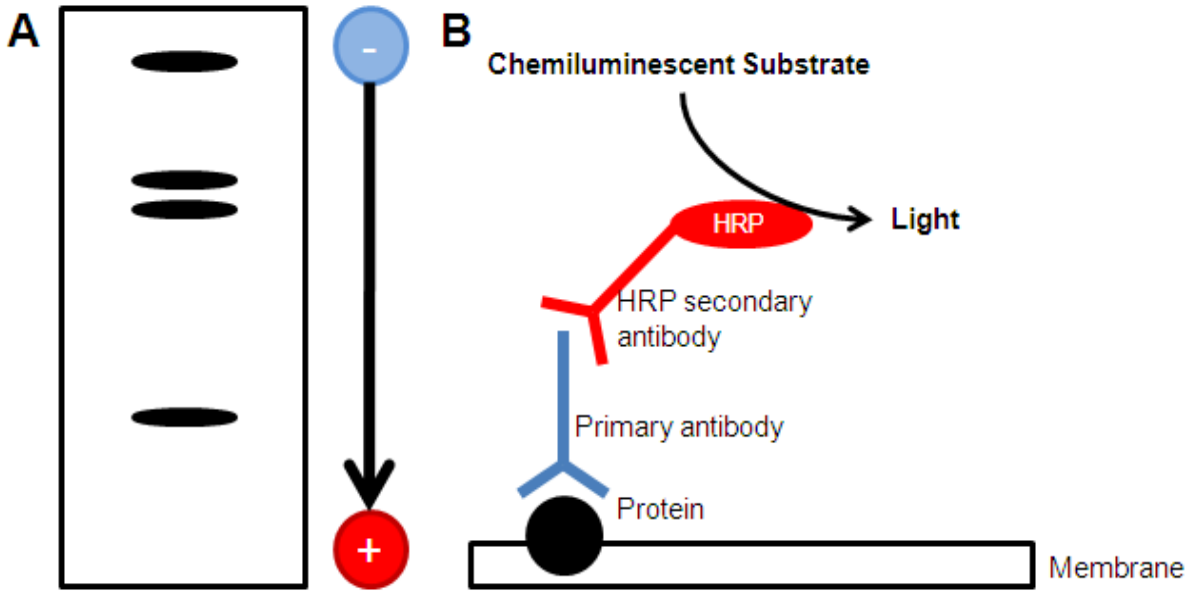

Figure 2.1. Principles of western blotting. (A) An electric current separates proteins along the gel according to their molecular weight. **(B)** Primary antibodies are used to bind to the protein of interest that has been transferred to a membrane, which is subsequently detected by a horseradish peroxidase (HRP) linked secondary antibody. HRP catalyses the oxidation of the chemiluminescent substrate, which subsequently decays and emits light. The intensity of light is proportional to the amount of the protein.

2.2.2. Polyacrylamide gel electrophoresis

8% Tris-glycine sodium dodecyl sulphate (SDS)-polyacrylamide gel electrophoresis (PAGE) gels were prepared comprising stacking and resolving gels **(Table 2.1)**. The cell lysate samples were defrosted on ice and equal amounts of protein (determined by BioRad protein Assay) the cell lysate was added to the 2X loading buffer (4% SDS, 20% glycerol, 2% 2-mercaptoethanol, 0.004% bromophenol blue and 0.125M Tris-HCl pH 6.8) and placed on a heat block at 90°C for 4 minutes to denature the protein. Proteins were separated by electrophoresis using a XCell SureLock™ system (Life Technologies) at 125V for 2 hours.

	Stacking Gel	8% Resolving Gel
Protogel™ (40% Acrylamide 0.8% Bisacrylamide Stabilised Solution; National diagnostics)	0.4ml	1.83ml
0.5M Tris/Cl pH 6.8	1.85ml	-
1.5M Tris/Cl pH 8.8	-	1.65ml
Distilled water	0.75ml	3.12ml
10% SDS	30µl	66µl
10% APS (ammonium persulfate)	15µl	23.1µl
TEMED (Tetramethylethylenediamine)	7.5µl	9.9µl

Table 2.1. SDS PAGE Gel composition. Amounts of each component used to make up the stacking and the 8% resolving gels.

2.2.3. Protein transfer and detection

An Immobilon-P PVDF membrane (Millipore, Watford, UK) was activated with 100% methanol (Fisher Scientific, Leicestershire, UK) and the proteins were electrophoretically transferred to the activated PVDF membrane over 2 hours at 25V using an XCell II^{TM} blot module (Life Technologies). After washing in TBST (0.12% Tris-base, 0.88% NaCl, pH 7.4, 0.05% Tween20), the membrane was incubated in blocking buffer (TBST, 5% dried skimmed milk; Marvel, Lincolnshire, UK) for 1 hour at room temperature. It was then incubated with primary antibody solution (TBST, 5% dried skimmed milk) on a tilting platform overnight at 4°C. The membrane was washed in TBST before being incubated with secondary HRP conjugated antibody solution (TBST, 5% dried skimmed milk) for 1hr at room temperature.

Immunoreactive protein bands were detected using an enhanced chemiluminescence (ECL) solution according to the manufacturer's protocol (GE Healthcare, Buckinghamshire, UK). Briefly, the membrane was covered with equal quantities of ECL detection reagent 1 and 2 and incubated for 1 minute before being placed in a cassette and exposured to Biomax Light film (Kodak, NY, USA). In order to detect other proteins of interest, the membrane was stripped and re-probed. Membranes were placed in stripping buffer (100mM glycine pH 2.9) for 30 minutes at room temperature before repeating the procedure outlined previously for the detection of proteins.

2.3. *In Vivo* Methods

2.3.1. Experimental animals

Adult male Sprague-Dawley rats (~250g; Charles River, Margate, UK) were housed in groups of 4 for experiments conducted in Chapter 3. Three week old Sprague-Dawley rats (~50g; Charles River, Massachusetts, USA and Margate, UK) were housed in litters in individual cages for experiments conducted in Chapters 4, 5 and 6. The rats were kept under a 12 hour light/dark cycle with free access to food and water. Animals were monitored daily for adverse effects of treatments, such as distress, lethargy, weight loss and seizures, and any animals showing severe adverse effects were euthanised. All efforts were made to minimise post-surgery discomfort and the number of animals used. The experiments conducted at the University of Birmingham were in accordance with the Animals and Scientific Procedures Act 1986, licensed by the UK Home Office (Home Office Project Licence PPL 30.2720) and approved by the University of Birmingham Ethics Committee, Those conducted at the University of Utah were carried out in accordance with the guidelines of the National Institutes of Health Care and Use of Laboratory Animals and procedures were approved by the University of Utah Ethics Committee.

2.3.2. Injection of kaolin into the prechiasmatic cistern (Chapter 3)

Rats were anaesthetised with 5% isoflurane (National Veterinary Supplies, Stoke, UK), maintained at 2-3% isoflurane and given a subcutaneous injection of Buprenorphine (National Veterinary Supplies). The head was shaved before the rat was

placed in the stereotactic apparatus (David Kopf Instruments, California, USA). A scalpel was used to make an incision along the midline on the top of the skull so that Bregma was revealed and marked. A Hamilton syringe was placed in the stereotactic frame and tilted 30° in the sagittal plane. The needle tip was placed 8mm anterior from Bregma and slightly lateral (to avoid hitting any major blood vessels) and the position on the cranium was marked. A dental drill was used to drill a burr hole through the cranium at this position. The needle was repositioned over the burr hole and slowly advanced until resistance was felt from the base of the skull (10mm from the surface of the brain; **Fig. 2.2.A)**. At this point 50µl of 25% Kaolin solution (250mg/ml; Fisher Scientific) in 0.9% sterile saline was slowly injected, and the needle withdrawn after being left in place for 1 minute after the injection. Control animals received 50µl sterile 0.9% saline solution. The skin was then sutured and the rat allowed to recover.

2.3.3. Injection of kaolin into the basal cisterns (Chapters 3, 4, 5 and 6)

The method of basal cistern injection of kaolin was described by Li *et al*. (2008) and used in several subsequent studies (Wagshul *et al.*, 2009, Nagra *et al.*, 2010, Rashid *et al.*, 2012). Rats were anaesthetised with 5% isoflurane, maintained at 2-3% and either given a subcutaneous injection of Buprenorphine (Chapters 3, 5 and 6) or Carprofen tablets (Chapter 4). Using aseptic techniques, the skin was incised along the ventral midline of the neck and the muscles mobilised to expose the atlanto-occipital membrane, the membrane between the occipital bone and the C1 vertebrae. A 30 gauge needle, angled at 30-45° was used to first puncture the membrane allowing CSF to leak out before being inserted into the subarachnoid space **(Fig. 2.2.B-F)**. The needle

was then advanced 1-2mm under the occipital bone and 30µl of 20% kaolin solution (200mg/ml; Fisher Scientific) in 0.9% sterile saline was injected over a period of 15 seconds. The skin was sutured and the rats were either allowed to recover or transferred to a stereotactic frame (David Kopf Instruments) for osmotic pump and intraventricular cannula implantations.

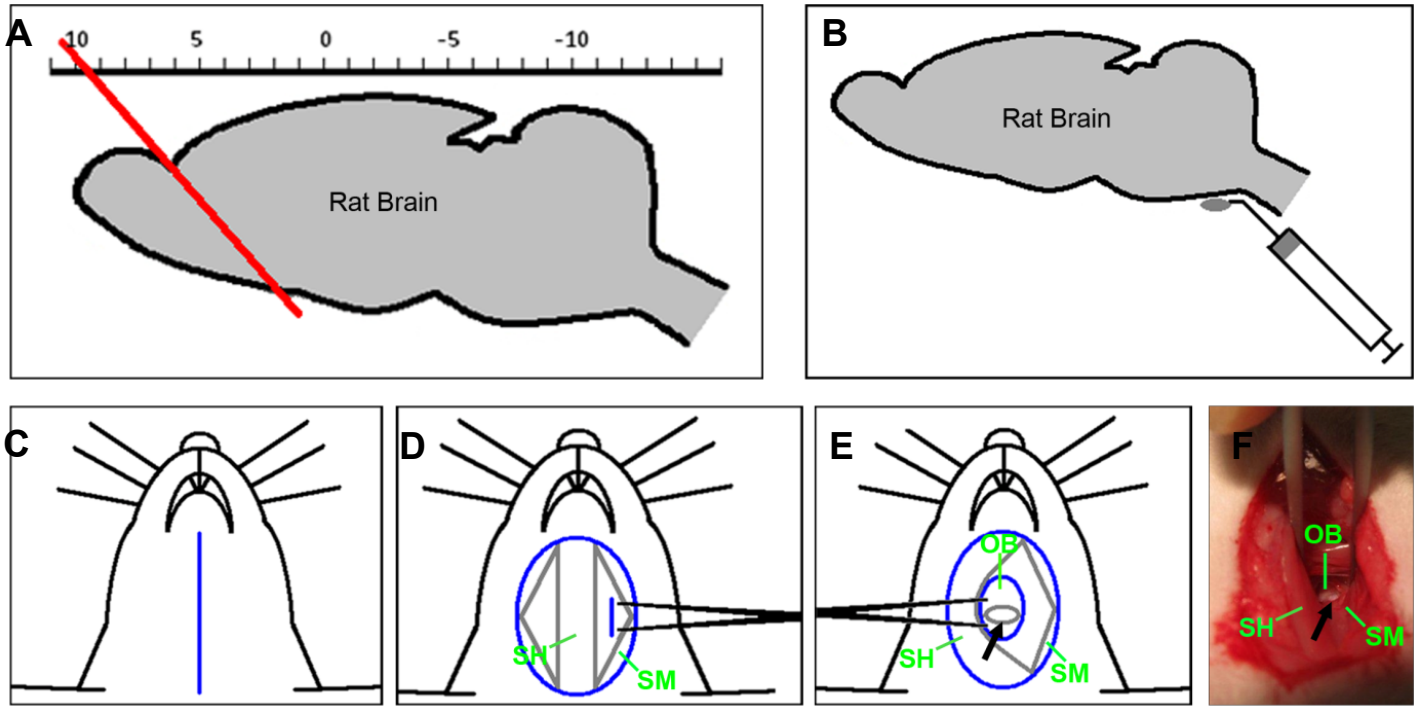

Figure 2.2. Diagrams explaining the *in vivo* models of hydrocephalus. (A) In the prechiasmatic cistern model, kaolin was injected using a needle angled at 30º through the brain to access the cistern. **(B)** In the basal cisterns model, kaolin was injected using an angled needle through the atlanto-occipital membrane. For the basal cistern approach, first an incision was made along the ventral midline of the neck **(C)** and forceps were used to blunt dissect the muscles apart to expose the atlanto-occipital membrane **(D)**. An angled needle was then used to inject kaolin through the membrane and into the basal cisterns (black arrow; **E)**. **(F)** Photo demonstrating the surgical approach. OB – occipital bone, SH – sternohyoid muscle, SM – sternomastoid muscle.

2.3.4. Implantation of the osmotic mini pump and brain cannula (Chapters 4, 5 and 6)

Osmotic pumps (model 2002, Alzet, Durect Corporation, California, USA) were prepared under sterile conditions. Pumps were adapted for MRI by replacing the metal flow moderator with PEEK tubing and using a customised 5mm long PEEK brain cannula (Plastics 1, Virginia, USA) attached to the pedestal. The catheter tubing was attached to the brain cannula and then in addition to the pumps, was filled with either 5mg/ml human recombinant Decorin (Galacorin™, Catalent, Pharma Solutions, New Jersey, USA) or PBS vehicle. The osmotic pumps were then connected to the brain cannula by the catheter tubing and primed in sterile saline overnight at 37°C to allow prompt delivery after implantation.

After fixing the heads of anaesthetised rats in a stereotactic frame, the dorsal skull was exposed and a burr hole sited in the parietal bone using co-ordinates 1mm posterior and 1.5mm lateral to Bregma. The cannula was inserted into the right lateral ventricle and fixed in place with glue and bone cement (Biomet UK Ltd, Bridgend, UK) to a stabilising screw (Plastics1) and the osmotic pump was implanted subcutaneously in the neck region **(Fig. 2.3)**. The surgical incision was sutured and the animal was allowed to recover.

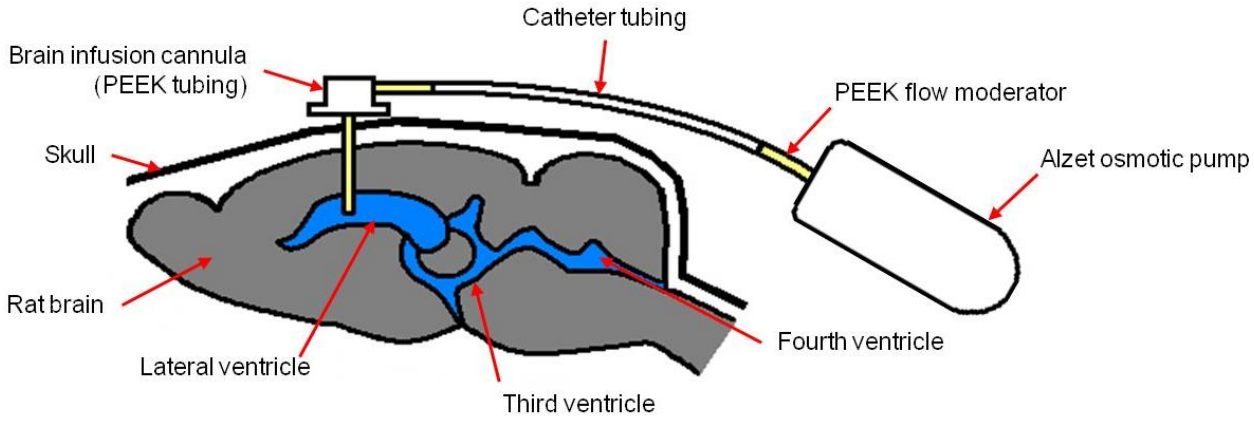

Figure 2.3. Diagram representing the osmotic mini pump implantation. The brain infusion cannula was implanted into the lateral ventricle. The pump was attached by tubing to the brain infusion cannula and implanted subcutaneously in the neck region.

2.3.5. CSF collection

For CSF removal, the rat was killed with an intraperitoneal injection of euthatol (National Veterinary Supplies) and then immediately placed in a head holder with the head fixed in a nose down position. Scissors were used to cut through the skin along the midline between the ears, and the superficial muscles were blunt dissected to expose the atlanto-occipital membrane at the back of the skull. A pulled glass micropipette made using a Flaming/Brown Micropipette puller (Sutter Instrument, California, USA), was inserted through this membrane and CSF allowed to flow out or removed gently with an attached syringe. On completion, the micropipette was slowly withdrawn, The CSF collected in eppendorf tubes and the rat perfused. The CSF was then frozen and stored at -20ºC.

2.3.6. Tissue preparation for histology

The rats were perfused transcardially with PBS followed by 4% paraformaldehyde (PFA; Alfa Aesar, Massachusetts, USA) in PBS at pH7.4. Brains were immersed in 4% PFA overnight at 4°C, cryoprotected by sequential immersion in 10%, 20% and 30% sucrose solutions in PBS at 4°C and embedded in optimum cutting temperature (OCT) embedding matrix (Fisher Scientific, Loughborough, UK).Coronal sections, 15µm thick, were cut on a Bright cryostat (Bright Instrument, Cambridgeshire, UK), placed onto Superfrost Plus slides (Thermo Scientific, Massachusetts, USA), and stored at -20°C before staining.

2.4. Immunohistochemistry and immunocytochemistry

2.4.1. Principles

Immunohistochemistry and immunocytochemistry are techniques used to identify and localise specific proteins within tissue or cell samples respectively, by exploiting the specificity of antigen-antibody interactions. Primary antibodies detect and bind to the specific protein (antigen) of interest. Secondary antibodies bind to the primary antibody as they have been raised against the animal species from which the primary antibody was generated. Secondary antibodies are usually used to amplify the signal to improve sensitivity. Two detection methods were used in this study, the indirect immunofluorescent method and the avidin-biotin complex (ABC) method. The indirect immunofluorescent method utilised secondary antibodies labelled with a fluorescent dye **(Fig. 2.4.A)**. The dye absorbs energy at a specific wavelength and emits it at a different wavelength, which can be detected using a fluorescence microscope. In the ABC method, the secondary antibody is conjugated to biotin, which binds to a preformed avidin-biotin complex containing biotin bound to HRP **(Fig. 2.4.B)**. The HRP catalyses the oxidation of added 3, 3'-diaminobenzidine (DAB) and produces a brown precipitate over the binding site that can be visualised under a light microscope.

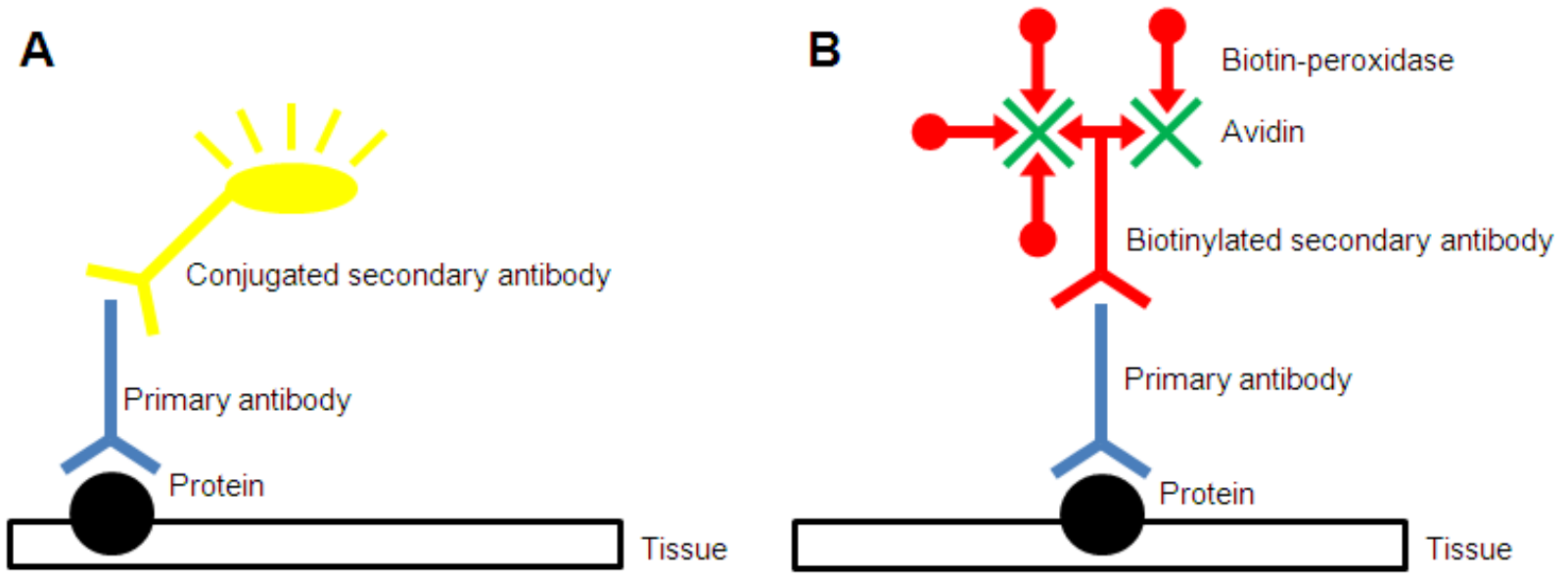

Figure 2.4. Immunohistochemistry methods. (A) Indirect immunofluorescent method. A secondary antibody conjugated to a fluorescent dye binds to the primary antibody. The dye emits a fluorescent light that can be detected using a fluorescence microscope. **(B)** Avidin-biotin complex (ABC) method. A biotinylated antibody binds to the primary antibody. This subsequently binds a preformed ABC that contains HRP. The HRP catalyses a substrate reaction which results in the precipitation of a coloured product over the binding site.

2.4.2. Immunocytochemistry

Rat meningeal fibroblasts were plated onto a chamber slide which had been pre-coated with 100µg/ml poly-D-lysine and incubated at 37°C in a humidified 5% CO_2 chamber for 48 hours until confluent. All subsequent incubations were performed at room temperature. The cells were washed in PBS then fixed in 4% PFA in PBS for 15 minutes. The cells were then washed again in PBS before non specific binding sites were blocked in PBS containing 0.3% Tween20 (PBST), 2% bovine serum albumin (BSA) and 15% normal serum (Vector Laboratories) for 10 minutes. This was followed by incubation of the cells in primary antibody solution (primary antibody in PBST with 2% BSA) for 1 hour. The cells were again washed in PBS before being incubated in secondary antibody solution (secondary antibody in PBST with 2% BSA and 1.5% normal serum) for 1 hour in the dark. Finally the cells were washed in PBS before being mounted in VectaShield mounting medium containing DAPI (Vector Laboratories, Peterborough, UK).

2.4.3. Immunofluorescence staining

Slides were removed from the freezer and allowed to thaw. A circle was drawn with a hydrophobic ImmEdge pen (Vector Laboratories) around the section and allowed to dry for 5 minutes. Sections were washed in PBST (PBS with 0.3% Tween20) before non-specific binding sites were blocked in PBST containing 2% BSA and 15% normal goat serum for 20 minutes at room temperature. Sections were then incubated in the primary antibody solution (primary antibody in PBST with 2% BSA) either at 4°C overnight or at room temperature for 1 hour. After washing in PBST, sections were

incubated with appropriate Alexa Fluor® 488 or 594 labelled secondary antibodies (Life Technologies, Paisley, UK) in secondary antibody solution (PBST with 2% BSA and 1.5% normal goat serum) for 1 hour at room temperature in the dark. Finally, sections were washed in PBST before mounting in Vectashield containing the nuclear stain DAPI (Vector Laboratories).

2.4.4. Immunoperoxidase staining

Slides were removed from the freezer and allowed to thaw. A circle was drawn with a hydrophobic ImmEdge pen (Vector Laboratories) around the section and allowed to dry for 5 minutes. The sections were washed in distilled water before being incubated with 0.3% H_2O_2 (70% methanol in PBS) for 30 minutes to inhibit endogenous peroxidase. Sections were washed in PBST before non-specific binding sites were blocked in PBST containing 2% BSA and 15% normal serum for 1 hour at room temperature, and then incubated in primary antibody solution at 4°C overnight. Sections were again washed in PBST before incubation in biotinylated secondary antibody solution (Vector Laboratories) for 30 minutes at room temperature. Sections were washed in PBST and then incubated for 30 minutes at room temperature in Avidin/Biotin Complex (ABC; Vectastain Elite ABC kit, Vector Laboratories) following the manufacturer's instructions. After rinsing in PBST, sections were treated with 3'3 diaminobenzidine (DAB) substrate (Vector Laboratories), washed in distilled water, counterstained with Mayer's haematoxylin, washed in running water before dehydration through an ascending series of alcohol concentrations, cleared in Histoclear (Fisher Scientific) and mounted in Vectamount medium (Vector Laboratories).

2.5. Enzyme-linked immunosorbent assay

2.5.1. Principles

Enzyme-linked immunosorbent assay (ELISA) is a technique used to quantify the amount of a specific protein in solution by exploiting the specificity of antigen-antibody interactions. A 96 well plate is coated with capture antibody that binds to the specific protein (antigen) of interest. A detection antibody conjugated to biotin, which is raised against a different epitope of the protein to the capture antibody, also binds to the protein of interest. Steptavidin bound to HRP is then added and binds to the detection antibody. Finally a substrate for HRP is added which results in the generation of a coloured product **(Fig. 2.5)**. The reaction is stopped and then the optical density of each well is measured using a microplate reader. This ELISA technique involves using antibodies either side of the substrate and so it is known as a sandwich ELISA.

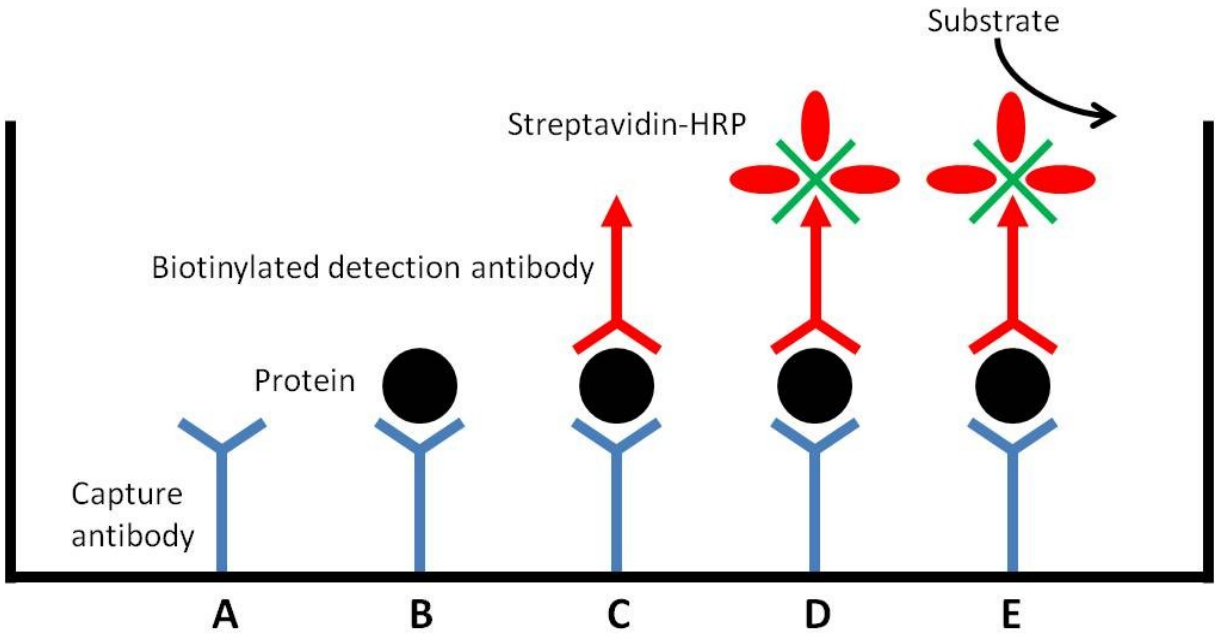

Figure 2.5. ELISA method. (A) First the wells of a 96 well plate are coated with capture antibody which subsequently binds to the protein of interest **(B)**. This protein is then detected with a biotinylated detection antibody **(C)**. **(D)** Streptavidin conjugated to horseradish peroxidise (HRP) binds the detection antibody. **(E)** Finally a substrate is added and the conjugated HRP catalyses a reaction which results in the precipitation of a coloured product.

2.5.2. Decorin ELISA

The ELISA kit used to detect and quantify Decorin was the human Decorin DuoSet (DY143, R&D Systems, UK) and both the protocol and reagents were supplied. All procedures were conducted at room temperature and between each step the wells were aspirated and washed with wash buffer (0.05% Tween20 in PBS). A 96 well plate was coated with capture antibody (2µg/ml monoclonal mouse anti-human Decorin diluted in PBS), covered and left overnight. Non specific binding sites in the wells were blocked with the reagent diluent (DY995, 1% BSA in PBS) for 1 hour followed by incubation with the CSF sample (1/10 dilution) or Decorin standards (recombinant human Decorin, serial dilutions up to 2000pg/ml) for 2 hours. The wells were then incubated with detection antibody (250ng/ml biotinylated mouse anti-human Decorin in reagent diluent) for 2 hours, after which the wells were incubated with streptavidin conjugated to HRP (1/200 in reagent diluent) in the dark for 20 minutes. Finally the wells were incubated in the substrate solution (DY999, equal amounts of H_2O_2 and tetramethylbenzidine) in the dark for 20 minutes and the reaction stopped with the stop solution (2N H_2SO_4). The optical density was determined immediately using a microplate reader set to 450nm (with the readings at 540/570nm subtracted for imperfections in the plate). All samples were run in duplicate and the average optical density of the two samples taken.

2.6. Antibodies

Antibody	Detects	Host	Dilution	Source	Catalogue number
α-smooth muscle actin		Mouse	1/100	Sigma-Aldrich, Poole, UK	
β-actin	β-actin	Mouse	1/1000 (WB)	Sigma-Aldrich, Poole, UK	A5441
βIII-Tubulin	Neurons	Mouse	1/400 (ICC)	Sigma-Aldrich, Poole, UK	T8660
CD11b (OX-42)	Microglia and macrophages	Mouse	1/50 (ICC), 1/500 (IF)	Serotec, Oxford, UK	MCA275R
CD68 (ED-1)	Macrophages and activated microglia	Mouse	1/100 (ICC), 1/400 (IF)	Serotec, Oxford, UK	MCA341R
Cleaved caspase 3	Apoptotic cells	Rabbit	1/200 (IF)	Cell Signalling, MA, USA	9661S
Collagen 1	Collagen 1	Rabbit	1/50 (ICC)	Abcam, Cambridge. UK	Ab292
Decorin	Human Decorin	Mouse	1/400 (IF)	Abcam, Cambridge, UK	Ab54728
Fibronectin	Fibronectin	Rabbit	1/200 (ICC/IF)	Sigma-Aldrich, Poole, UK	F3648
GFAP	Astrocytes	Mouse	1/500 (ICC/IF)	Sigma-Aldrich, Poole, UK	G3893
Ki67	Cell proliferation	Rabbit	1/400 (IF)	Abcam, Cambridge, UK	Ab16667
Laminin	Laminin	Rabbit	1/200 (IF)	Sigma-Aldrich, Poole, UK	L9393
Nestin	Neuroprogenitor cells	Mouse	1/50 (IF)	BD Biosciences, Oxford, UK	556309
NG2	NG2	Rabbit	1/200 (ICC), 1/500 (WB)	Millipore, MA, USA	AB5320
RECA-1	Rat endothelial cells	Mouse	1/50 (ICC)	Serotec, Oxford, UK	MCA970R
TGF-β1	TGF-β1	Mouse	1/200 (IP)	Abcam, Cambridge, UK	Ab27969
TGF-β1	TGF-β1	Rabbit	1/200 (IP)	Santa Cruz Biotechnology, Texas, USA	Sc-146

Phosphorylated Smad2/3	Phosphorylated Smad2/3	Rabbit	1/200 (IP)	Santa Cruz Biotechnology, Texas, USA	Sc-11769-R
Vimentin	Vimentin	Rabbit	1/200 (ICC)	Abcam, Cambridge, UK	Ab92547
Alexa Fluor 488	Mouse IgG	Goat	1/500 (ICC), 1/1000 (IF)	Life Technologies, Paisley, UK	A11029
Alexa Fluor 488	Rabbit IgG	Goat	1/500 (ICC), 1/1000 (IF)	Life Technologies, Paisley, UK	A11034
Alexa Fluor 594	Mouse IgG	Goat	1/500 (ICC), 1/1000 (IF)	Life Technologies, Paisley, UK	A11032
Alexa Fluor 594	Rabbit IgG	Goat	1/500 (ICC), 1/1000 (IF)	Life Technologies, Paisley, UK	A11037
Biotinylated	Human IgG	Donkey	1/500 (IP)	Jackson ImmunoResearch Laboratories, PA,USA	709-005-149
Biotinylated	Mouse IgG	Horse	1/500 (IP)	Vector Laboratories, Peterborough, UK	BA2001
Biotinylated	Rabbit IgG	Goat	1/1000 (IP)	Vector Laboratories. Peterborough, UK	BA1000
ECL HRP linked	Mouse IgG	Sheep	1/1000 (WB)	GE Healthcare, Buckinghamshire, UK	NA931-1ML
ECL HRP linked	Rabbit IgG	Donkey	1/1000 (WB)	GE Healthcare, Buckinghamshire, UK	NA934-1ML

Table 2.2. Table of Antibodies. Antibodies used for Western blotting (WB), immunocytochemistry (ICC), immunofluorescent staining (IF) and immunoperoxidase staining (IP).

2.7. Haematoxylin and Eosin (H&E)

Slides were removed from the freezer and allowed to thaw. Sections were incubated in Harris haematoxylin for 2 minutes, washed in distilled water and briefly differentiated in 1% acid alcohol (1% HCl in 70% ethanol). The sections were then washed in water, followed by the blueing agent 0.1% sodium bicarbonate and then 90% ethanol. This was followed by incubation in alcoholic eosin (VWR International, Dublin, Ireland) for 1 minute followed by 90% then 100% ethanol, cleared in Histoclear (Fisher Scientific) and mounted in Vectamount medium (Vector Laboratories).

2.8. Semi-quantitative analysis

Stained sections were viewed on an Axioplan 2 imaging epifluorescent microscope (Carl Zeiss, Germany) and micrographs were captured using an AxioCam HRc (Carl Zeiss). Images were analysed semi-quantitatively using ImageJ analysis software (Abramoff, 2004).

2.8.1. Evaluation of GFAP immunofluorescent staining in Chapters 4, 5 and 6

Nine regions of interest (3 regions x 3 coronal sections) per rat were selected from images of the corpus callosum, periventricular white matter **(Fig. 2.6.A)** or olfactory tubercle, and the percentage of immunofluorescent pixels above a set threshold calculated using ImageJ. First the region of interest (ROI) manager was opened using the tabs Analyze→ Tools→ROI Manager **(Fig. 2.7.A)**. This was to allow the ROI to be saved so that the same size area was used on all the images. Then the ROI was drawn

using the Rectangle Tool and was added to the ROI manager **(Fig. 2.7.B)**. The threshold window was opened using the tabs Image→Adjust →Threshold and the threshold was set by adjusting the brightness to include as much of the staining as possible. The threshold colour was changed to B&W so that the background was white and the staining was black **(Fig. 2.8.A)**. The initial threshold was set on an image with a medium amount of staining and the same threshold value would then be used in all subsequent images. The ROI was then selected and the histogram was opened using the tabs Analyze→Histogram. The graph had two peaks showing 0 and 255, the Count value was the total number of pixels, the mode was usually the number of white pixels from which the black pixel value was calculated and the percentage of black pixels measured **(Fig. 2.8.B)**.

2.8.2. Evaluation of ED-1 immunofluorescent staining in Chapter 5

A composite image of the basal subarachnoid space was created using a series of images captured at x100 from a posterior coronal section of the brain (5.8mm post-Bregma). A region of interest was drawn around the subarachnoid space and the percentage of pixels that were immunofluorescent above a set threshold was calculated as described in section 2.8.1.

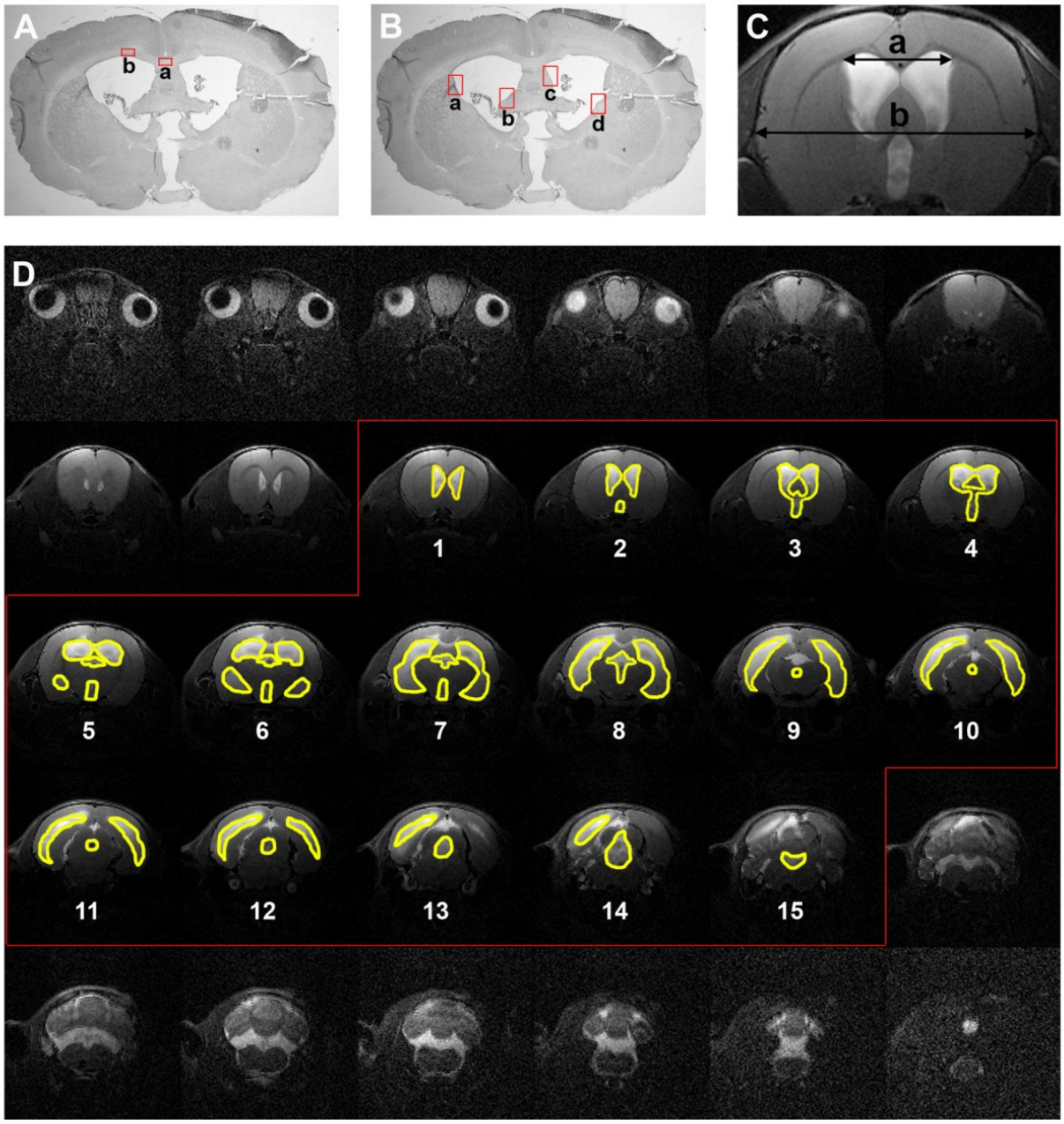

Figure legend on following page...

Figure 2.6. Analysis of data. Images representing the areas of the brain where high magnification images were taken to analyse: **(A)**, GFAP immunofluorescent staining in the corpus callosum (a) and the periventricular white matter (b); and **(B)**, TGF-β1 and pSmad2/3 immunoperoxidase staining intensity in the ependyma of 4 ventricular regions (a-d). **(C)** The Evan's ratio was calculated as the ratio of the greatest width of both lateral ventricles (a) to the greatest width of the brain (b), at the level of the foramen of Monro. **(D)** Example of a complete series of 30 coronal MRI scans, 0.75mm apart, from a Kaolin treated rat. The total ventricular volume was calculated as the sum of the lateral, third and fourth ventricular areas (*yellow*) in 15 sequential MRI scans multiplied by the distance between the scans (0.75mm).

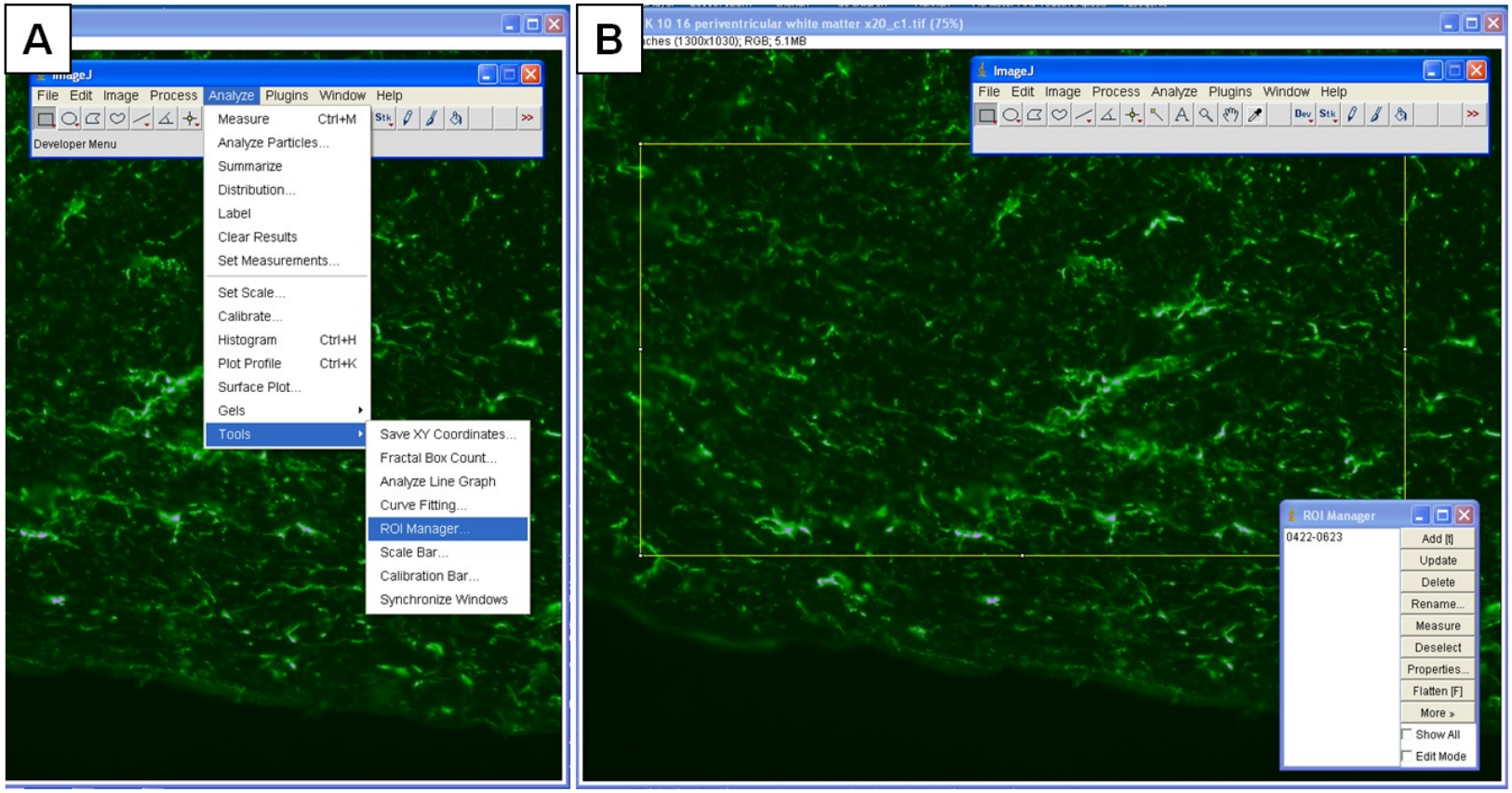

Figure 2.7. Instructions for selecting a region of interest in ImageJ. (A) The region of interest (ROI) manager was opened using the tabs Analyze→ Tools→ROI Manager. **(B)** The ROI was drawn using the Rectangle Tool and was added to the ROI manager.

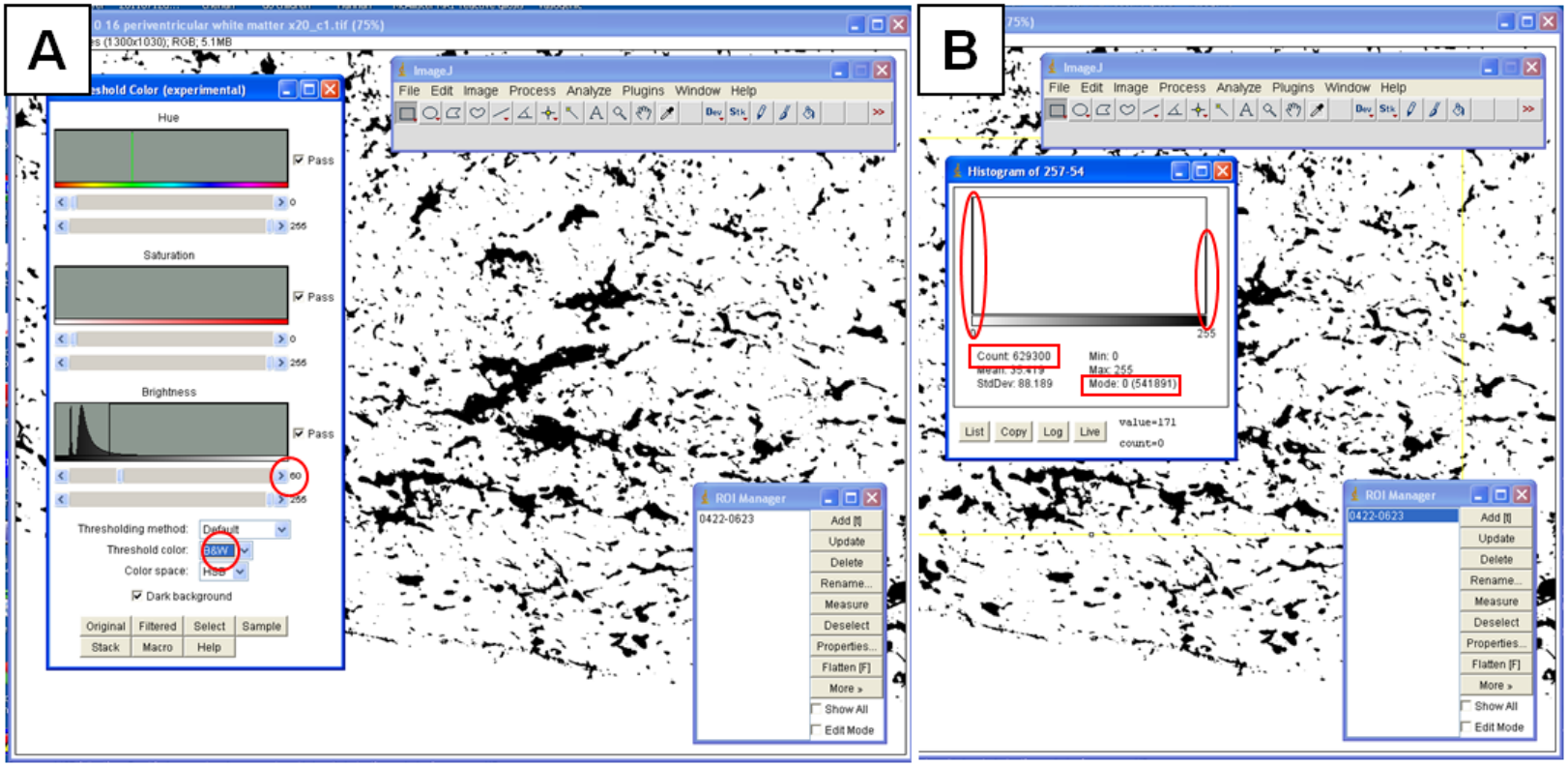

Figure 2.8. Instructions on setting the threshold and determining the number of black pixels in ImageJ. (A) The threshold window was opened using the tabs Image→Adjust →Threshold and the threshold was set by adjusting the brightness and selecting the threshold colour as B&W. **(B)**. The histogram was opened using the tabs Analyze→Histogram. The graph has two peaks showing 0 (white) and 255 (black) and the number of black pixels was calculated as the count value minus the mode value (white pixels).

2.8.3. Quantification of inflammatory cells in the subarachnoid space in Chapter 5

To evaluate the acute inflammatory response in the subarachnoid space the number of eosinophils, neutrophils and macrophages were estimated on two posterior coronal sections per rat stained with haematoxylin and eosin. Up to 50 x1000 images (field of view 93.16x69.82μm) were taken at random within the subarachnoid space (the number depending upon the total area of the subarachnoid space in the section) and the number of cells within each field of view was counted manually. Eosinophils contained bright pink granules in the cytoplasm, Neutrophils had multi-lobed nuclei and pale pink cytoplasm and macrophages had an acentric large round or kidney shaped nucleus surrounded by light bluish cytoplasm **(Fig. 5.4.A. in Chapter 5)**. Macrophages could only be definitively identified at the edge of the kaolin deposits and were therefore probably under-represented in the counts. Also cells that could not be positively identified by these criteria were classed as unidentified. The relative frequency of each cell type were represented as a percentage of the total number of cells.

2.8.4. Evaluation of TGF-β1 and pSmad2/3 immunoperoxidase staining in chapters 4 & 6

In the ependyma, 12 regions of interest (4 regions x 3 coronal sections) per rat were selected from images of the lateral ventricular ependyma **(Fig. 2.6.B)**, and the mean pixel intensity (arbitrary units of pixel intensity) above background threshold (established using the no primary antibody control sections) was calculated. First an ROI was drawn using the polygon tool around the ependyma **(Fig. 2.9.A)** then the colour of the ROI was inverted by using the tabs

Edit→Invert. The histogram was then opened using the tabs Analyze→Histogram and the Mean value represented the mean pixel intensity of the ependyma **(Fig. 2.9.B)**.

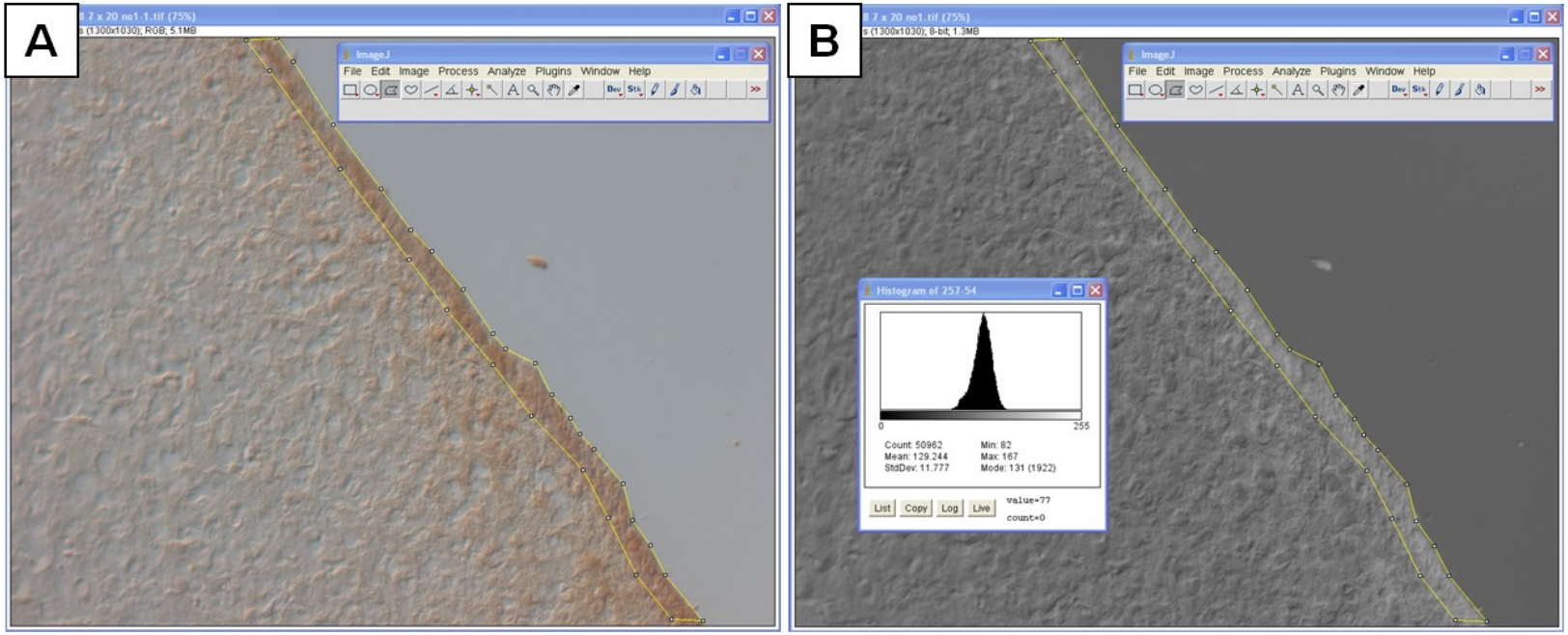

Figure 2.9. Instructions on determining pixel intensity in ImageJ. (A) An ROI was drawn using the polygon tool around the ependyma and the colour inverted. **(B)** The histogram was then opened and the Mean value represented the mean pixel intensity of the ependyma.

2.9. Evaluation of ventricular size

2.9.1. Principles of magnetic resonance imaging (MRI)

MRI is a technique that exploits the fact that hydrogen nuclei (protons) in the body rotate on an axis and therefore generate a magnetic field. The nuclei precess (move in a conical motion) around the direction of the magnetic field **(Fig. 2.10.A)**. If a magnetic field is applied to a specific tissue, the nuclei align parallel to the field and together they form a net magnetisation (in the longitudinal direction; **Fig. 2.10.B+C)**. During excitation, a perpendicular oscillating magnetic field (for example a coil with alternating currents) is applied at the same frequency as precession of the nuclei causing the net magnetisation to be rotated away from equilibrium in a perpendicular direction **(Fig. 2.10.D)**. However after magnetisation, the nuclei do not remain in the same direction, as neighbouring nuclei precess at different frequencies causing dephasing to occur, leading to the nuclei pointing in all directions perpendicular to the magnetic field **(Fig. 2.10.E)**. In firm tissue dephasing occurs relatively quickly as the neighbouring nuclei are constant, whereas in fluids the nuclei are more mobile and are interacting with new neighbouring nuclei all the time causing dephasing to happen relatively slowly. These interactions cause the magnetisation to constantly approach equilibrium and this is known as relaxation. The time it takes for the magnetisation to decrease in the perpendicular plane is known as T2 and the time it takes to decrease in the longitudinal plane is known as T1 **(Fig. 2.10.F)**. Dephasing causes a loss of signal however this can be regained through a refocusing pulse which realigns the nuclei in the perpendicular plane leading to an echo

which emits a signal and can be measured. Therefore magnetic resonance is measured using sequences that include the elements excitation, dephasing and refocusing.

To create an image it is necessary to excite tissue in slices using gradient coils. These induce a gradient in the strength of the magnetic field from left to right which will only excite nuclei at a particular frequency causing them to emit a signal, thus creating a tissue ‘slice’. In each slice, gradients are then applied to cause different patterns of magnetisation and similarities between the pattern and the object being scanned will cause a signal to be emitted at a particular strength. Different patterns in each tissue slice can then be used to build up a total image resulting in the final magnetic resonance image.

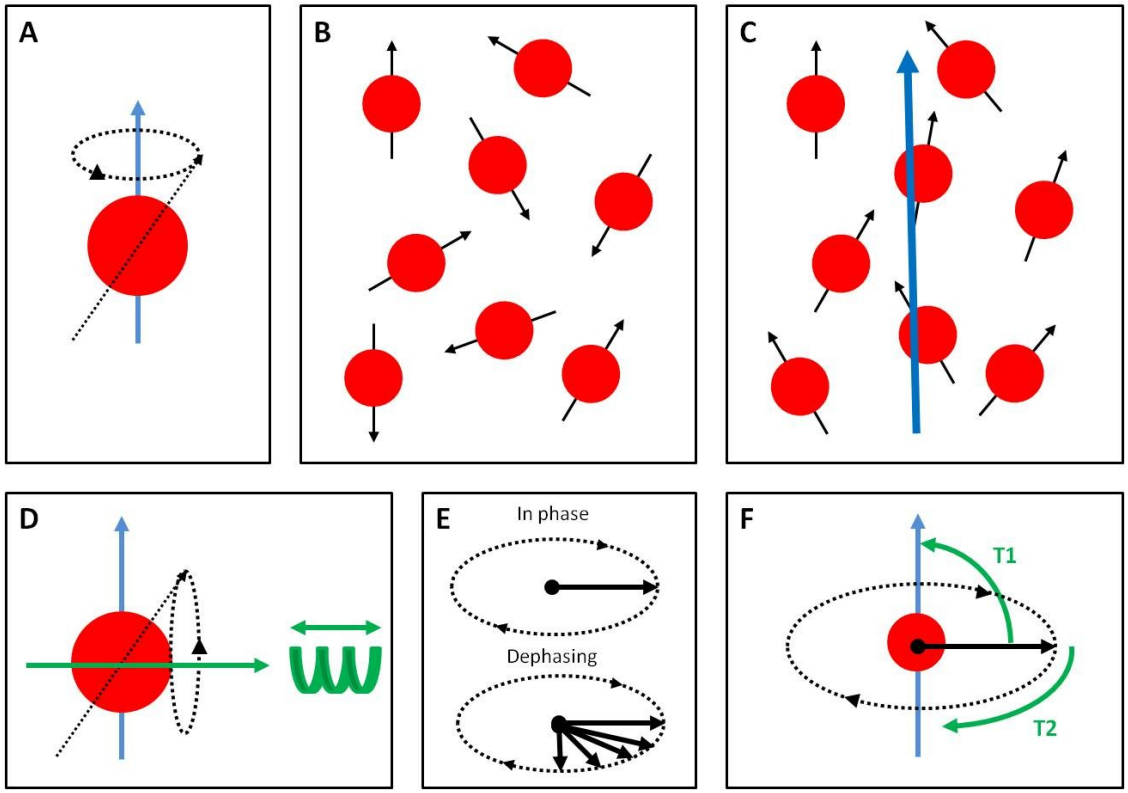

Figure 2.10. Basic principles of MRI. (A) Nuclei have a magnetic field (blue arrow) and precess around it. **(B)** Nuclei in tissue point in all directions, however when a magnetic field is applied they will try and align, resulting in net magnetisation (blue arrow, **C)**. **(D)** A coil with alternating currents (green) can cause the net magnetisation to rotate in a perpendicular direction (green arrow). **(E)** After, the nuclei will begin in phase but will slowly dephase due to differing precession frequencies. **(F)** The time it takes for the magnetisation to decrease in the perpendicular plane is T2, the time it takes to decrease in the longitudinal plane is T1.

2.9.2. MRI

Imaging experiments were conducted using a Bruker Biospec 7T scanner (Bruker Biospin, Ettlington, Germany) equipped with a high performance gradient system (with 600mT/m maximum gradient amplitude, and 0.25ms rise time). Animals were anesthetised using 1–3% Isoflurane and their vital signs (respiration, rectal temperature, heart rate and oxygen saturation percentage) were continuously monitored using a MR compatible physio-logical monitoring system (SA Instruments, Stony Brook, NY, USA). Animals were placed in a 72-mm volume coil for signal transmission, and a quadrature surface coil that was placed on the animal's head was used for signal reception. T_2-weighted scans were acquired using rapid acquisition with a relaxation enhancement sequence of 4000ms repetition time, 40ms effective echo time, 8 echoes per image, 4 averages, 30 coronal slices of 0.75mm slice thickness in a 2.5cm × 2.5cm field-of-view with a 98μm × 98μm in-plane resolution.

2.9.3. Ventricular area on tissue sections

Sections were stained with H&E using the protocol outlined in section 2.7. The degree of ventricular dilation was determined by measuring the size of the lateral ventricles in a defined anatomical plane. The area of both lateral ventricles was measured on the H&E coronal sections of brain at 0.3mm posterior to Bregma where the fornix and the anterior commissure were visible. Tissue sections were observed under bright field microscopy and images were captures using an Axiocam digital camera (Carl Zeiss, Germany), and the ventricular area was calculated using the appropriate software (Axiovision 4.8, Carl Zeiss).

2.9.4. Evan's ratio on tissue sections and MRI scans

The Evan's ratio is used clinically to diagnose hydrocephalus and a ratio of greater than 0.3 is classed as hydrocephalic (Shprecher *et al.,* 2008).The Evan's ratio (ratio of the greatest width of both lateral ventricles to the greatest width of the brain) was measured in one tissue section or one coronal MRI scan from each experimental animal, at the level of the foramen of Monro (**Fig. 2.6.C**).

2.9.5. Ventricular volume measured on MRI scans

Ventricular volume was estimated by measuring the total ventricular area of the lateral, third and fourth ventricles, using ImageJ, in 15 sequential coronal MRI scans from each experimental animal (**Fig. 2.6.D**) and multiplying this value by 0.75 (distance in mm between each scan).

2.10. Statistical Analysis

The 'resources equation' was used to confirm that the appropriate number of animals were included in this study (NC3Rs, 2012). Statistical analyses were carried out using SPSS PASW statistics 18 (IBM, NY, USA) to determine if there was any significant difference between treatment groups at the various time points.

The data were tested using the Shapiro-Wilk test to evaluate the normal distribution of the residual values for the data. This test indicated that the oedema, TGF-β1 and pSmad2/3 data were normally distributed and therefore it was analysed using the one way ANOVA and *post hoc* Tukey tests. Similarly, after transformation (Log_{10}), ventricular

volume, Evan's ratio and GFAP data were shown to be normally distributed and so were analysed using the one way ANOVA. Data were reported as group means ± standard error of the mean (SEM).

Chapter 3

Developing an experimental rat model of communicating hydrocephalus

3.1. Rationale

Post-haemorrhagic communicating hydrocephalus is thought to develop due to fibrosis in the subarachnoid space obstructing CSF drainage. Transforming growth factor-β1 (TGF-β1) plays a significant role in the development of fibrosis through promoting inflammation and extracellular matrix (ECM) deposition in multiple tissues, and has also been implicated in the aetiology of post-haemorrhagic hydrocephalus. Therefore a TGF-β antagonist may be useful as a therapeutic agent to prevent post-haemorrhagic hydrocephalus. Post-haemorrhagic hydrocephalus is difficult to induce in a rat therefore other experimental models of hydrocephalus such as an injection of kaolin may be more useful. The injection of kaolin into the cisterna magna produces non-communicating hydrocephalus but this is not appropriate for studying the development of post-haemorrhagic communicating hydrocephalus. Therefore the first aim of this study was to generate a reliable *in vivo* rat model of communicating hydrocephalus and assess endogenous levels of TGF-β1. The second aim was to generate an *in vitro* model of rat meningeal fibroblasts to determine the bioactive range of TGF-β1 required to promote maximum fibrosis, and to assess the effects of a TGF-β antagonist (Decorin) on TGF-β1 induced meningeal fibrogenesis.

3.2. Experimental design

3.2.1. Model of communicating hydrocephalus

Kaolin was either injected into the prechiasmatic cistern or the basal cisterns to induce communicating hydrocephalus as described in sections 2.3.2 and 2.3.3

respectively. The rats were killed 2, 7, 14 and 28 days later in the prechiasmatic cistern model and 14 days later in the basal cisterns model **(Table 3.1)**. Ventricular enlargement and TGF-β immunohistochemistry were determined on coronal sections as outlined in sections 2.9.3, 2.9.4 and 2.4.4.

Hydrocephalus model	Group	Day 2	Day 7	Day 14	Day 28
Prechiasmatic cistern model	Saline	3	4	3	3
	Kaolin	2	2	3	2
Basal cistern model	Saline	-	-	4	-
	Kaolin	-	-	7	-

Table 3.1. Hydrocephalus models. The number of rats in each group for the prechiasmatic cistern model and the basal cistern model of hydrocephalus

3.2.2. Primary rat meningeal cell cultures

Adult rat meninges were removed and cultured to produce a rat meningeal cell culture as described in sections 2.1.1 and 2.1.2. To determine the type of cells present in the culture the cells were passaged 3 or 4 times before being cultured on poly-D-lysine coated chamber slides for 48 hours, fixed and stained with antibodies for specific cell markers as described in section 2.4.2. To examine the effects of TGF-β1 and Decorin on the production of extracellular matrix (ECM) molecules, the meningeal cell cultures were treated with TGF-β1 (0, 10, 25 and 50ng/ml) and/or 20µg/ml Decorin as described in section 2.1.3. The cells were then lysed and the levels of NG2 determined by western blot as described in section 2.2.

3.3. Results

3.3.1. Prechiasmatic cistern model of hydrocephalus

3.3.1.1. Kaolin injection into the prechiasmatic cistern did not reliably induce hydrocephalus

At 7 and 28 days the ventricular area (mm^2) was similar between the Saline group (1.63mm^2 and 1.11mm^2, respectively) and the Kaolin group (1.50±0.28mm^2 and 1.24±0.13mm^2, respectively). However at 14 days the Kaolin group (2.85±0.30mm^2) had larger ventricles compared to the Saline group (1.84±0.10mm^2) although the difference was not statistically significant **(Fig. 3.1)**. This data suggests that kaolin injected into the prechiasmatic is not a reliable or reproducible model of hydrocephalus.

3.3.1.2. Raised TGF-β1 levels after prechiasmatic cistern injection

TGF-β1 positive staining was localised to the meninges in both the Kaolin and Saline groups at all time points (data not shown). At 2 days after the prechiasmatic cistern injection, intense TGF-β1 staining was localised to the cytoplasm of cells in the ependyma, choroid plexus, cortex and corpus callosum in both the Saline and the Kaolin groups **(Fig. 3.2)**. TGF-β1 positive staining was associated with neurones in the cortex and glial cells such as oligodendrocytes in the corpus callosum based on their morphology and distribution in these areas **(Fig. 3.2)**. At 7, 14 and 28 days the staining in the cortex and corpus callosum was lost.

TGF-β1 positive staining in ependymal cells demonstrated a biphasic response, with more intense TGF-β1 staining at 2 and 14 days compared to the low levels of TGF-

β1 observed at 7 and 28 days in both the Kaolin and Saline groups **(Fig. 3.3)**. This data suggests that changes in endogenous TGF-β1 levels were not related to the kaolin injection or enlargement of ventricles.

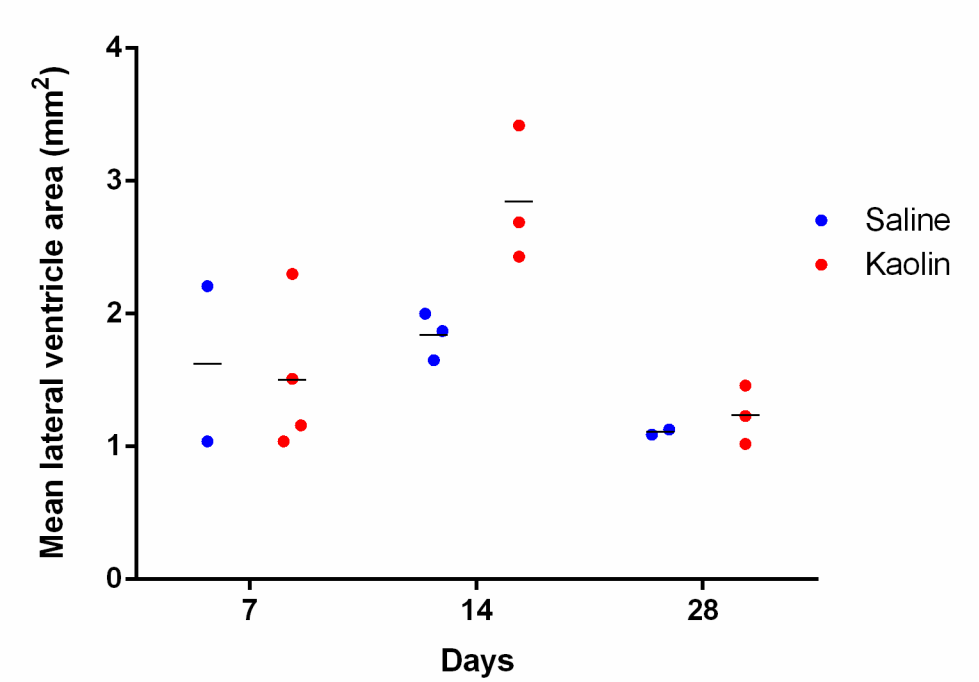

Figure 3.1. Lateral ventricle area in the prechiasmatic cistern model. The scatter plot summarises the mean of the ventricular area in the Saline and Kaolin groups at 7, 14 and 28 days. Ventricular enlargement was only observed in the Kaolin group 14 days after the injection of kaolin into the prechiasmatic cistern.

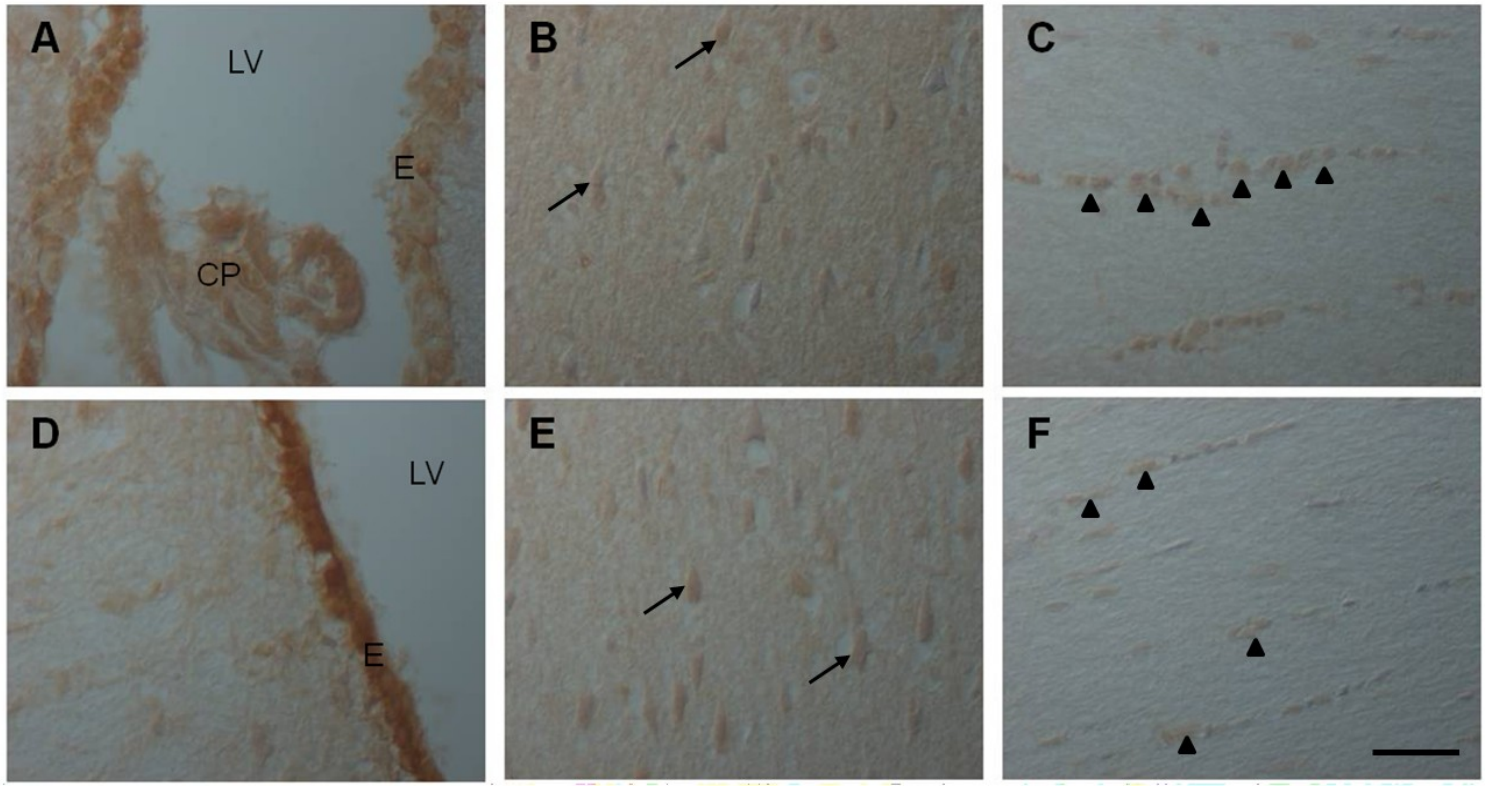

Figure 3.2. TGF-β1 staining in the ependyma, choroid plexus, cortex and corpus callosum at 2 days. Representative images of TGF-β1 staining in the Saline **(A-C)** and Kaolin **(D-E)** groups. There was intense cytoplasmic TGF-β1 staining in the ependyma and choroid plexus in both treatment groups **(A+D)**. TGF-β1 staining in the cortex appeared to be mainly associated with neurones (black arrows; **B+E)** and in the white matter associated with glial cells (black arrow heads) based on their morphology and typical arrangement in these areas of the brain **(C+F)**. Scale bar - 50μm; CP – choroid plexus, E – ependyma, LV – lateral ventricle.

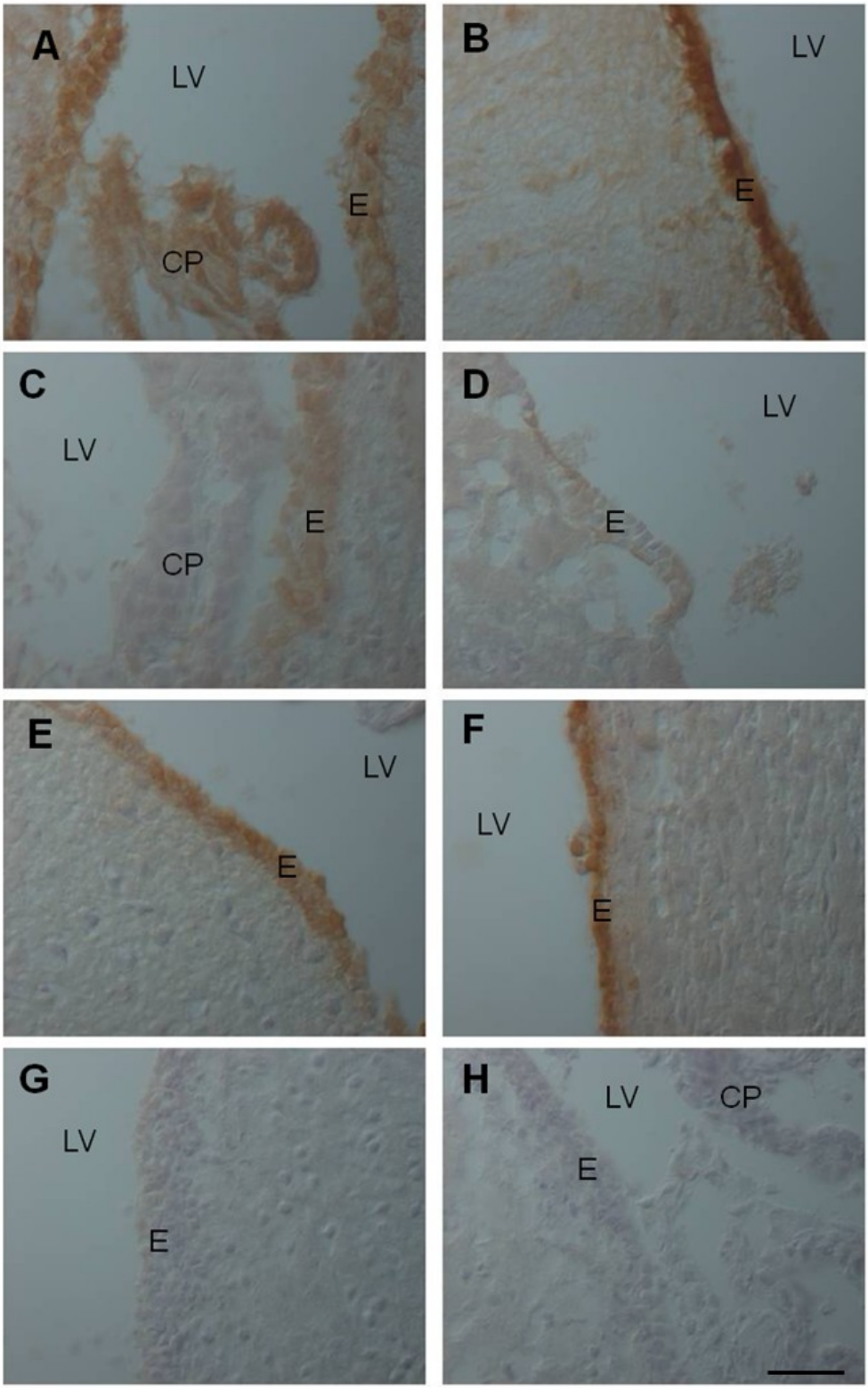

Figure legend on following page...

Figure 3.3. TGF-β1 staining in the ependyma at time points 2, 7, 14 and 28 days. Representative images of TGF-β1 positive staining in the Saline **(A,C,E,G)** and Kaolin **(B,D,F,H)** groups. There was intense cytoplasmic TGF-β1 staining in the ependyma of both the Saline and Kaolin groups at 2 **(A-B)** and 14 days **(E-F)**. The intensity of TGF-β1 staining was relatively reduced at 7 **(C-D)** and 28 days **(G-H)** in the ependyma of the Saline and Kaolin groups. Scale bar - 50μm; CP – choroid plexus, E – ependyma, LV – lateral ventricle.

3.3.2. Basal cistern model of hydrocephalus

3.3.2.1. Kaolin injection into the basal cistern induced hydrocephalus

The second model used in this study has already been used previously to induce communicating hydrocephalus (Li *et al*., 2008). After basal cistern injection of kaolin, the lateral ventricle area was larger in the Kaolin group (2.69±0.66mm^2) compared to the Saline group (1.52±0.57mm^2; **Fig. 3.4.A)**. In addition, the Evans ratio was greater in the Kaolin group (0.32±0.01) compared to the Saline group (0.26±0.01; **Fig. 3.4.B)**. This data suggests that the basal cistern injection is a reliable and reproducible experimental model of communicating hydrocephalus.

3.3.2.2. Hydrocephalus was associated with raised endogenous TGF-β1 levels

In the Saline group, there was weak cytoplasmic TGF-β1 staining of the ependymal and choroid plexus epithelium cells **(Fig. 3.4.C)**, and strong staining of meninges (not shown). There was more intense TGF-β1 staining in the ependymal and sub-ependymal cells of the Kaolin group **(Fig. 3.4.D)**. In addition in the Kaolin group, animals with the largest increase in ventricular size had more intense TGF-β1 staining. This suggests that the basal cistern injection induced hydrocephalus was associated with an increase in TGF-β1 levels in the ependyma.

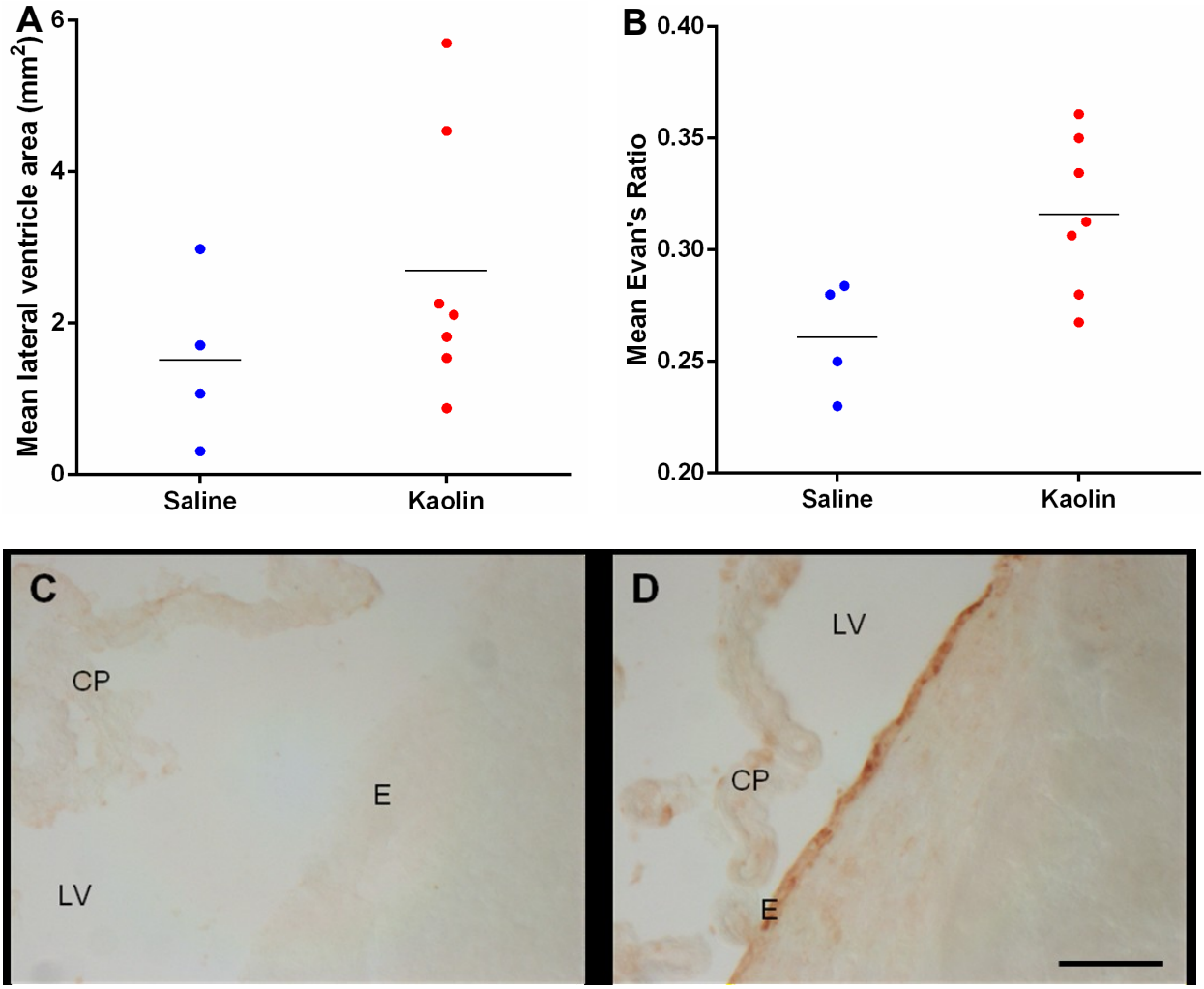

Figure 3.4. Lateral ventricle area, Evan's ratio and TGF-β1 levels in the basal cistern model. The scatter plots summarise the mean of the ventricular volumes **(A)** and Evan's Ratio **(B)** in the Saline and Kaolin groups. Ventricular enlargement was observed in the Kaolin group after the injection of kaolin into the basal cisterns. Representative images of ependymal TGF-β1 staining in the brains of Saline **(C)** and Kaolin **(D)** groups. TGF-β1 staining was more intense in the ependyma of the Kaolin group compared to the Saline group. Scale bar - 100μm; CP – choroid plexus, E – ependyma, LV – lateral ventricle.

3.3.3. Characterisation of rat meningeal fibroblasts

There were no specific markers of meningeal fibroblasts available, therefore the cells that were isolated and cultured from meningeal tissue were characterised for the presence of cell types known to be present within the meninges and brain parenchyma (Manwaring *et al*., 2001). The cells were stained for endothelial cells (RECA-1), astrocytes (GFAP), macrophages (ED-1), monocytes and microglia (OX-42) and neurones (βIII-tubulin). Cells that were positive for vimentin, an intermediate filament which is highly expressed in fibroblasts, and negative for the other cells types were assumed to be meningeal fibroblasts.

As expected, in the cell culture the majority of cells stained positive for vimentin and vimentin positive fibres were observed in the cytoplasm **(Fig. 3.5.A)**. In addition the cells had elongated cytoplasm, a hallmark of fibroblastic-like morphology. βIII-tubulin staining was confined to small round neurones in the cultures **(Fig. 3.5. B)**, and around 2% of the total cell population were positive for ED-1, GFAP and OX-42 **(Fig. 3.5.C-E)**. No cells were RECA-1 positive (data not shown). The cultures were therefore assumed to be >95% enriched for meningeal fibroblasts. Numerous cells of the meningeal cultures were also associated with ECM molecules including collagen, fibronectin and NG2 **(Fig. 3.5.F-H)**.

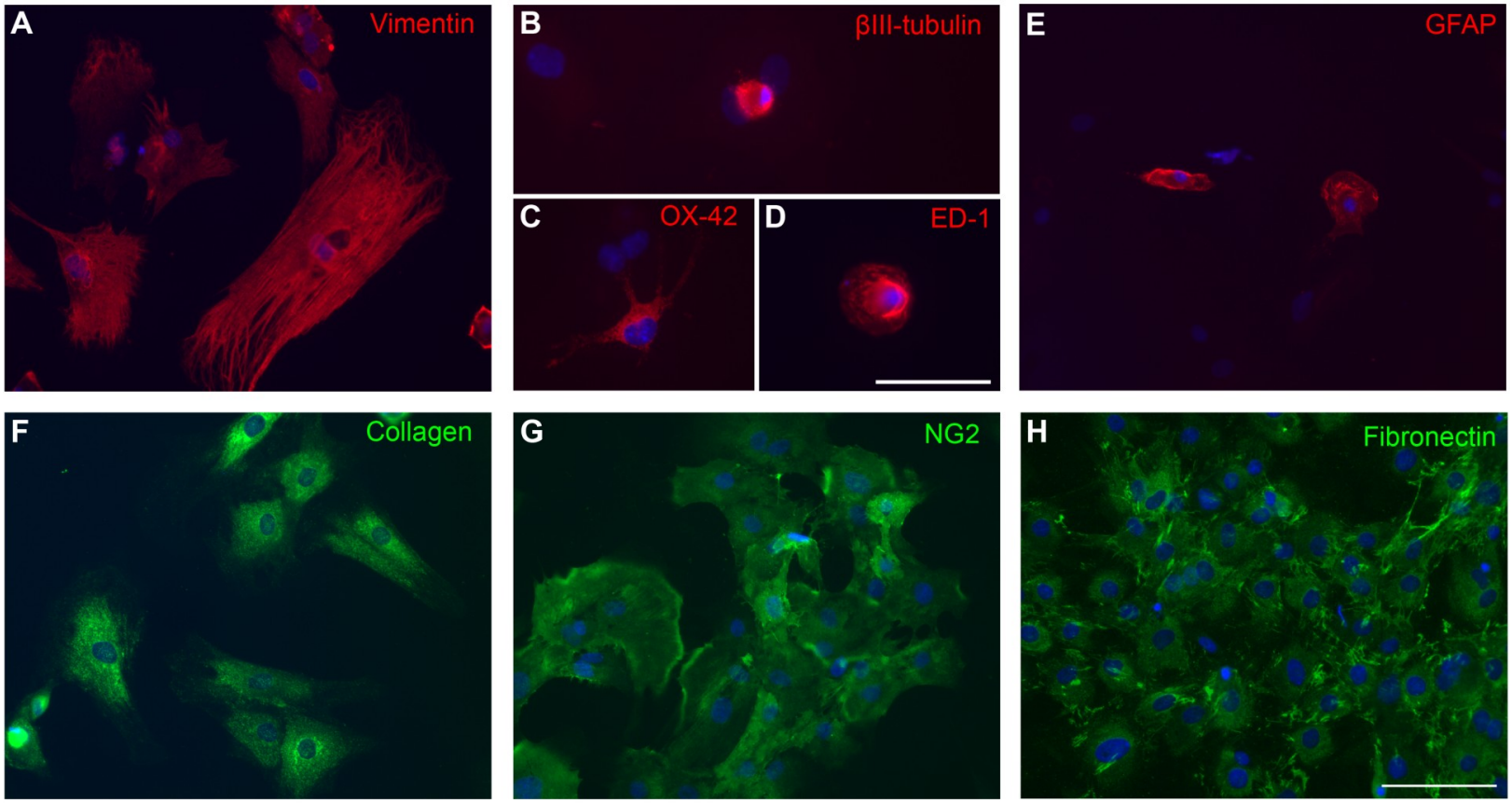

Figure 3.5. Characterisation of rat brain meningeal cell cultures. Cells were cultured for 48 hours then fixed and stained for cell markers. **(A)** The majority of cell stained positive for vimentin *(red)*. Occasional cells stained positive *(red)* for βIII-tubulin **(B)**, OX-42 **(C)**, ED-1 **(D)**, and GFAP **(E)**. Numerous cells in the cultures also stained postive (*green)* for the extracellular matrix molecules collagen **(F)**, NG2 **(G)** and fibronectin **(H)**. DAPI (*blue*) was used as a generic nuclear marker; scale bars A+E-H - 50μm, B-D - 10μm.

3.3.4. TGF-β1 increases NG2 protein levels in primary rat meningeal cell cultures

To determine whether the primary rat meningeal cell culture responds to TGF-β1, the levels of NG2, an extracellular matrix (ECM) molecule, were determined by Western blot of the cell lysate. Untreated meningeal cells showed negligible levels of NG2. TGF-β1 induced an increase in NG2 protein levels which was concentration dependent, with 25ng/ml inducing the greatest response. Rat central nervous system tissue lysate was used as a positive control **(Fig 3.6)**. This data suggests that at specific concentration TGF-β1 induces the production of ECM molecules.

3.3.5. Decorin attenuates TGF-β1 induced NG2 protein levels

To test the efficacy of the human recombinant Decorin we examined the effects of Decorin on TGF-β1 induced NG2 protein levels. Decorin treatment alone showed similar negligible NG2 levels to the untreated meningeal cell cultures. Decorin attenuated TGF-β1 induced NG2 levels and was dependent on the concentration of TGF-β1. Decorin had a greater effect on NG2 protein expression induced by 10ng/ml TGF-β1 compared with 25ng/ml TGF-β1 **(Fig. 3.6)**. These results suggest that Decorin inhibits the TGF-β1 induced ECM deposition in meningeal cultures.

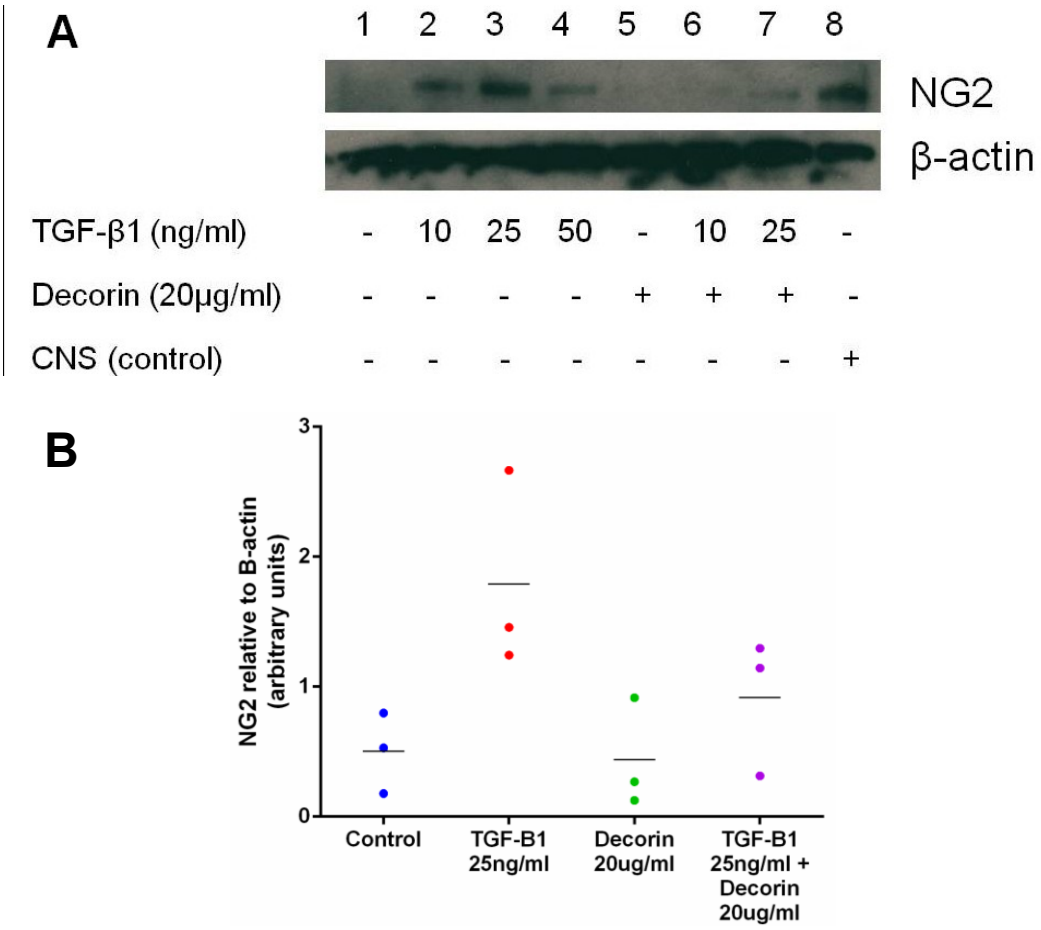

Figure 3.6. Western blot analysis of meningeal culture lysate after treatment with TGF-β1 and Decorin. (A) Primary rat meningeal cell cultures were treated with TGF-β1 (0, 10, 25 and 50 ng/ml) and/or Decorin (20µg/ml). NG2 protein levels were increased dependent on the concentration of TGF-β1, with 25ng/ml TGF-β1 inducing the greatest response (lane 3). Decorin reduced the TGF-β1 induced expression of NG2 and this effect was dependent on the dose of TGF-β1 (lanes 6 and 7). A rat central nervous system tissue lysate was used as a positive control for NG2 (lane 8). **(B)** The scatter plot summarises the mean of the intensity of the NG2 band to the β-actin band (n=3). TGF-β1 increased the levels of NG2 produced by meningeal cell cultures while Decorin attenuated this response.

3.4. Discussion

3.4.1. Prechiasmatic cistern model of hydrocephalus

The prechiasmatic cistern model of SAH uses a simple technique of blood injection that is well tolerated, reliable and reproducible, and distributes blood throughout the basal subarachnoid space (Prunell *et al*., 2002). Here, the prechiasmatic cistern model was adapted by injecting 50µl of kaolin instead of blood. It was hypothesised that this would also induce fibrosis in the subarachnoid space and subsequently the development of communicating hydrocephalus. The rats were killed at 7, 14 and 28 days after the injection of kaolin to establish the time course of hydrocephalus development. Unfortunately, ventricular enlargement was only observed at the 14 day time point. It is unlikely that the hydrocephalus developed transiently in all kaolin-injected rats and reduce to normal levels by 28 days and has not been described in any other studies. Therefore it can be assumed that hydrocephalus did not develop in the 28 day rats. During the injection the needle is advanced until resistance is felt, however the needle may have gone too far and injected kaolin between the dura mater and the bone. This could account for the variation in the induction of hydrocephalus as kaolin injected between the dura mater and bone would have no effect on subarachnoid fibrosis.

In addition, levels of TGF-β in the ependyma were similar between the saline and kaolin injected rats. Although care was taken to minimise brain damage, the needle could still cause an injury and induce bleeding around the olfactory bulbs. As this bleeding is not controlled it could also occur in the saline injected rats and confound the assessment of TGF-β as it is released by activated platelets (Assoian *et al.,*1983).

Moreover, around the lesion site activated astrocytes, microglia and macrophages would produce TGF-β (Logan *et al*., 1992). These sources of TGF-β production could have contributed to the similar levels of ependymal TGF-β observed between the kaolin and saline injected rats. Altogether, this suggests the prechiasmatic cistern injection of kaolin is not a reliable or reproducible model of hydrocephalus.

3.4.2. Basal cisterns model of hydrocephalus

Most studies investigating hydrocephalus inject kaolin into the cisterna magna which produces obstructive non-communicating hydrocephalus. The basal cisterns model of hydrocephalus was adapted to model communicating hydrocephalus by injecting kaolin into the subarachnoid space at the base of the brain. It is a complicated technique as the basal cisterns are accessed through the atlanto-occipital membrane localised in the ventral region of the neck. In addition, the injections are performed blind as the surgeon is unable to see the end of the needle and therefore the risk of lesioning the brainstem is high (Li *et al*., 2008). However it results in an 80% hydrocephalus induction rate and the saline injection is a reliable control. In this study the basal cistern injection of kaolin reliably induced hydrocephalus. Although the basal cisterns injection technique is more complex compared to the prechiasmatic cistern route, it is more reliable and reproducible and therefore was used in further studies.

Moreover, the experiments were performed in 3-week old rats as neonates tolerate the induction of hydrocephalus better and produce a greater severity of hydrocephalus (Del Bigio and Enno, 2008). While most neonatal studies are conducted in 7 day old rats, they are quite small for the implantation of the osmotic mini pumps and

the brain cannulae required in these studies. Also there could be problems with the mother rejecting the pups or attempting to remove the brain cannulae. Rats are weaned at 3 weeks, therefore 3-week old rats were chosen for subsequent studies.

3.4.3. TGF-βs in hydrocephalus

TGF-β1 was only present at low levels in the meninges and the choroid plexus of the normal rat brain (Unsicker *et al*., 1991). After injury, TGF-β1 gene and protein expression were increased around the wound in macrophages, microglia and astrocytes for up to 14 days post lesion, with the levels highest in the first 2-3 days. Also the levels of TGF-β1 in the meninges and choroid plexus were increased (Logan *et al*., 1992). In a model of neonatal IVH, there was a correlation between ventricular enlargement and TGF-β1 levels in the brain. The hydrocephalus was also associated with increased levels of the ECM molecules laminin and fibronectin. In rats injected with either blood or artificial CSF without ventricular enlargement, patchy ependymal TGF-β1 immunostaining was observed at 14 days (Cherian *et al*., 2004).

In the study reported here, there was intense ependymal TGF-β1 staining detected in the rats with a saline injection into the prechiasmatic cistern. This suggests that the injury caused by the needle induced an increase in TGF-β1 staining in the ependyma. In the hydrocephalic rats from the both prechiasmatic and basal cisterns models, TGF-β1 immunostaining was observed in the ependyma periventricular white matter and al low levels in the cortex at 14 days. This is in agreement with the study by Cherian *et al.* (2004) who observed raised levels of TGF-β1 in the periventricular white matter, blood vessels and cortex after blood injection. In addition, Hatta *et al* (2006)

demonstrated that hydrocephalus was associated with TGF-β1 increases in macrophages in the subarachnoid space, meninges and choroid plexus. In the basal cisterns model of hydrocephalus it was apparent that TGF-β1 levels were higher in the Kaolin group compared to the Saline group. Together these results further support a role for TGF-β1 in the development of hydrocephalus.

3.4.4. *In vitro* rat meningeal cell cultures respond to TGF-β1 and Decorin

Adult rat brain meninges were removed and cultured to generate an enriched primary meningeal cell culture so that the fibrotic responsiveness of the cells to TGF-β1 and Decorin inhibition could be determined. The results demonstrated that in these primary cell cultures there was less than 5% contamination from non-fibroblast cells after 3-4 passages of the cell culture. Manwaring *et al*. (2001) also used this approach with cultured rat brain meningeal tissue from postnatal day 1 rats, and found that by 24 hours there was less than 15% cell contamination which was further reduced to 4% when the cells reached confluency.

The cultured meningeal fibroblasts responded to TGF-β1 by producing ECM molecules such as NG2 and this fibrogenic response was attenuated by human recombinant Decorin. These results confirm previous studies from our laboratory (Mahay, unpublished data) in which adult rat spinal cord meningeal cells in culture produced increased levels of NG2 protein in response to TGF-β2 and this response was attenuated with the addition of human recombinant Decorin. A similar modulation of the response to fibrogenic agents in cultured meningeal fibroblasts has been reported Minor *et al.* (2010). They demonstrated that decorin suppressed the meningeal fibroblast

levels of Semaphorin 3A, a molecule thought to be an inhibitor of axonal regeneration by promoting growth cone collapse. The results presented here demonstrated that this bioassay is very useful for assessing the efficacy of anti-fibrotic agents.

3.4.5. Conclusion

Although an injection of kaolin into the basal cisterns is more complex compared to the prechiasmatic cistern approach, it demonstrates better reliability and reproducibility compared to the prechiasmatic cistern model. Therefore, the basal cisterns model was used as a model of communicating hydrocephalus in the further studies. This preliminary study also demonstrated that primary rat meningeal cell cultures respond to TGF-β1 by producing ECM and that human recombinant Decorin was able to suppress the fibrogenic effects of TGF-β1. This suggests that human recombinant Decorin has the potential to reduce TGF-β1-induced fibrogenesis after an *in vivo* basal cistern injection of kaolin, thereby preventing the development of of communicating hydrocephalus.

Chapter 4

Decorin prevents the development of communicating hydrocephalus in juvenile rats

Published in

Hannah Botfield, Ana Maria Gonzalez, Osama Abdullah, Anders Daehli Skjolding, Martin Berry, James Pat McAllister II, Ann Logan. *Decorin prevents the development of juvenile communicating hydrocephalus.* Brain 2013 136: 2842-2858

4.1. Rationale

Post-haemorrhagic hydrocephalus develops because fibrosis in the subarachnoid space obstructs CSF drainage. Transforming growth factor-β1 (TGF-β1) plays a significant role in the development of fibrosis through promoting inflammation and extracellular matrix (ECM) deposition, and has also been implicated in the aetiology of post-haemorrhagic hydrocephalus. Therefore it was hypothesised that a TGF-β antagonist would be useful as a therapeutic agent to prevent the development of post-haemorrhagic hydrocephalus. The aim of this study was to test this hypothesis by investigating the effects of continuous intraventricular Decorin treatment on the development of kaolin-induced communicating hydrocephalus.

4.2. Experimental design

Kaolin was injected into the basal cistern to induce communicating hydrocephalus as described in section 2.3.3. In this model the kaolin does not obstruct the ventricular system (like in cisterna magna injections) but causes a cellular response that obstructs flow in the subarachnoid space, hence it relates more closely to the communicating hydrocephalus that develops after a haemorrhage. As TGF-β1 is continually produced by different cell types throughout the development of post-haemorrhagic fibrosis a bolus injection of Decorin may not be sufficient to inhibit TGF-β1. Therefore, immediately after kaolin injection, osmotic pumps were implanted subcutaneously and connected through a catheter to a cannula placed in the right lateral ventricle for continuous intraventricular infusion of either Decorin or phosphate buffered saline (PBS) vehicle for 14 days (**Fig**

4.1) as described in section 2.3.4. *In vivo* magnetic resonance imaging (MRI) was conducted after 14 days of treatment to assess the extent of hydrocephalus prior to sacrifice as described in section 2.9.1, followed by tissue collection and immunohistochemical analyses of the brain as described in sections 2.3.6. and 2.4.

Three week old rats were randomly assigned to 4 groups: (1), intact age-matched controls (Intact group, n=4), with no kaolin injection and no intraventricular infusion to obtain baseline data; (2), basal cistern kaolin injections only (Kaolin group, n=8) to evaluate the effects of subarachnoid kaolin without intraventricular cannulation and agent delivery; (3), kaolin injection with intraventricular infusion of PBS (Kaolin+PBS group; n=8), to determine the effect of vehicle delivery and ventricular cannulation on kaolin-induced subarachnoid fibrosis and ventriculomegaly; and (4), kaolin injection with intraventricular infusion of Decorin (Kaolin+Decorin group; n=8), to measure the effects of Decorin on kaolin-induced TGF-β levels, subarachnoid fibrosis, ventricular enlargement and brain damage caused by hydrocephalus.

Eight rats were excluded from the final analyses because they either did not develop hydrocephalus or because they died before the end of the study (**Table 4.1.**). Equal numbers of rats died in Decorin and non-Decorin treated groups, suggesting that the deaths were not Decorin related. Residual numbers in each group that were included in the analyses were as follows: Intact n=4, Kaolin n=5, Kaolin+PBS n=6, and Kaolin+Decorin n=5.

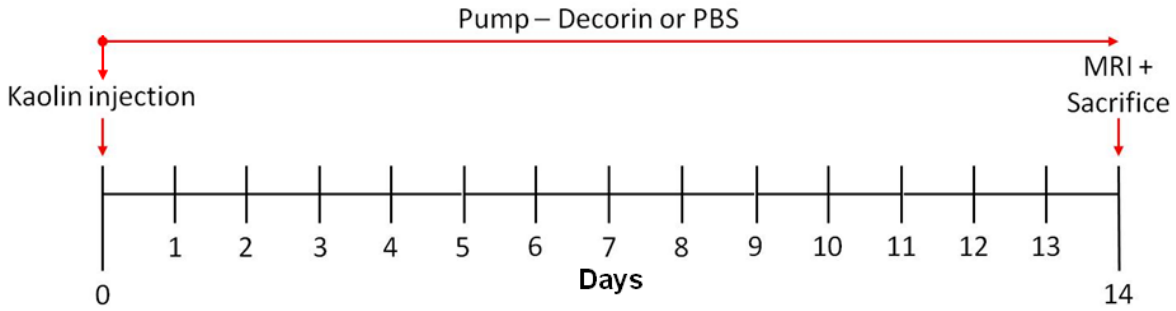

Figure 4.1. Experimental protocol. Kaolin was injected into the basal cisterns on day 0 followed immediately by implantation of the osmotic pump delivering either Decorin or PBS (control). Decorin or PBS was continually infused into the lateral ventricle for 14 days at which point MRI was conducted followed by sacrifice and tissue collection.

Animal	Group	Reason
1	Kaolin	Non responder (no hydrocephalus)
2	Kaolin	Non responder (no hydrocephalus)
3	Kaolin	Found dead (day 2)
4	Kaolin+PBS	Euthanised (day 6)
5	Kaolin+PBS	Euthanised (day 11)
6	Kaolin+Decorin	Euthanised (day 3)
7	Kaolin+Decorin	Found dead (day 6)
8	Kaolin+Decorin	Found dead (day 14 before MRI)

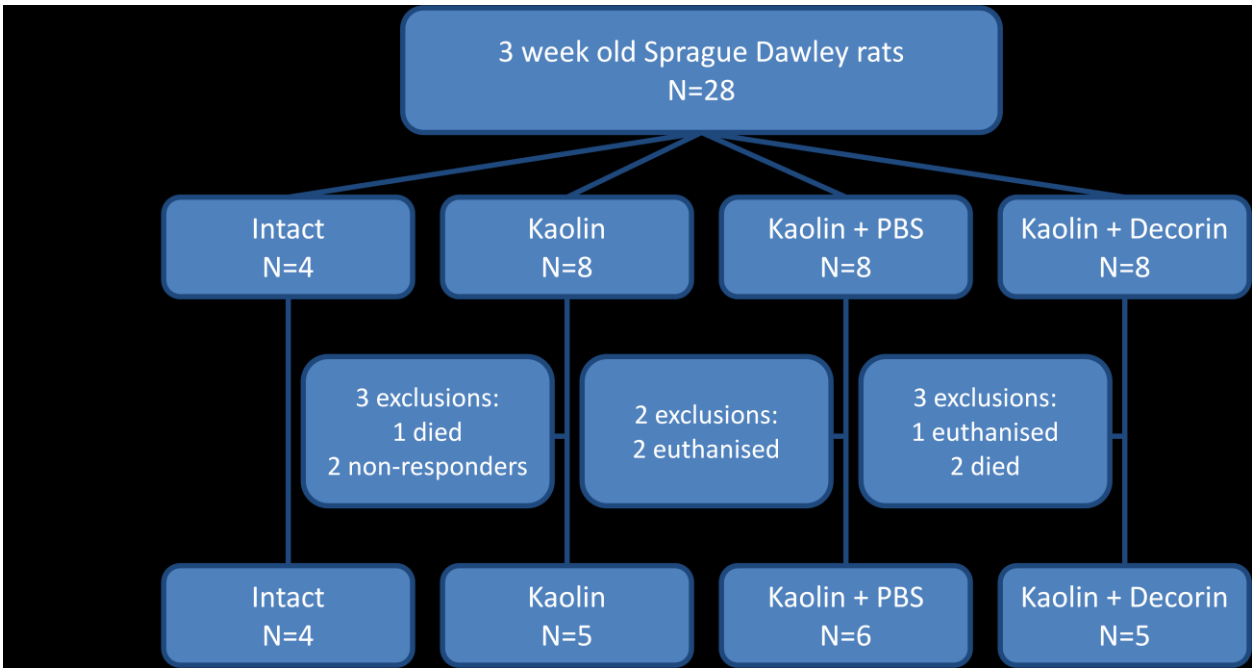

Table 4.1. Table of Animal exclusions and consort diagram. Eight animals were excluded from the study. Two animals from the Kaolin group did not develop hydrocephalus (had normal ventricular volumes) and were excluded from the analysis. Animals were euthanised if they showed severe adverse effects of treatment, including rapid weight loss, distress, lethargy and seizures.

4.3. Results

4.3.1. Decorin prevented the development of communicating hydrocephalus

The model used in this study was developed in adult rats but had not previously been optimised in neonatal or juvenile rats. In the present study hydrocephalus developed in 87% of juvenile rats in the Kaolin and Kaolin + PBS groups, which is comparable to the induction rate reported in adult rats by Li *et al* (2008). MRI demonstrated that, in the Kaolin and Kaolin+PBS groups, the lateral ventricles enlarged bilaterally through all anterior-posterior levels **(Fig. 4.2)** and had Evan's ratios of greater than 0.3. Ventricular volumes in the Kaolin and Kaolin+PBS groups were similar **(Fig. 4.3)**, indicating that cannulation of the ventricles did not affect the development of ventriculomegaly. Oedema was often observed posteriorly in the corpus callosum and periventricular white matter of hydrocephalic brains **(Fig. 4.2**.). In all groups the aqueduct of Sylvius and foramina of Luschka were patent, confirming the induction of communicating hydrocephalus and large kaolin deposits could be seen in the basal subarachnoid space in the Kaolin and Kaolin+PBS groups (not shown).

Hydrocephalus development was initially determined in all the animals in each group (baseline numbers; **Table 4.1**). Hydrocephalus was determined as either an Evan's ratio of greater than 0.3 or a ventricular volume of greater than 50mm^3 (in 2 cases hydrocephalus could not be determined and therefore they was classed as unknown). Significantly more rats (Kruskal Wallis test, P=0.003) developed hydrocephalus in the Kaolin and Kaolin+PBS groups compared to the Kaolin+Decorin group **(Table 4.2)**. The majority of studies into hydrocephalus do not include data on

animals that do not develop hydrocephalus after kaolin injection. Two rats in the Kaolin group demonstrated normal ventricular volumes which was most likely due to an unsuccessful kaolin injection into the basal cisterns and therefore were not included in the final analysis. In addition the main comparison will be between the Kaolin+PBS group and the Kaolin+Decorin group. Data from the animals that died or were euthanised were incomplete (lack of MRI scans and viable tissue) therefore further analysis was only conducted on the final numbers presented in **Table 4.1**.

Group	Hydrocephalic	Non-hydrocephalic	Unknown
Kaolin	5	2	1
Kaolin+PBS	8	0	0
Kaolin+Decorin	1	6	1

Table 4.2. Analysis of hydrocephalus development in all animals (including exclusions). Hydrocephalus was determined as either an Evan's ratio of greater than 0.3 or a ventricular volume of greater than 50mm^3. Significantly more rats (Kruskal Wallis test, P=0.003) were hydrocephalic in the Kaolin and Kaolin+PBS groups compared to the Kaolin+Decorin group.

After basal cistern injection of kaolin, ventricular volumes were significantly enlarged ($P<0.001$) in the Kaolin ($155.7\pm31.9mm^3$) and Kaolin+PBS ($198.3\pm92.9mm^3$) groups, compared to normal ventricular volumes measured in the Intact group ($10.9\pm1.0mm^3$). Also the Evan's ratio was significantly greater ($P<0.05$) in the Kaolin (0.39 ± 0.02) and Kaolin+PBS (0.38 ± 0.04) groups compared to the Intact group (0.27 ± 0.02). Decorin treatment prevented ventricular enlargement, so that the ventricular volume and the Evan's ratio in the Kaolin+Decorin group ($21.1\pm5.4mm^3$ and 0.27 ± 0.01 respectively) were indistinguishable from the normal values of the Intact group (**Fig. 4.2** and **Fig 4.3**). Thus, continuous Decorin infusion prevented the development of hydrocephalus after basal cistern injection of kaolin.

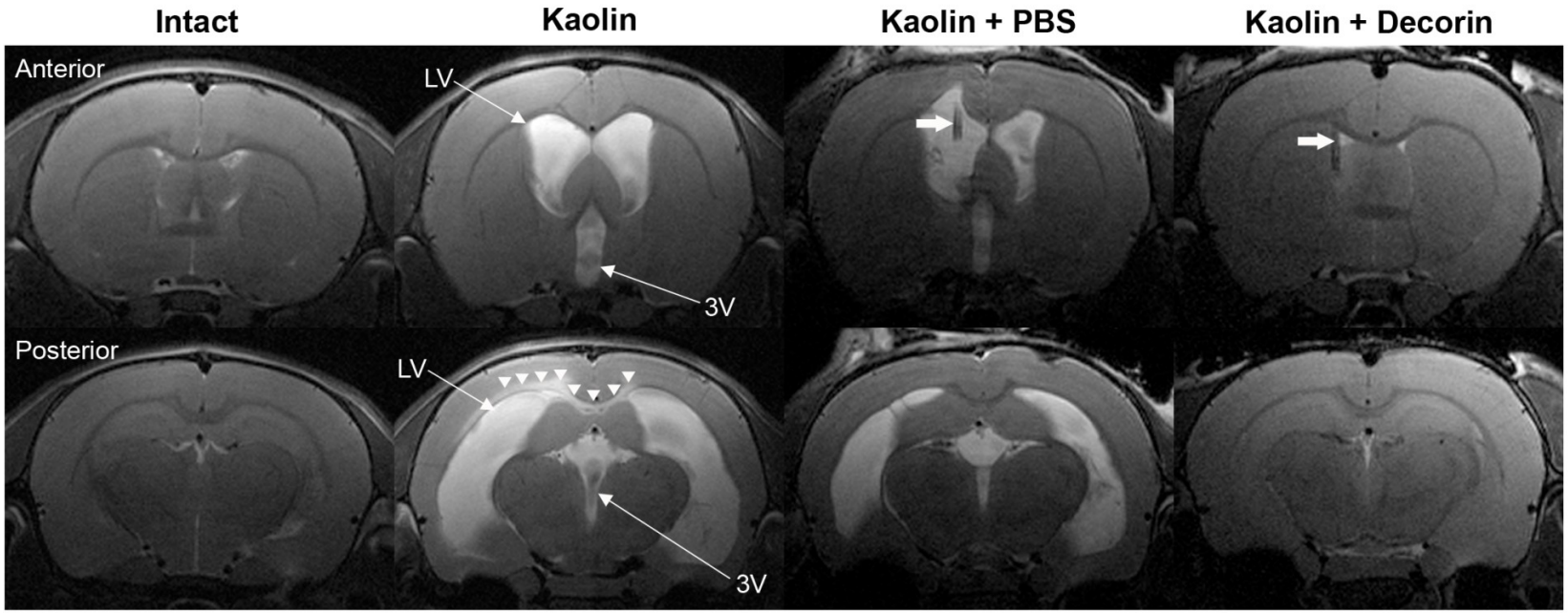

Figure 4.2. Representative coronal T-2 weighted MRI anterior and posterior images from Intact, Kaolin, Kaolin+PBS and Kaolin+Decorin groups. Ventriculomegaly developed in the Kaolin and Kaolin+PBS groups, however the ventricles in the Kaolin+Decorin group appeared similar to the Intact group. The intraventricular cannula (*bold arrow*), delivering either Decorin or PBS, is seen within the right lateral ventricle. White matter oedema was often observed in the hydrocephalic animals (*arrowheads*). LV – lateral ventricle; 3V – third ventricle.

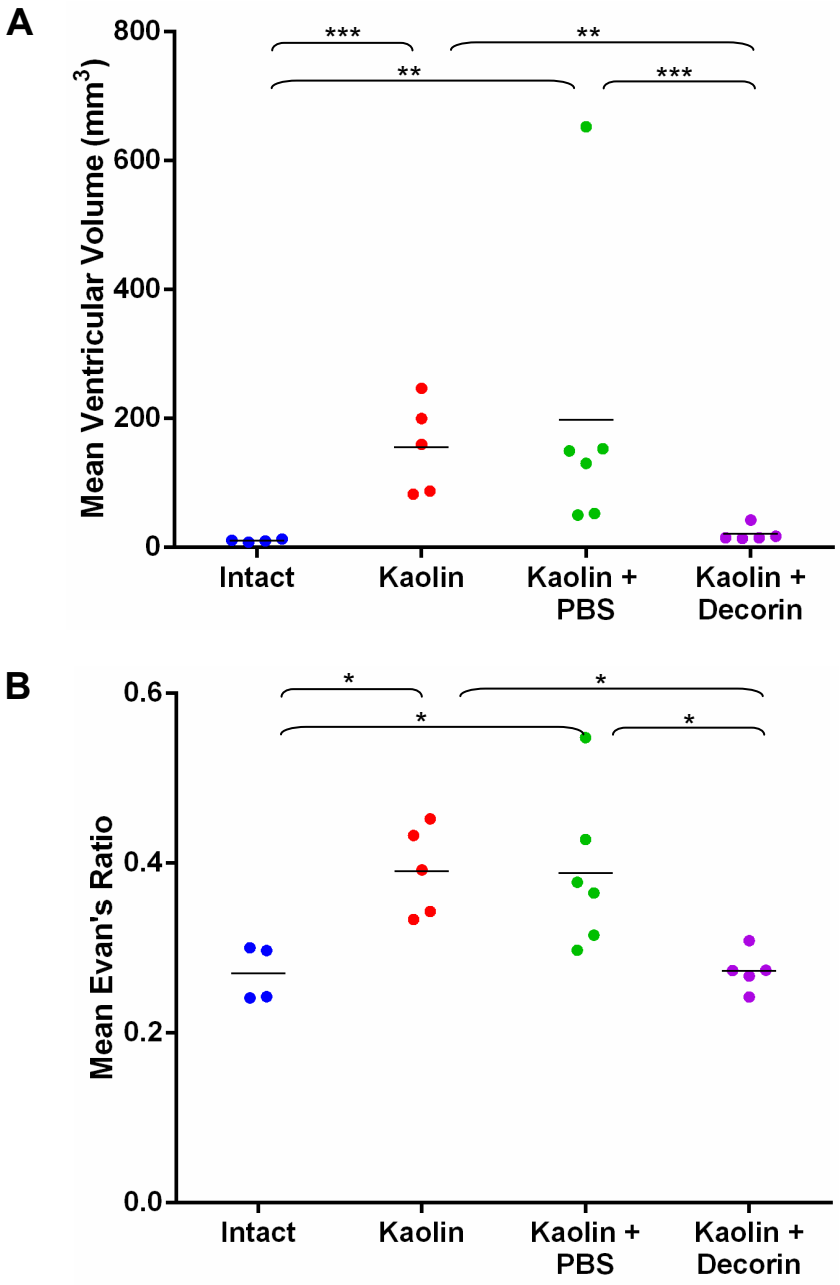

Figure 4.3. Ventricular volume measurements and Evan's ratios. The scatter plots summarise the mean of the ventricular volumes **(A)** and Evan's Ratio **(B)** in the 4 groups. Ventriculomegaly that characterised the Kaolin and Kaolin+PBS groups did not develop in the Kaolin+Decorin group in which intact volumes/ratios were recorded. *P<0.05, ***P<0.001.

4.3.2. Decorin was delivered throughout the entire ventricular system and basal subarachnoid space

MRI located the cannula in the frontal horn of the right lateral ventricle **(Fig. 4.2)**. There was no positive human Decorin staining in the brains of Intact, Kaolin and Kaolin+PBS groups, as illustrated in the Intact group **(Fig. 4.4.A)**. By contrast, in the Kaolin+Decorin group, Decorin staining was observed throughout the ventricular system on the apical surface of the choroid plexus epithelium and lateral ventricle ependymal cells **(Fig. 4.4.B, C)**. Decorin staining was also abundant in the basal cisterns through the entire rostral-caudal axis of the brain, especially in the basement membranes of subarachnoid vessels and in the meninges over the cortex **(Fig. 4.4.D)**. The wide distribution of Decorin throughout the subarachnoid space confirmed successful delivery.

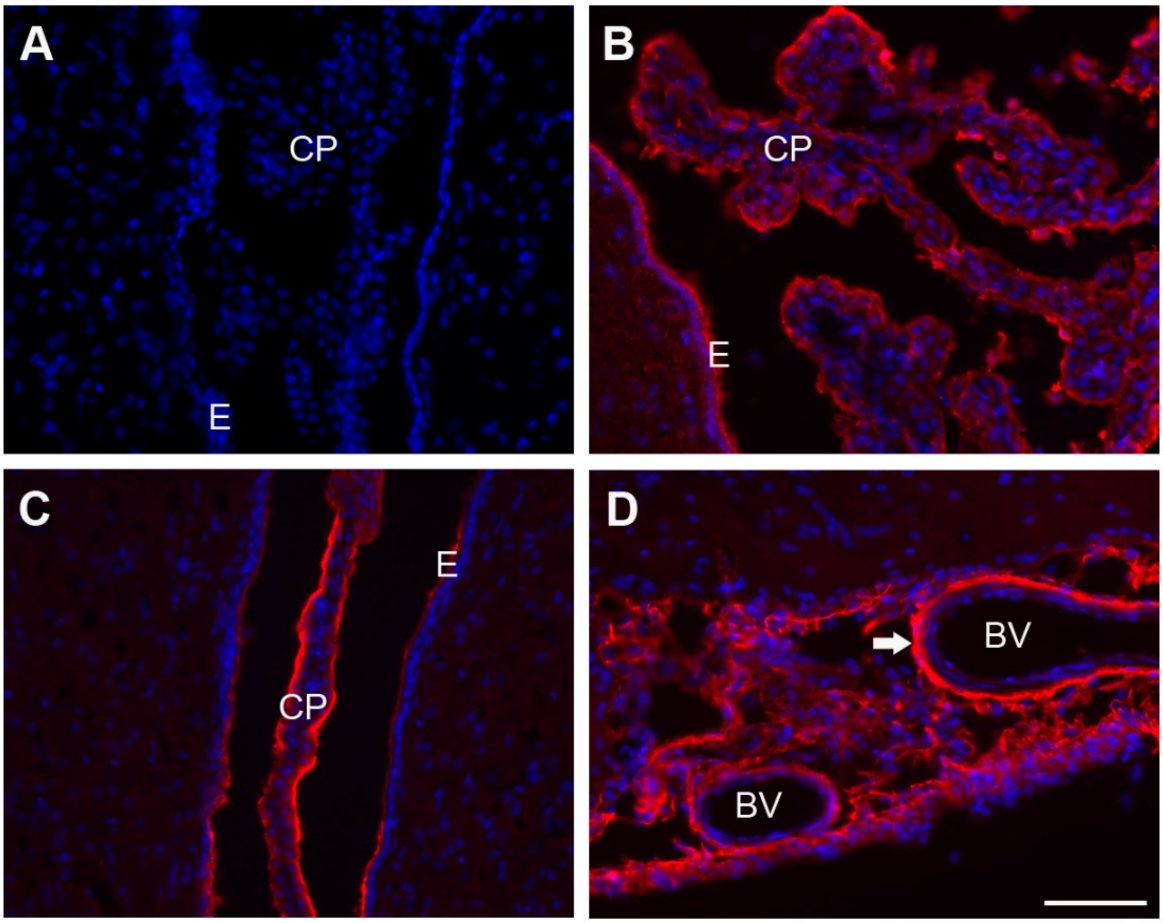

Figure 4.4. Distribution of human Decorin in the brain and subarachnoid space in the Kaolin+Decorin group. No human Decorin was detected in the lateral ventricles of Intact rats **(A)**. In the Kaolin+Decorin group, Decorin staining (*red*) was observed on the apical surface of the choroid plexus epithelial and ependymal cells in the ipsilateral **(B)** and contralateral ventricles **(C)**. Decorin staining was also detected in the basal subarachnoid space **(D)**, with intense staining in the basement membranes of the arachnoid vasculature (*arrow*). DAPI (*blue*) was used as a generic nuclear marker; scale bar – 100μm; CP – choroid plexus; E – ependyma; BV – blood vessel.

4.3.3. Decorin reduced TGF-β1 staining intensity in the ependyma

Decorin is a TGF-β antagonist therefore it is important to first characterise TGF-β1 in the hydrocephalic brain and then determine whether Decorin influences TGF-β1 levels. In the Intact group, there was weak cytoplasmic TGF-β1 staining of the ependymal and choroid plexus epithelium cells in the lateral ventricles **(Fig. 4.5.A)**, and strong staining of meningeal cells and cells of the ependyma in the third ventricle (not shown). In the Kaolin and Kaolin+PBS groups, there was more intense TGF-β1 staining in ependymal and sub-ependymal cells **(Fig. 4.5.B,C)**, macrophages and fibroblasts within sites of subarachnoid fibrosis and in occasional astrocytes and oligodendrocytes in the corpus callosum (data not shown). The intensity of ependymal TGF-β1 staining (arbitrary units of pixel intensity) in the Kaolin (40.5±4.2) and Kaolin+PBS (44.0±5.6) groups was statistically greater ($p<0.05$) compared to the Intact group (21.6±2.3). The intensity of TGF-β1 staining in the ependyma of the Kaolin+Decorin (23.3±1.2) group was indistinguishable from that in the Intact group, and significantly lower than in the Kaolin and Kaolin+PBS groups indicating widespread antagonism of the kaolin-induced cytokine elevation by Decorin **(Fig. 4.5.D, E)**. There was also a high frequency of TGF-β1 positive macrophages in areas of subarachnoid fibrosis in the Kaolin and Kaolin+PBS groups, but numbers were much lower in the Kaolin+Decorin group **(Fig. 4.6)**. Thus, Decorin prevented both the increase in ependymal TGF-β1 and the ingress of TGF-β1 positive macrophages into the subarachnoid space after Kaolin injection into the basal cistern.

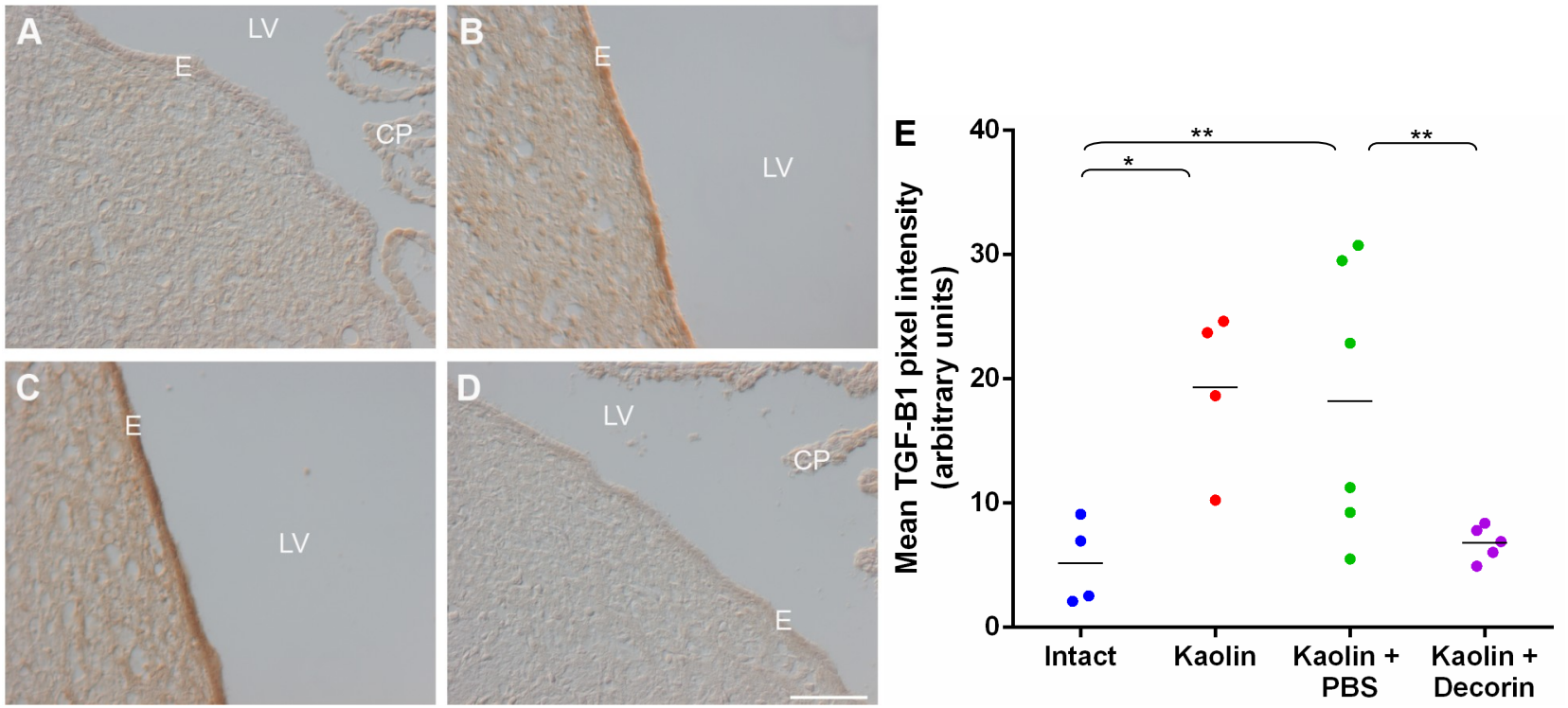

Figure 4.5. TGF-β1 staining in the ependyma. Representative images of ependymal TGF-β1 staining in Intact **(A)**, Kaolin **(B)**, Kaolin+PBS **(C)** and Kaolin+Decorin **(D)** groups. **(E)** Scatter plot of mean TGF-β1 pixel intensities in the 4 groups. The normal constitutive levels of TGF-β1 that were observed in the Intact group were significantly increased in the ependyma of the Kaolin and Kaolin+PBS groups, however TGF-β1 staining in the Kaolin+Decorin group remained at the constitutive levels seen in Intact group. Scale bar – 100μm; *P<0.05; **P<0.01; CP – choroid plexus; E – ependyma; LV – lateral ventricle.

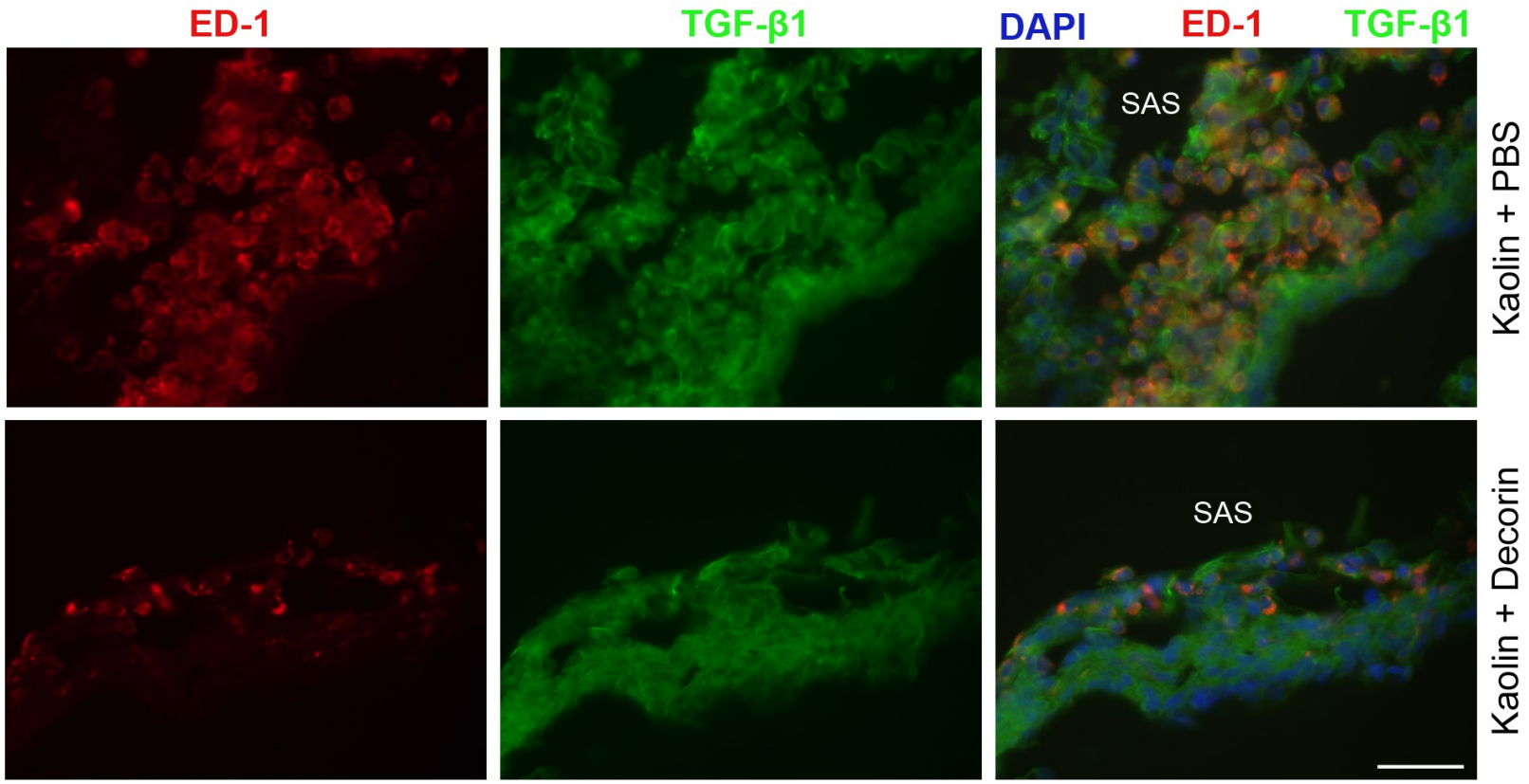

Figure 4.6. TGF-β1 staining in macrophages in the subarachnoid space. In areas of subarachnoid fibrosis, there was a high frequency of ED-1 positive macrophages (*red*) that also stained positive for TGF-β1 (*green*) in the Kaolin and Kaolin+PBS (top panels) groups compared to markedly lower numbers in the Kaolin+Decorin group (bottom panels). DAPI (*blue*) was used as a generic nuclear marker; scale bars – 200μm; SAS – subarachnoid space.

4.3.4. Decorin reduced Smad2/3 phosphorylation in the ependyma

The widespread bioactivity of intraventricular Decorin against TGF-β1 was also reflected by differences in elements of the TGF-β intracellular signalling cascades. Accordingly, patterns of phosphorylated Smad 2/3 (pSmad2/3) staining of meningeal, choroid plexus epithelial and ependymal cells were similar to those of TGF-β1 staining. Thus, ependymal cell pSmad2/3 staining was weak and cytoplasmic in the Intact group and more intense, especially at apical surfaces of ependymal cells in the lateral ventricles of the Kaolin and Kaolin+PBS groups **(Fig. 4.7.A-D)**. The intensity of ependymal pSmad2/3 staining (arbitrary units of pixel intensity) in the Kaolin (37.7±2.7) and Kaolin+PBS (36.8±0.8) groups was statistically greater ($p<0.001$) compared to the Intact group (15.2±3.5). The intensity of pSmad2/3 staining in the ependyma of the Kaolin+Decorin (19.0±3.0) group was indistinguishable from the Intact group **(Fig. 4.7.E)**. This finding suggests that Decorin suppressed TGF-β receptor activation and the induction of downstream Smad2/3 signalling.

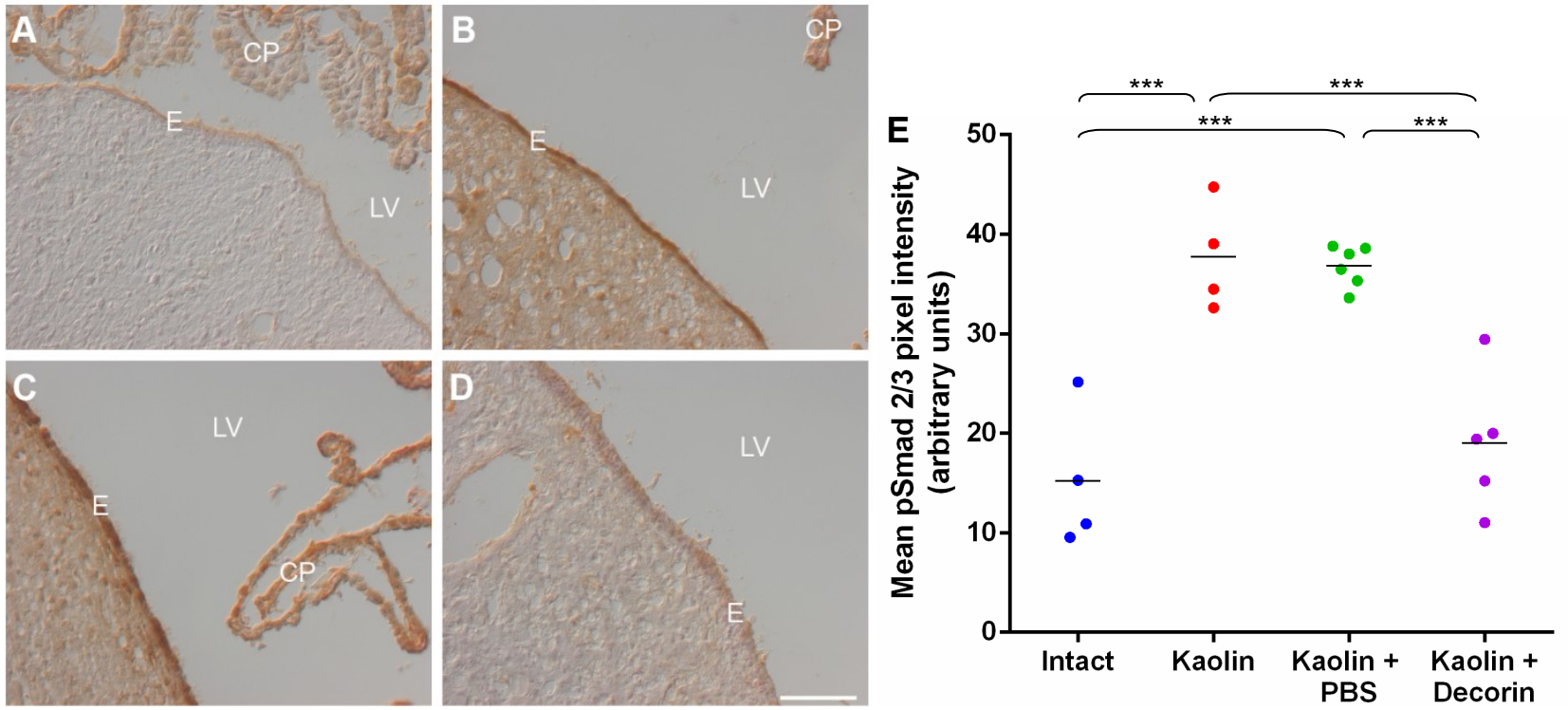

Figure 4.7. Phosphorylated Smad 2/3 staining in the ependyma. Representative images of ependymal pSmad2/3 staining in Intact **(A)**, Kaolin **(B)**, Kaolin+PBS **(C)** and Kaolin+Decorin **(D)** groups. **(E)** Scatter plot of mean pSmad2/3 pixel intensity in the 4 groups. After induction of hydrocephalus, there was an increase in pSmad2/3 levels in the Kaolin and Kaolin+PBS groups, however pSmad2/3 staining in the Kaolin+Decorin group remained at the constitutive levels seen in the intact group. Scale bar – 100μm; ***P<0.001; CP – choroid plexus; E – ependyma; LV – lateral ventricle, pSmad2/3 – phosphorylated Smad2/3.

4.3.5. Decorin reduced astrogliosis and fibrosis in the subarachnoid space

Astrogliosis and fibrosis in the subarachnoid space have not previously been examined in this model of hydrocephalus, therefore glial fibrillary acidic protein (GFAP) levels and the deposition of ECM such as molecules laminin and fibronectin in the subarachnoid space was investigated. In the Intact group, laminin immunostaining was present in thin strands of ECM in the subarachnoid space and vascular basement membranes. Laminin and GFAP co-immunostained the glial limitans externa **(Fig. 4.8)**. In both the Kaolin and Kaolin+PBS groups at 14 days post-kaolin injection, the deposition of laminin extended throughout the basal subarachnoid space into which GFAP positive astrocytic processes infiltrated **(Fig. 4.8)** where the glial limitans externa was disrupted. The laminin staining in the subarachnoid space of the Kaolin+Decorin group was similar to that seen in the Intact group, largely confined to the glial limitans and vascular basement membranes. Laminin deposits were also present on the apical surface of ependymal cells in the Kaolin and Kaolin+PBS groups (data not shown), but not in the Intact or Kaolin+Decorin groups. By 14 days a dense disorganised network of fibronectin was deposited in the fibrosed subarachnoid space of Kaolin and Kaolin+PBS groups but was absent from the Intact and Kaolin+Decorin groups **(Fig. 4.9)**. Thus, Decorin prevented astrogliosis, ECM deposition and fibrosis in the subarachnoid space of Kaolin-treated rats.

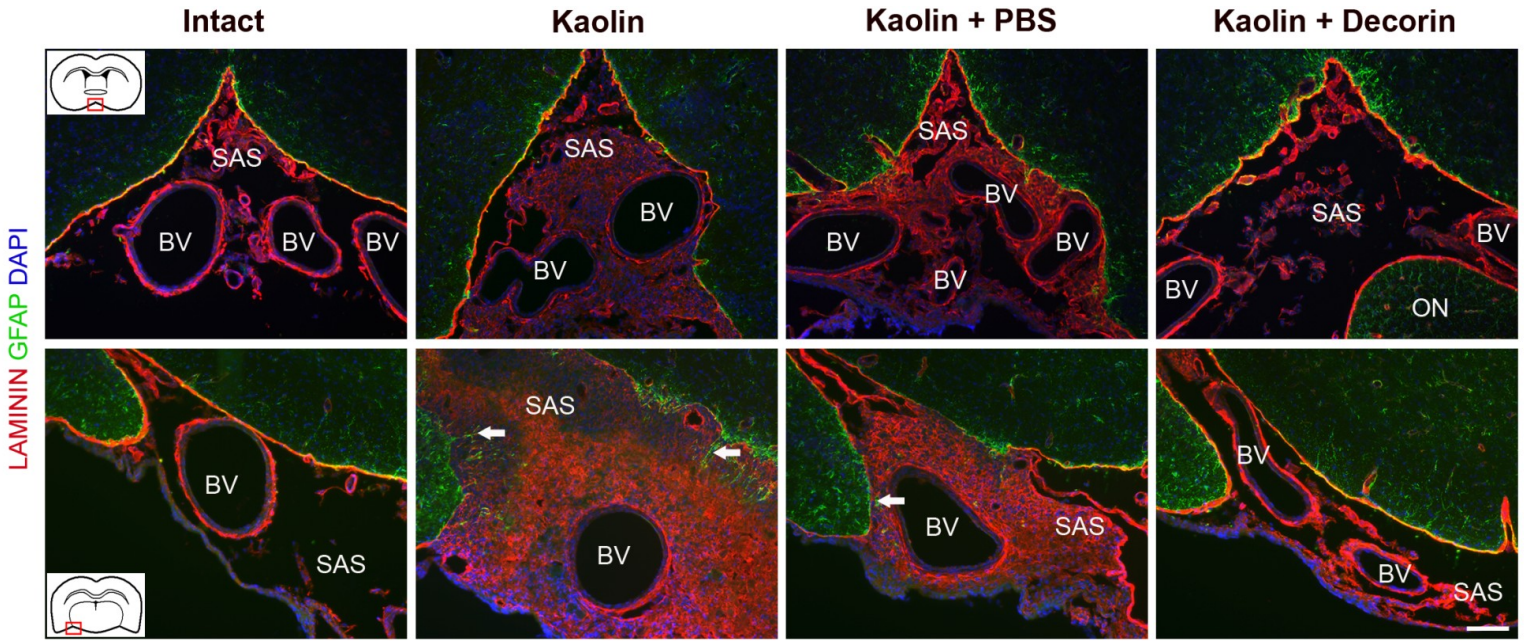

Figure 4.8. Laminin deposition in the subarachnoid space. Images of coronal sections of brain illustrating areas of fibrosis in the basal subarachnoid space. In the figure, panels in the upper row show sections taken at the level of Bregma and in the lower row at a level 5mm posterior to Bregma (see inserts); boxed areas in the inserts indicate the areas of basal subarachnoid space selected for analysis and illustrated in each row. Representative images show more laminin (*red*) staining in areas of fibrosis in the basal subarachnoid space in the Kaolin and Kaolin+PBS groups compared to the Intact and Kaolin+Decorin groups. In the Kaolin and Kaolin+PBS groups, GFAP positive (*green*) astrocytic processes (*arrows*) penetrated fibrotic areas. DAPI (*blue*) was used as a generic nuclear marker; scale bars – 100μm; BV – blood vessels; SAS – subarachnoid space; ON – optic nerve.

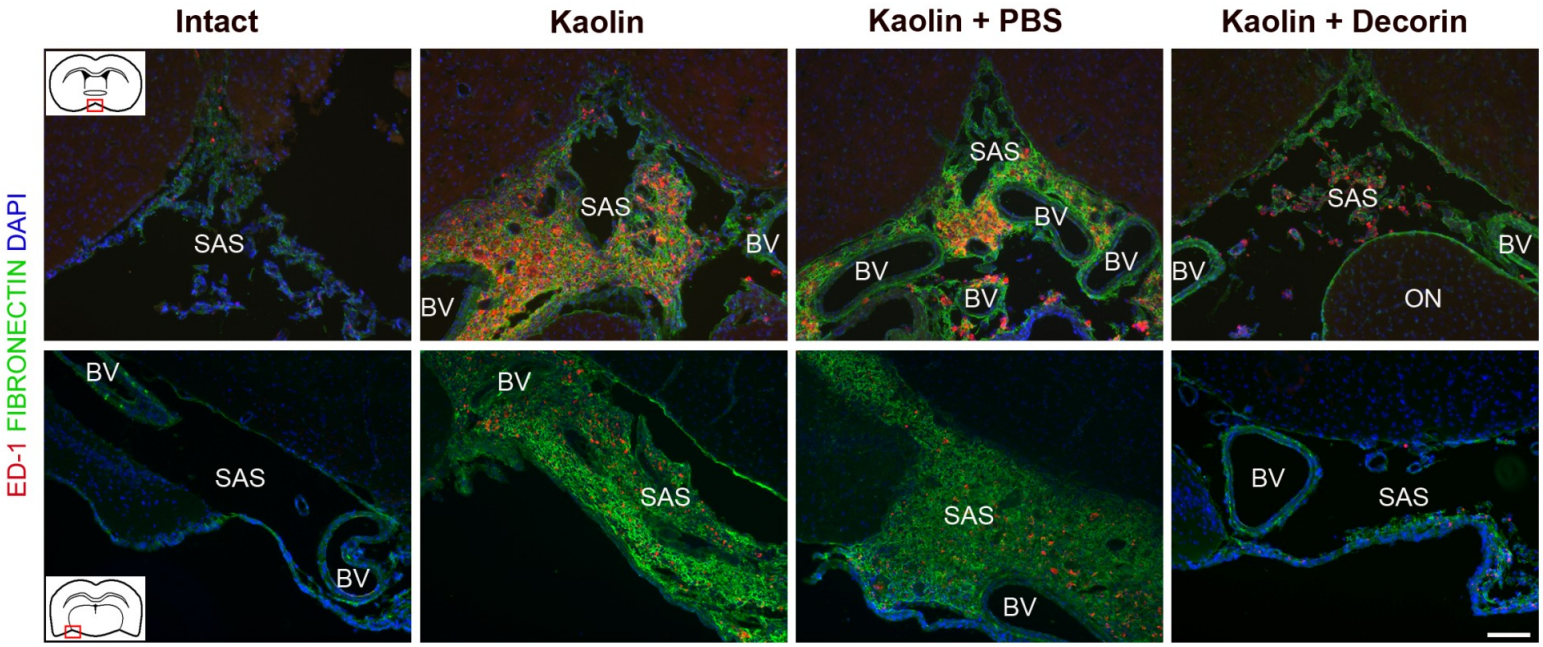

Figure 4.9. Fibronectin deposition in the subarachnoid space. Images of coronal sections illustrating areas of fibrosis in the subarachnoid space. In the figure, panels in the upper row show sections taken at the level of Bregma and in the lower row at a level 5mm posterior to Bregma (see inserts); boxed areas in the inserts indicate the areas of basal subarachnoid space selected for analysis and illustrated in each row. Fibronectin (*green*) staining was increased in the fibrosed subarachnoid space of Kaolin and Kaolin+PBS groups compared to the Intact and Kaolin+Decorin groups. ED1 positive macrophages (*red*) amassed in the fibrotic areas of the Kaolin and Kaolin+PBS groups but few invaded the subarachnoid space of the Kaolin+Decorin group. DAPI (*blue*) was used as a generic nuclear marker; scale bars – 100μm; BV – blood vessels; SAS – subarachnoid space; ON – optic nerve.

4.3.6. Decorin protected against hydrocephalus-induced brain damage

There are various pathological consequences of hydrocephalus, including astrogliosis and reactive microglia within compromised neural tissue. Therefore, it was important to determine whether Decorin treatment had any effect on hydrocephalic brain damage. GFAP is a marker of astrocytes and is upregulated during reactive astrogliosis. After induction of hydrocephalus, the levels of GFAP immunostaining (percentage of immunofluorescent pixels per area) in both the corpus callosum and periventricular white matter were higher in the Kaolin (7.0±2.4% and 10.7±1.9%, respectively) and Kaolin+PBS (11.6±4.7% and 12.8±4.40%, respectively) groups compared to the Intact group (1.7±0.7% and 1.9±0.4%, respectively). The levels of GFAP immunostaining in the Kaolin+Decorin group (1.0±0.3% and 1.4±0.4%, respectively) were similar to the normal levels observed in the Intact group **(Fig. 4.10.A,B)**. In the corpus callosum, perivascular basement membrane laminin staining was increased in the Kaolin and Kaolin+PBS groups compared to the Kaolin + Decorin group **(Fig. 4.11)**. Also, in the Kaolin and Kaolin+PBS groups, OX-42 positive microglia accumulated in areas adjacent to ependymal rupture in the walls of the expanded lateral ventricles **(Fig. 4.12)** demonstrating a distinctive amoeboid morphology with shortened, thicker processes characteristic of activated microglia. Numerous ED-1 positive haematogenous macrophages accumulated in areas of fibrosis in the subarachnoid space in the Kaolin and Kaolin+PBS groups but very few macrophages immigrated into the subarachnoid space of the Kaolin+Decorin group **(Fig. 4.9)**. These findings are consistent with the hypothesis that Decorin protects against ventriculomegaly and the development of hydrocephalus associated pathology.

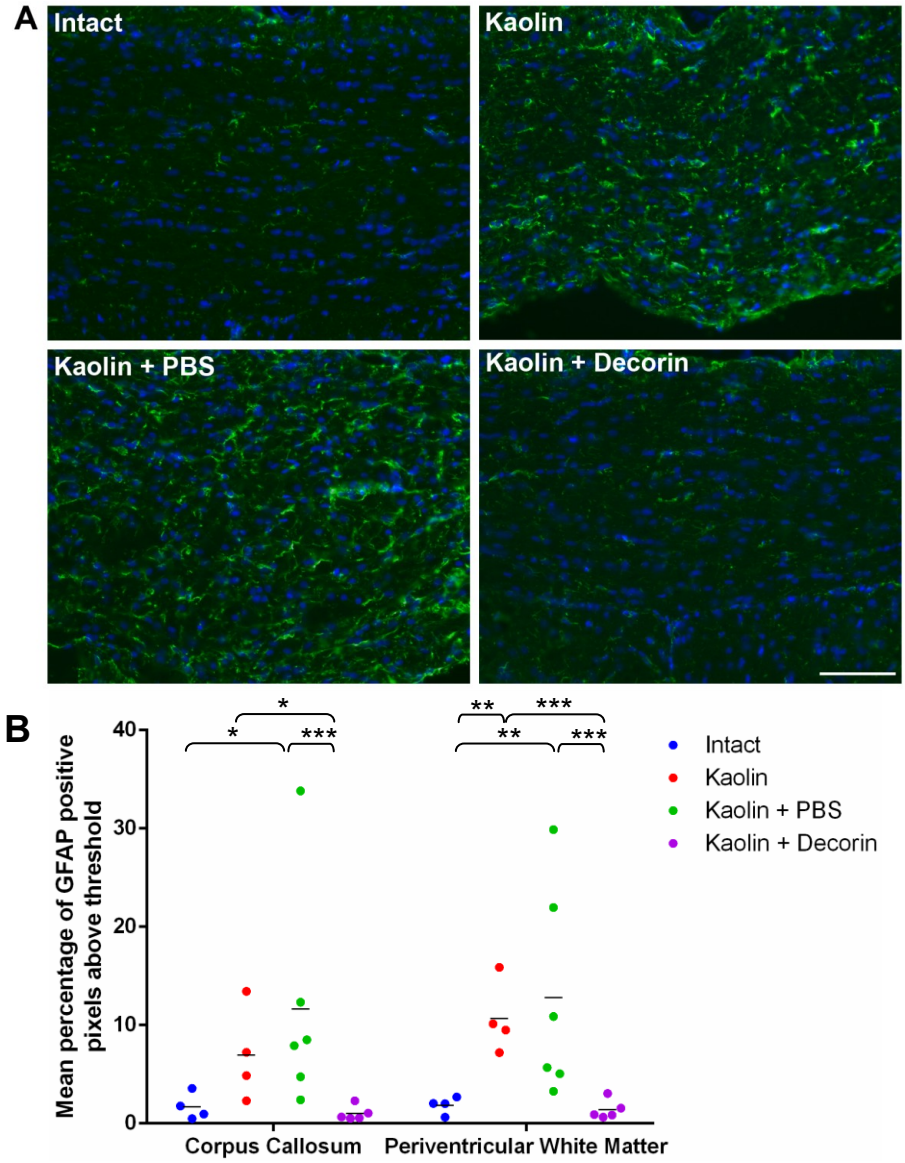

Figure 4.10. Astrogliosis in hydrocephalic brains (A) Representative images of GFAP positive staining (*green*) in the corpus callosum of the 4 treatment groups. **(B)** Scatter plot of the mean percentage GFAP positive staining in the corpus callosum and periventricular white matter in the 4 groups. Above normal levels of GFAP were observed in the Kaolin and Kaolin+PBS groups, whilst normal constitutive levels were maintained in the Kaolin+Decorin group. DAPI (*blue*) was used as a generic nuclear marker; scale bar – 100μm; *P<0.05, **P<0.01, ***P<0.001.

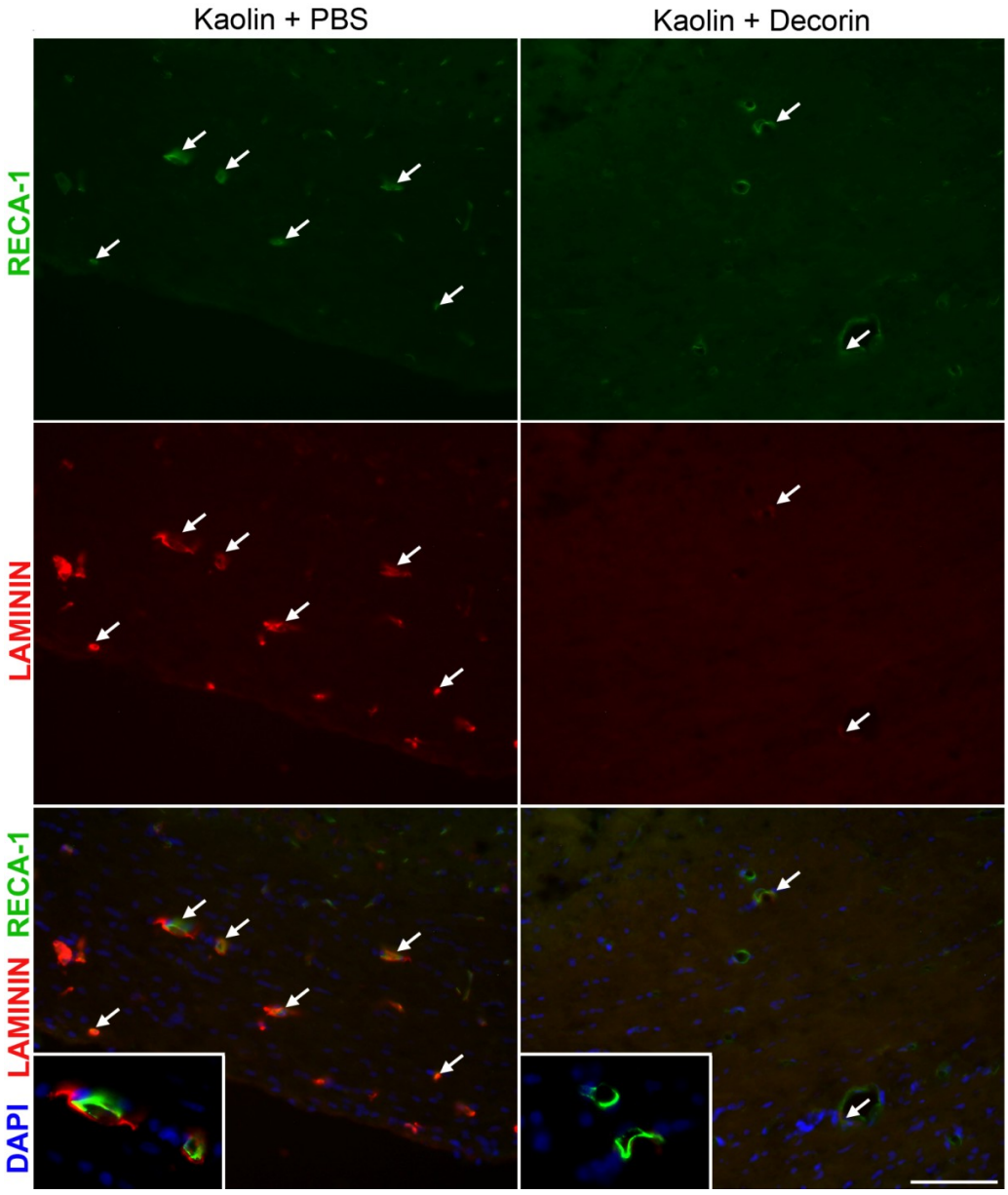

Figure 4.11. Laminin staining associated with blood vessels in the corpus callosum. (A) In the corpus callosum of the Kaolin and Kaolin+PBS groups there was intense perivascular laminin staining (*red*) around RECA-1 positive (*green*) vessels (white arrows) compared to the weak laminin staining seen in the vasculature of the Kaolin+Decorin group. DAPI (*blue*) was used as a generic nuclear marker; scale bar – 100µm.

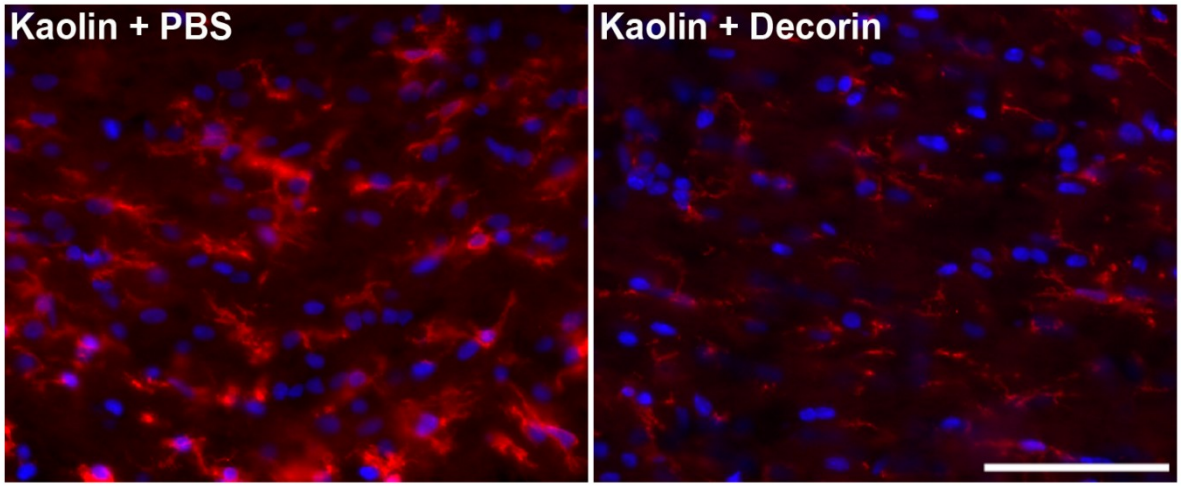

Figure 4.12. Reactive microglia in hydrocephalic brains. Increased OX-42 (*red*) staining reflecting microglia activation was observed in the periventricular white matter of the Kaolin and Kaolin+PBS groups, especially in areas where the ependyma was lost in the expanding lateral ventricles, was not apparent in the brains of the Kaolin+Decorin group. DAPI (*blue*) was used as a generic nuclear marker; scale bar – 50μm.

4.4. Discussion

This study demonstrated that continuous intraventricular delivery of human recombinant Decorin prevented the development of ventriculomegaly in a kaolin model of juvenile communicating hydrocephalus. Moreover, Decorin treatment was associated with reduced laminin and fibronectin deposition, inflammation and astrogliosis, showing that Decorin prevents the development of fibrosis and protects against hydrocephalic brain damage. Furthermore, in the hydrocephalic animals, the kaolin-induced increase in subarachnoid fibrosis was associated with raised levels of TGF-β/Smad2/3 signalling, whereas Decorin treatment suppressed a key stimulus for the development of subarachnoid fibrosis, maintaining normal levels of TGF-β/Smad2/3 signalling. These findings support the hypothesis that the arrested development of subarachnoid fibrosis, hydrocephalus and associated brain pathology are to some extent causally linked with Decorin-mediated blockade of TGF-β signalling, despite the range of Decorin influences described in the introduction (Chapter 1).

4.4.1. Induction of hydrocephalus in juvenile rats

MRI analysis confirmed that a basal cistern injection of kaolin induced hydrocephalus in 3-week old rats, whilst immunohistochemistry demonstrated that this was accompanied by inflammation plus fibronectin and laminin ECM accumulation in the subarachnoid space. Comparison of the Kaolin and Kaolin+PBS group data confirmed that the implanted intraventricular cannula did not ameliorate ventricular enlargement by shunting CSF subcutaneously. The combined incidence of induction of hydrocephalus in

the Kaolin and Kaolin+PBS groups was 87%, giving a projected incidence of induction of hydrocephalus in the Kaolin+Decorin group (n=5) of 4.3 rats. Thus, the normal ventricular volume in the Kaolin+Decorin group was attributed to the Decorin-induced suppression of hydrocephalus by blockade of subarachnoid fibrosis and not to either shunting effects or failure of the kaolin injection technique.

The relevance of the kaolin model of communicating hydrocephalus to clinical post-haemorrhagic communicating hydrocephalus has been demonstrated by observations that intraventricular or subarachnoid injection of blood generates a pattern of ventriculomegaly similar to that induced by kaolin (Suzuki *et al.,* 1977; Cherian *et al.,* 2004). The present study also corroborates the findings of Slobodian *et al.* (2007), demonstrating that kaolin injection causes acute inflammatory cell infiltration into the subarachnoid space, with subsequent phagocytosis of the kaolin granules by macrophages and deposition of ECM.

4.4.2. TGF-β's involvement in hydrocephalus

Low TGF-β levels occur in the CSF and brain parenchyma of healthy humans (Mogi *et al*., 1995; Krupinski *et al*., 1996; Flood *et al*., 2001) and rats (Unsicker *et al*., 1991; Logan *et al*., 1992). TGF-β1 levels are increased in the meninges, subarachnoid macrophages and choroid plexus after kaolin injection into the cisterna magna (Hatta *et al.,* 2006), in the CSF and choroid plexus of post-haemorrhagic communicating hydrocephalus patients, (Kitazawa *et al*., 1994; Whitelaw *et al*., 1999; Flood *et al*., 2001; Heep *et al*., 2004; Douglas *et al*., 2009) and in experimental intraventricular haemorrhage (IVH; Cherian *et al*., 2004). In this study the kaolin and Kaolin+PBS

groups showed upregulation of the TGF-β/Smad signalling throughout the ventricular system including the choroid plexus, suggesting that raised CSF levels of TGF-β mediate the progression from meningeal inflammation through to subarachnoid fibrosis. Although the Smad intracellular signalling pathway is central to the actions of the TGF-β family, TGF-β also signals through the mitogen-activated protein kinase (MAPK), Rho-like GTPase and phosphatidylinositol-3-kinase (PI3K)/AKT signalling pathways, which mediate a wide range of other cellular functions including epithelial-mesenchymal transition, activating fibroblasts and promoting ECM production (Zhang, 2009; Nakerakanti and Trojanowska, 2012). For example, in an experimental model of IVH, it was demonstrated that phosphorylated MAPK levels are increased in the ependymal and sub-ependymal glia (Cherian *et al.,* 2004), providing a possible alternative supplementary fibrogenic signalling pathway in hydrocephalus. In the studies described here, Decorin suppression of subarachnoid deposition of fibronectin and laminin after kaolin injection was linked to the maintenance of constitutive levels of TGF-β1 and down-stream Smad signalling. Since Decorin sequestration of TGF-β into ECM blocks all forms of TGF-β signalling, suppression of activation of non-Smad pathways also probably occurred in these studies.

4.4.3. Decorin and hydrocephalus

Aquilina *et al*. (2008) and Hoque *et al*. (2011) have reported no protection against ventriculomegaly in a neonatal rat model of IVH after administration of the TGF-β antagonists Perfenidone, Losartan, and Colchicine (administered by gavage) and Decorin (injected into the lateral ventricle 1 and 6 days after the induction of

hydrocephalus). One explanation for these findings could be that, since the former three reagents target TGF-β transcription, they were ineffective in neutralising translated TGF-β stored in platelet granules and released on haemorrhage. Platelet release accounts for the initial phase of the biphasic TGF-β surge in the CSF (Flood *et al*., 2001; Douglas *et al*., 2009) which initiates TGF-β-mediated subarachnoid fibrosis. Macrophages and monocytes subsequently immigrate into the CSF and release a second wave of TGF-β which is supplemented by a sustained supply from ependymal, choroid plexus epithelial and meningeal cell sources (Wahl *et al.,* 1989; Flood *et al.,* 2001). The two-bolus injection regime of Decorin, used by Hoque *et al*. (2011), was unlikely to have blocked sustained high levels of TGF-β production, since the findings from this study indicate that continuous delivery of Decorin was required for effective neutralisation of TGF-β signalling in the kaolin model of communicating hydrocephalus. The results presented here clearly suggest that initiation of continuous Decorin delivery immediately after basal cistern kaolin injection suppressed the development of hydrocephalus by blocking TGF-β signalling from the outset as a prophylactic treatment and thus maintained normal ventricular volumes.

4.4.4. Decorin prevents hydrocephalic induced brain pathology

Hydrocephalic brain damage developing from multiple insults, including compression, stretch, ischaemia and hypoxia, ultimately leads to periventricular oedema, demyelination, axonal degeneration, metabolic impairments, accumulation of metabolic waste products, gliosis and inflammation (Silva, 2004; McAllister, 2012). In the thinned corpus callosum and periventricular white matter of the hydrocephalic rats, MRI

detected oedema and immunohistochemistry demonstrated increased perivascular laminin and astrocytic GFAP staining. Similar increases in perivascular laminin staining have been seen in hydrocephalic transgenic mice over-expressing TGF-β1 (Wyss-Coray *et al.,* 1995) and in blood vessels local to brain lesions (Szabo and Kalman, 2004), suggesting similar mechanisms may affect the integrity of the blood brain barrier and contribute to the development of oedema in both these conditions.

Meningeal inflammation and progressive reactive astrogliosis and microgliosis in the periventricular matter are prevalent features of hydrocephalus (Fukumizu *et al*., 1996; Khan *et al.,* 2006; Del Bigio, 2010b; McAllister, 2012). Reactive astrogliosis in the brain is reflected by an upregulation of GFAP and hypertrophy of the astrocytic processes. After CNS injury, activated astrocytes may be beneficial in the acute stages but detrimental in the latter stages (Pekny and Nilsson, 2005). In hydrocephalus, ongoing reactive astrogliosis makes the brain less compliant, affecting shunt success, and could prevent axon regeneration and remyelination (McAllister, 2012). In the current study, GFAP positive staining increased in the corpus callosum and periventricular white matter after induction of hydrocephalus and this astrogliosis correlated with the magnitude of ventricular enlargement irrespective of treatment. These results extend previous research findings showing a positive correlation between the severity of ventriculomegaly and the mRNA and protein levels of GFAP (Yamada et al., 1992; Deren et al., 2010; Eskandari et al., 2011; Xu et al., 2012). Unlike sustained intraventricular infusion of Decorin that normalises gliosis and prevents oedema, shunting reduces but does not restore GFAP to normal levels (Miller and McAllister, 2007; Eskandari et al., 2011). Ependymal disruption of the enlarged ventricles of the

hydrocephalic rats was similar to that described by Del Bigio *et al*. (2010b) in post-haemorrhagic communicating hydrocephalus and associated with the underlying accumulation of reactive microglia.

4.4.5. Conclusion

In summary, continuous intraventricular Decorin infusion prevented the development of Kaolin-induced hydrocephalus by blockade of TGF-β-mediated subarachnoid fibrosis, protecting against the development of hydrocephalic brain damage. As post-haemorrhagic communicating hydrocephalus develops after a readily diagnosed haemorrhagic insult, it is likely that initiating Decorin delivery immediately after the bleed would block the effects of TGF-β signalling from the outset as a prophylactic rather than a curative treatment. Therefore, these findings demonstrate that sustained intraventricular Decorin is a potential therapeutic treatment that prevents the development of acute juvenile post-haemorrhagic communicating hydrocephalus and its associated morbidity. Further studies are required to investigate whether Decorin is also able to treat established hydrocephalus.

Chapter 5

Decorin suppresses the early kaolin-induced inflammatory and glial cell response in juvenile rats

Published in

Hannah Botfield, Ana Maria Gonzalez, Osama Abdullah, Anders Daehli Skjolding, Martin Berry, James Pat McAllister II, Ann Logan. *Decorin prevents the development of juvenile communicating hydrocephalus.* Brain 2013 136: 2842-2858

5.1. Rationale

Kaolin injected into the basal cisterns induces a robust inflammatory response in the subarachnoid space which leads to the development of fibrosis, astrogliosis and hydrocephalus. In the previous chapter it was demonstrated that Decorin prevented the development of kaolin-induced hydrocephalus in juvenile rats, probably by inhibiting TGF-β1 induced fibrosis. The aim of this study was to determine whether Decorin influenced the early inflammatory response after kaolin injection.

5.2. Experimental Design

Kaolin was injected into the basal cistern to induce communicating hydrocephalus in 3-week old rats as described in section 2.3.3. Immediately after kaolin injection, osmotic pumps were implanted subcutaneously and connected through a catheter to a cannula placed in the right lateral ventricle for continuous intraventricular infusion of either human recombinant Decorin or phosphate buffered saline (PBS) for 3 days as described in section 2.3.4. The rats were killed 3 days after kaolin injection, the brains removed and processed for histology and immunohistochemistry to assess the early cellular response to kaolin injection **(Fig. 5.1)** as outlined in sections 2.3.6. and 2.4. Rats were randomly assigned to 4 groups: Intact group n=4, Kaolin group n=5, Kaolin+PBS group n=3 and Kaolin+Decorin group n=5.

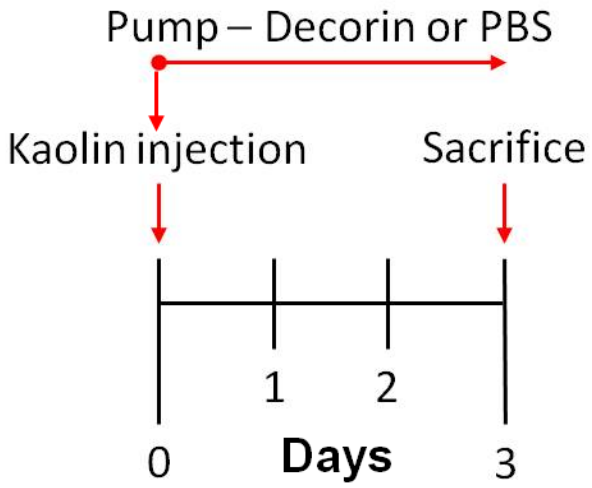

Figure 5.1. Experimental protocol. Kaolin was injected into the basal cisterns on day 0 followed immediately by implantation of an osmotic pump containing either human recombinant Decorin or PBS (control). Decorin or PBS was continuously infused into the lateral ventricle for 3 days, at which point the rats were sacrificed.

5.3. Results

5.3.1. Human Decorin was detected in the CSF

Human recombinant Decorin was infused into the lateral ventricles at a rate of 2.5µg/0.5µl/hour in the Kaolin+Decorin group. A human Decorin ELISA kit was used to measure the levels of human Decorin in the CSF removed from the rat cistern magna on day 3 as described in sections 2.3.5 and 2.5.2. The levels of human Decorin in the intact, Kaolin and Kaolin+PBS groups were negligible. Levels in the Kaolin+Decorin group ranged from 1.7ng/ml to 16.3ng/ml (mean of 8.6±3.0ng/ml; **Fig. 5.2)**. These results demonstrate the levels of Decorin achieved in the CSF through continuous infusion into the lateral ventricles.

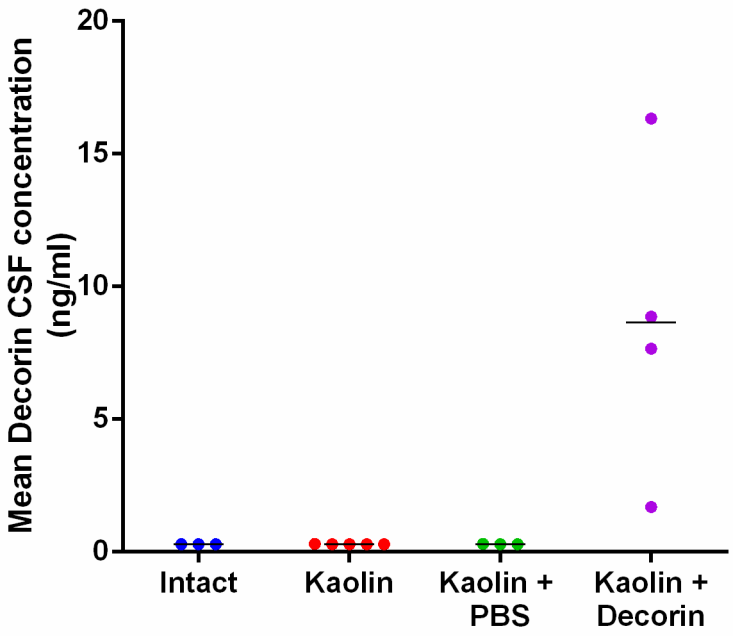

Figure 5.2. Human Decorin levels in the CSF. Scatter plot of the mean concentration of human Decorin in the rat CSF measured by ELISA. Human Decorin was only detected in the CSF after infusion of 2.5µg/0.5µl/hour into the lateral ventricles in the Kaolin+Decorin group.

5.3.2. Decorin reduced the kaolin-induced inflammatory response in the basal subarachnoid space

At 3 days, the basal subarachnoid space in the Kaolin and Kaolin+PBS groups contained thick kaolin deposits associated with a considerable accumulation of inflammatory cells including neutrophils, macrophages and eosinophils **(Fig. 5.3.A,C-E)**. Eosinophils were identified by their bright pink granules in the cytoplasm, Neutrophils by their multi-lobed nuclei and pale pink cytoplasm and macrophages had an acentric large round or kidney shaped nucleus surrounded by light bluish cytoplasm **(Fig. 5.4.A)**. The distribution of these cells within the basal subarachnoid space was not homogeneous. Eosinophils tended to form large accumulations in close proximity to meningeal blood vessels while numerous macrophages and neutrophils amassed on the edges of the kaolin deposits. Within kaolin deposits the cell density was considerably lower and while it was difficult to identify the cell types based on their morphology, the majority of them stained positive for ED-1 suggesting they were macrophages **(Fig. 5.5)**. Under the microscope kaolin appeared as reflective granules and could be observed within the cytoplasm of macrophages suggesting that phagocytosis of kaolin had begun within the first 3 days **(Fig. 5.4.B)**. In the Kaolin+Decorin group, the subarachnoid space appeared smaller, containing fewer inflammatory cells and only small kaolin deposits **(Fig. 5.3.B and 5.3.F-H)** compared to the Kaolin and Kaolin+PBS groups.

The relative percentages of eosinophils, neutrophils and macrophages in the subarachnoid space were similar between the Kaolin (1.7±0.6%, 22.2±1.9% and 13.7±0.9%, respectively), Kaolin+PBS (3.2±1.3%, 23.5±2.1% and 20.1±2.6%,

respectively) and Kaolin+Decorin groups (5.4±1.7%, 17.0±4.3% and 14.8±1.1%, respectively; **Fig. 5.4.C)**. In contrast, the extent of ED-1 positive staining (expressed as the percentage of immunofluorescent pixels in the subarachnoid space) showed a trend towards being lower in the Kaolin+Decorin group (10.6±1.0%) compared to the Kaolin (19.3±3.7%) and Kaolin+PBS groups (18.6±3.5%; **Fig. 5.5)**. These findings suggest that Decorin treatment suppressed the kaolin-induced inflammatory response from as early as day 3.

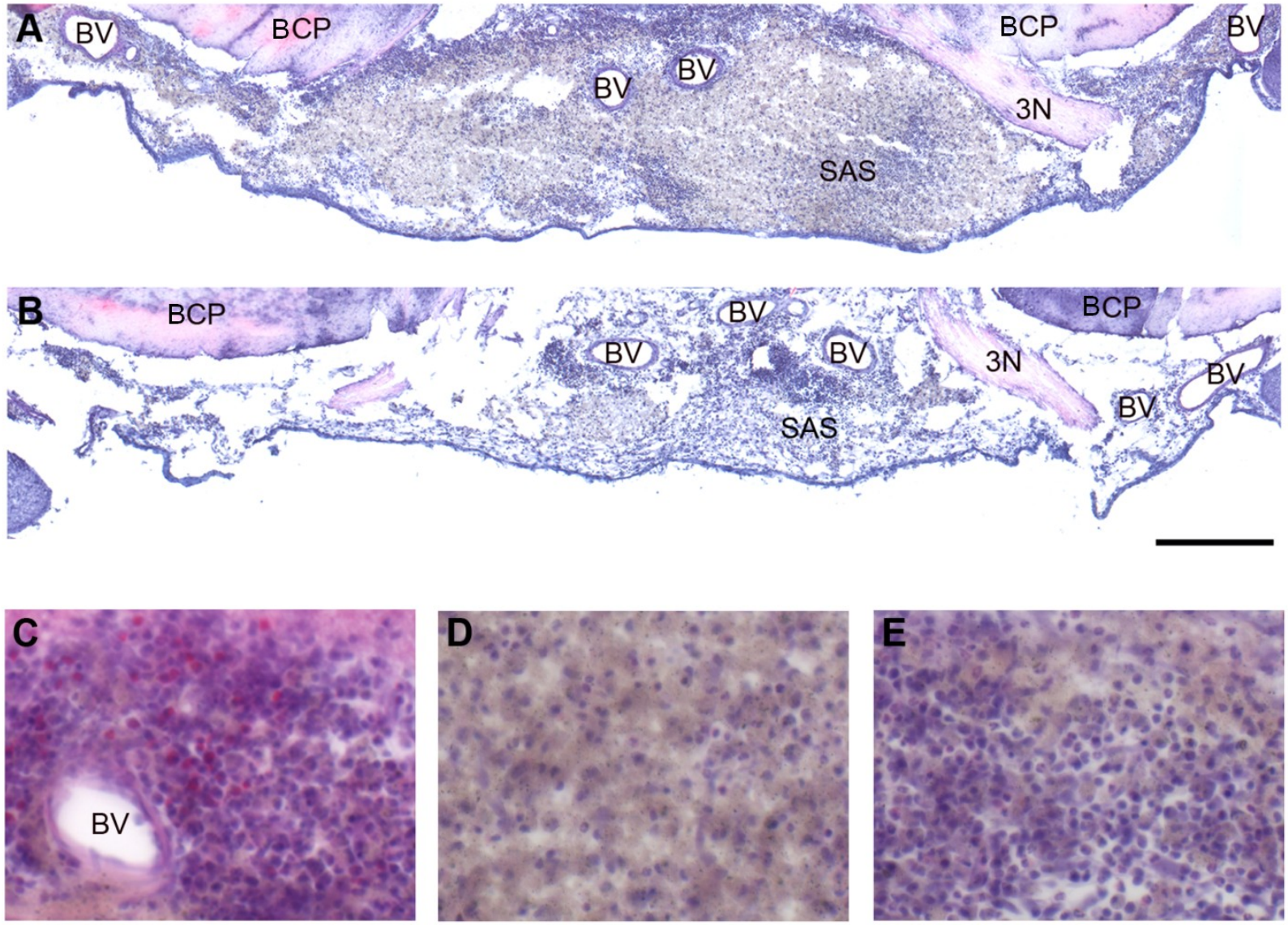
A
BV
BCP
BV
BV
BV
BCP
BV
3N
SAS
B
BCP
BV
BV
BV
BCP
3N
BV
BV
SAS
C
BV
D
E

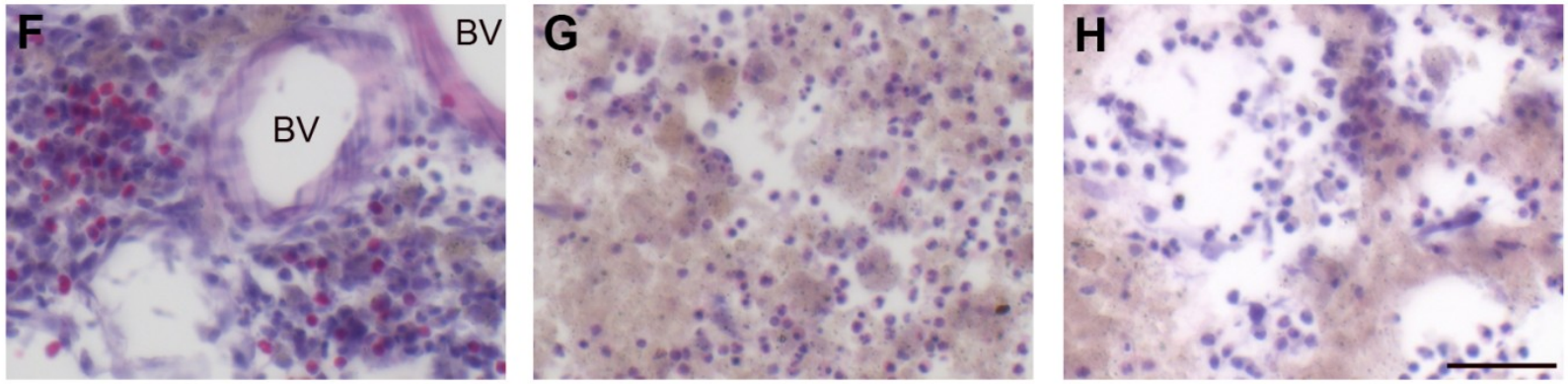

Figure 5.3. The basal subarachnoid space 3 days after kaolin injection. Representative composite images of the basal subarachnoid space from posterior coronal sections of the brain stained with H&E in the Kaolin+PBS **(A)** and Kaolin+Decorin **(B)** groups. The 6 lower panels show higher magnification images of the subarachnoid space from Kaolin+PBS **(C-E)** and Kaolin+Decorin **(F-H)** groups. In general, there were large accumulations of cells around blood vessels **(C+F)**, fewer cells embedded within kaolin deposits **(D+G)** and more cells amassing on the edges of the kaolin deposits **(E+H)** in both groups. However, the subarachnoid space in the Kaolin and Kaolin+PBS groups contained thicker kaolin deposits and greater accumulations of inflammatory cells compared to the Kaolin+Decorin group. Scale bars A-B – 500μm, C-H – 100μm; BCP – basal cerebral peduncle; BV – blood vessels; SAS – subarachnoid space; 3N – oculomotor nerve.

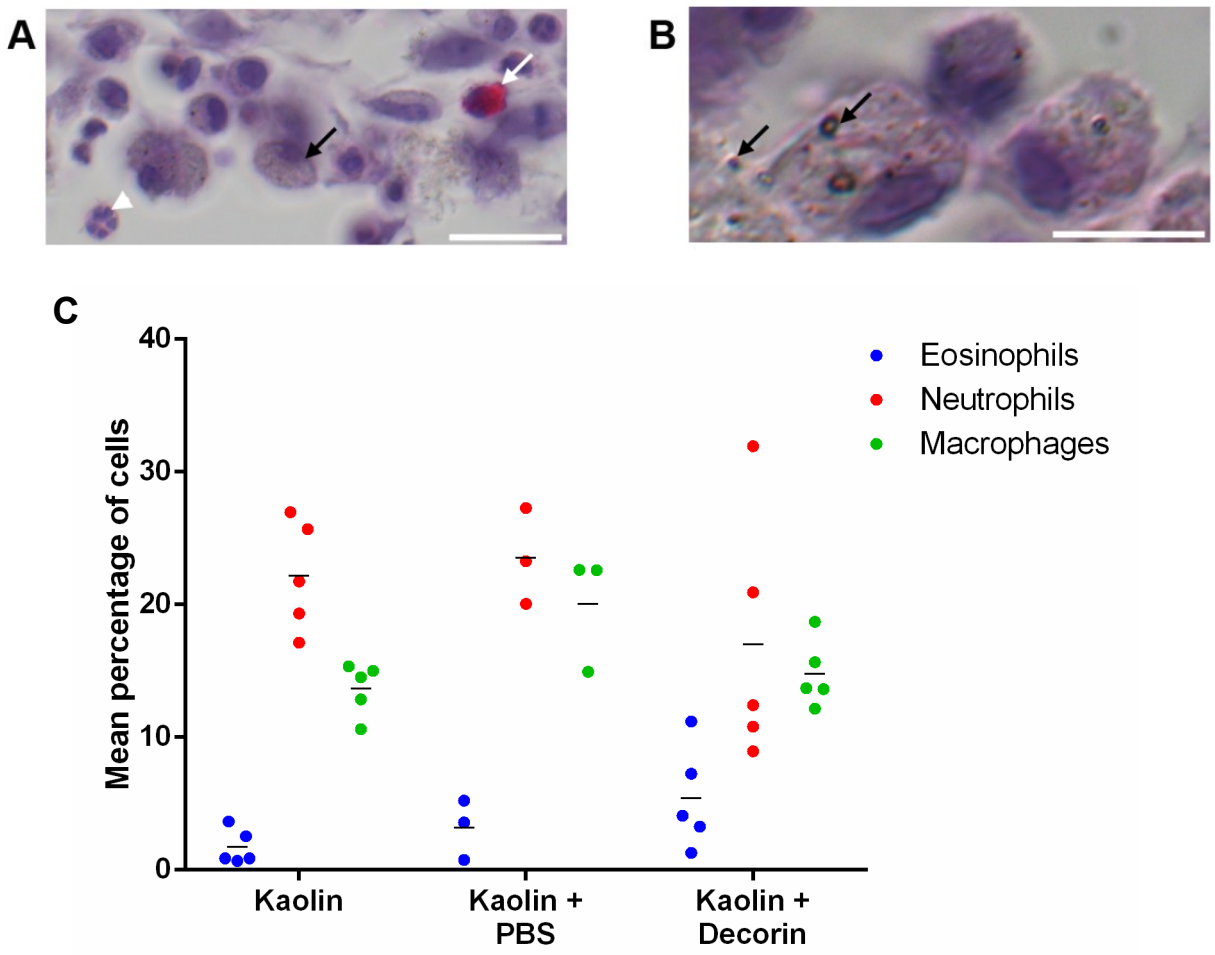

Figure 5.4. Inflammatory cells types in the basal subarachnoid space. (A) A high magnification image identifying the various inflammatory cell types in the subarachnoid space including eosinophils (*white arrow*) with bright pink cytoplasm, neutrophils (*white arrowhead*) with a multi-lobed nuclei and macrophages (*black arrow*) with an acentric round nucleus. **(B)** Kaolin granules (*black arrows)* could be seen in the subarachnoid space and within the cytoplasm of macrophages. **(C)** Scatter plot of the mean percentage of eosinophils, neutrophils and macrophages in the subarachnoid space of Kaolin, Kaolin+PBS and Kaolin+Decorin groups showing that the distribution of each cell type was similar between the 3 groups. Scale bars A – 20µm, B – 10µm.

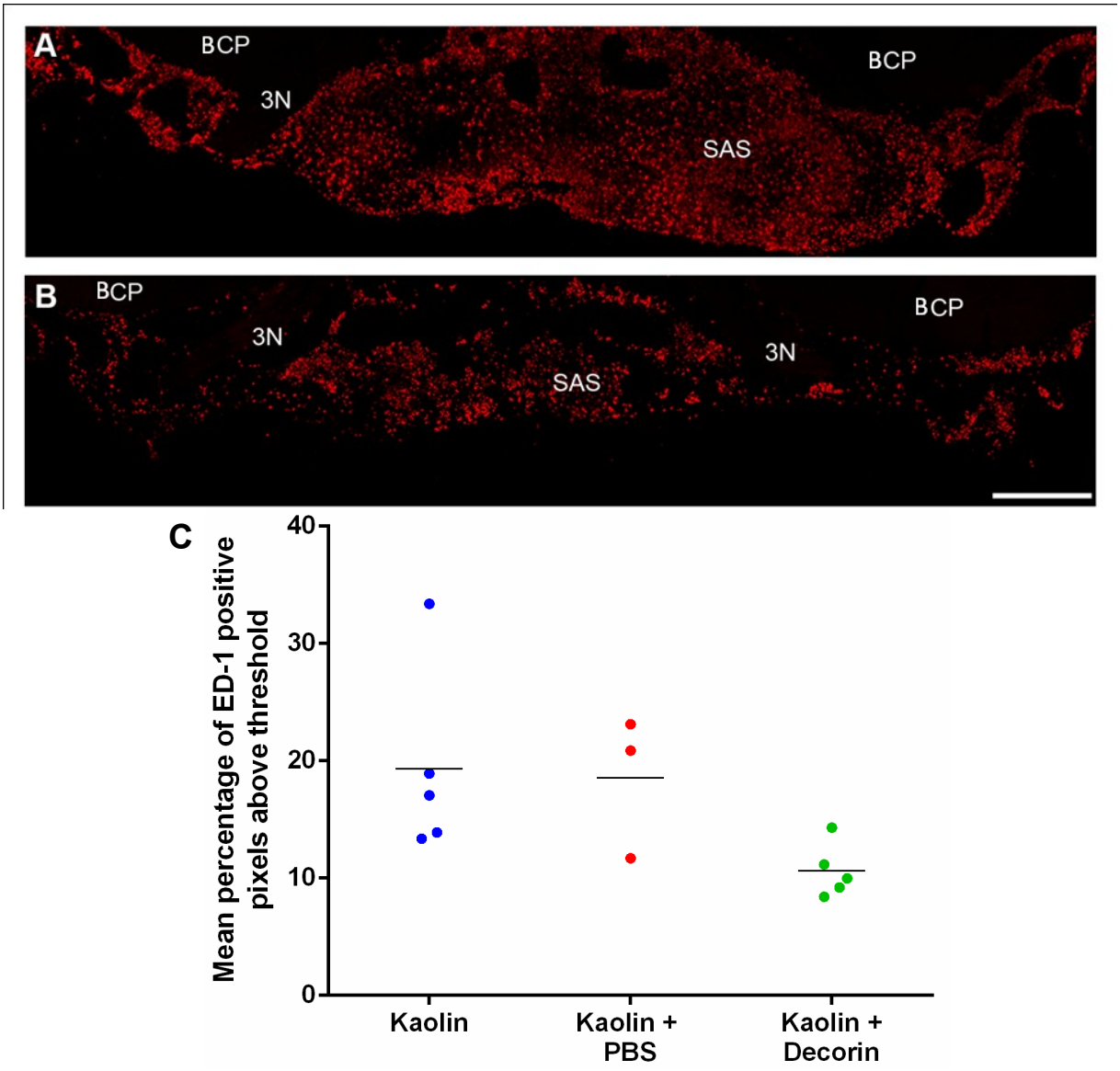

Figure 5.5. ED-1 positive macrophages in the basal subarachnoid space. Representative composite images of ED-1 staining (*red*) in the basal subarachnoid space of the Kaolin+PBS **(A)** and Kaolin+Decorin **(B)** groups. **(C)** Scatter plot of the mean percentage of ED-1 positive pixels in the subarachnoid space in the 3 groups. ED-1 staining was increased in the Kaolin and Kaolin+PBS groups compared to the Kaolin+Decorin group. Scale bar – 500μm; BCP – basal cerebral peduncle; BV – blood vessels; SAS – subarachnoid space; 3N – oculomotor nerve.

5.3.3. Decorin reduced the inflammatory response in the lateral ventricles

In addition to the meningeal blood vessels, inflammatory cells are able to enter the CNS through the choroid plexus (Chodobski *et al*., 2011). In the choroid plexus of intact rat brains, occasional OX-42 positive cells were detected on the apical side of the epithelium, and based on their morphology and location these cells were identified as macrophages **(Fig. 5.6.A)**. In the Kaolin and Kaolin+PBS groups these OX-42 positive macrophages were more numerous and formed clusters (**Fig. 5.6.B+C)** while in the Kaolin+Decorin group their numbers were clearly lower **(Fig. 5.6.D)**. These results suggest that Decorin treatment may decrease the influx of macrophages through the choroid plexus.

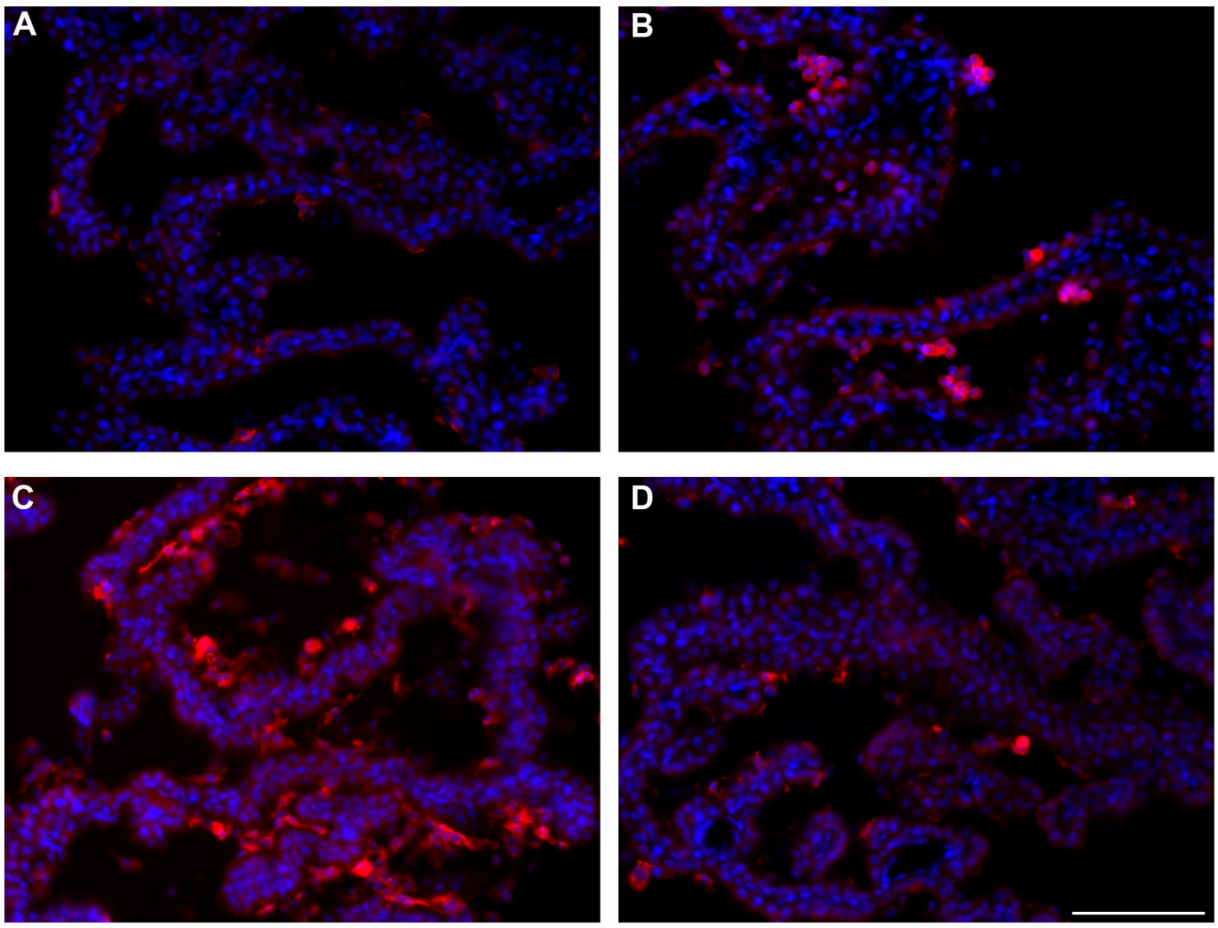

Figure 5.6. OX-42 positive macrophages associated with the choroid plexus. Representative images of OX-42 positive cells (*red*) in the lateral ventricles in Intact **(A)**, Kaolin **(B)**, Kaolin+PBS **(C)** and Kaolin+Decorin **(D)** groups. There were more OX-42 positive macrophages associated with the choroid plexus in the Kaolin and Kaolin+PBS compared to the Kaolin+Decorin group. DAPI (*blue*) was used as a generic nuclear marker; scale bar – 100µm.

5.3.4. Decorin did not affect the proliferation or apoptosis of macrophages in the basal subarachnoid space

TGF-β1 can influence chemotaxis, proliferation and apoptosis of inflammatory cells (Wahl *et al*., 1989; Xaus *et al.,* 2001; Comalada *et al.,* 2003) and therefore, Decorin's effects on reducing the inflammatory response could be due to a combination of these factors. In all groups injected with kaolin there were cells positive for Ki67 (marker of proliferation) and cleaved caspase-3 (marker of apoptosis) present in the basal subarachnoid space. The majority of these cells were not ED-1 positive **(Fig. 5.7)**. This suggests that the macrophages in the subarachnoid space were not proliferating or dying 3 days after kaolin injection.

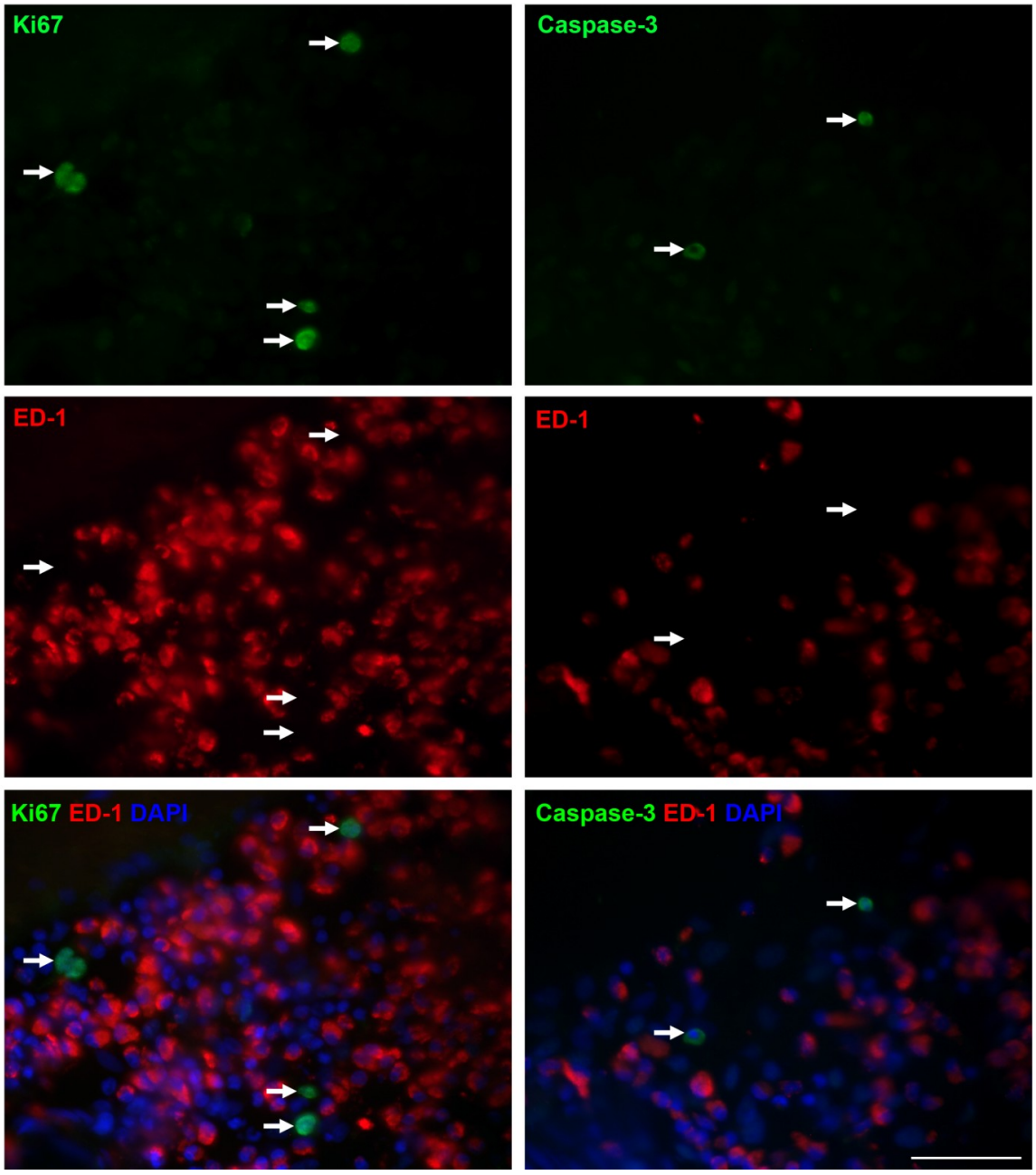

Figure 5.7. Proliferation and apoptosis in the basal subarachnoid space. Images showing Ki67 (left panels) and cleaved caspase-3 positive cells (right panels) in the basal subarachnoid space of rats injected with kaolin. The majority of cells (white arrows) that were positive for Ki67 (*green*) or cleaved caspase-3 (*green*) were not ED-1 positive (*red*). DAPI (*blue*) was used as a generic nuclear marker; scale bar – 50μm.

5.3.5. Decorin reduced astrogliosis and reactive microglia at 3 days after kaolin injection

Three days after the injection of kaolin, the levels of GFAP immunostaining (measured as the percentage of immunofluorescent pixels per unit area) at the base of the brain (olfactory tubercle) located close to kaolin deposits, and in the corpus callosum demonstrated a trend to being higher in the Kaolin (19.6±4.3% and 15.6±1.9%, respectively) and Kaolin+PBS (20.2±3.1% and 12.8±1.3%, respectively) groups compared to the Intact group (3.7±0.3% and 5.4±0.8%, respectively). The levels of GFAP immunostaining in brain tissue adjacent to kaolin deposits and in the corpus callosum of the Kaolin+Decorin group (12.8±3.4% and 9.5±2.5%, respectively) were higher compared to the Intact group but did not reach the levels seen in the Kaolin and Kaolin+PBS groups **(Fig. 5.8 and 5.9)**.

The OX-42 immunostaining (microglia) was more intense in the corpus callosum and periventricular white matter in the Kaolin and Kaolin+PBS groups compared to the Intact group at 3 days after the injection of kaolin **(Fig. 5.10)**. The OX-42 positive microglia had thicker processes and took on an amoeboid morphology which is characteristic of activated microglia. This was especially evident in close proximity to the injury site left by the cannula (in the Kaolin+PBS group) and along the ventricle wall. In the Kaolin+Decorin group, OX-42 immunostaining was more intense at the injury site where cannulation occurred, while in distal portions of the corpus callosum and periventricular white matter the staining was similar to that in the Intact group **(Fig. 5.10)**. In both the Kaolin+PBS and Kaolin+Decorin groups, the OX-42 positive microglia appeared to be migrating along the white matter towards the injury site produced by the

cannula. These results suggest that Decorin may affect the early microglial and astrocytic responses to the injection of kaolin.

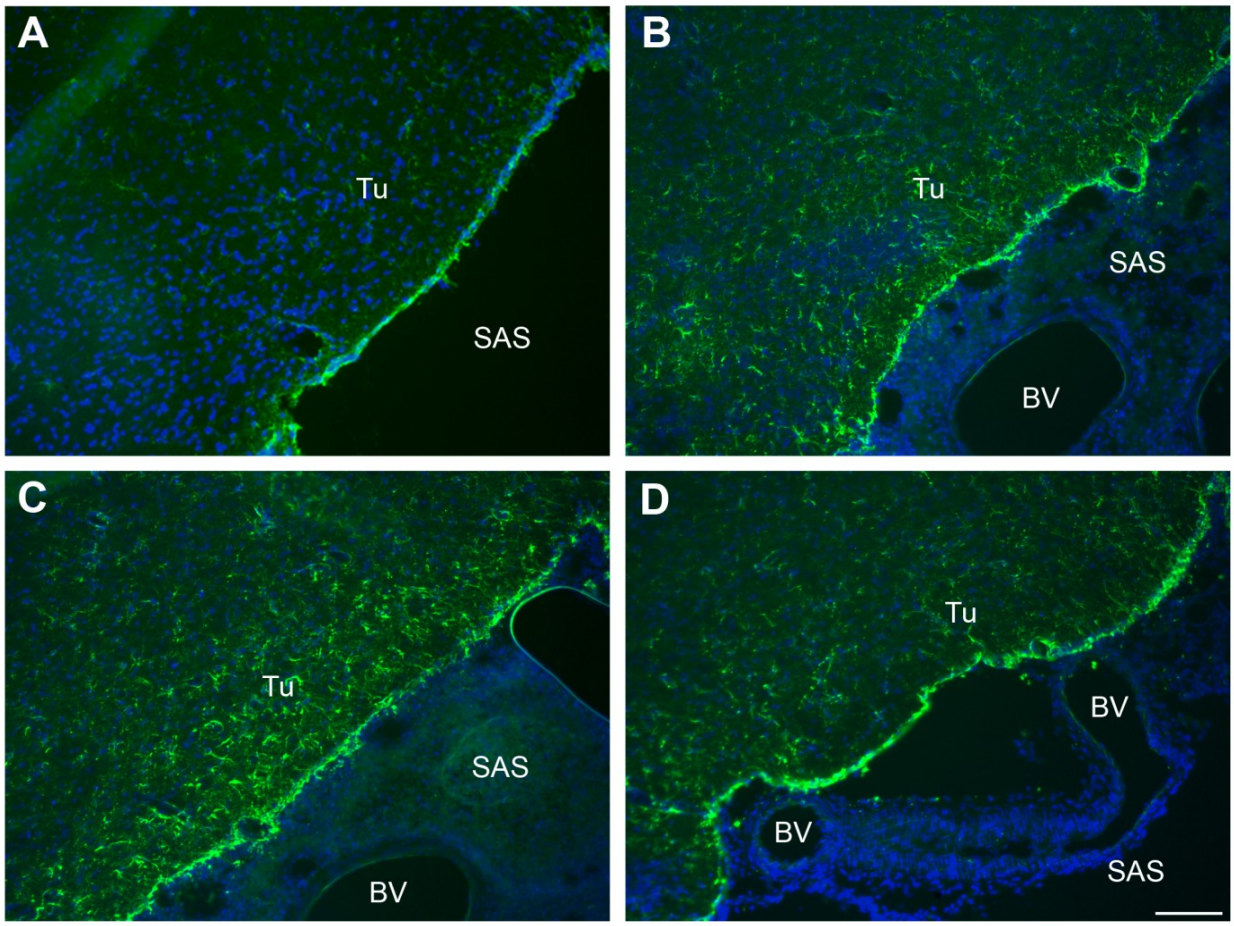

Figure 5.8. Astrogliosis at the base of the brain. Representative images of GFAP positive staining (*green*) in the neural parenchyma at the base of the brain in the Intact **(A)**, Kaolin **(B)**, Kaolin+PBS **(C)** and Kaolin+Decorin **(D)** groups. Increased GFAP staining was observed in the Kaolin and Kaolin+PBS groups at the base of the brain in close proximity to kaolin deposits when compared to the Intact group. The levels of GFAP staining in the Kaolin+Decorin group was lower when compared to the Kaolin and Kaolin+PBS groups. DAPI (*blue*) was used as a generic nuclear marker; scale bar – 200μm; BV – blood vessel, SAS – subarachnoid space, Tu - olfactory tubercle.

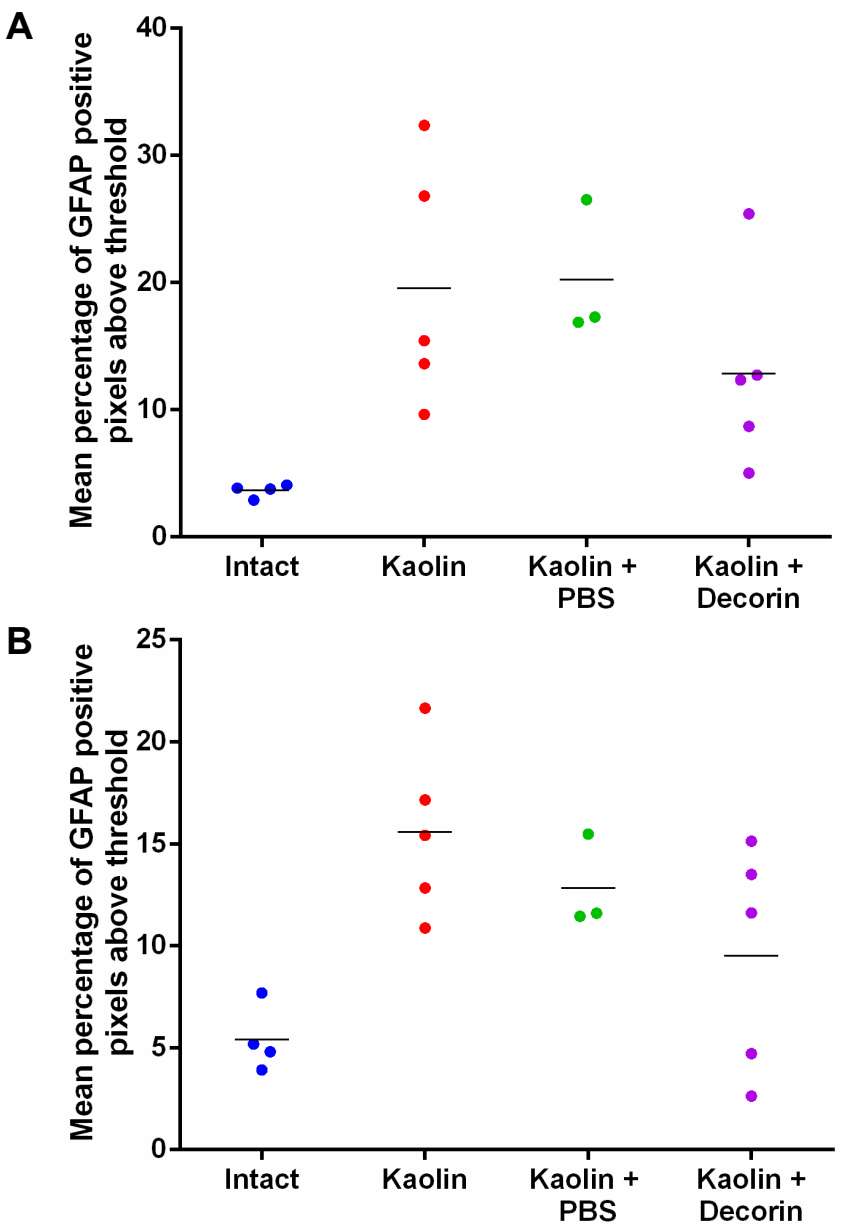

Figure 5.9. Astrogliosis 3 days after the injection of kaolin. Scatter plots of the mean percentage of GFAP positive staining at the base of the brain (olfactory tubercle; **A)** and in the corpus callosum **(B)**. Increased levels of GFAP were observed in the Kaolin and Kaolin+PBS groups compared to the Intact group. In the Kaolin+Decorin group the levels were reduced compared to the Kaolin and Kaolin+PBS groups but did not reach the constitutive levels seen in the Intact group.

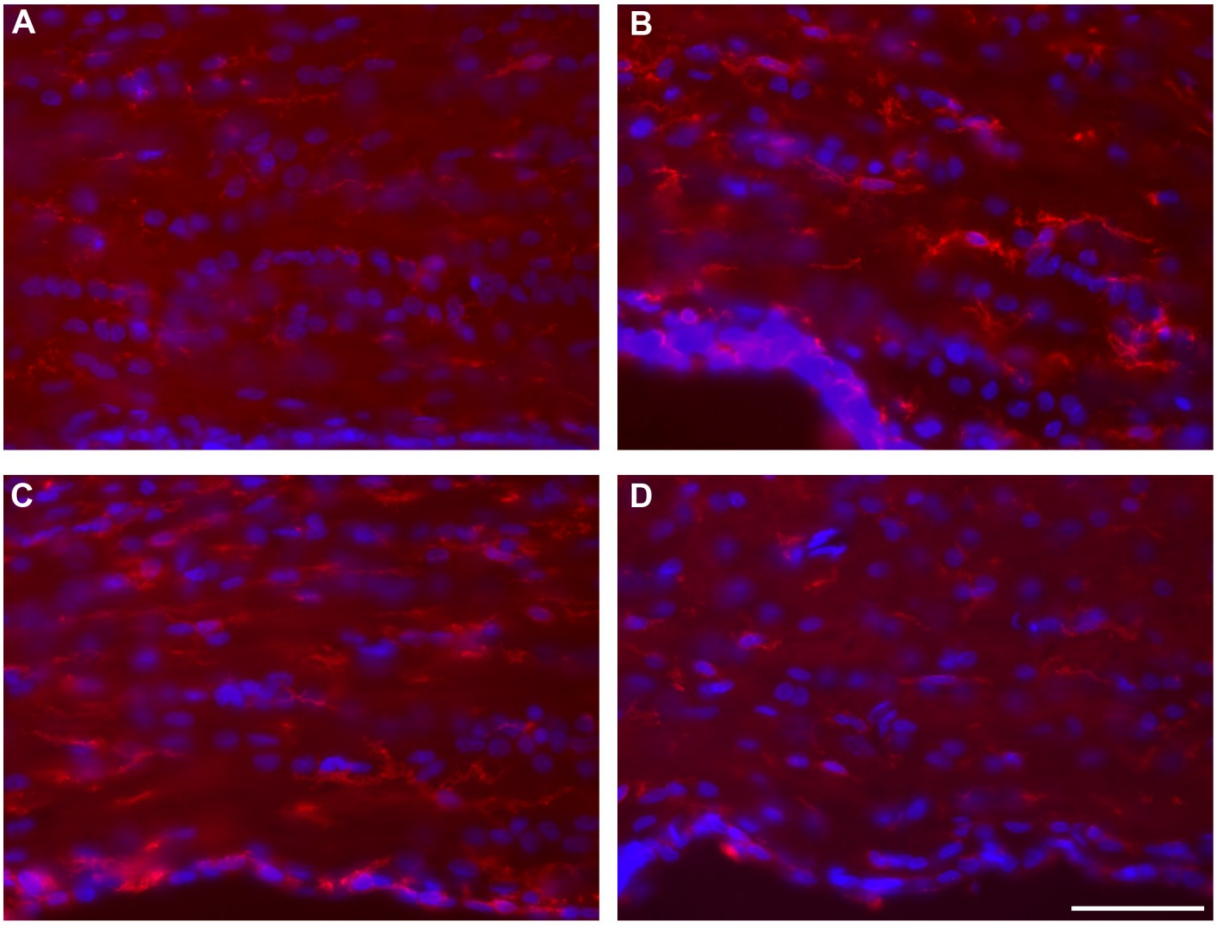

Figure 5.10. Reactive microglia in the periventricular white matter. Representative images showing OX-42 positive microglia (*red*) in the periventricular white matter in the Intact **(A)**, Kaolin **(B)**, Kaolin+PBS **(C)** and Kaolin+Decorin **(D)** groups. Microglia with more intense OX-42 staining were observed in the Kaolin and Kaolin+PBS groups compared to the Intact group, whilst normal constitutive levels of OX-42 stained cells were maintained in the Kaolin+Decorin group. DAPI (*blue*) was used as a generic nuclear marker; scale bar – 50μm.

5.3.6. Injection of kaolin increased nestin positive staining in the subventricular zone and subarachnoid space

One of the main sources of neural progenitor cells is the subventricular zone of the lateral ventricle. Nestin, an intermediate filament protein, is expressed by neural progenitor cells and is down regulated upon differentiation (Hendrickson *et al*., 2011). The ependyma and underlying subventricular zone are the first areas to be affected by expansion of the ventricles therefore sections were stained using antibodies against nestin to determine any changes in the neural progenitor population. In the Intact group there were nestin positive cytoplasmic processes associated with the meninges in the subarachnoid space, and in particular surrounding blood vessels. Compared to intact brains, in the Kaolin and Kaolin+PBS groups there was an increase in the extent of nestin staining with more nestin positive cytoplasmic processes observed throughout the subarachnoid space, particularly within and around kaolin granules. There was also an increase in nestin positive processes in the Kaolin+Decorin group although not to the same extent as that seen in the Kaolin and Kaolin+PBS groups **(Fig. 5.11)**. In addition, the extent of nestin staining appeared to be relative to the inflammatory response and kaolin deposits present in the subarachnoid space **(Fig. 5.3.A+B)**.

Furthermore in the subventricular zone and ependymal cell layer there were more nestin positive cells and processes in the Kaolin and Kaolin+PBS groups compared to the Intact group. Nestin positive cells were also increased in the Kaolin+Decorin group although to a lesser extent in the subventricular zone **(Fig. 5.12.A-D)**. However, in all the kaolin injected groups there were ‘pockets’ of nestin positive cells present just beneath the ependyma and in certain instances, these cells extended into the lateral ventricle

(Fig. 5.12.E+F). Therefore, the results from these studies suggest that Decorin treatment reduces the Kaolin induced nestin staining in the subventricular zone and subarachnoid space.

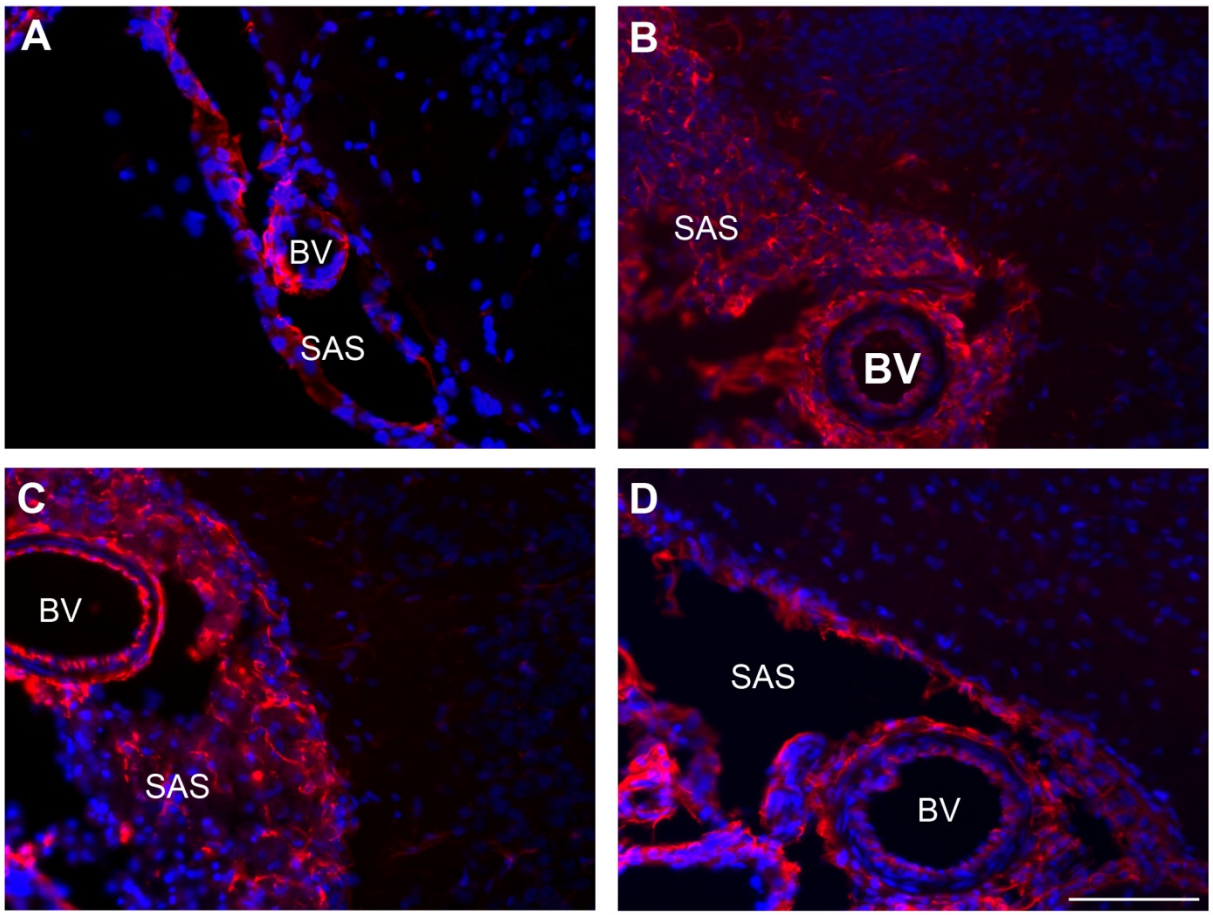

Figure 5.11. Nestin positive processes in the basal subarachnoid space at 3 days after kaolin injection. Representative images of nestin positive staining (*red*) in the subarachnoid space in the Intact **(A)**, Kaolin **(B)**, Kaolin+PBS **(C)** and Kaolin+Decorin **(D)** groups. Nestin positive cytoplasmic processes were observed in the Intact group associated with the meninges and blood vessels in the subarachnoid space. Increased nestin positive processes were observed in the Kaolin and Kaolin+PBS groups compared to the Intact group. The extent of nestin positive processes in the Kaolin+Decorin group was lower compared to the Kaolin and Kaolin+PBS groups. DAPI (*blue*) was used as a generic nuclear marker; scale bar – 100µm; BV – blood vessel, SAS – subarachnoid space.

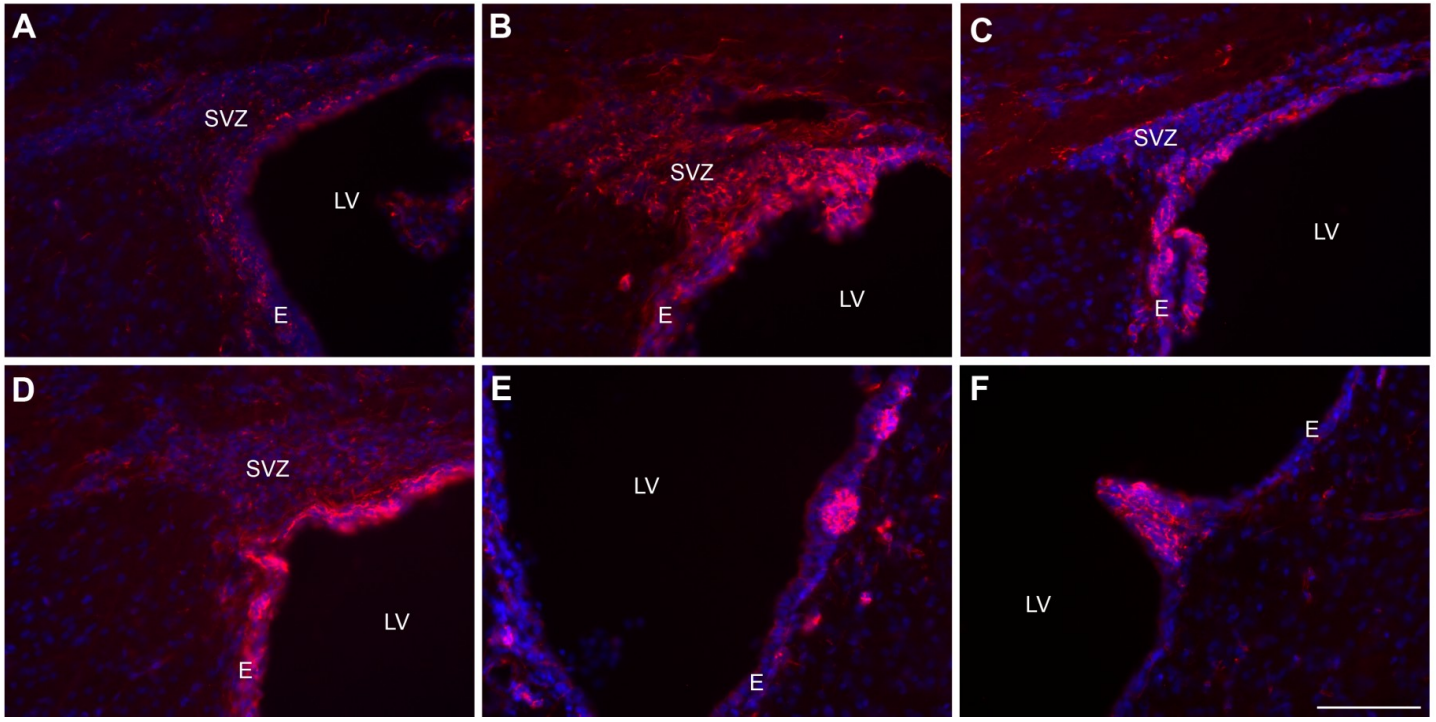

Figure 5.12. Nestin staining in the subventricular zone at 3 days after kaolin injection. Representative images of nestin positive staining (*red*) in the subventricular zone in the Intact **(A)**, Kaolin **(B)**, Kaolin+PBS **(C)** and Kaolin+Decorin **(D)** groups. There was an increase in nestin positive cells and processes seen in the Kaolin and Kaolin+PBS groups compared to the Intact group. The extent of nestin staining in the Kaolin+Decorin group was lower when compared to the Kaolin and Kaolin+PBS groups. Distinct 'pockets' of nestin positive cells were observed beneath the ependyma in the Kaolin+PBS **(E)** and Kaolin+Decorin **(F)** groups. DAPI (*blue*) was used as a generic nuclear marker; scale bar – 100μm; E – ependyma, LV – lateral ventricle.

5.3.7. α-smooth muscle actin positive cells in the third ventricle ependyma at 3 days after kaolin injection

In order to determine whether the fibrogenic response had begun at the 3 day time point, sections were stained for α-smooth muscle actin (α-SMA) which is expressed by smooth muscle cells of blood vessels and myofibroblasts. Myofibroblasts are activated fibroblasts that are involved in producing extracellular matrix and contracting the wound (Gabbiani *et al*., 2003). In the Intact group, as expected, α-SMA positive staining was observed in blood vessels in the brain parenchyma and subarachnoid space. While in the kaolin-injected rat brains there were no changes in the staining pattern for α-SMA in the subarachnoid space (data not shown), α-SMA positive cells were detected in close proximity to the ependymal lining of the third ventricle **(Fig. 5.13)**. The α-SMA positive staining in the Kaolin+Decorin group was clearly lowered compared to the Kaolin and Kaolin+PBS groups. These results suggest that by 3 days after kaolin injection there was an increase in fibroblastic-like cells in the third ventricle and that Decorin reduced this response.

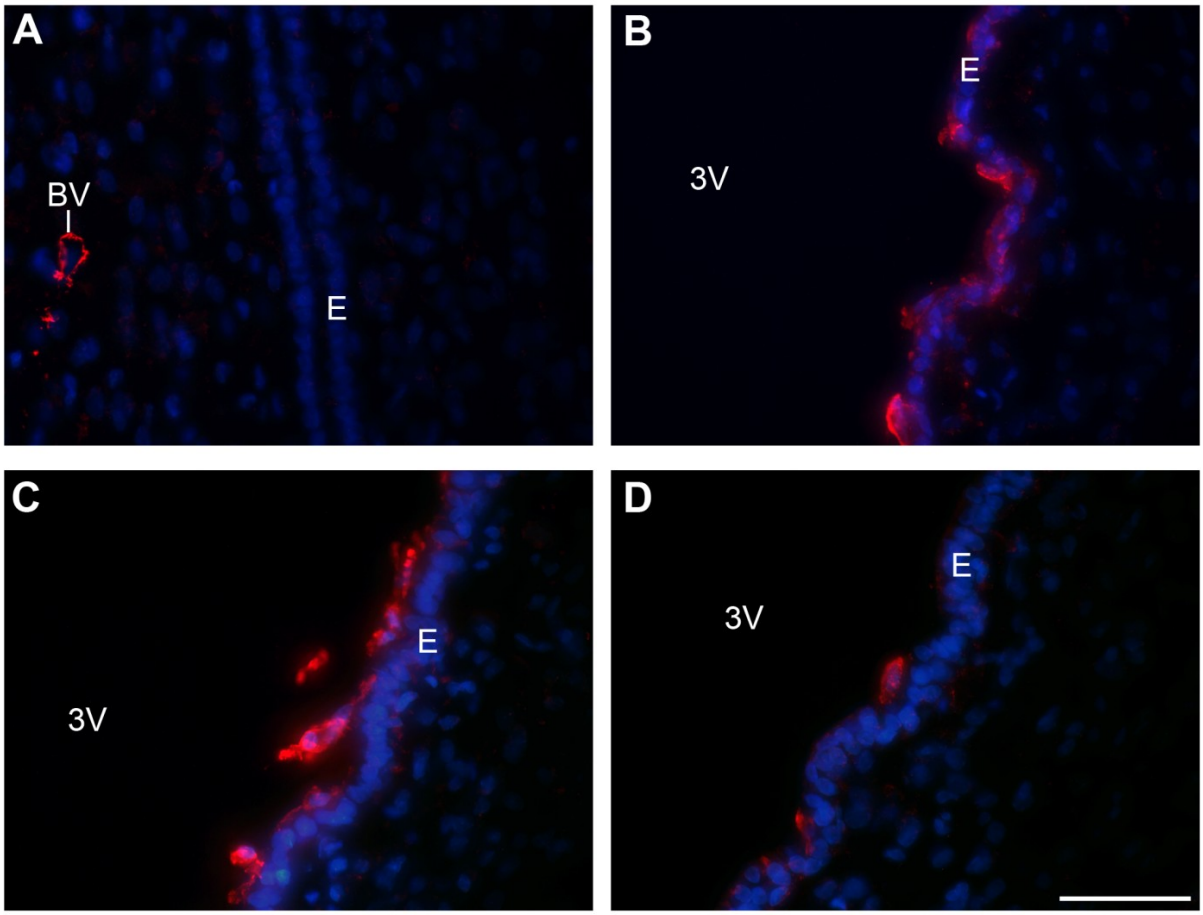

Figure 5.13. α-SMA in the third ventricle at 3 days after kaolin injection. Representative images of α-SMA positive staining (*red*) in the third ventricle ependyma of the Intact **(A)**, Kaolin **(B)**, Kaolin+PBS **(C)** and Kaolin+Decorin **(D)** groups. In the Intact group there were no α-SMA positive cells observed along the surface of the ependyma. There was an increase in α-SMA positive cells in the Kaolin and Kaolin+PBS groups and, to a lesser extent, also in the Kaolin+Decorin group. DAPI (*blue*) was used as a generic nuclear marker; scale bar – 50μm; BV – blood vessel, E – ependyma, 3V – third ventricle.

5.4. Discussion

In the previous chapter (Chapter 4) it was demonstrated that continuous intraventricular delivery of human recombinant Decorin prevented the development of ventriculomegaly in a kaolin model of juvenile communicating hydrocephalus by reducing neuroinflammation and fibrosis in the subarachnoid space. This acute phase study further supports the previous observations by demonstrating that the suppressive effect of Decorin on the inflammatory response was seen as early as 3 days after kaolin injection, with reduced numbers of inflammatory cells populating the subarachnoid space. In addition, Decorin suppressed the response of other populations of cells to the kaolin injection in periventricular regions and the subarachnoid space.

5.4.1. Decorin's effects on the early inflammatory response

After a haemorrhage or blood injection, the cisternal subarachnoid space is filled with erythrocytes embedded within a fibrin matrix containing TGF-β-rich platelets that evoke an inflammatory response characterised by the recruitment of leukocytes (Dumont *et al.,* 2003), the invasion of cytokine expressing macrophages supplemented by the transformation of pial cells into macrophages that phagocytose erythrocytes and debris (Jackowski *et al.,* 1990), and the production of ECM by meningeal fibroblasts (Sajanti *et al.,* 1999a, 1999b). This study corroborates the findings of Slobodian *et al.* (2007), demonstrating that kaolin injection causes acute inflammatory cell infiltration into the subarachnoid space, with subsequent phagocytosis of kaolin granules by macrophages and deposition of ECM. Hence, at 3 days there were eosinophils, neutrophils and macrophages present in the

subarachnoid space. The ratio of each cell type was similar between all the groups injected with kaolin, however the numbers of ED-1 positive macrophages were reduced with Decorin treatment. During inflammation, leukocytes are able to gain entry to the CNS through blood vessels in the meninges, parenchyma and choroid plexus (Muldoon *et al*., 2013). In the present study, the bulk of the inflammatory cells in the subarachnoid space were located in close proximity to meningeal blood vessels and clusters of inflammatory cells were also present near to the choroid plexus suggesting a large influx of these cells from the bloodstream.

TGF-β1 is chemotactic for monocytes, macrophages (Wahl *et al*., 1987) neutrophils (Lagraoui and Gagnon, 1997) and eosinophils (Luttmann *et al*., 1998), and the influx of these cells to sites of injury can be attenuated by TGF-β antibodies (Bottoms *et al*., 2010). This suggests that through inhibition of TGF-β1, Decorin could influence chemotaxis of inflammatory cells into the subarachnoid space. However, there is conflicting evidence regarding Decorin's effects on inflammatory cell infiltration and the majority of this research has been conducted in Decorin deficient mice. In a model of diabetic nephropathy, a lack of Decorin appeared to lead to an increase in the accumulation of inflammatory cells in perivascular regions of the kidney (Merline *et al*., 2009), implying a role for Decorin in the reduction of inflammatory cell recruitment. In contrast, in a model of contact allergy, there was a reduction in leukocyte influx to the site of insult, due to increased adhesion of inflammatory cells to endothelial cells and a reduction in their migration across the endothelium (Seidler *et al*., 2011). Further research conducted by Logan *et al* (1999a) have shown that after a cerebral lesion, continuous Decorin treatment reduced the number of ED-1-positive macrophages in and around the wound site. In

addition, Xaus *et al.* (2001) and Comalada *et al.* (2003) reported that Decorin inhibited macrophage proliferation through $p27^{Kip1}$, protects macrophages from apoptosis through $p21^{Waf1}$ and prevented TGF-β1-induced inhibition of macrophage activation. In the present study, there were very few, if any, ED-1 positive macrophages that were positive for either Ki67 or cleaved caspase-3, suggesting that Decorin did not influence the proliferation or apoptosis of macrophages within the first 3 days of treatment. Altogether, these results suggest that the anti-inflammatory actions of Decorin are achieved by both reducing the number of ED-1 positive macrophages recruited from the blood stream and increasing their efficiency to clear debris from the subarachnoid space.

5.4.2. The acute effects of Decorin on astrogliosis and reactive microglia

The results presented in this chapter suggest that the induction of reactive gliosis in hydrocephalus is due to astrocytes responding to the mechanical stresses placed upon them by increasing intracranial pressure (ICP), which causes distortion of the brain parenchyma. Astrocytes respond to those mechanical stresses by increasing intracellular calcium through mechanosensitive ion channels such as the stretch activated channel, and propagating the signal to surrounding astrocytes (Ostrow and Sachs, 2005). Consequently during the genesis of hydrocephalus, molecular mediators of astrogliosis may not be responsible for the initial glial response but involved in progressing its severity. Therefore, the initial astrogliosis induced by the early increase in ICP (caused by kaolin) may not be preventable. This could explain why Decorin reduces, but not completely abolishes, the early reactive astrogliosis and microgliosis. Nevertheless, this may not be a disadvantage as mild

reactive astrogliosis can be beneficial to compromised neural tissue (Pekny and Nilsson, 2005). Complete prevention of reactive astrogliosis can lead to a lack of astrocytic hypertrophy, failed glial scar formation, increased inflammation and lesion size, a lack of blood brain barrier repair and degeneration of neurones (Bush *et al*., 1999; Herrmann *et al*, 2008). In addition, reactive microglia surround the injury site, protecting neurones from damage and removing cellular debris (Nimmerjahn *et al*., 2005; Raivich *et al*., 1999) which, if abolished, could cause further damage to neurones.

5.4.3. Neuroprogenitor response to kaolin injection

Krueger *et al*., (2006) demonstrated that there were nestin positive neural progenitor cells present in the CSF of post haemorrhagic hydrocephalic infants and hypothesised that these cells entered the CSF through the disrupted ependyma. However, it is also known that cells of the subventricular zone will proliferate and migrate to areas of brain damage (Fallon *et al*., 2000) probably in response chemotactic molecules. In the present study, pockets of nestin positive cells were identified beneath the ependyma and appeared to be proliferating towards the ventricle. Together this data suggests that the injection of kaolin induces the proliferation and possibly the migration of neural progenitor cells in the subventricular zone towards the lateral ventricles, most likely in response to cytokines released into the CSF. The progressive loss of these neural progenitor cells into the CSF could result in a reduction of neural progenitor cells present in the subventricular zone to repopulate the hydrocephalic brain (Rodriguez *et al*., 2012). Moreover, the results from the present study demonstrate an increase in nestin positive cell processes in

the subarachnoid space of hydrocephalic animals. Recently it has been demonstrated that the meninges contain nestin positive cells resembling neural progenitor cells (Bifari *et al*., 2009; Nakagomi *et al*., 2011), which are able to migrate into damaged brain parenchyma (Nakagomi *et al*., (2012). This, together with our data suggests that these cells may represent an important pool of cells in the repair of the brain after hydrocephalus.

Studies from Owen-Lynch *et al* (2003) have shown that CSF from hydrocephalic animals has anti-neurogenic properties and prevents the proliferation of neural progenitor cells. It is tempting to speculate that TGF-β1 could play a role in the proliferation of these neural progenitor cells since the levels of TGF-β1 are increased in the CSF of post-haemorrhagic hydrocephalus patients (Douglas *et al*., 2009), and inhibition of TGF-β1 results in reduced apoptosis and increased proliferation of neural progenitor cells (Pineda *et al*., 2013). The lower levels of nestin staining observed in the subventricular zone of Decorin treated animals may not necessarily indicate a role for Decorin in reducing the neural progenitor cell response, but could be related to Decorin attenuating the hydrocephalic cues.

5.4.4. α-smooth muscle actin positive cells; myobibroblasts or macrophages?

Fibroblasts and activated myofibroblasts (α-SMA positive) respond to pro-fibrotic molecules such as TGF-β1 by increasing their production of ECM molecules (Kisseleva and Brenner, 2008). In the present study there was no increase in immunoreactive α-SMA in cells of the subarachnoid space at 3 days after kaolin injection. These findings are corroborated by Darby *et al* (1990) who demonstrated that in a wound healing model, α-SMA is not expressed within the lesion site until 6

days after injury. In these studies α-SMA positive cells were associated with the ependymal lining of the third ventricle 3 days after kaolin injection. These cells could be inflammatory cells as a small subset of monocytes and macrophages have been shown to express α-SMA (Ludin *et al*., 2012), but as these cells are very rare, it is unlikely that the α-SMA positive cells observed in the third ventricle were all macrophages. Unfortunately, co-immunostaining of α-SMA with ED-1 or OX-42 antibodies could not be performed (all mouse antibodies) to confirm this, and it would have been difficult to identify macrophages based on morphology in this area using H&E.

Alternatively, these α-SMA positive cells could represent ependymal cells undergoing epithelial-mesenchymal transition (EMT). Whether ependymal cells can undergo EMT or if this mechanism is involved in the aetiology of hydrocephalus has not been investigated, however there is evidence that supports this hypothesis. For example, it is well known that ependymal cells are damaged in hydrocephalus due to stretching during the ventricular enlargement, a feature that leads to ependymal denudation (Sarnat, 1995). Epithelial cell damage often precedes EMT and increased α-SMA expression is one of the critical steps in EMT (Kisseleva and Brenner, 2008). Furthermore, TGF-β1 levels are increased in post-haemorrhagic hydrocephalus and TGF-β1 is a potent inducer of EMT and directly induces α-SMA expression (Sarrazy *et al*., 2011). Therefore, this data suggests that the ependyma could potentially be a source of fibroblastic cells that contribute to the deposition of ECM in the subarachnoid space. The lower numbers of these cells observed in the Decorin treated group could indicate that Decorin has attenuated TGF-β1 induced EMT.

5.4.5. Variation in the early development of hydrocephalus

In this acute phase study the differences observed between the groups did not reach statistical significance and therefore only demonstrated trends. This was due to the high variation of the responses observed within each treatment group, particularly in the immunostaining parameters evaluated in periventricular tissue. It is recognised that the development of kaolin-induced hydrocephalus is not always uniform. Analysis of the MRI scan images in the previous chapter indicated that there was a correlation between the rapid enlargement of the ventricles and the appearance of oedema in the periventricular area. Therefore, there may have been a lot of variation in the timing of responses in the periventricular tissue at this early 3 day time point. Also within the Decorin group, the amount of human Decorin present in the CSF was very variable and ranged between 1.7-16.3ng/ml. It is possible that the high variability in the levels of Decorin observed in the CSF of the animals in these studies could be due technical problems with the pumps used for continuous delivery of Decorin. In this acute study there were air bubbles observed in the tubing of some of the pumps before they were implanted, which could have affected the early phase efficiency of Decorin delivery.

However, this study does demonstrate that infusion of Decorin into the lateral ventricles leads to the continuous delivery of low levels of Decorin to the CSF, compared to a 25µg/5µl bolus injection that results in around 5µg/ml Decorin in the CSF after 30 minutes (Lisa Hill, unpublished work). Continuous delivery of Decorin should inhibit the sustained release of TGF-β1 that occurs during the development of hydrocephalus while reducing the side effects associated with overdosing.

5.4.6. Conclusion

In summary, the results from these studies show that continuous Decorin infusion suppresses the acute phase inflammatory and cellular responses in the subarachnoid space and periventricular regions resulting from the kaolin injection. This work further demonstrates the potential use of Decorin as a therapeutic agent in reducing inflammation in the early stages of post-haemorrhagic hydrocephalus,

Chapter 6

Decorin's effects on degrading subarachnoid fibrosis in established hydrocephalus

6.1. Rationale

Post-haemorrhagic hydrocephalus is thought to develop due to fibrosis in the subarachnoid space obstructing CSF drainage. Transforming growth factor β1 (TGF-β1) plays a significant role in the development of fibrosis through promoting inflammation and extracellular matrix (ECM) deposition, as well as in reducing degradation of ECM in established fibrosis. As such it has been implicated in post-haemorrhagic hydrocephalus. Therefore it was hypothesised that a TGF-β antagonist may be useful as a therapeutic agent to prevent the development and degradation of subarachnoid fibrosis to protect against post-haemorrhagic hydrocephalus. Previously in Chapter 4 it was demonstrated that Decorin was able to prevent the development of kaolin-induced communicating hydrocephalus. Therefore the aim of this study was to investigate the effects of continuous Decorin treatment on degrading subarachnoid fibrosis and resolving established hydrocephalus.

6.2. Experimental design

Kaolin was injected into the basal cistern to induce communicating hydrocephalus in 3 week old rats as described in section 2.3.3. I*n vivo* magnetic resonance imaging (MRI) was conducted 6 days after the injection of kaolin to determine the development of hydrocephalus as described in section 2.9.2. Rats that had not developed hydrocephalus at this point were excluded from the study (n=5). Twenty-two rats were paired up based on their ventricular volumes and randomly assigned to either receive an osmotic pump containing phosphate buffered saline (PBS) or Decorin and became the Kaolin+PBS group (n=11) and the Kaolin+Decorin group (n=11) respectively. The surgeon was blinded to the treatment each rat

received. The remaining rats received no further surgery and became the Kaolin group (n=6). On day 7 the osmotic pumps were implanted subcutaneously and connected through a catheter to a cannula placed in the right lateral ventricle for continuous intraventricular infusion of either Decorin or PBS for 14 days as described in section 2.3.4. *In vivo* MRI was conducted on day 20 to assess the extent of hydrocephalus and the rats were sacrificed on day 21, followed by immunohistochemical analyses of the brain as described in section 2.4 **(Fig. 6.1)**. Age matched intact rats were sacrificed immediately after receiving an MRI scan and became the Intact group (n=5).

Three rats from the Kaolin+Decorin group pulled the tubing off the pump which allowed CSF to leak out, so that it acted similar to a shunt. These rats were sacrificed as soon as the disconnection of the pump was discovered. Immunohistochemical analyses were still conduced on these rat brains and they were put into a separate group named the Kaolin+Decorin-Pump group (n=3). Severe hydrocephalus developed in 4 rats (2 from the Kaolin+PBS group and 2 from the Kaolin+Decorin group) and they were euthanised before the end of the study (days 17-19) as they had reached a pre-defined humane endpoint. Fortunately MRI scans were conducted before sacrifice and therefore these rats were included in this study. Therefore the residual numbers in each group that were included in the analyses were as follows: Intact n=5, Kaolin n=6, Kaolin+PBS n=11 (includes 2 severely hydrocephalic rats), Kaolin+Decorin n=8 (includes 2 severely hydrocephalic rats) and Kaolin+Decorin-Pump n=3.

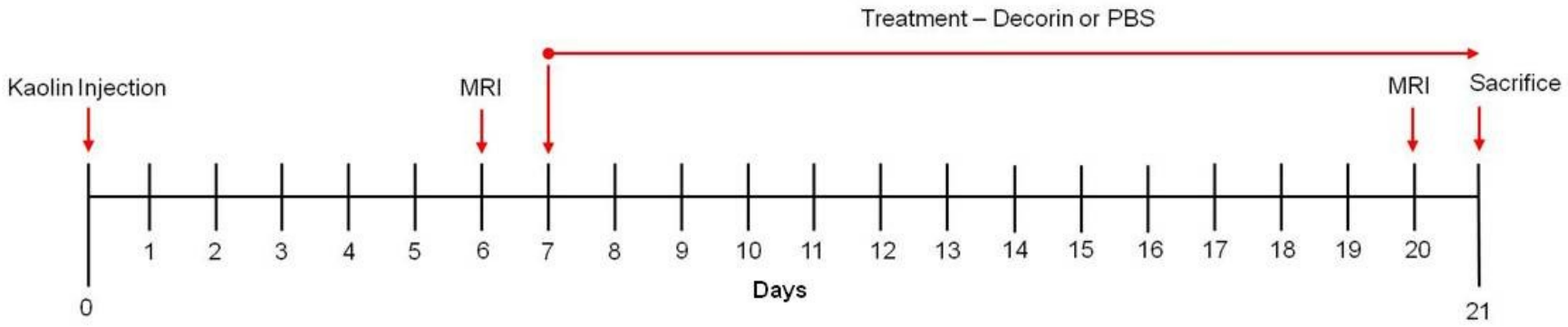

Figure 6.1. Experimental protocol. Kaolin was injected into the basal cisterns on day 0 followed by the first MRI scan on day 6. Osmotic pumps containing either Decorin or PBS (control) were implanted on day 7 in hydrocephalic animals. Decorin or PBS was continually infused into the lateral ventricles for 14 days. A second MRI scan was conducted on day 20 followed by sacrifice on day 21.

6.3. Results

6.3.1. Early development of hydrocephalus and oedema

In this study hydrocephalus developed in 85% of juvenile rats injected with kaolin and was comparable to the induction rate in Chapter 4. The first MRI scan conducted on day 6 determined that hydrocephalus had already developed within 6 days of the kaolin injection with the ventricles expanding significantly ($P<0.001$) to $203.8\pm14.3mm^3$ compared to $10.7\pm0.8mm^3$ in intact rats **(Fig. 6.2)**. In the T_2-weighted MRI scans, fluid appeared lighter compared to the brain parenchyma therefore oedema was identified as lighter areas present within the brain parenchyma that were not part of the ventricular system. Further analysis of the 6 day MRI scan indicated the presence of oedema in the white matter (periventricular white matter and corpus callosum) and cortex in 17 out of 28 rats (61%) injected with kaolin **(Fig. 6.3)**. Oedema was not present on the MRI scans from the Intact group. Rats with oedema had significantly ($P<0.01$) larger ventricles ($236.3\pm8.3mm^3$) compared to those rats without oedema ($153.5\pm28.7mm^3$, **Fig. 6.4)**. This data suggests that ventricles that enlarge quickly are associated with oedema in the periventricular white matter and cortex.

6.3.2. Hydrocephalic characteristics

The rats injected with kaolin demonstrated classic hydrocephalus associated behaviour. The day after the injection of kaolin, the rats had porphyrin secretions around the eyes and nose, piloerection of the fur and weight loss compared to intact rats. During the following days the rats improved and most were walking round the cage normally, although some rats demonstrated weakness and lethargy. The 4 rats

with severe hydrocephalus were killed early due to severe weight loss, lethargy, agitation and gait problems.

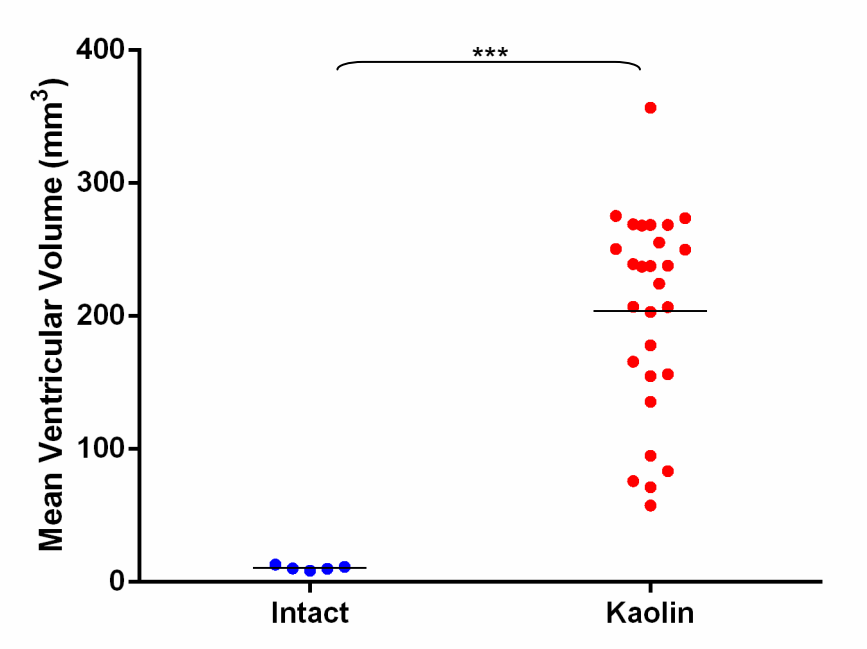

Figure 6.2. Induction of hydrocephalus. The scatter plot summarises the mean of the ventricular volumes of intact rats (n=5) and kaolin injected rats (n=28). Hydrocephalus was induced within 6 days of the kaolin injection. ***P<0.001.

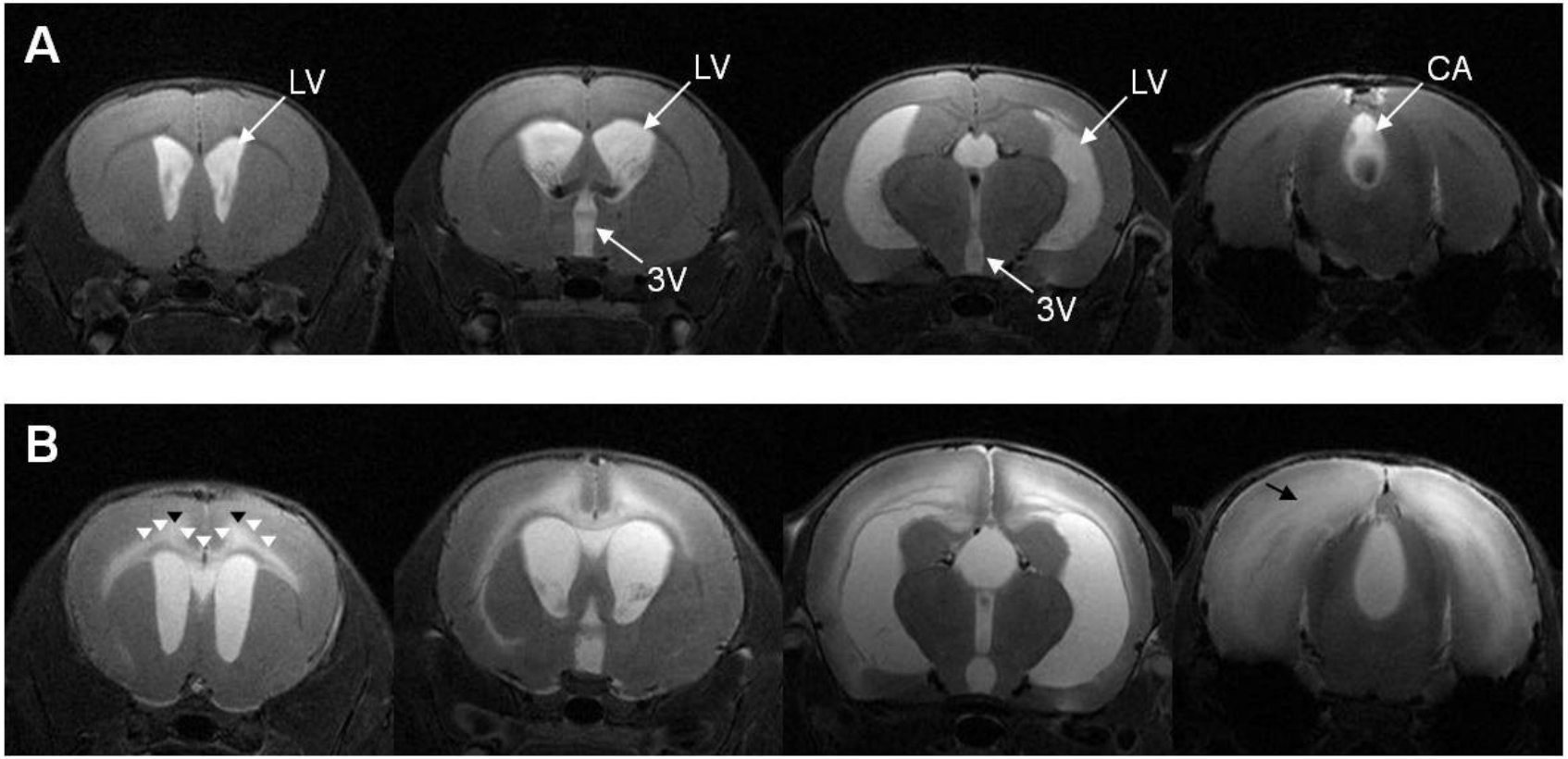

Figure 6.3. Representative coronal T-2 weighted MRI images from kaolin injected rats at 6 days. Ventriculomegaly developed by 6 days after kaolin injection. **(A)** Images (Left to right – anterior to posterior) from a kaolin injected rat whose ventricles enlarged to 135.6mm^3 and showed no oedema. **(B)** Images from a kaolin injected rat whose ventricles enlarged to 275.5mm^3 and demonstrated oedema in the white matter (white arrow heads, periventricular white matter and corpus callosum) and cortex (black arrow heads and black arrow). CA – cerebral aquaduct, LV – lateral ventricle, 3V – third ventricle.

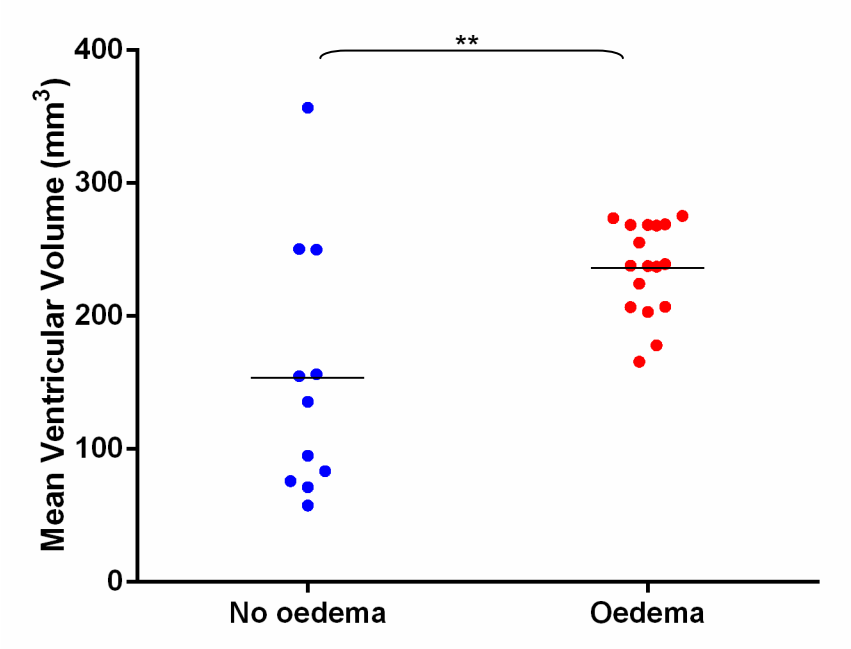

Figure 6.4. Comparison of ventricular volumes with oedema on day 6 MRI scans. The scatter plot summarise the mean of the ventricular volumes of rats presenting with and without oedema. At 6 days after the kaolin injection, larger ventricular volumes were associated with the presence of oedema in the white matter and cortex. **P<0.01.

6.3.3. Delayed Decorin treatment did not affect ventriculomegaly

On the 6 day MRI (before pump implantation) there was no difference between the ventricular volumes of the Kaolin (237.9±12.2mm^3), Kaolin+PBS (197.7±26.3mm^3) and Kaolin+Decorin (207.9±24.2mm^3) groups. Overall on the 20 day MRI scan there was an increase in ventricular volume in the Kaolin (288.7±46.8mm^3), Kaolin+PBS (299.7±85.2mm^3) and Kaolin+Decorin (346.7±108.8mm^3) groups compared to the 6 day measurements. At 20 days there was no significant difference between the three groups **(Fig. 6.5)**. The scatter plot **(Fig. 6.6)** shows the ventricular volume changes for each rat. The results demonstrated that there were 3 types of hydrocephalus that developed;

a) Progressive – increase in ventricular volume between the two MRI scans
b) Stable – similar ventricular volumes on both MRI scans (±10mm^3)
c) Declining – decrease in ventricular volume between the two MRI scans.

In progressive hydrocephalus the lateral ventricles continued to expand throughout all anterior-posterior sections. In stable hydrocephalus the lateral ventricles remained a similar size with slight changes in shape. In declining hydrocephalus the majority of changes occurred posterior with the lateral ventricle horns, cerebral aqueduct and fourth ventricle reducing in size **(Fig. 6.7).** These 3 types of hydrocephalus were present in all the groups **(Table 6.1)**. There were 4 rats, 2 from the Kaolin+PBS group and 2 from the Kaolin+Decorin group, that developed severe hydrocephalus and were killed early **(Fig. 6.8)** with the ventricles enlarging more than 250% between MRI scan 1 and the MRI scan conducted on the day they were killed (day 17-19).

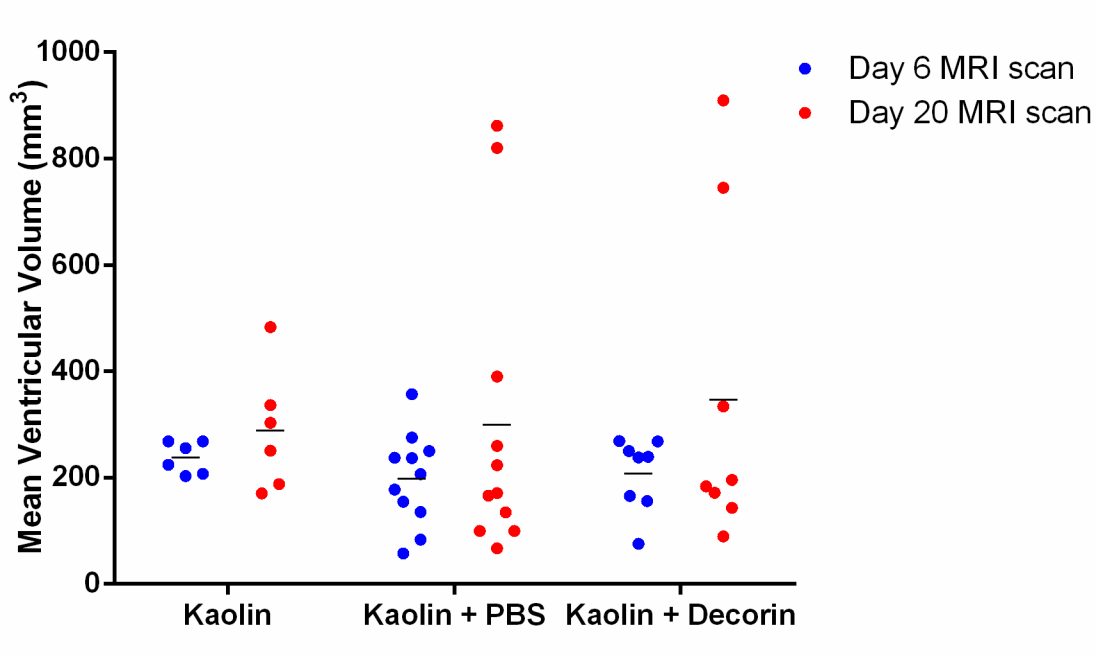

Figure 6.5. Ventricular volumes from day 6 and day 20 MRI scans. The scatter plot summarises the mean of the ventricular volumes from the MRI scans on day 6 and day 20 in the Kaolin, Kaolin+PBS and Kaolin+Decorin groups. In all three groups the mean ventricular enlargement increased between the MRI scans. There was no significant difference between the 3 groups.

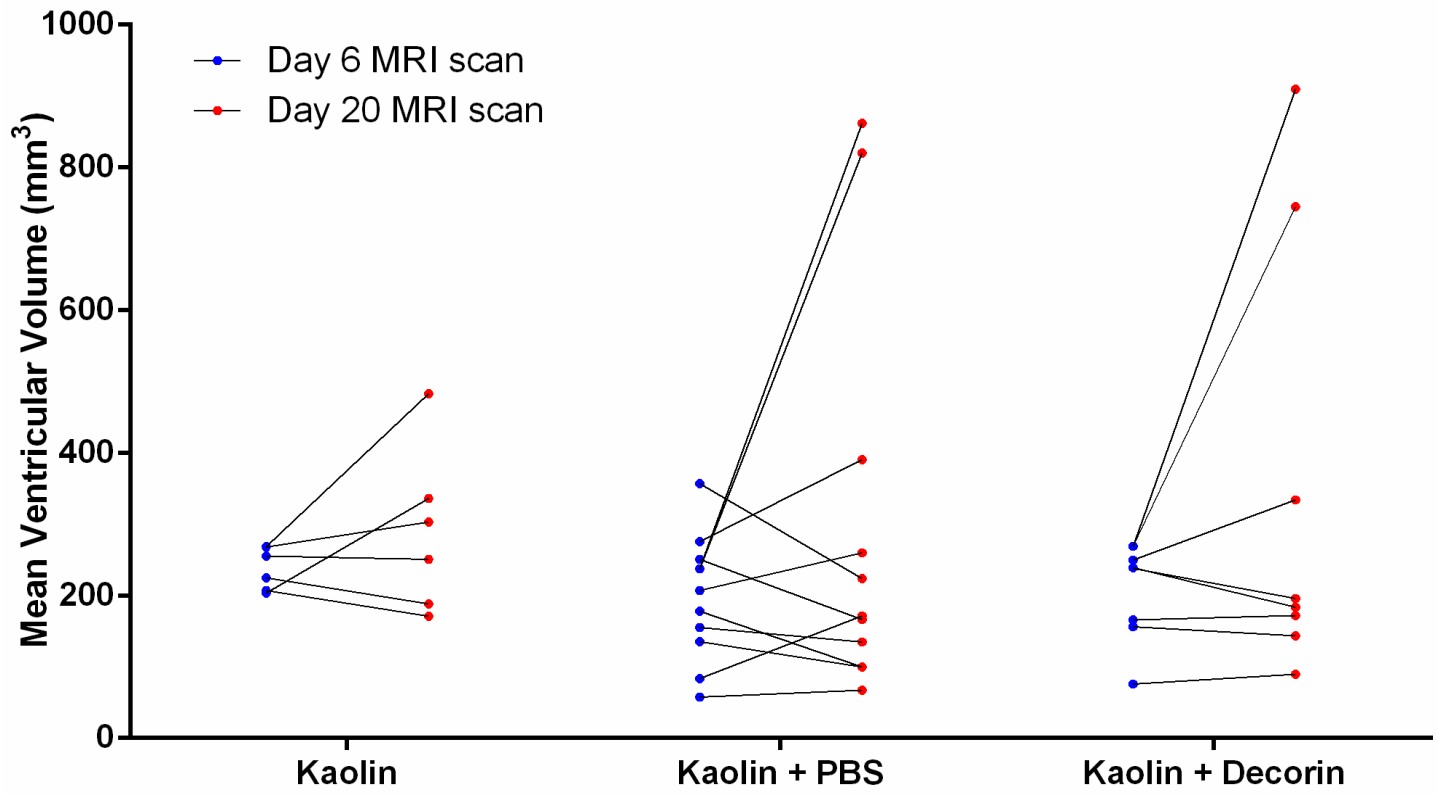

Figure 6.6. Individual rat ventricular volumes from day 6 and 20 MRI scans. The scatter plot summarises the data from the MRI scans on day 6 and day 20 in the Kaolin, Kaolin+PBS and Kaolin+Decorin groups. The ventricular volumes between the day 6 and day 20 MRI scan demonstrated 3 types of hydrocephalus; progressive, stable and declining. There were 4 rats (2 from the Kaolin+PBS group and 2 from the Kaolin+Decorin group) with severe hydrocephalus that demonstrated ventricular volumes of over 700mm^3 on the day 20 MRI scan.

Group	Progressive	Stable (±10mm^3)	Declining
Kaolin (n=6)	3	1	2
Kaolin + PBS (n=11)	5	1	5
Kaolin +Decorin (n=8)	4	1	3

Table 6.1. Types of hydrocephalus. The number of rats in the Kaolin, Kaolin+PBS and Kaolin+Decorin groups that showed progressive, stable and declining hydrocephalus between the MRI scans on day 6 and day 20.

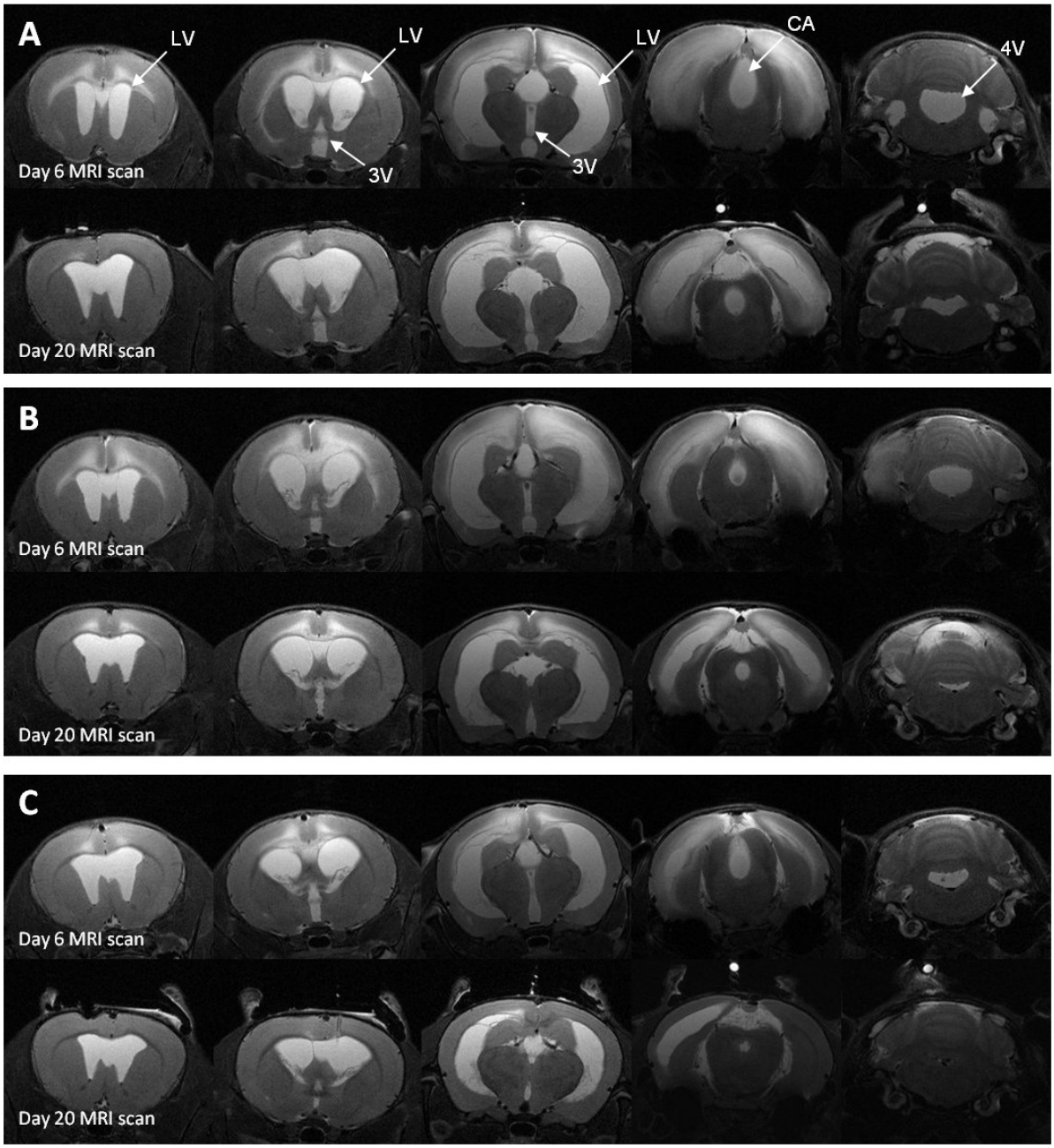

Figure legend on following page…

Figure 6.7. Representative coronal T-2 weighted MRI images of the three types of hydrocephalus. Images (Left to right – anterior to posterior) from MRI scans conducted on day 6 and day 20 illustrating the 3 types of hydrocephalus. **(A)** A rat from the Kaolin+PBS group demonstrating progressive hydrocephalus with enlargement of the lateral ventricles throughout the brain. **(B)** A rat from the Kaolin group demonstrating stable hydrocephalus with little or no change in size of the lateral ventricles and sometimes a smaller fourth ventricle. **(C)** A rat from the Kaolin+Decorin group with declining hydrocephalus which mainly affected the posterior of the brain leading to reductions in the size of the lateral ventricles, cerebral aqueduct and the fourth ventricle. CA – cerebral aquaduct, LV – lateral ventricle, 3V – third ventricle, 4V – fourth ventricle.

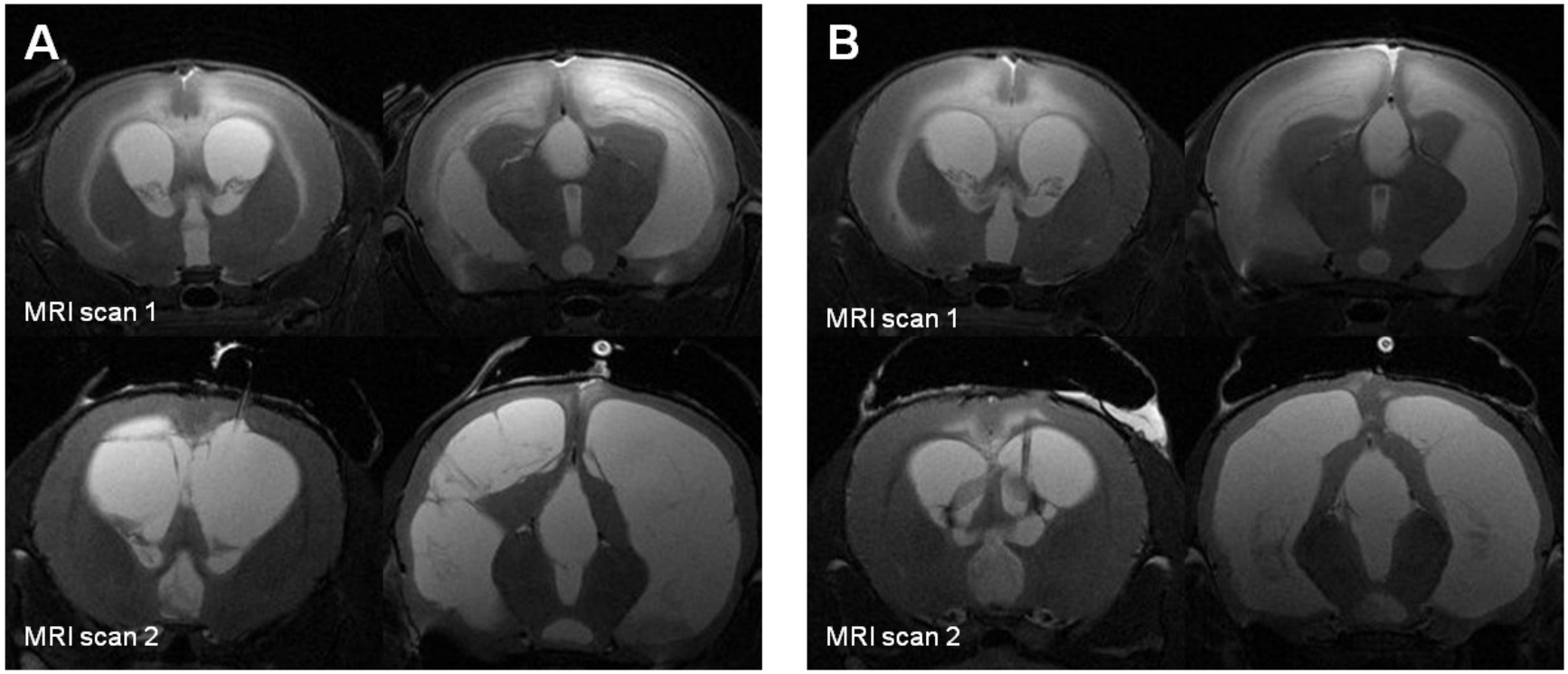

Figure 6.8. Representative coronal T-2 weighted MRI images of the development severe hydrocephalus. MRI was conducted on day 6 (MRI scan 1) before the implantation of the pump and just before sacrifice (day 17-19; MRI scan 2). Images (left to right – anterior to posterior) of rats with severe hydrocephalus from the Kaolin+PBS group **(A)** and the Kaolin+Decorin group **(B).**

6.3.4. Early oedema leads to greater enlargement of the ventricles

There was a reduction in the number of rats with oedema in the 20 day MRI scan (11/25 rats, 44%) compared to the 6 day MRI scan. In addition, if rats exhibited oedema on the day 6 MRI scan they had significantly larger ventricles on the day 20 MRI scan (398.2±69.5mm^3) compared to those rats without oedema (159.0±27.0mm^3, **Fig. 6.9.A)**. In comparison, rats with oedema only present on the day 20 MRI scan had similar ventricular volumes on the day 20 MRI scan (309.0±54.8mm^3) to rats without oedema (314.5±81.6mm^3; **Fig. 6.9.B)**. The 4 rats with severe hydrocephalus demonstrated major oedema on the day 6 MRI scan, which was reduced to little or no oedema in the day 20 MRI scan most likely due to the progressive expansion of the ventricles **(Fig. 6.8)**.

In the Kaolin+PBS group there appeared to be an association between ventricular enlargement and oedema. 4/6 (67%) of rats without oedema in the day 6 MRI scan demonstrated a reduction in ventricular volume between the two scans while 4/5 (80%) of rats with oedema showed an increase in ventricular volume. This comparison could not be done in the Kaolin group as there were no rats without oedema in the day 6 MRI scan and in the Kaolin+Decorin group there was no association.

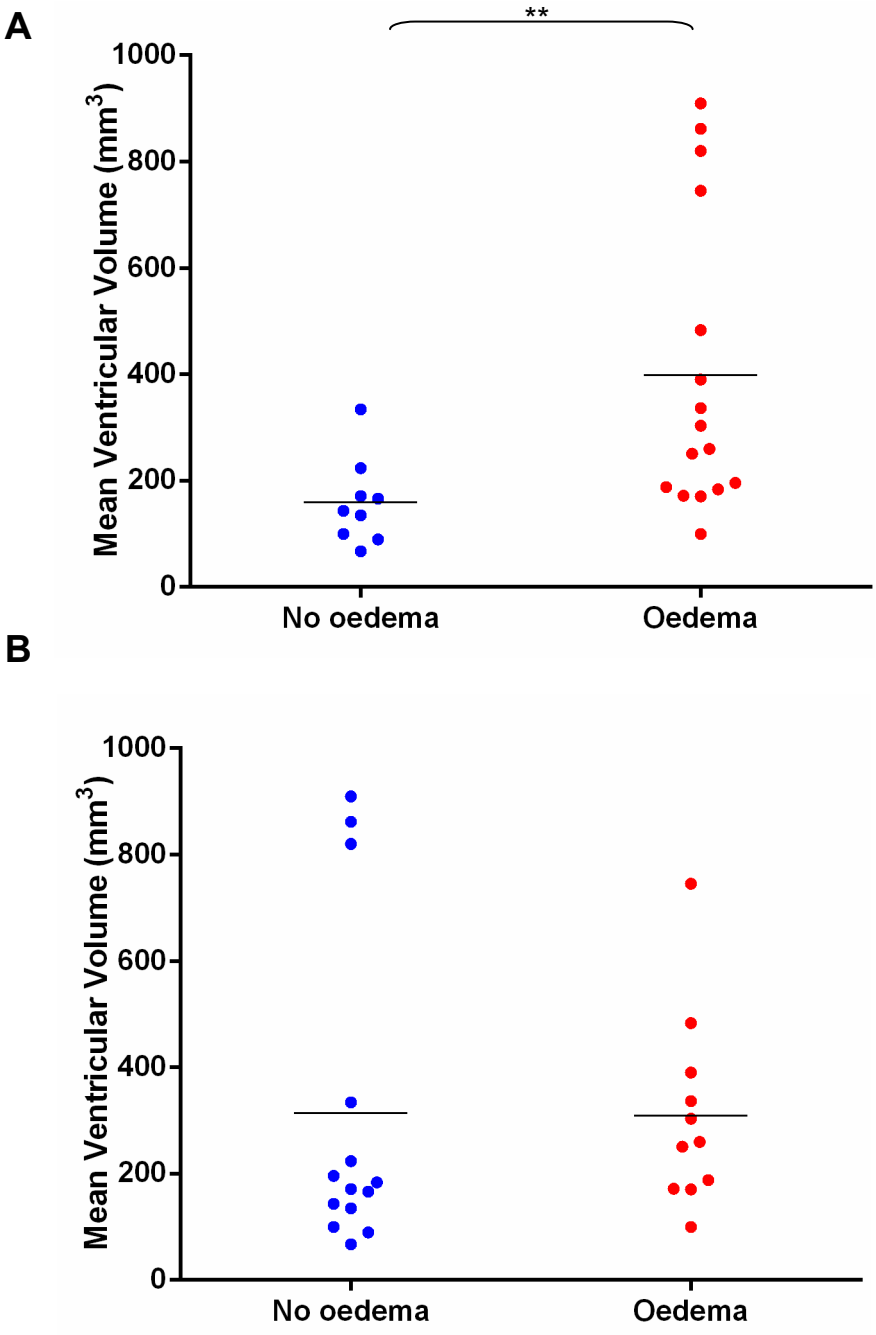

Figure 6.9. Comparison of ventricular volumes and oedema. The scatter plots summarise the mean of the ventricular volumes of rats on day 20 MRI scans. **(A)** Rats with oedema on the day 6 MRI scan went on to develop larger ventricles on the day 20 MRI scan compared to rats without oedema on day 6. **(B)** The presence of oedema only on the day 20 MRI scan was not correlated to higher ventricular volume. **P<0.01.

6.3.5. Human Decorin was undetectable in brains with severe hydrocephalus

Human Decorin staining was performed in this study to determine the distribution of the infused human Decorin throughout the brain. The staining was also conducted in rats from the Kaolin+Decorin group described in Chapter 4 to determine whether there were any differences in distribution resulting from the delayed delivery of Decorin. In the acute Kaolin+Decorin group described in Chapter 4, intraventricular Decorin infusion began on the same day as the injection of kaolin into the basal cistern used to induce hydrocephalus. Human Decorin staining was observed in the subarachnoid space and on the apical surface of the choroid plexus and ependymal cells **(Fig. 4.4 and Fig. 6.10.A-B)**. In the chronic Kaolin+Decorin group, Decorin infusion began 7 days after the injection of kaolin. In this chronic group there were varying intensities of human Decorin staining apparent in the subarachnoid space. In 3 rats there was no detectable human Decorin staining and in the remaining 5 rats the levels varied from low to moderate intensities. Human Decorin staining was only observed in the lateral ventricles of 1 rat **(Fig. 6.10.C-F)**. This data suggests that the distribution of Decorin is not as efficient when Decorin is infused after fibrotic blockade of CSF flow and hydrocephalus has developed.

Further investigations revealed that all the rats with no detectable human Decorin staining in the subarachnoid space showed an increase in ventricular volume between the 2 MRI scans and this included the 2 rats with severe hydrocephalus. Out of the remaining rats with positive human Decorin staining in the subarachnoid space, 3 rats had declining hydrocephalus, 1 rat had stable hydrocephalus and 1 rat had progressive hydrocephalus, although the increase in ventricular volume was only 13.5mm^3 (76.0 to 89.5mm^3).

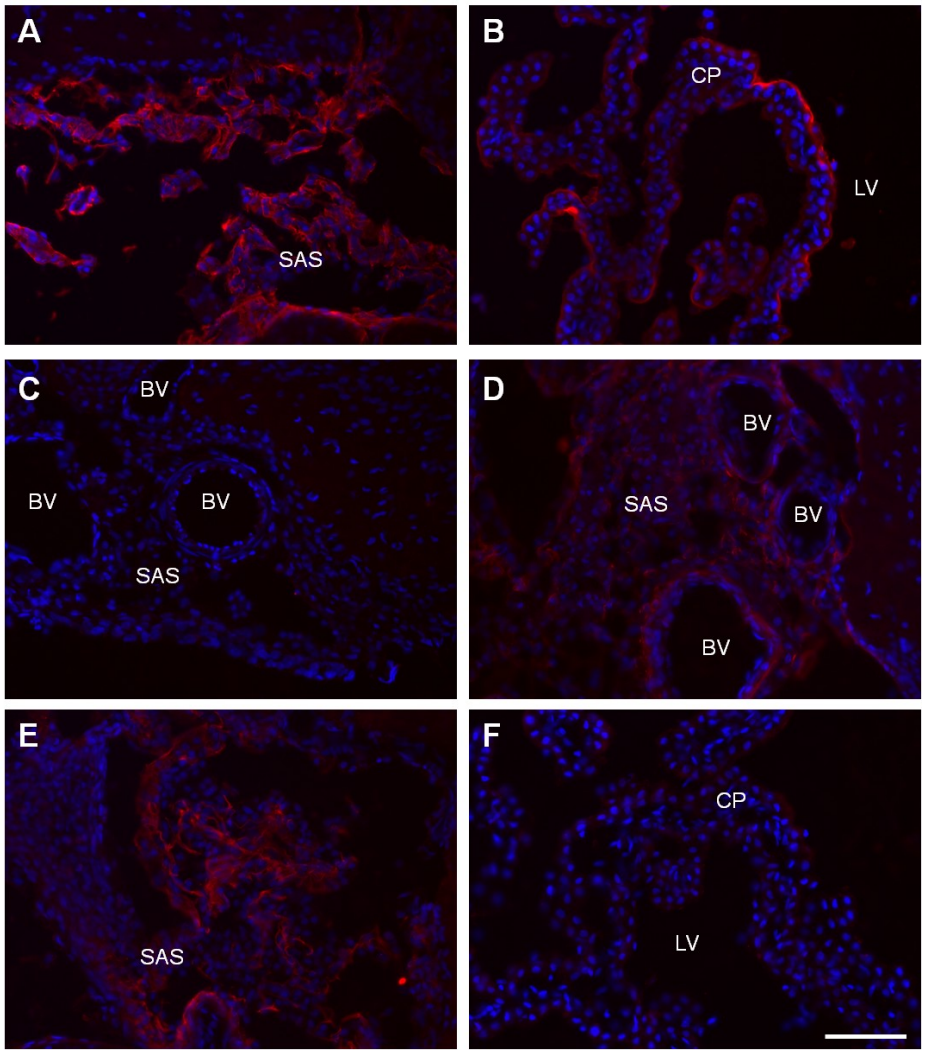

Figure 6.10. Distribution of Decorin in the brain and subarachnoid space in the acute and chronic Kaolin+Decorin groups. When Decorin infusion began the same day as the kaolin injection (acute), human Decorin (*red*) staining was observed in the subarachnoid space **(A)** and on the apical surface of the choroid plexus in the lateral ventricles **(B)**. When Decorin infusion began 7 days after the kaolin injection (chronic), the intensity of Decorin staining in the subarachnoid space varied from no detectable Decorin **(C)** to low **(D)** and medium **(E)** intensities. Human Decorin staining was not observed in the lateral ventricles **(F)**. DAPI (*blue*) was used as a generic nuclear marker; scale bar – 100μm; BV – blood vessel, CP – choroid plexus, LV – lateral ventricle, SAS – subarachnoid space.

6.3.6. Decorin did not affect the levels of fibronectin in the subarachnoid space

In the Intact group, thin strands of fibronectin were present in the subarachnoid space. In all kaolin injected groups there was an increase in fibronectin staining in the subarachnoid space, and there were no apparent differences between the groups **(Fig 6.11)**. There did not appear to be any correlation between the amount of fibronectin staining and the treatment group or the size of the ventricles. This data suggests that delayed Decorin treatment did not reduce ECM deposition in the subarachnoid space.

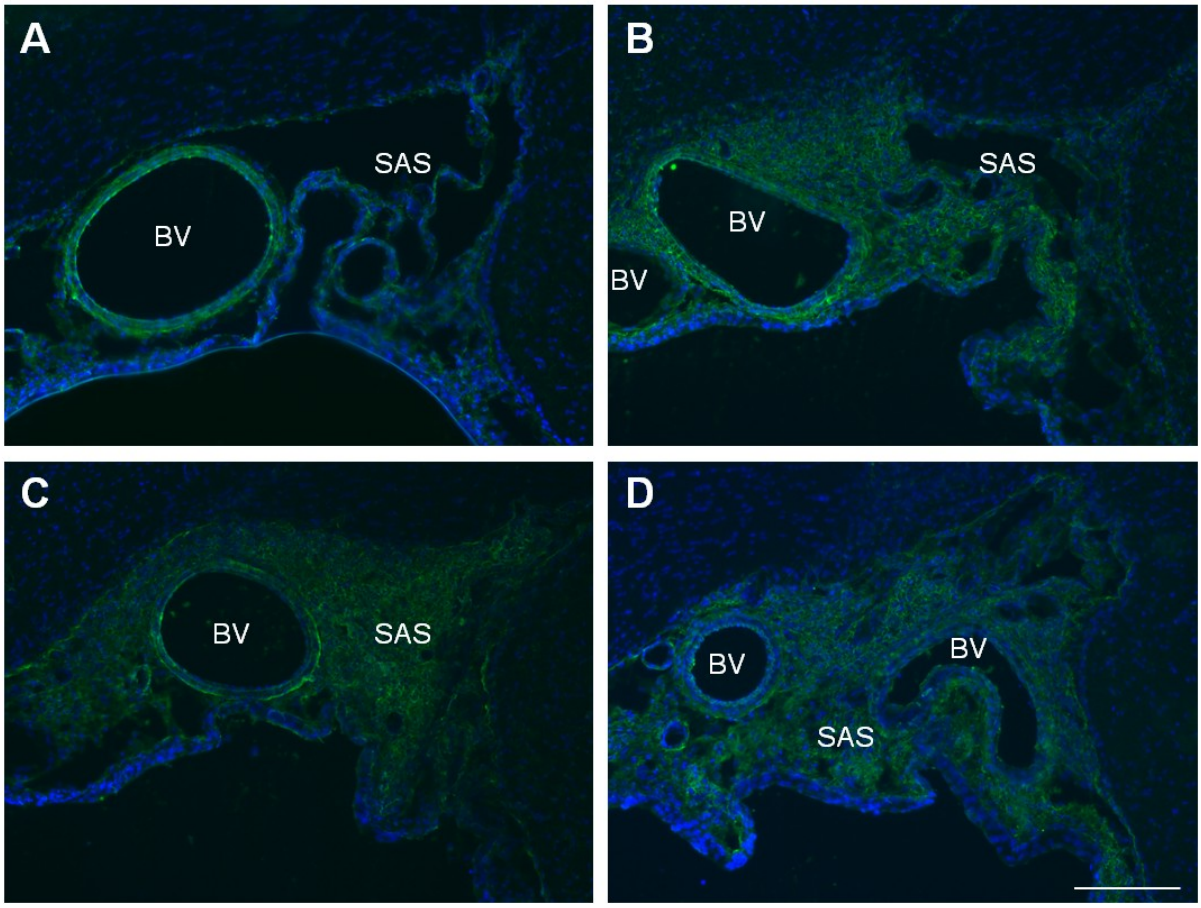

Figure 6.11. Fibrosis in the subarachnoid space 21 days after kaolin injection. Representative images of fibronectin (*green*) staining in the Intact **(A)**, Kaolin **(B)**, Kaolin+PBS **(C)** and Kaolin+Decorin **(D)** groups. The amount of fibronectin positive staining increased in the Kaolin, Kaolin+PBS and Kaolin+Decorin groups compared to the Intact group. DAPI (*blue*) was used as a generic nuclear marker; scale bar – 200μm; BV – blood vessel, SAS – subarachnoid space.

6.3.7. Delayed intraventricular Decorin did not affect TGF-β levels in the ependyma

Previously (in Chapter 4) it was demonstrated that acutely delivered human Decorin prevented the kaolin-induced increase in TGF-β1 levels in the ependyma, therefore in this study the same approach was used to determine whether delayed Decorin treatment could influence ependymal TGF-β1 levels. Interestingly, the intensity of ependymal TGF-β1 staining (arbitrary units of pixel intensity) was similar between the Intact (36.8±3.3), Kaolin (40.7±9.7), Kaolin+PBS (45.7±6.7) and Kaolin+Decorin (47.4±3.7) groups. The intensity of TGF-β1 staining in the ependyma of the Kaolin+Decorin-Pump (29.8±9.3) group showed a trend to being lower compared to the other 4 groups **(Fig 6.12.A-C)**. The TGF-β1 staining appeared patchy in places and this may be due to denuadation of the ependyma caused by hydrocephalus **(Fig. 6.12.D)**. In addition, there were numerous cells beneath the ependyma that were positive for TGF-β1, especially in the periventricular white matter **(Fig. 6.12.E)**. This data suggests that delayed Decorin treatment did not affect ependymal TGF-β1 levels possibly due to poor Decorin delivery and distribution.

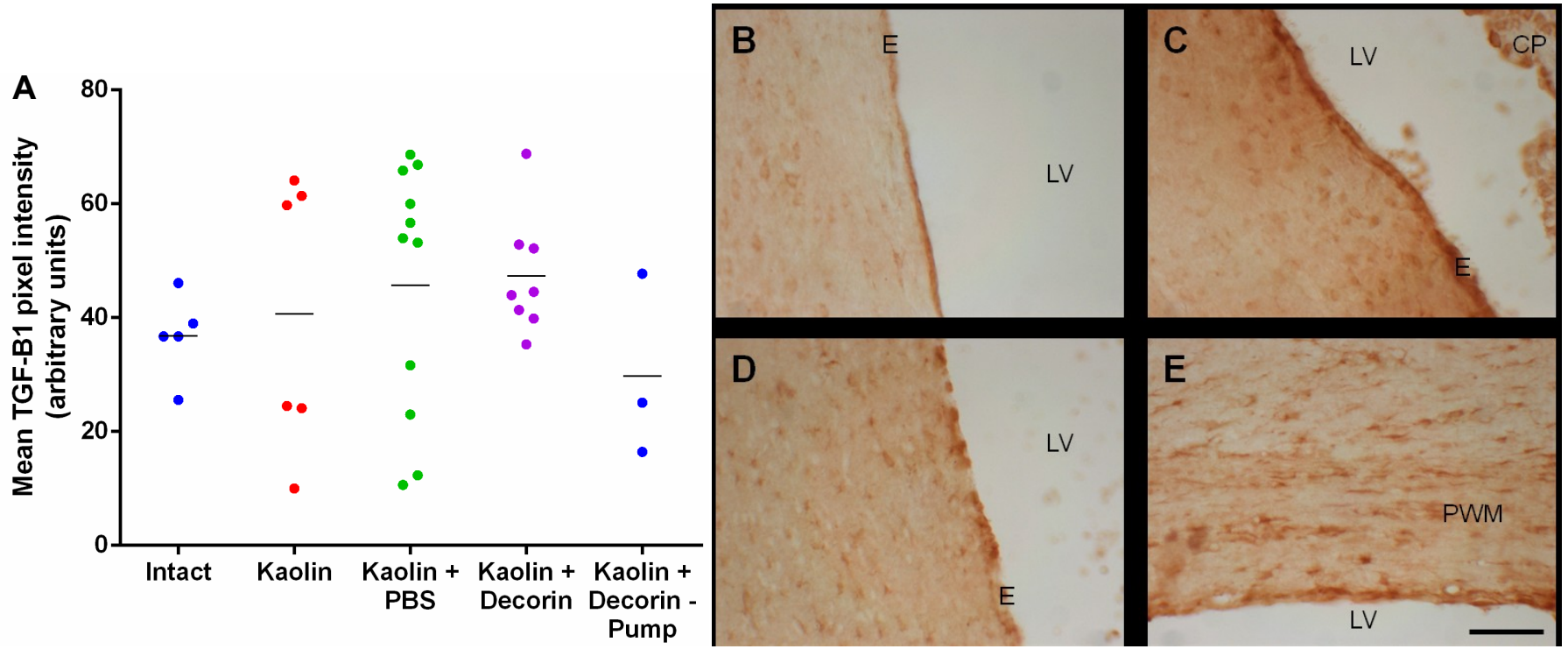

Figure 6.12. TGF-β1 staining in the white matter and ependyma after 21 days. **(A)** Scatter plot of mean TGF-β1 pixel intensities in the 5 groups. The levels of TGF-β1 staining in the ependyma was similar between the Intact, Kaolin, Kaolin+PBS, Kaolin+Decorin and Kaolin+Decorin-Pump group. Representative images of TGF-β1 positive staining in the ependyma from an Intact rat **(B)** and a hydrocephalic rat **(C). (D)** Denudation of the ependyma could be observed as patchy TGF-β1 staining in hydrocephalic rats. **(E)** Subependymal cells and cells in the periventricular white matter were also positive for TGF-β1. Scale bar–100μm; CP – choroid plexus; E – ependyma; LV – lateral ventricle, PWM – periventricular white matter.

6.3.8. Decorin did not affect GFAP levels in the corpus callosum

In Chapter 4 it was demonstrated that Decorin prevented the increase in kaolin-induced GFAP levels in the corpus callosum, most likely by preventing the enlargement of the ventricles and the underlying tissue damage. Therefore in this study it was important to determine whether Decorin had any impact on GFAP once hydrocephalus had developed. The levels of GFAP immunostaining (percentage of immunofluorescent pixels per area) in the corpus callosum showed a trend to being higher in the Kaolin (11.6±3.1%) and Kaolin+PBS (10.2±3.0%) groups compared to the Intact group (3.3±0.8%). The levels of GFAP immunostaining showed a trend to being lower in the Kaolin+Decorin (7.0±1.6%) and Kaolin+Decorin-Pump (5.0±3.7%) groups compared to the Kaolin and Kaolin+PBS groups **(Fig. 6.13.A)**. Also in the Kaolin+Decorin group the highest levels of GFAP were observed in the 3 rats with no visible Decorin staining in the subarachnoid space. Therefore these results suggest that Decorin did not affect astrogliosis associated with hydrocephalus. The levels of GFAP in the corpus callosum were also compared in rats with and without oedema as the corpus callosum is one of the areas that is most affected by oedema. The rats that had oedema on the day 6 MRI scan had significantly ($P<0.001$) higher levels of GFAP (12.6±2.0%) compared to rats without oedema (4.1±1.5%; **Fig. 6.13.B)**. This suggests that oedema may influence astrogliosis in the corpus callosum.

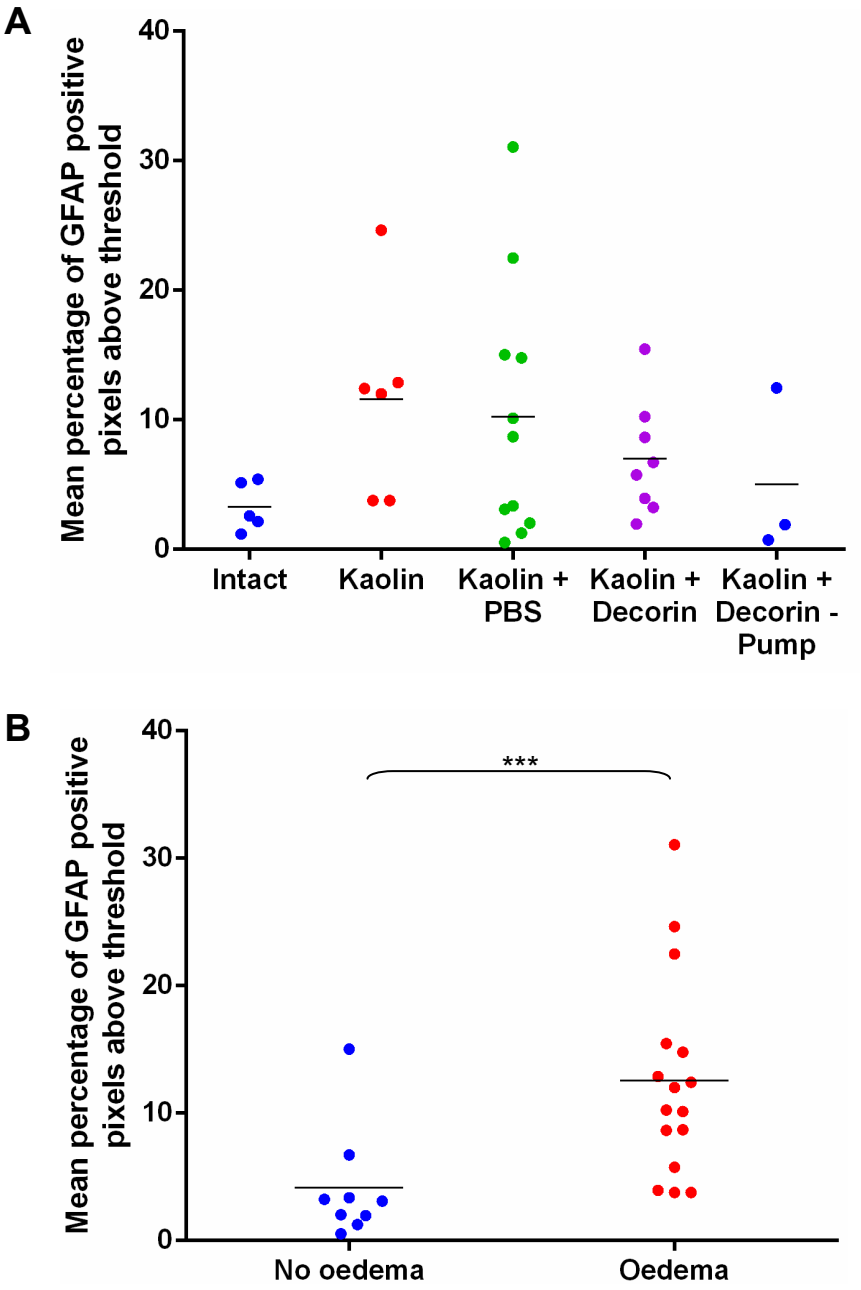

Figure 6.13. Astrogliosis in the corpus callosum at 21 days after kaolin injection. Scatter plots of the mean percentage GFAP positive staining in the corpus callosum. **(A)** The levels of GFAP were similar between all the groups however there was a trend towards the Kaolin and Kaolin+PBS groups being higher compared to the Intact, Kaolin+Decorin and Kaolin+Decorin-Pump groups. **(B)** Rats with oedema in the day 6 MRI scan had significantly higher levels of GFAP compared to those rats which did not have oedema. ***P<0.001.

6.4. Discussion

This study demonstrated that continuous intraventricular infusion of human recombinant Decorin delivered by osmotic min pump, 7 days after the injection of kaolin to induce hydrocephalus, did not affect ventriculomegaly. In addition, infused Decorin did not affect the kaolin-induced increase in subarachnoid fibrosis, ependymal TGF-β1 levels or astrogliosis in the corpus callosum. These findings suggest that intraventricular delivery of human Decorin by osmotic mini pump is not a useful treatment strategy or regime for hydrocephalus after fibrosis has developed, probably because of problems with drug delivery.

6.4.1. Decorin's effects on degradation of extracellular matrix molecules

Chapter 4 demonstrated that Decorin is able to prevent the deposition of ECM leading to the subsequent development of subarachnoid fibrosis and hydrocephalus. TGF-βs not only increase the deposition of ECM but also reduce the degradation of ECM through inhibition of matrix metalloproteinases (MMPs) and enhancing tissue inhibitors of metalloproteinases (TIMPs; Border and noble, 1994). Therefore, Decorin may have a role in ECM degradation (fibrolysis) through its inhibition of TGF-β and consequent action of proteases. ECM deposition occurs as early as 3 days after the injection of kaolin and therefore this study was set up to determine whether delayed intraventricular Decorin was also able to treat established hydrocephalus by degrading mature subarachnoid fibrosis. The results demonstrated that intraventricular human Decorin had no effect on the amount of fibrosis present in the subarachnoid space and therefore did not affect the degradation of ECM. In previous studies, exogenous human Decorin was able to increase the levels of MMP-2 and

cause a decrease in TIMP-2 in a model of chronic spinal cord injury, thereby aiding tissue remodelling in chronic fibrotic wounds (Z. Ahmed and D Mahay, unpublished data). In addition, Decorin deficient mice with hepatic fibrosis demonstrate reduced MMP-9 and -2 and increased TIMP-1 levels when compared to wild type mice (Baghy *et al*., 2011). On the other hand, Decorin has also been shown to reduce MMP-1 and -3 in gingival fibroblasts, possibly through its induction of interleukin 4 (Al Haj Zen *et al*., 2003). These inconsistencies indicate that Decorin's actions may be cell specific and possibly TGF-β independent.

The results presented here and in Chapter 4 suggest that intraventricular Decorin delivery via osmotic mini pump is better suited to preventing the formation of subarachnoid fibrosis rather than degrading established ECM when CSF circulation is compromised.

6.4.2. Efficiency of Decorin delivery

An alternative interpretation of the results is that Decorin was not delivered efficiently through intraventricular infusion to elicit a therapeutic response. The lack of detectable levels of Decorin in the subarachnoid space of 3/4 rats with progressive hydrocephalus could be evidence towards this theory. ICP increases significantly in hydrocephalus and accounts for some of the pathology associated with the disease, however it usually reduces to normal levels by 6 weeks (Kondzeilla *et al*., 2002). Therefore, it could be postulated that the osmotic mini pumps were unable to infuse efficiently into a high pressure environment. These pumps were used in studies to deliver agents that induce hydrocephalus (Krishnamurthy *et al.,* 2009) however there is limited information about their use in treating established hydrocephalus. Tada *et*

al, (2006) induced hydrocephalus and then implanted an osmotic mini pump containing hepatocyte growth factor (HGF), an anti-fibrotic agent that counteracts TGF-β activity, 6 weeks after the induction of hydrocephalus. It was demonstrated that continual infusion of HGF for 14 days caused a reduction in ventricular size (measured on one MRI scan). Implanting the pumps after 6 weeks, when ICP has reduced to normal levels, may have allowed the pump to work efficiently. Hence, studies need to be conducted to determine the efficiency of the pumps in high pressure situations. It may be pointed out that when implanting the pump, CSF was able to leak out before the cannula was permanently attached to the skull thereby reducing ICP. However this would have only been for a short period of time as it only takes 2 hours for CSF to be completely replaced in a rat (Preston, 2001) and therefore ICP would have increased again relatively rapidly. The results presented here also demonstrate the need to measure ICP changes in the model. It may be that the treatment needs to be delayed until ICP has returned to normal levels.

6.4.3. Decorin and TGF-β1

In Chapter 4 it was shown that infused human Decorin was detected in the lateral ventricles on the apical surface of the choroid plexus and ependyma. In addition Decorin infusion prevented the kaolin-induced increase in ependymal TGF-β1 levels. In this study there was a lack of detectable human Decorin in the lateral ventricles and furthermore ependymal TGF-β1 levels were similar between the rats receiving PBS and human Decorin. This data suggests that human Decorin was not present in the lateral ventricles at bioactive levels to inhibit TGF-β1. In hydrocephalus the flow of CSF will be affected, causing stagnation of CSF in the ventricles.

Consequently it was presumed that there would be higher levels of Decorin in the lateral ventricles compared to the subarachnoid space, however this was not the case. Furthermore there was denudation of the ependyma which could have affected the levels of TGF-β1 observed lining the ventricle. Immunohistochemistry is extremely useful for establishing the localisation of molecules within the tissue however it only indicates differences in the levels of molecules and therefore is at best semi-quantitative. Additional studies where the ependyma is removed and processed are required to get definitive quantitative results on TGF-β1 protein and gene expression.

6.4.4. Oedema, ventricular enlargement and astrogliosis

This study demonstrated the importance of early oedema in the development of hydrocephalus. The presence of oedema in the early day 6 MRI scan was associated with a greater increase in ventricular size by the day 20 MRI scan. In addition, there was a link between the levels of GFAP in the white matter and the early presence of oedema. Oedema is closely associated with raised ICP as oedema often reduces once ICP levels have normalised (Braun *et al*., 1997, 1998). Also in hydrocephalic rats, GFAP levels dramatically increase at the same time as ICP begins to rise, and shunting, which effectively reduces ICP causes a reduction in GFAP levels (Miller and McAllister, 2007). Together this data suggests that raised ICP and oedema are causally linked, which is also associated with a worse outcome. More studies need to be conducted to measure the direct effect of ICP on oedema, ventricular enlargement and the associated neural pathologies.

6.4.5. Diversity in hydrocephalus development

The kaolin-induced model of communicating hydrocephalus used here is relatively new and had not previously been used in 3 week-old rats, therefore the aetiology and progression of hydrocephalus is unknown. The results from this study corroborate the work conducted in the kaolin model of non-communicating hydrocephalus where 3 types of hydrocephalus development were proposed; progressive, stable and declining (Braun *et al*.,1998). In this study all types of hydrocephalus were observed in the Kaolin group, which suggests that the pump implantation, which could potentially release a small amount of CSF thereby lowering ICP, had no bearing on the progression of hydrocephalus.

This experiment has brought to light the diversity of hydrocephalus development in this model which most likely reflects the development of hydrocephalus in humans. It also highlights the fact that other factors need to be taken into account when assessing outcomes including oedema and ICP. In this study the appearance of oedema in the early scan appeared to be predictive in the progression of hydrocephalus. ICP was not measured in this study, however it would be beneficial to further aid in the understanding of the changes in ventricular volume with time.

6.4.6. The Kaolin+Decorin-Pump group

During this chronic experiment, 3 rats in the Kaolin+Decorin group removed the pump from the catheter tubing, which would stop the delivery of Decorin but more importantly would mean that the cannulae acted similar to a shunt draining CSF. These rats were therefore put into a separate group called the Kaolin+Decorin-Pump

group. While the data from this group cannot give any definitive results, it indicates what changes may occur with shunting. There was a non-significant trend towards a reduction in TGF-β1 in the ependyma and GFAP in the corpus callosum in this group. Previously shunting in HTx rats had also shown a reduction in GFAP levels in the cortex although not to control levels (Miller and McAllister, 2007). Therefore, shunting is able to reduce the effects of hydrocephalus, although generally not to normal levels.

6.4.7. Conclusion

There is diversity in the development of hydrocephalus in response to blocking CSF drainage and therefore it is important that treatments are given at the right time to have a beneficial effect. In the chronic study reported here intraventricular Decorin delivered by osmotic mini pump began 7 days after the injection of kaolin, and the results showed that this treatment regime had no significant effects on resolving established subarachnoid fibrosis and hydrocephalus. Future studies need to be conducted to investigate the effects of ICP in the model of communicating hydrocephalus and on the delivery of Decorin into the lateral ventricles.

Chapter 7

Discussion

7.1. General conclusions

The studies described in this thesis aimed to investigate the effects of the transforming growth factor-β (TGF-β) antagonist Decorin on the development of juvenile communicating hydrocephalus. An advantage of this study was that the human recombinant Decorin was manufactured at a GMP grade that would be suitable for use in humans, and therefore highlights the potential for Decorin treatment to be translated from experimental research to clinical trials.

Initial studies were conducted to establish a suitable *in vivo* model of communicating hydrocephalus and to explore the efficacy of human recombinant Decorin on fibrogenesis in rat brain meningeal cell cultures. Two models of kaolin induced hydrocephalus were assessed; the prechiasmatic cistern model and the basal cisterns model. After the initial studies, it was established that the basal cisterns model was more appropriate for future studies as it reliably induced ventricular enlargement and changes in endogenous TGF-β1 levels. These studies support a role for TGF-β in the development of hydrocephalus. In addition, the *in vitro* studies showed that recombinant human Decorin reproducibly blocked TGF-β1-induced extracellular matrix (ECM) production by meningeal fibroblasts.

Post-haemorrhagic hydrocephalus develops after a bleed due to the formation of fibrotic lesions in the subarachnoid space that obstruct the flow and drainage of cerebrospinal fluid (CSF; Motohashi *et al.*, 1995a; Massicotte and Del Bigio, 1999). Therefore initiating Decorin delivery immediately after the bleed should block the effects of TGF-β signalling from the outset as a prophylactic therapy. This hypothesis formed the basis for the acute experiment (Chapter 4), which was set up to determine if Decorin could prevent the formation of fibrosis in the subarachnoid

space. To achieve this, Decorin delivery began immediately after the injection of kaolin and continued for 14 days. It was established that continuous intraventricular infusion of Decorin prevented the development of kaolin-induced hydrocephalus. Decorin reduced inflammation and ECM deposition in the subarachnoid space, maintained normal levels of TGF-β1/Smad signalling in the ependyma and prevented the kaolin-induced increase in astrogliosis in white matter. These findings suggest that Decorin prevents the formation of subarachnoid fibrosis by inhibiting the TGF-β signalling pathway, thus protecting against the development of hydrocephalus and associated brain pathology.

Chapter 5 further supported this work by investigating the early effects of Decorin treatment on kaolin-induced inflammation. In these studies, the early cellular response after the onset of hydrocephalus was assessed. The results from these studies clearly indicate that Decorin reduces the inflammatory response in the subarachnoid space, potentially by reducing inflammatory cell infiltration. In addition, Decorin reduces the response of resident cells in the subarachnoid space and periventricular regions, and also reduces astrogliosis and microgliosis in the white matter. These findings further signify the importance of early application of human recombinant Decorin, as it suppresses the early inflammatory response which will subsequently influence subarachnoid fibrosis.

Finally the chronic experiment (Chapter 6) was set up to investigate whether Decorin is able to degrade subarachnoid fibrosis in an *in vivo* model of established hydrocephalus. In this chronic study intraventricular human recombinant Decorin infusion via osmotic mini pump began 7 days after the injection of kaolin to induce fibrosis and hydrocephalus. Under these experimental conditions Decorin has no

effect on ventriculomegaly, subarachnoid fibrosis or ependymal TGF-β1 levels. Together, all these findings suggest continuous intraventricular Decorin infusion can attenuate inflammation, subarachnoid fibrosis and hydrocephalus. In contrast, it is likely that alternative methods of Decorin delivery need to be developed to assess whether it can degrade subarachnoid fibrosis and resolve established hydrocephalus.

7.2. Recent advances in haemorrhagic hydrocephalus

There are four recent studies that have contributed to our knowledge of post-haemorrhagic hydrocephalus. Okubo *et al*. (2013) have induced subarachnoid haemorrhage (SAH) in rats using the endovascular perforation model and measured ventricular volume on MRI scans 24 hours later. They demonstrated that ventricular enlargement was apparent in 44% (12/27) of rats at 24 hours, which was associated with ventricular wall damage and activation of microglia. Although the hydrocephalus induced was most likely non-communicating and caused by blood clots blocking the ventricular system, it often leads to communicating hydrocephalus. Lackner *et al.* (2013) advanced this work and allowed the rats to survive for 21 days and measured intracranial pressure (ICP) at 7, 14 and 21 days. They demonstrated 40% (4/10) of the SAH rats had raised ICP and that these rats had enlarged ventricles compared the SAH without raised ICP. Together these studies demonstrated that the endovascular perforation model was able to induce post-haemorrhagic hydrocephalus in rats. On the other hand these studies also highlight the drawback of this model; that the perforation technique releases inconsistent amount of blood leading to high variability and low induction rates of hydrocephalus. If there was a way to regulate the amount of blood released, the endovascular perforation model

would be more viable for testing therapeutic agents. In addition, these studies showed that increased ICP was related to ventricular enlargement. This suggests that ICP could be used as surrogate marker for determining the development of hydrocephalus.

An interesting study by Li *et al.* (2013) demonstrated that thrombin injected into the lateral ventricles induced proliferative changes in the meninges. In addition, the effects of thrombin were reversed by a TGF-β inhibitor. This work corroborated previous *in vitro* studies where thrombin and other growth factors including TGF-β, have been shown to induce proliferation of leptomeningeal cells (Motohashi *et al*., 1995). Therefore, this study further supports the significant role of TGF-β in the development of hydrocephalus.

Finally Ahn *et al.* (2013) investigated the effect of human umbilical cord blood derived mesenchymal stem cells on post-haemorrhagic hydrocephalus. The experiment was based on the model developed by Cherian *et al.* (2004). Cherian *et al* (2004) injected 80µl of citrated adult rat blood into each ventricle on consecutive days in postnatal day 7 rat pups. Artificial CSF was injected in control rats. In the rats injected bilaterally with blood, there was a 20% mortality rate and 65% of surviving rats developed ventricular enlargement. Rats injected with artificial CSF had a 27% mortality rate and 50% developed ventricular enlargement. They did not use more than 80µl blood as it resulted in leakage of blood around the needle tract, and suggested that the increased ventricular enlargement in the rats injected with CSF was due to distension of the ventricles and increased ICP induced by the injection. In the study by Ahn *et al.* (2013) IVH was generated in postnatal day 4 rats by injecting 100µl of maternal whole blood into each lateral ventricle on the same day. A sham

operation without blood injection was performed in control rats. In the rats injected with blood, there was a 16% mortality rate and 85% developed ventricular enlargement. On postnatal day 7, rats either received an injection of mesenchymal stem cells, fibroblasts or saline. Only the injection of mesenchymal stem cells reduced the ventricular volume and was associated with a reduction in the inflammatory cytokines. These results are promising as they corroborate the findings presented in this thesis and suggest that reducing the blood induced-inflammatory response is important in preventing the development of post-haemorrhagic hydrocephalus.

7.3. Future Experiments

7.3.1. Cyclooxygenase-2 inhibition and Decorin

In the chronic study (Chapter 6), it was concluded that intraventricular Decorin was unable to degrade subarachnoid fibrosis or resolve hydrocephalus and therefore differences between the acute (Chapter 4) and the chronic (Chapter 6) experiments were examined. At this point it was discovered that different types of analgesics had been used. Due to restrictions at the University of Utah in 2012, Buprenophine was not permitted as an analgesic in the acute experiment, therefore the rats received Carprofen tablets the night before the kaolin injection and for the subsequent 2 days after the injection. In 2013 these restrictions were lifted and in the chronic experiment the rats received subcutaneous injections of Buprenophine before the surgery, and twice daily for the following 3 days. Carprofen is a non-steroidal anti-inflammatory drug mainly used for managing pain in animals. It specifically inhibits cyclooxygenase-2 (COX-2) and affects the synthesis of prostaglandins with pro-

inflammatory activity (Mitchell and Warner, 2006). In a model of traumatic brain injury, Carprofen was neuroprotective and reduced oedema, reactive microglia and pro-inflammatory cytokines (Thau-Zuchman *et al*., 2012). Moreover, levels of COX-2 have been shown to be increased after IVH (Lekic *et al*., 2012) and another COX-2 inhibitor, Celecoxib, reduced prostaglandin E2, neurophil infiltration, reactive astrogliosis and microgliosis in a rabbit model of IVH (Vinukonda *et al*., 2010). In wound healing, Prostaglandin E2 was involved in promoting inflammation however it was also anti-fibrotic as it reduced fibroblast proliferation and inhibited collagen production (Su *et al*., 2010). Therefore these studies suggest that Carprofen could have influenced the kaolin-induced subarachnoid fibrosis.

Carprofen was only given acutely for 2 days in the acute experiment therefore it would potentially reduce early inflammation while still allowing the anti-fibrotic properties of prostaglandins in the later stages. When observing the ventricular volumes for the two Kaolin groups from the acute and chronic experiments, the Kaolin group with Carprofen had lower ventricular volumes at 14 days ($155.7\pm31.9mm^3$, n=5) compared to the Kaolin group without Carprofen at 6 and 20 days ($237.9\pm12.2mm^3$ and $288.7\pm46.8mm^3$, respectively, n=6, significance at 20 day $P<0.05$). This demonstrates that Carprofen potentially reduced ventricular volume after the induction of hydrocephalus, however on its own it is not able to completely prevent it. This data suggests that Carprofen may have been acting synergistically with Decorin as the combination of the two did prevent hydrocephalus, but further studies are required to assess this association. Continuous Decorin infusion for 14 days would need to be given with and without Carprofen tablets for the first 2 days. In addition to determining ventricular volume, changes in the levels of inflammatory

cytokines and prostaglandin E2, a product of COX-2, could be measured in the brain and subarachnoid space to determine the effect on the inflammatory response.

7.3.2. Decorin treatment in a haemorrhagic model

The results presented in this thesis are very promising and demonstrate Decorin's therapeutic potential for preventing the development of post-haemorrhagic hydrocephalus. Accordingly, to progress the work described in this thesis, the Decorin treatment regime needs to be tested in a haemorrhagic model to determine whether Decorin is able to prevent haemorrhage-induced subarachnoid fibrosis and hydrocephalus. Haemorrhagic models would be more clinically relevant and more closely resemble the events that occur in humans. The basal cisterns injection of kaolin was used to induce communicating hydrocephalus in this thesis because at the time haemorrhagic models rarely demonstrated ventricular enlargement or had low induction rates. More recent studies have demonstrated that previous haemorrhagic models can be modified to produce a greater induction rate. Adapting both the Cherian *et al.* (2004) and the Ahn *et al.* (2013) models could produce a reliable model of post-IVH hydrocephalus. Injecting lower amounts (around 80ul) of citrated blood into both lateral ventricles would limit leakage of blood up the needle tract and would increase the haematocrit to levels required for inducing ventricular enlargement (Cherian *et al*., 2004), however injecting on the same day would better model a single IVH event (Ahn *et al*., 2013). Once established, this model would be more clinically relevant to test the therapeutic potential of human recombinant Decorin.

Throughout these studies immunohistochemistry has been performed so that the location of specific proteins could be elucidated and different cell types could be identified. Although changes in protein levels can be assessed semi-quantitatively by immunohistochemistry, it is not as accurate as other techniques such as western blotting or enzyme-linked immunosorbent assay (ELISA). Ideally the number of animals in each group would have been increased so that half of the animals could have been used for gene and protein analysis. In addition, it is important to take into account that Decorin interacts with a diverse number of molecules other than TGF-β including ECM molecules, growth factors and growth factor receptors. Hence, it would be critical to establish whether Decorin influences other pathways that may contribute to the prevention of hydrocephalus.

7.3.3. Finding the therapeutic window for successful Decorin treatment

In the acute experiment, it was established that when continuous Decorin infusion was started immediately after the injection of kaolin, it prevented subarachnoid fibrosis and hydrocephalus. Unfortunately, starting Decorin treatment immediately after an IVH in premature infants would not be possible, as IVH can clinically present without symptoms and is often only picked up on routine cranial ultrasound (Martin, 2011). Therefore further experiments where Decorin is delivered in the days after the induction of hydrocephalus are required to establish the window of therapeutic opportunity and increase its clinical relevance. Border *et al.* (1992) suggested that there was a window of therapeutic opportunity for successful Decorin treatment of fibrosis. Administration of Decorin within the first two days has no effect on preventing ECM deposition, however Decorin treatment from day 3 onwards

suppressed the production of ECM. It was hypothesised that Decorin was only effective after 2 days as this was the time point when the cells surrounding the injury started producing detectable levels of TGF-β. Therefore subsequent studies need to be conducted to determine the optimum timing for Decorin treatment, ideally in a clinically relevant window but before substantial ECM has been deposited in the subarachnoid space.

In addition, altering the duration and dose of Decorin may improve efficacy. The dose used in these studies was based on experiments conducted in spinal cord (Minor *et al*., 2010) where Decorin was infused locally into the lesion site. In the studies presented here, intraventricularly delivered Decorin was distributed throughout the ventricular system and therefore susceptible to dilution so that higher doses may be required. Also it would be beneficial to determine the long term effects of Decorin infusion on hydrocephalus after treatment has stopped.

7.3.4. Improving the efficiency of Decorin delivery

The chronic study highlighted the importance of efficient Decorin delivery. It is not known whether the osmotic mini pumps were able to infuse efficiently into the high pressure hydrocephalic environment. Therefore the results from the chronic study are inconclusive as it cannot be established that Decorin was delivered at a suitable concentration to the required sites of action to elicit a biological response. Ideally it would have been useful to have measured the levels of Decorin in the CSF in all the studies, however this was complicated by the lack of necessary equipment in the Utah laboratories. Therefore studies need to be conducted to establish whether osmotic mini pumps are able to work efficiently to deliver Decorin throughout the

ventricular system and subarachnoid space in a high pressure environment. This may be through filling the pumps with dyes and testing them in *ex vivo* or *in vivo* high pressure situations. On the other hand after establishing hydrocephalus development, intraventricular Decorin infusion could be combined with a shunt which would reduce ventricular volume and ICP. After the 14 days of continuous Decorin treatment the shunt could be removed and the progression of hydrocephalus from this point assessed. This experiment would examination whether Decorin is able to degrade subarachnoid fibrosis, providing the shunt did not affect Decorin delivery to the subarachnoid space.

Further work using ICP measuring devices would also be extremely valuable. ICP rises during the injection of blood into the ventricles and returns to normal levels soon after the injection (Cherian *et al*., 2004). Rats that go on to develop post-haemorrhagic hydrocephalus have increased ICP at 14 and 21 days (Lackner *et al*., 2013), then in kaolin-induced hydrocephalus ICP usually normalises at around 6 weeks (Konziella *et al*., 2002). In subsequent experiments it would be extremely interesting to monitor ICP with an indwelling device daily and be able to correlate this with oedema and ventricular enlargement on MRI scans to further characterise the progression of hydrocephalus. Not only would this increase our understanding of the model but it may give us markers that could influence when Decorin treatment is started. For example, treatment could begin as soon as ICP has reduced back to normal levels.

Alternatively, other techniques for continually delivering Decorin into the high pressure ventricular system and subarachnoid space could be considered. A ventricular access device or reservoir is often implanted in premature infants with

post-haemorrhagic hydrocephalus to facilitate repeat ventricular tapping (Brouwer *et al*., 2011). This device could be used to deliver Decorin by giving daily injections into the device that would replicate a delivery technique usable in premature infants. Nasal delivery could also be another potential route for Decorin administration as it is a non-invasive way of getting drugs into the CNS. However, a significant amount of work would need to be invested into getting the formulation right so that there is efficient uptake of Decorin without it being distributed systemically (Dhuria *et al*., 2010). In this laboratory a hydrogel is being developed that is in liquid form at room temperature but solidifies at 37ºC. Hence there is the potential for incorporating Decorin into the gel and injecting it into the subarachnoid space so it slowly releases Decorin, however its effects on obstructing CSF flow would need to be established.

References

Abbott NJ. Evidence for bulk flow of brain interstitial fluid: significance for physiology and pathology. Neurochem Int. 2004 Sep;45(4):545-52.

Adeeb N, Deep A, Griessenauer CJ, Mortazavi MM, Watanabe K, Loukas M, et al. The intracranial arachnoid mater : a comprehensive review of its history, anatomy, imaging, and pathology. Childs Nerv Syst. 2013a Jan;29(1):17-33.

Adeeb N, Mortazavi MM, Deep A, Griessenauer CJ, Watanabe K, Shoja MM, et al. The pia mater: a comprehensive review of literature. Childs Nerv Syst. 2013b Oct;29(10):1803-10.

Adeeb N, Mortazavi MM, Tubbs RS, Cohen-Gadol AA. The cranial dura mater: a review of its history, embryology, and anatomy. Childs Nerv Syst. 2012 Jun;28(6):827-37.

Aguzzi A, Barres BA, Bennett ML. Microglia: scapegoat, saboteur, or something else? Science. 2013 Jan 11;339(6116):156-61.

Ahn SY, Chang YS, Sung DK, Sung SI, Yoo HS, Lee JH, et al. Mesenchymal stem cells prevent hydrocephalus after severe intraventricular hemorrhage. Stroke. 2013 Feb;44(2):497-504.

Al-Shahi R, White PM, Davenport RJ, Lindsay KW. Subarachnoid haemorrhage. BMJ. 2006 Jul 29;333(7561):235-40.

Al Haj Zen A, Lafont A, Durand E, Brasselet C, Lemarchand P, Godeau G, et al. Effect of adenovirus-mediated overexpression of decorin on metalloproteinases, tissue inhibitors of metalloproteinases and cytokines secretion by human gingival fibroblasts. Matrix Biol. 2003 May;22(3):251-8.

Allen NJ. Role of glia in developmental synapse formation. Curr Opin Neurobiol. 2013 Jul 17.

anonymous. International randomised controlled trial of acetazolamide and furosemide in posthaemorrhagic ventricular dilatation in infancy. International PHVD Drug Trial Group. Lancet. 1998 Aug 8;352(9126):433-40.

Aquilina K, Hobbs C, Tucker A, Whitelaw A, Thoresen M. Do drugs that block transforming growth factor beta reduce posthaemorrhagic ventricular dilatation in a neonatal rat model? Acta Paediatr. 2008 Sep;97(9):1181-6.

Assoian RK, Komoriya A, Meyers CA, Miller DM, Sporn MB. Transforming growth factor-beta in human platelets. Identification of a major storage site, purification, and characterization. J Biol Chem. 1983 Jun 10;258(11):7155-60.

Baghy K, Dezso K, Laszlo V, Fullar A, Peterfia B, Paku S, et al. Ablation of the decorin gene enhances experimental hepatic fibrosis and impairs hepatic healing in mice. Lab Invest. 2011 Mar;91(3):439-51.

Balasubramaniam J, Del Bigio MR. Analysis of age-dependant alteration in the brain gene expression profile following induction of hydrocephalus in rats. Exp Neurol. 2002 Jan;173(1):105-13.

Ballabh P. Intraventricular hemorrhage in premature infants: mechanism of disease. Pediatr Res. 2010 Jan;67(1):1-8.

Ballabh P, Braun A, Nedergaard M. The blood-brain barrier: an overview: structure, regulation, and clinical implications. Neurobiol Dis. 2004 Jun;16(1):1-13.

Banizs B, Pike MM, Millican CL, Ferguson WB, Komlosi P, Sheetz J, et al. Dysfunctional cilia lead to altered ependyma and choroid plexus function, and result in the formation of hydrocephalus. Development. 2005 Dec;132(23):5329-39.

Bederson JB, AANS Publications Committee. Subarachnoid hemorrhage : pathophysiology and management. Park Ridge, Ill.: American Association of Neurological Surgeons; 1997.

Bergsneider M, Egnor MR, Johnston M, Kranz D, Madsen JR, McAllister JP, 2nd, et al. What we don't (but should) know about hydrocephalus. J Neurosurg. 2006 Mar;104(3 Suppl):157-9.

Bhowmick NA, Ghiassi M, Bakin A, Aakre M, Lundquist CA, Engel ME, et al. Transforming growth factor-beta1 mediates epithelial to mesenchymal transdifferentiation through a RhoA-dependent mechanism. Mol Biol Cell. 2001 Jan;12(1):27-36.

Bidanset DJ, LeBaron R, Rosenberg L, Murphy-Ullrich JE, Hook M. Regulation of cell substrate adhesion: effects of small galactosaminoglycan-containing proteoglycans. The Journal of Cell Biology. 1992 September 15, 1992;118(6):1523-31.

Bifari F, Decimo I, Chiamulera C, Bersan E, Malpeli G, Johansson J, et al. Novel stem/progenitor cells with neuronal differentiation potential reside in the

leptomeningeal niche. Journal of cellular and molecular medicine. 2009 Sep;13(9B):3195-208.
Border WA, Noble NA. Transforming growth factor beta in tissue fibrosis. N Engl J Med. 1994 Nov 10;331(19):1286-92.
Border WA, Noble NA, Yamamoto T, Harper JR, Yamaguchi Y, Pierschbacher MD, et al. Natural inhibitor of transforming growth factor-[beta] protects against scarring in experimental kidney disease. Nature. [10.1038/360361a0]. 1992;360(6402):361-4.
Bottinger EP. TGF-beta and Fibrosis. In: Derynck R, Miyazono, K., editor. the TGF-beta Family: Cold Spring Harbor Laboratory Press; 2008. p. 989-1022.
Bottner M, Krieglstein K, Unsicker K. The transforming growth factor-betas: structure, signaling, and roles in nervous system development and functions. J Neurochem. 2000 Dec;75(6):2227-40.
Bottoms SE, Howell JE, Reinhardt AK, Evans IC, McAnulty RJ. Tgf-Beta isoform specific regulation of airway inflammation and remodelling in a murine model of asthma. PLoS One. 2010;5(3):e9674.
Boulton M, Flessner M, Armstrong D, Mohamed R, Hay J, Johnston M. Contribution of extracranial lymphatics and arachnoid villi to the clearance of a CSF tracer in the rat. Am J Physiol. 1999 Mar;276(3 Pt 2):R818-23.
Braun KP, de Graaf RA, Vandertop WP, Gooskens RH, Tulleken KA, Nicolay K. In vivo 1H MR spectroscopic imaging and diffusion weighted MRI in experimental hydrocephalus. Magn Reson Med. 1998 Dec;40(6):832-9.
Braun KP, Dijkhuizen RM, de Graaf RA, Nicolay K, Vandertop WP, Gooskens RH, et al. Cerebral ischemia and white matter edema in experimental hydrocephalus: a combined in vivo MRI and MRS study. Brain Res. 1997 May 23;757(2):295-8.
Braun KP, van Eijsden P, Vandertop WP, de Graaf RA, Gooskens RH, Tulleken KA, et al. Cerebral metabolism in experimental hydrocephalus: an in vivo 1H and 31P magnetic resonance spectroscopy study. J Neurosurg. 1999 Oct;91(4):660-8.
Breuer B, Schmidt G, Kresse H. Non-uniform influence of transforming growth factor-beta on the biosynthesis of different forms of small chondroitin sulphate/dermatan sulphate proteoglycan. Biochem J. 1990 Jul 15;269(2):551-4.

Brinker T, Beck H, Klinge P, Kischnik B, Oi S, Samii M. Sinusoidal intrathecal infusion for assessment of CSF dynamics in kaolin-induced hydrocephalus. Acta Neurochir (Wien). 1998;140(10):1069-75.

Brouwer A. Treatment and outcome of neonatal haemorrhagic brain injury. Utrecht: Utrecht University; 2011.

Brown CT, Nugent MA, Lau FW, Trinkaus-Randall V. Characterization of proteoglycans synthesized by cultured corneal fibroblasts in response to transforming growth factor beta and fetal calf serum. J Biol Chem. 1999 Mar 12;274(11):7111-9.

Brown DC, Vogel KG. Characteristics of the in vitro interaction of a small proteoglycan (PG II) of bovine tendon with type I collagen. Matrix. 1989;9(6):468-78.

Bruni JE, Del Bigio MR, Clattenburg RE. Ependyma: normal and pathological. A review of the literature. Brain Res. 1985 Apr;356(1):1-19.

Buraschi S, Pal N, Tyler-Rubinstein N, Owens RT, Neill T, Iozzo RV. Decorin antagonizes Met receptor activity and down-regulates {beta}-catenin and Myc levels. J Biol Chem. 2010 Dec 31;285(53):42075-85.

Bush TG, Puvanachandra N, Horner CH, Polito A, Ostenfeld T, Svendsen CN, et al. Leukocyte infiltration, neuronal degeneration, and neurite outgrowth after ablation of scar-forming, reactive astrocytes in adult transgenic mice. Neuron. 1999 Jun;23(2):297-308.

Caner H, Atasever A, Kilinc K, Durgun B, Peker S, Ozcan OE. Lipid peroxide level increase in experimental hydrocephalus. Acta Neurochir (Wien). 1993;121(1-2):68-71.

Caner H, Peker S, Ozcan OE. Effects of hydrocephalus on the sympathetic nerves of cerebral arteries, investigated with WGA-HRP anterograde tracing in the rat. Acta Neurochir (Wien). 1991;111(3-4):143-6.

Carpenter RC, Miao L, Miyagi Y, Bengten E, Zhang JH, Muizelaar JP. Altered Expression of P2 Receptor mRNAs in the Basilar Artery in a Rat Double Hemorrhage Model • Editorial Comment. Stroke. 2001 February 1, 2001;32(2):516-22.

Chen Y, Blom IE, Sa S, Goldschmeding R, Abraham DJ, Leask A. CTGF expression in mesangial cells: involvement of SMADs, MAP kinase, and PKC. Kidney Int. 2002 Oct;62(4):1149-59.

Cherian S, Whitelaw A, Thoresen M, Love S. The pathogenesis of neonatal post-hemorrhagic hydrocephalus. Brain Pathol. 2004 Jul;14(3):305-11.
Chodobski A, Szmydynger-Chodobska J. Choroid plexus: target for polypeptides and site of their synthesis. Microsc Res Tech. 2001 Jan 1;52(1):65-82.
Chodobski A, Zink BJ, Szmydynger-Chodobska J. Blood-brain barrier pathophysiology in traumatic brain injury. Transl Stroke Res. 2011 Dec;2(4):492-516.
Chu SH, Feng DF, Ma YB, Zhang H, Zhu ZA, Li ZQ, et al. Expression of HGF and VEGF in the cerebral tissue of adult rats with chronic hydrocephalus after subarachnoid hemorrhage. Mol Med Report. 2011 Jun 2.
Comalada M, Cardo M, Xaus J, Valledor AF, Lloberas J, Ventura F, et al. Decorin reverses the repressive effect of autocrine-produced TGF-beta on mouse macrophage activation. J Immunol. 2003 May 1;170(9):4450-6.
Csordas G, Santra M, Reed CC, Eichstetter I, McQuillan DJ, Gross D, et al. Sustained down-regulation of the epidermal growth factor receptor by decorin. A mechanism for controlling tumor growth in vivo. J Biol Chem. 2000 Oct 20;275(42):32879-87.
Curl FD, Pollay M. Transport of water and electrolytes between brain and ventricular fluid in the rabbit. Exp Neurol. 1968 Apr;20(4):558-74.
Danielson KG, Baribault H, Holmes DF, Graham H, Kadler KE, Iozzo RV. Targeted disruption of decorin leads to abnormal collagen fibril morphology and skin fragility. J Cell Biol. 1997 Feb 10;136(3):729-43.
Darby I, Skalli O, Gabbiani G. Alpha-smooth muscle actin is transiently expressed by myofibroblasts during experimental wound healing. Lab Invest. 1990 Jul;63(1):21-9.
Davies JE, Tang X, Denning JW, Archibald SJ, Davies SJ. Decorin suppresses neurocan, brevican, phosphacan and NG2 expression and promotes axon growth across adult rat spinal cord injuries. Eur J Neurosci. 2004 Mar;19(5):1226-42.
De Luca A, Santra M, Baldi A, Giordano A, Iozzo RV. Decorin-induced growth suppression is associated with up-regulation of p21, an inhibitor of cyclin-dependent kinases. J Biol Chem. 1996 Aug 2;271(31):18961-5.
de Rooij NK, Linn FHH, van der Plas JA, Algra A, Rinkel GJE. Incidence of subarachnoid haemorrhage: a systematic review with emphasis on region, age,

gender and time trends. Journal of Neurology, Neurosurgery & Psychiatry. 2007 December 1, 2007;78(12):1365-72.
Del Bigio MR. Calcium-mediated proteolytic damage in white matter of hydrocephalic rats? J Neuropathol Exp Neurol. 2000 Nov;59(11):946-54.
Del Bigio MR. Cellular damage and prevention in childhood hydrocephalus. Brain Pathol. 2004 Jul;14(3):317-24.
Del Bigio MR. Ependymal cells: biology and pathology. Acta Neuropathol. 2010a Jan;119(1):55-73.
Del Bigio MR. Neuropathology and structural changes in hydrocephalus. Dev Disabil Res Rev. 2010b;16(1):16-22.
Del Bigio MR, Enno TL. Effect of hydrocephalus on rat brain extracellular compartment. Cerebrospinal Fluid Res. 2008;5:12.
Del Bigio MR, Zhang YW. Cell Death, Axonal Damage, and Cell Birth in the Immature Rat Brain Following Induction of Hydrocephalus. Exp Neurol. [doi: DOI: 10.1006/exnr.1998.6922]. 1998;154(1):157-69.
Deren KE, Packer M, Forsyth J, Milash B, Abdullah OM, Hsu EW, et al. Reactive astrocytosis, microgliosis and inflammation in rats with neonatal hydrocephalus. Exp Neurol. 2010 Nov;226(1):110-9.
Dhuria SV, Hanson LR and Frey WH. Intranasal delivery to the central nervous system: mechansms and experimental considerations. J Pharm Sci. 2010 Apr; 99(4):1654-73.
Di Terlizzi R, Platt S. The function, composition and analysis of cerebrospinal fluid in companion animals: part I - function and composition. Vet J. 2006 Nov;172(3):422-31.
Ding Y, McAllister JP, 2nd, Yao B, Yan N, Canady AI. Axonal damage associated with enlargement of ventricles during hydrocephalus: a silver impregnation study. Neurol Res. 2001a Sep;23(6):581-7.
Ding Y, McAllister JP, 2nd, Yao B, Yan N, Canady AI. Neuron tolerance during hydrocephalus. Neuroscience. 2001b;106(4):659-67.
Dorai Z, Hynan LS, Kopitnik TA, Samson D. Factors Related to Hydrocephalus after Aneurysmal Subarachnoid Hemorrhage. Neurosurgery. 2003;52(4):763-71

Douglas MR, Daniel M, Lagord C, Akinwunmi J, Jackowski A, Cooper C, et al. High CSF transforming growth factor beta levels after subarachnoid haemorrhage: association with chronic communicating hydrocephalus. J Neurol Neurosurg Psychiatry. 2009 May;80(5):545-50.

Dumont AS, Dumont RJ, Chow MM, Lin CL, Calisaneller T, Ley KF, et al. Cerebral vasospasm after subarachnoid hemorrhage: putative role of inflammation. Neurosurgery. 2003 Jul;53(1):123-33; discussion 33-5.

Edwards RJ, Dombrowski SM, Luciano MG, Pople IK. Chronic hydrocephalus in adults. Brain Pathol. 2004 Jul;14(3):325-36.

Egawa T, Mishima K, Egashira N, Fukuzawa M, Abe K, Yae T, et al. Impairment of spatial memory in kaolin-induced hydrocephalic rats is associated with changes in the hippocampal cholinergic and noradrenergic contents. Behav Brain Res. 2002 Feb 1;129(1-2):31-9.

Engel S, Isenmann S, Stander M, Rieger J, Bahr M, Weller M. Inhibition of experimental rat glioma growth by decorin gene transfer is associated with decreased microglial infiltration. J Neuroimmunol. 1999 Sep 1;99(1):13-8.

Eskandari R, Harris CA, McAllister JP, 2nd. Reactive astrocytosis in feline neonatal hydrocephalus: acute, chronic, and shunt-induced changes. Childs Nerv Syst. 2011 Dec;27(12):2067-76.

Fallon J, Reid S, Kinyamu R, Opole I, Opole R, Baratta J, et al. In vivo induction of massive proliferation, directed migration, and differentiation of neural cells in the adult mammalian brain. Proc Natl Acad Sci U S A. 2000 Dec 19;97(26):14686-91.

Faulkner JR, Herrmann JE, Woo MJ, Tansey KE, Doan NB, Sofroniew MV. Reactive astrocytes protect tissue and preserve function after spinal cord injury. J Neurosci. 2004 Mar 3;24(9):2143-55.

Faust SM, Lu G, Wood SC, Bishop DK. TGFbeta neutralization within cardiac allografts by decorin gene transfer attenuates chronic rejection. J Immunol. 2009 Dec 1;183(11):7307-13.

Ferro JM, Canhao P, Peralta R. Update on subarachnoid haemorrhage. J Neurol. 2008 Apr;255(4):465-79.

Flood C, Akinwunmi J, Lagord C, Daniel M, Berry M, Jackowski A, et al. Transforming growth factor-beta1 in the cerebrospinal fluid of patients with

subarachnoid hemorrhage: titers derived from exogenous and endogenous sources. J Cereb Blood Flow Metab. 2001 Feb;21(2):157-62.
Fukumizu M, Takashima S, Becker LE. Glial reaction in periventricular areas of the brainstem in fetal and neonatal posthemorrhagic hydrocephalus and congenital hydrocephalus. Brain Dev. 1996 Jan-Feb;18(1):40-5.
Gabbiani G. The myofibroblast in wound healing and fibrocontractive diseases. J Pathol. 2003 Jul;200(4):500-3.
Galbreath E, KIM S-J, PARK K, BRENNER M, MESSING A. Overexpression of TGF-[beta]1 in the Central Nervous System of Transgenic Mice Results in Hydrocephalus. Journal of Neuropathology & Experimental Neurology. 1995;54(3):339-49.
Gaskell A, Crennell S, Taylor G. The three domains of a bacterial sialidase: a [beta]-propeller, an immunoglobulin module and a galactose-binding jelly-roll. Structure. [doi: DOI: 10.1016/S0969-2126(01)00255-6]. 1995;3(11):1197-205.
Go KG, Molenaar I. Some applications of scanning electron microscopy for the study of biopsies in central nervous system pathology. Scan Electron Microsc. 1983(Pt 1):143-50.
Goldoni S, Humphries A, Nystrom A, Sattar S, Owens RT, McQuillan DJ, et al. Decorin is a novel antagonistic ligand of the Met receptor. J Cell Biol. 2009 May 18;185(4):743-54.
Goldoni S, Seidler DG, Heath J, Fassan M, Baffa R, Thakur ML, et al. An antimetastatic role for decorin in breast cancer. Am J Pathol. 2008 Sep;173(3):844-55.
Gopinath G, Bhatia R, Gopinath PG. Ultrastructural observations in experimental hydrocephalus in the rabbit. J Neurol Sci. 1979 Nov;43(3):333-4.
Goumans MJ, Valdimarsdottir G, Itoh S, Rosendahl A, Sideras P, ten Dijke P. Balancing the activation state of the endothelium via two distinct TGF-beta type I receptors. EMBO J. 2002 Apr 2;21(7):1743-53.
Graff-Radford NR, Torner J, Adams HP, Jr., Kassell NF. Factors associated with hydrocephalus after subarachnoid hemorrhage. A report of the Cooperative Aneurysm Study. Arch Neurol. 1989 Jul;46(7):744-52.

Greenwood S, Swetloff A, Wade A, Terasaki T, Ferretti P. Fgf2 is expressed in human and murine embryonic choroid plexus and affects choroid plexus epithelial cell behaviour. Cerebrospinal Fluid Research. 2008;5(1):20.

Grisanti S, Szurman P, Warga M, Kaczmarek R, Ziemssen F, Tatar O, et al. Decorin modulates wound healing in experimental glaucoma filtration surgery: a pilot study. Invest Ophthalmol Vis Sci. 2005 Jan;46(1):191-6.

Grondona JM, Perez-Martin M, Cifuentes M, Perez J, Jimenez AJ, Perez-Figares JM, et al. Ependymal denudation, aqueductal obliteration and hydrocephalus after a single injection of neuraminidase into the lateral ventricle of adult rats. J Neuropathol Exp Neurol. 1996 Sep;55(9):999-1008.

Gul S, Bahadir B, Hanci V, Acikgoz S, Bektas S, Ugurbas E, et al. Effects of ebselen versus nimodipine on cerebral vasospasm subsequent to experimental subarachnoid hemorrhage in rats. J Clin Neurosci. 2010 May;17(5):608-11.

Gules I, Satoh M, Clower BR, Nanda A, Zhang JH. Comparison of three rat models of cerebral vasospasm. American Journal of Physiology - Heart and Circulatory Physiology. 2002 December 1, 2002;283(6):H2551-H9.

Hartsough MT, Mulder KM. Transforming growth factor-beta signaling in epithelial cells. Pharmacol Ther. 1997;75(1):21-41.

Hatta J, Hatta T, Moritake K, Otani H. Heavy water inhibiting the expression of transforming growth factor-beta1 and the development of kaolin-induced hydrocephalus in mice. J Neurosurg. 2006 Apr;104(4 Suppl):251-8.

Hayamizu TF, Chan PT, Johanson CE. FGF-2 immunoreactivity in adult rat ependyma and choroid plexus: responses to global forebrain ischemia and intraventricular FGF-2. Neurol Res. 2001 Jun;23(4):353-8.

Heep A, Stoffel-Wagner B, Bartmann P, Benseler S, Schaller C, Groneck P, et al. Vascular endothelial growth factor and transforming growth factor-beta1 are highly expressed in the cerebrospinal fluid of premature infants with posthemorrhagic hydrocephalus. Pediatr Res. 2004 Nov;56(5):768-74.

Hendrickson ML, Rao AJ, Demerdash ON, Kalil RE. Expression of nestin by neural cells in the adult rat and human brain. PLoS One. 2011;6(4):e18535.

Herrmann JE, Imura T, Song B, Qi J, Ao Y, Nguyen TK, et al. STAT3 is a critical regulator of astrogliosis and scar formation after spinal cord injury. J Neurosci. 2008 Jul 9;28(28):7231-43.

Hidaka M, Matsumae M, Yamamura M, Tsugane R, Sato O. Glucose metabolism and protective biochemical mechanisms in a rat brain affected by kaolin-induced hydrocephalus. Childs Nerv Syst. 1997 Apr;13(4):183-8.

Higashi K, Asahisa H, Ueda N, Kobayashi K, Hara K, Noda Y. Cerebral blood flow and metabolism in experimental hydrocephalus. Neurol Res. 1986 Sep;8(3):169-76.

Hocevar BA, Brown TL, Howe PH. TGF-beta induces fibronectin synthesis through a c-Jun N-terminal kinase-dependent, Smad4-independent pathway. EMBO J. 1999 Mar 1;18(5):1345-56.

Hochwald GM, Nakamura S, Camins MB. The rat in experimental obstructive hydrocephalus. Z Kinderchir. 1981 Dec;34(4):403-10.

Hocking AM, Shinomura T, McQuillan DJ. Leucine-rich repeat glycoproteins of the extracellular matrix. Matrix Biol. 1998 Apr;17(1):1-19.

Hoppe-Hirsch E, Laroussinie F, Brunet L, Sainte-Rose C, Renier D, Cinalli G, et al. Late outcome of the surgical treatment of hydrocephalus. Childs Nerv Syst. 1998 Mar;14(3):97-9.

Hoque N, Thoresen M, Aquilina K, Hogan S, Whitelaw A. Decorin and colchicine as potential treatments for post-haemorrhagic ventricular dilatation in a neonatal rat model. Neonatology. 2011;100(3):271-6.

Hwang YS, Shim I, Chang JW. The behavioral change of locomotor activity in a kaolin-induced hydrocephalus rat model: evaluation of the effect on the dopaminergic system with progressive ventricle dilatation. Neurosci Lett. 2009 Oct 25;462(3):198-202.

Iozzo RV, Moscatello DK, McQuillan DJ, Eichstetter I. Decorin is a biological ligand for the epidermal growth factor receptor. J Biol Chem. 1999 Feb 19;274(8):4489-92.

Irigoin C, Rodriguez EM, Heinrichs M, Frese K, Herzog S, Oksche A, et al. Immunocytochemical study of the subcommissural organ of rats with induced postnatal hydrocephalus. Exp Brain Res. 1990;82(2):384-92.

Jackowski A, Crockard A, Burnstock G, Russell RR, Kristek F. The time course of intracranial pathophysiological changes following experimental subarachnoid haemorrhage in the rat. J Cereb Blood Flow Metab. 1990 Nov;10(6):835-49.

Jahanyar J, Joyce DL, Southard RE, Loebe M, Noon GP, Koerner MM, et al. Decorin-mediated transforming growth factor-beta inhibition ameliorates adverse cardiac remodeling. J Heart Lung Transplant. 2007 Jan;26(1):34-40.

Jayatilaka AD. Arachnoid Granulations and Arachnoid villi in Mammals. The Ceylon Journal of Medical Science. 1969;18(1):25-30.

Jeon H, Ai J, Sabri M, Tariq A, Shang X, Chen G, et al. Neurological and neurobehavioral assessment of experimental subarachnoid hemorrhage. BMC Neurosci. 2009;10:103.

Jimenez AJ, Tome M, Paez P, Wagner C, Rodriguez S, Fernandez-Llebrez P, et al. A programmed ependymal denudation precedes congenital hydrocephalus in the hyh mutant mouse. J Neuropathol Exp Neurol. 2001 Nov;60(11):1105-19.

Johanson C, Stopa E, McMillan P, Roth D, Funk J, Krinke G. The distributional nexus of choroid plexus to cerebrospinal fluid, ependyma and brain: toxicologic/pathologic phenomena, periventricular destabilization, and lesion spread. Toxicologic pathology. 2011 Jan;39(1):186-212.

Johanson CE, Szmydynger-Chodobska J, Chodobski A, Baird A, McMillan P, Stopa EG. Altered formation and bulk absorption of cerebrospinal fluid in FGF-2-induced hydrocephalus. Am J Physiol. 1999 Jul;277(1 Pt 2):R263-71.

Johnston M, Zakharov A, Papaiconomou C, Salmasi G, Armstrong D. Evidence of connections between cerebrospinal fluid and nasal lymphatic vessels in humans, non-human primates and other mammalian species. Cerebrospinal Fluid Res. 2004 Dec 10;1(1):2.

Kahari VM, Larjava H, Uitto J. Differential regulation of extracellular matrix proteoglycan (PG) gene expression. Transforming growth factor-beta 1 up-regulates biglycan (PGI), and versican (large fibroblast PG) but down-regulates decorin (PGII) mRNA levels in human fibroblasts in culture. J Biol Chem. 1991 Jun 5;266(16):10608-15.

Kalluri R, Neilson EG. Epithelial-mesenchymal transition and its implications for fibrosis. J Clin Invest. 2003 Dec;112(12):1776-84.

Kanaji M, Tada T, Kobayashi S. A murine model of communicating hydrocephalus: Role of TGF-beta1. J Clin Neurosci. 1997 Jan;4(1):51-6.

Kandasamy J, Jenkinson MD, Mallucci CL. Contemporary management and recent advances in paediatric hydrocephalus. BMJ. 2011;343:d4191.

Kapoor KG, Katz SE, Grzybowski DM, Lubow M. Cerebrospinal fluid outflow: an evolving perspective. Brain Res Bull. 2008 Dec 16;77(6):327-34.

Kawamata T, Katayama Y, Tsuji N, Nishimoto H. Metabolic derangements in interstitial brain edema with preserved blood flow: selective vulnerability of the hippocampal CA3 region in rat hydrocephalus. Acta Neurochir Suppl. 2003;86:545-7.

Kettenmann H, Hanisch UK, Noda M, Verkhratsky A. Physiology of microglia. Physiol Rev. 2011 Apr;91(2):461-553.

Khan OH, Enno TL, Del Bigio MR. Brain damage in neonatal rats following kaolin induction of hydrocephalus. Exp Neurol. 2006 Aug;200(2):311-20.

Kida S, Pantazis A, Weller RO. CSF drains directly from the subarachnoid space into nasal lymphatics in the rat. Anatomy, histology and immunological significance. Neuropathol Appl Neurobiol. 1993 Dec;19(6):480-8.

Kida S, Yamashima T, Kubota T, Ito H, Yamamoto S. A light and electron microscopic and immunohistochemical study of human arachnoid villi. J Neurosurg. 1988 Sep;69(3):429-35.

Kiefer M, Eymann R, von Tiling S, Muller A, Steudel WI, Booz KH. The ependyma in chronic hydrocephalus. Childs Nerv Syst. 1998 Jun;14(6):263-70.

Kim YL, Im YJ, Ha NC, Im DS. Albumin inhibits cytotoxic activity of lysophosphatidylcholine by direct binding. Prostaglandins Other Lipid Mediat. 2007 Feb;83(1-2):130-8.

Kimelberg HK, Nedergaard M. Functions of astrocytes and their potential as therapeutic targets. Neurotherapeutics. 2010 Oct;7(4):338-53.

Kisseleva T, Brenner DA. Mechanisms of fibrogenesis. Exp Biol Med (Maywood). 2008 Feb;233(2):109-22.

Kitazawa K, Tada T. Elevation of transforming growth factor-beta 1 level in cerebrospinal fluid of patients with communicating hydrocephalus after subarachnoid hemorrhage. Stroke. 1994 Jul;25(7):1400-4.

Klinge P, Muhlendyck A, Lee S, Ludemann W, Groos S, Samii M, et al. Temporal and regional profile of neuronal and glial cellular injury after induction of kaolin hydrocephalus. Acta Neurochir Suppl. 2002;81:275-7.

Klinge PM, Samii A, Muhlendyck A, Visnyei K, Meyer GJ, Walter GF, et al. Cerebral hypoperfusion and delayed hippocampal response after induction of adult kaolin hydrocephalus. Stroke. 2003 Jan;34(1):193-9.

Klinge PM, Samii A, Niescken S, Brinker T, Silverberg GD. Brain amyloid accumulates in aged rats with kaolin-induced hydrocephalus. Neuroreport. 2006 Apr 24;17(6):657-60.

Knuckey NW, Preston J, Palm D, Epstein MH, Johanson C. Hydrocephalus decreases chloride efflux from the choroid plexus epithelium. Brain Research. [doi: DOI: 10.1016/0006-8993(93)91282-W]. 1993;618(2):313-7.

Kobe B, Deisenhofer J. Proteins with leucine-rich repeats. Curr Opin Struct Biol. 1995 Jun;5(3):409-16.

Kolb M, Margetts PJ, Sime PJ, Gauldie J. Proteoglycans decorin and biglycan differentially modulate TGF-β-mediated fibrotic responses in the lung. American Journal of Physiology - Lung Cellular and Molecular Physiology. 2001 June 1, 2001;280(6):L1327-L34.

Kondziella D, Eyjolfsson EM, Saether O, Sonnewald U, Risa O. Gray matter metabolism in acute and chronic hydrocephalus. Neuroscience. 2009 Mar 17;159(2):570-7.

Kondziella D, Ludemann W, Brinker T, Sletvold O, Sonnewald U. Alterations in brain metabolism, CNS morphology and CSF dynamics in adult rats with kaolin-induced hydrocephalus. Brain Res. 2002 Feb 8;927(1):35-41.

Kondziella D, Qu H, Ludemann W, Brinker T, Sletvold O, Sonnewald U. Astrocyte metabolism is disturbed in the early development of experimental hydrocephalus. J Neurochem. 2003 Apr;85(1):274-81.

Kondziella D, Sonnewald U, Tullberg M, Wikkelso C. Brain metabolism in adult chronic hydrocephalus. J Neurochem. 2008 Aug;106(4):1515-24.

Kreutzberg GW. Microglia: a sensor for pathological events in the CNS. Trends Neurosci. 1996 Aug;19(8):312-8.

Krishnamurthy S, Li J, Schultz L, McAllister JP, 2nd. Intraventricular infusion of hyperosmolar dextran induces hydrocephalus: a novel animal model of hydrocephalus. Cerebrospinal Fluid Res. 2009;6:16.

Krueger RC, Jr., Wu H, Zandian M, Danielpour M, Kabos P, Yu JS, et al. Neural progenitors populate the cerebrospinal fluid of preterm patients with hydrocephalus. The Journal of pediatrics. 2006 Mar;148(3):337-40.

Krumdieck R, Hook M, Rosenberg L, Volanakis J. The proteoglycan decorin binds C1q and inhibits the activity of the C1 complex. The Journal of Immunology. 1992 December 1, 1992;149(11):3695-701.

Krupinski J, Kumar P, Kumar S, Kaluza J. Increased expression of TGF-beta 1 in brain tissue after ischemic stroke in humans. Stroke. 1996 May;27(5):852-7.

Kuchiwaki H, Nagasaka M, Inao S, Sugita K. Progression of kaolin-induced hydrocephalus and changes in performance of operant tasks by rats. J Neurol Sci. 1994 Jan;121(1):32-8.

Kumar R, Friedman J. Subarachnoid Hemorrhage: The First 24 hours. A Surgeon's Perspective. Neurocritical Care. 2011;14(2):287-90.

Lackner P, Vahmjanin A, Hu Q, Krafft PR, Rolland W, Zhang JH. Chronic hydrocephalus after experimental subarachnoid hemorrhage. PLoS One. 2013;8(7):e69571.

Lagraoui M, Gagnon L. Enhancement of human neutrophil survival and activation by TGF-beta 1. Cell Mol Biol (Noisy-le-grand). [In Vitro]. 1997 May;43(3):313-8.

Lan HY. Diverse roles of TGF-beta/Smads in renal fibrosis and inflammation. Int J Biol Sci. 2011;7(7):1056-67.

Lawson RF, Raimondi AJ. Hydrocephalus-3, a murine mutant: I. Alterations in fine structure of choroid plexus and ependyma. Surg Neurol. 1973 Mar;1(2):115-28.

Lee JY, Sagher O, Keep R, Hua Y, Xi G. Comparison of experimental rat models of early brain injury after subarachnoid hemorrhage. Neurosurgery. 2009 Aug;65(2):331-43; discussion 43.

Lekic T, Manaenko A, Rolland W, Krafft PR, Peters R, Hartman RE, et al. Rodent neonatal germinal matrix hemorrhage mimics the human brain injury, neurological consequences, and post-hemorrhagic hydrocephalus. Exp Neurol. 2012 Jul;236(1):69-78.

Li J, McAllister JP, 2nd, Shen Y, Wagshul ME, Miller JM, Egnor MR, et al. Communicating hydrocephalus in adult rats with kaolin obstruction of the basal cisterns or the cortical subarachnoid space. Exp Neurol. 2008 Jun;211(2):351-61.

Li T, Zhang P, Yuan B, Zhao D, Chen Y, Zhang X. Thrombin-induced TGF-beta1 pathway: a cause of communicating hydrocephalus post subarachnoid hemorrhage. International journal of molecular medicine. 2013 Mar;31(3):660-6.

Li Y, Foster W, Deasy BM, Chan Y, Prisk V, Tang Y, et al. Transforming growth factor-beta1 induces the differentiation of myogenic cells into fibrotic cells in injured skeletal muscle: a key event in muscle fibrogenesis. Am J Pathol. 2004 Mar;164(3):1007-19.

Li Y, Li J, Zhu J, Sun B, Branca M, Tang Y, et al. Decorin gene transfer promotes muscle cell differentiation and muscle regeneration. Mol Ther. 2007 Sep;15(9):1616-22.

Liu W, Tang Y, Feng J. Cross talk between activation of microglia and astrocytes in pathological conditions in the central nervous system. Life Sci. 2011 Aug 1;89(5-6):141-6.

Lodhia KR, Shakui P, Keep RF. Hydrocephalus in a rat model of intraventricular hemorrhage. Acta Neurochir Suppl. 2006;96:207-11.

Logan A, Baird A, Berry M. Decorin Attenuates Gliotic Scar Formation in the Rat Cerebral Hemisphere. Exp Neurol. [doi: 10.1006/exnr.1999.7180]. 1999a;159(2):504-10.

Logan A, Frautschy S, Gonzalez A, Baird A. A time course for the focal elevation of synthesis of basic fibroblast growth factor and one of its high-affinity receptors (flg) following a localized cortical brain injury. The Journal of Neuroscience. 1992a October 1, 1992;12(10):3828-37.

Logan A, Frautschy SA, Gonzalez A-M, Sporn MB, Baird A. Enhanced expression of transforming growth factor [beta]1 in the rat brain after a localized cerebral injury. Brain Research. [doi: 10.1016/0006-8993(92)91000-5]. 1992b;587(2):216-25.

Logan A, Green J, Hunter A, Jackson R, Berry M. Inhibition of glial scarring in the injured rat brain by a recombinant human monoclonal antibody to transforming growth factor-beta2. Eur J Neurosci. 1999b Jul;11(7):2367-74.

Longden TA, Dunn KM, Draheim HJ, Nelson MT, Weston AH, Edwards G. Intermediate-conductance calcium-activated potassium channels participate in neurovascular coupling. Br J Pharmacol. 2011 Oct;164(3):922-33.

Lopes LD, Slobodian I, Del Bigio MR. Characterization of juvenile and young adult mice following induction of hydrocephalus with kaolin. Exp Neurol. 2009 Sep;219(1):187-96.

Lu YB, Iandiev I, Hollborn M, Korber N, Ulbricht E, Hirrlinger PG, et al. Reactive glial cells: increased stiffness correlates with increased intermediate filament expression. FASEB J. 2011 Feb;25(2):624-31.

Ludin A, Itkin T, Gur-Cohen S, Mildner A, Shezen E, Golan K, et al. Monocytes-macrophages that express alpha-smooth muscle actin preserve primitive hematopoietic cells in the bone marrow. Nat Immunol. 2012 Nov;13(11):1072-82.

Luedemann W, Kondziella D, Tienken K, Klinge P, Brinker T, Berens von Rautenfeld D. Spinal cerebrospinal fluid pathways and their significance for the compensation of kaolin-hydrocephalus. Acta Neurochir Suppl. 2002;81:271-3.

Luttmann W, Franz P, Matthys H, Virchow JC, Jr. Effects of TGF-beta on eosinophil chemotaxis. Scandinavian journal of immunology. 1998 Feb;47(2):127-30.

Mack J, Squier W, Eastman JT. Anatomy and development of the meninges: implications for subdural collections and CSF circulation. Pediatr Radiol. 2009 Mar;39(3):200-10.

Manwaring ME, Biran R, Tresco PA. Characterization of rat meningeal cultures on materials of differing surface chemistry. Biomaterials. [doi: 10.1016/S0142-9612(01)00068-0]. 2001;22(23):3155-68.

Martin J. Prevention of Intraventricular Hemorrhages and Periventricular Leukomalacia in the Extremely Low Birth Weight Infant. Newborn and Infant Nursing Reviews. 2011;11(3):141-52.

Massicotte EM, Buist R, Del Bigio MR. Altered diffusion and perfusion in hydrocephalic rat brain: a magnetic resonance imaging analysis. J Neurosurg. 2000 Mar;92(3):442-7.

Massicotte EM, Del Bigio MR. Human arachnoid villi response to subarachnoid hemorrhage: possible relationship to chronic hydrocephalus. J Neurosurg. 1999 Jul;91(1):80-4.

Massimi L, Paternoster G, Fasano T, Di Rocco C. On the changing epidemiology of hydrocephalus. Childs Nerv Syst. 2009 Jul;25(7):795-800.

Matsumae M, Sogabe T, Miura I, Sato O. Energy metabolism in kaolin-induced hydrocephalic rat brain. Assessed by phosphorus (31P) magnetic resonance spectroscopy and the diversity of lactate-dehydrogenase and its isoenzyme patterns. Childs Nerv Syst. 1990 Nov;6(7):392-6.

Matsuyama A, Iwata H, Okumura N, Yoshida S, Imaizumi K, Lee Y, et al. Localization of basic fibroblast growth factor-like immunoreactivity in the rat brain. Brain Research. [doi: 10.1016/0006-8993(92)91427-G]. 1992;587(1):49-65.

McAllister JP, 2nd. Pathophysiology of congenital and neonatal hydrocephalus. Semin Fetal Neonatal Med. 2012 Jul 15.

Merhar S. Biomarkers in neonatal posthemorrhagic hydrocephalus. Neonatology. 2012;101(1):1-7.

Merline R, Lazaroski S, Babelova A, Tsalastra-Greul W, Pfeilschifter J, Schluter KD, et al. Decorin deficiency in diabetic mice: aggravation of nephropathy due to overexpression of profibrotic factors, enhanced apoptosis and mononuclear cell infiltration. Journal of physiology and pharmacology : an official journal of the Polish Physiological Society. 2009 Oct;60 Suppl 4:5-13.

Meunier A, Sawamoto K and Spassky N. Ependyma, Choroid. Patterning and cell type specification in the developing CNS and PNS: comprehensive developmental neuroscience, Volume 1. 2013, p 819-833.

Miller JM, McAllister JP, 2nd. Reduction of astrogliosis and microgliosis by cerebrospinal fluid shunting in experimental hydrocephalus. Cerebrospinal Fluid Res. 2007;4:5.

Minor KH, Bournat JC, Toscano N, Giger RJ, Davies SJ. Decorin, erythroblastic leukaemia viral oncogene homologue B4 and signal transducer and activator of transcription 3 regulation of semaphorin 3A in central nervous system scar tissue. Brain. 2010 Nov 28.

Mitchell JA, Warner TD. COX isoforms in the cardiovascular system: understanding the activities of non-steroidal anti-inflammatory drugs. Nature reviews Drug discovery. 2006 Jan;5(1):75-86.

Miyake H, Eghwrudjakpor PO, Sakamoto T, Mori K. Catecholamine alterations in experimental hydrocephalus. Childs Nerv Syst. 1992 Aug;8(5):243-6.
Mogi M, Harada M, Kondo T, Narabayashi H, Riederer P, Nagatsu T. Transforming growth factor-beta 1 levels are elevated in the striatum and in ventricular cerebrospinal fluid in Parkinson's disease. Neurosci Lett. 1995 Jun 30;193(2):129-32.
Mohan RR, Gupta R, Mehan MK, Cowden JW, Sinha S. Decorin transfection suppresses profibrogenic genes and myofibroblast formation in human corneal fibroblasts. Exp Eye Res. 2010 Aug;91(2):238-45.
Moinuddin SM, Tada T. Study of cerebrospinal fluid flow dynamics in TGF-beta 1 induced chronic hydrocephalic mice. Neurol Res. 2000 Mar;22(2):215-22.
Morganti-Kossmann MC, Kossmann T, Brandes ME, Mergenhagen SE, Wahl SM. Autocrine and paracrine regulation of astrocyte function by transforming growth factor-beta. J Neuroimmunol. 1992 Jul;39(1-2):163-73.
Moscatello DK, Santra M, Mann DM, McQuillan DJ, Wong AJ, Iozzo RV. Decorin suppresses tumor cell growth by activating the epidermal growth factor receptor. J Clin Invest. 1998 Jan 15;101(2):406-12.
Motohashi O, Suzuki M, Shida N, Umezawa K, Ohtoh T, Sakurai Y, et al. Subarachnoid haemorrhage induced proliferation of leptomeningeal cells and deposition of extracellular matrices in the arachnoid granulations and subarachnoid space. Immunhistochemical study. Acta Neurochir (Wien). 1995a;136(1-2):88-91.
Motohashi O, Suzuki M, Yanai N, Umezawa K, Shida N, Yoshimoto T. Thrombin and TGF-beta promote human leptomeningeal cell proliferation in vitro. Neurosci Lett. 1995b May 5;190(2):105-8.
Muldoon LL, Alvarez JI, Begley DJ, Boado RJ, Del Zoppo GJ, Doolittle ND, et al. Immunologic privilege in the central nervous system and the blood-brain barrier. J Cereb Blood Flow Metab.. 2013 Jan;33(1):13-21.
Munger JS, Huang X, Kawakatsu H, Griffiths MJ, Dalton SL, Wu J, et al. The integrin alpha v beta 6 binds and activates latent TGF beta 1: a mechanism for regulating pulmonary inflammation and fibrosis. Cell. 1999 Feb 5;96(3):319-28.
Myer DJ, Gurkoff GG, Lee SM, Hovda DA, Sofroniew MV. Essential protective roles of reactive astrocytes in traumatic brain injury. Brain. 2006 Oct;129(Pt 10):2761-72.

Nagra G, Koh L, Aubert I, Kim M, Johnston M. Intraventricular injection of antibodies to beta1-integrins generates pressure gradients in the brain favoring hydrocephalus development in rats. Am J Physiol Regul Integr Comp Physiol. 2009 Nov;297(5):R1312-21.

Nagra G, Li J, McAllister JP, 2nd, Miller J, Wagshul M, Johnston M. Impaired lymphatic cerebrospinal fluid absorption in a rat model of kaolin-induced communicating hydrocephalus. Am J Physiol Regul Integr Comp Physiol. 2008 May;294(5):R1752-9.

Nagra G, Wagshul ME, Rashid S, Li J, McAllister JP, 2nd, Johnston M. Elevated CSF outflow resistance associated with impaired lymphatic CSF absorption in a rat model of kaolin-induced communicating hydrocephalus. Cerebrospinal Fluid Res. 2010;7(1):4.

Nakagawa Y, Cervos-Navarro J, Artigas J. Tracer study on a paracellular route in experimental hydrocephalus. Acta Neuropathol. 1985;65(3-4):247-54.

Nakagomi T, Molnar Z, Nakano-Doi A, Taguchi A, Saino O, Kubo S, et al. Ischemia-induced neural stem/progenitor cells in the pia mater following cortical infarction. Stem cells and development. 2011 Dec;20(12):2037-51.

Nakagomi T, Molnar Z, Taguchi A, Nakano-Doi A, Lu S, Kasahara Y, et al. Leptomeningeal-derived doublecortin-expressing cells in poststroke brain. Stem cells and development. 2012 Sep 1;21(13):2350-4.

Nakamura S, Hochwald GM. Spinal fluid formation and glucose influx in normal and experimental hydrocephalic rats. Exp Neurol. 1983 Oct;82(1):108-17.

Nakazato F, Tada T, Sekiguchi Y, Murakami K, Yanagisawa S, Tanaka Y, et al. Disturbed spatial learning of rats after intraventricular administration of transforming growth factor-beta 1. Neurol Med Chir (Tokyo). 2002 Apr;42(4):151-6; discussion 7.

Nakerakanti S, Trojanowska M. The Role of TGF-beta Receptors in Fibrosis. Open Rheumatol J. 2012;6:156-62.

Nassar K, Luke J, Luke M, Kamal M, Abd El-Nabi E, Soliman M, et al. The novel use of decorin in prevention of the development of proliferative vitreoretinopathy (PVR). Graefes Arch Clin Exp Ophthalmol. 2011 Nov;249(11):1649-60.

Neal JW, Gasque P. How does the brain limit the severity of inflammation and tissue injury during bacterial meningitis? J Neuropathol Exp Neurol. 2013 May;72(5):370-85.

Neill T, Jones HR, Crane-Smith Z, Owens RT, Schaefer L, Iozzo RV. Decorin induces rapid secretion of thrombospondin-1 in basal breast carcinoma cells via inhibition of Ras homolog gene family, member A/Rho-associated coiled-coil containing protein kinase 1. FEBS J. 2013 May;280(10):2353-68.

Neill T, Painter H, Buraschi S, Owens RT, Lisanti MP, Schaefer L, et al. Decorin antagonizes the angiogenic network: concurrent inhibition of Met, hypoxia inducible factor 1alpha, vascular endothelial growth factor A, and induction of thrombospondin-1 and TIMP3. J Biol Chem. 2012a Feb 17;287(8):5492-506.

Neill T, Schaefer L, Iozzo RV. Decorin: a guardian from the matrix. Am J Pathol. 2012b Aug;181(2):380-7.

Nelimarkka L, Kainulainen V, Schonherr E, Moisander S, Jortikka M, Lammi M, et al. Expression of small extracellular chondroitin/dermatan sulfate proteoglycans is differentially regulated in human endothelial cells. J Biol Chem. 1997 May 9;272(19):12730-7.

Nilsson C, Lindvall-Axelsson M, Owman C. Neuroendocrine regulatory mechanisms in the choroid plexus-cerebrospinal fluid system. Brain Res Brain Res Rev. 1992 May-Aug;17(2):109-38.

Nimmerjahn A, Kirchhoff F, Helmchen F. Resting microglial cells are highly dynamic surveillants of brain parenchyma in vivo. Science. 2005 May 27;308(5726):1314-8.

O'Kelly CJ, Kulkarni AV, Austin PC, Urbach D, Wallace MC. Shunt-dependent hydrocephalus after aneurysmal subarachnoid hemorrhage: incidence, predictors, and revision rates. Clinical article. J Neurosurg. 2009 Nov;111(5):1029-35.

Ohmiya M, Fukumitsu H, Nitta A, Nomoto H, Furukawa Y, Furukawa S. Administration of FGF-2 to embryonic mouse brain induces hydrocephalic brain morphology and aberrant differentiation of neurons in the postnatal cerebral cortex. Journal of Neuroscience Research. 2001;65(3):228-35.

Ohta K, Inokuchi T, Hayashida Y, Mizukami T, Yoshida T, Kawahara T. Regional diminution of von Willebrand factor expression on the endothelial covering arachnoid granulations of human, monkey and dog brain. Kurume Med J. 2002;49(4):177-83.

Oi S. Hydrocephalus research update--controversies in definition and classification of hydrocephalus. Neurol Med Chir (Tokyo). 2010;50(9):859-69.

Oi S, Kim DS, Hidaka M. "Hydrocephalus-parkinsonism complex": progressive hydrocephalus as a factor affecting extrapyramidal tract disorder-an experimental study. Childs Nerv Syst. 2004 Jan;20(1):37-40.

Oka N, Nakada J, Endo S, Takaku A. Angioarchitecture in experimental hydrocephalus. Pediatr Neurosci. 1985;12(6):294-9.

Okajima F, Sato K, Tomura H, Kuwabara A, Nochi H, Tamoto K, et al. Stimulatory and inhibitory actions of lysophosphatidylcholine, depending on its fatty acid residue, on the phospholipase C/Ca2+ system in HL-60 leukaemia cells. Biochem J. 1998 Dec 1;336 (Pt 2):491-500.

Okii N, Amano T, Seki T, Matsubayashi H, Mukai H, Ono Y, et al. Fragmentation of protein kinase N (PKN) in the hydrocephalic rat brain. Acta Histochem Cytochem. 2007 Aug 30;40(4):113-21.

Okubo S, Strahle J, Keep RF, Hua Y, Xi G. Subarachnoid hemorrhage-induced hydrocephalus in rats. Stroke. 2013 Feb;44(2):547-50.

Oreskovic D, Klarica M. Development of hydrocephalus and classical hypothesis of cerebrospinal fluid hydrodynamics: Facts and illusions. Prog Neurobiol. 2011 Aug;94(3):238-58.

Ostrow LW, Sachs F. Mechanosensation and endothelin in astrocytes--hypothetical roles in CNS pathophysiology. Brain Res Brain Res Rev. 2005 Jun;48(3):488-508.

Owen-Lynch PJ, Draper CE, Mashayekhi F, Bannister CM, Miyan JA. Defective cell cycle control underlies abnormal cortical development in the hydrocephalic Texas rat. Brain. 2003 Mar;126(Pt 3):623-31.

Park IS, Meno JR, Witt CE, Suttle TK, Chowdhary A, Nguyen TS, et al. Subarachnoid hemorrhage model in the rat: modification of the endovascular filament model. J Neurosci Methods. 2008 Jul 30;172(2):195-200.

Pearce RKB, Collins P, Jenner P, Emmett C, Marsden CD. Intraventricular infusion of basic fibroblast growth factor (bFGF) in the MPTP-treated common marmoset. Synapse. 1996;23(3):192-200.

Pekny M, Nilsson M. Astrocyte activation and reactive gliosis. Glia. 2005 Jun;50(4):427-34.

Pham AC, Fan C, Owler BK. Treating pediatric hydrocephalus in Australia: a 3-year hospital-based cost analysis and comparison with other studies. J Neurosurg Pediatr. 2013 Apr;11(4):398-401.

Pineda JR, Daynac M, Chicheportiche A, Cebrian-Silla A, Sii Felice K, Garcia-Verdugo JM, et al. Vascular-derived TGF-beta increases in the stem cell niche and perturbs neurogenesis during aging and following irradiation in the adult mouse brain. EMBO molecular medicine. 2013 Apr;5(4):548-62.

Pollay M. The function and structure of the cerebrospinal fluid outflow system. Cerebrospinal Fluid Res. 2010;7:9.

Porter S. The role of the fibroblast in wound contraction and healing. Wounds UK. 2007;3(1):33-40.

Preston JE. Ageing choroid plexus-cerebrospinal fluid system. Microsc Res Tech. 2001 Jan 1;52(1):31-7.

Prunell GF, Mathiesen T, Svendgaard NA. A new experimental model in rats for study of the pathophysiology of subarachnoid hemorrhage. Neuroreport. 2002 Dec 20;13(18):2553-6.

Raivich G, Bohatschek M, Kloss CU, Werner A, Jones LL, Kreutzberg GW. Neuroglial activation repertoire in the injured brain: graded response, molecular mechanisms and cues to physiological function. Brain Res Brain Res Rev. 1999 Jul;30(1):77-105.

Redzic ZB, Segal MB. The structure of the choroid plexus and the physiology of the choroid plexus epithelium. Adv Drug Deliv Rev. 2004 Oct 14;56(12):1695-716.

Reed CC, Waterhouse A, Kirby S, Kay P, Owens RT, McQuillan DJ, et al. Decorin prevents metastatic spreading of breast cancer. Oncogene. 2005 Feb 3;24(6):1104-10.

Rekate HL. The definition and classification of hydrocephalus: a personal recommendation to stimulate debate. Cerebrospinal Fluid Res. 2008;5:2.

Rendu F, Brohard-Bohn B. The platelet release reaction: granules' constituents, secretion and functions. Platelets. 2001 Aug;12(5):261-73.

Rodriguez EM, Guerra MM, Vio K, Gonzalez C, Ortloff A, Batiz LF, et al. A cell junction pathology of neural stem cells leads to abnormal neurogenesis and hydrocephalus. Biological research. 2012;45(3):231-42.

Romaris M, Heredia A, Molist A, Bassols A. Differential effect of transforming growth factor beta on proteoglycan synthesis in human embryonic lung fibroblasts. Biochim Biophys Acta. 1991 Jul 10;1093(2-3):229-33.

Sajanti J, Bjorkstrand AS, Finnila S, Heikkinen E, Peltonen J, Majamaa K. Increase of collagen synthesis and deposition in the arachnoid and the dura following subarachnoid hemorrhage in the rat. Biochim Biophys Acta. 1999 Aug 30;1454(3):209-16.

Sajanti J, Heikkinen E, Majamaa K. Transient increase in procollagen propeptides in the CSF after subarachnoid hemorrhage. Neurology. 2000 Aug 8;55(3):359-63.

Sajanti J, Heikkinen E, Majamaa K. Rapid induction of meningeal collagen synthesis in the cerebral cisternal and ventricular compartments after subarachnoid hemorrhage. Acta Neurochir. 2001;143(8):821-6.

Sajanti J, Majamaa K. Detection of meningeal fibrosis after subarachnoid haemorrhage by assaying procollagen propeptides in cerebrospinal fluid. J Neurol Neurosurg Psychiatry. 1999 Aug;67(2):185-8.

Sakka L, Coll G, Chazal J. Anatomy and physiology of cerebrospinal fluid. Eur Ann Otorhinolaryngol Head Neck Dis. 2011 Dec;128(6):309-16.

Santra M, Santra S, Zhang J, Chopp M. Ectopic decorin expression up-regulates VEGF expression in mouse cerebral endothelial cells via activation of the transcription factors Sp1, HIF1alpha, and Stat3. J Neurochem. 2008 Apr;105(2):324-37.

Sarnat HB. Ependymal reactions to injury. A review. J Neuropathol Exp Neurol. [Review]. 1995 Jan;54(1):1-15.

Sarrazy V, Billet F, Micallef L, Coulomb B, Desmouliere A. Mechanisms of pathological scarring: role of myofibroblasts and current developments. Wound Repair Regen. 2011 Sep;19 Suppl 1:s10-5.

Schilling SH, Hjelmeland, A.B., Rich, J.N., Wang, X.F. TGF-beta: a multipotential cytokine. In: Derynck R, Miyazono, K., editor. The TGF-beta Family: Cold Spring Harbor Laboratory Press; 2008. p. 45-78.

Schonherr E, Jarvelainen HT, Kinsella MG, Sandell LJ, Wight TN. Platelet-derived growth factor and transforming growth factor-beta 1 differentially affect the synthesis

of biglycan and decorin by monkey arterial smooth muscle cells. Arterioscler Thromb. 1993 Jul;13(7):1026-36.

Scott PG, Dodd CM, Ghahary A, Shen YJ, Tredget EE. Fibroblasts from post-burn hypertrophic scar tissue synthesize less decorin than normal dermal fibroblasts. Clin Sci (Lond). 1998 May;94(5):541-7.

Seidler DG, Mohamed NA, Bocian C, Stadtmann A, Hermann S, Schafers K, et al. The role for decorin in delayed-type hypersensitivity. J Immunol. 2011 Dec 1;187(11):6108-19.

Shafritz TA, Rosenberg LC, Yannas IV. Specific effects of glycosaminoglycans in an analog of extracellular matrix that delays wound contraction and induces regeneration. Wound Repair Regen. 1994 Oct;2(4):270-6.

Shim I, Ha Y, Chung JY, Lee HJ, Yang KH, Chang JW. Association of learning and memory impairments with changes in the septohippocampal cholinergic system in rats with kaolin-induced hydrocephalus. Neurosurgery. 2003 Aug;53(2):416-25; discussion 25.

Shooman D, Portess H, Sparrow O. A review of the current treatment methods for posthaemorrhagic hydrocephalus of infants. Cerebrospinal Fluid Res. 2009;6:1.

Siegenthaler JA, Sohet F, Daneman R. 'Sealing off the CNS': cellular and molecular regulation of blood-brain barriergenesis. Curr Opin Neurobiol. 2013 Jul 15.

Silva MCD. Pathophysiology of Hydrocephalus. In: Giuseppe Cinalli WJM, Christian Sainte-Rose, editor. Pediatric Hydrocephalus. Milano: Springer-Verlag; 2004. p. 65-76.

Silverberg GD, Miller MC, Machan JT, Johanson CE, Caralopoulos IN, Pascale CL, et al. Amyloid and Tau accumulate in the brains of aged hydrocephalic rats. Brain Res. 2010 Mar 4;1317:286-96.

Simon TD, Riva-Cambrin J, Srivastava R, Bratton SL, Dean JM, Kestle JR. Hospital care for children with hydrocephalus in the United States: utilization, charges, comorbidities, and deaths. J Neurosurg Pediatr. 2008 Feb;1(2):131-7.

Slobodian I, Krassioukov-Enns D, Del Bigio MR. Protein and synthetic polymer injection for induction of obstructive hydrocephalus in rats. Cerebrospinal Fluid Res. 2007;4:9.

Sofroniew MV. Molecular dissection of reactive astrogliosis and glial scar formation. Trends Neurosci. 2009 Dec;32(12):638-47.

Sofroniew MV, Vinters HV. Astrocytes: biology and pathology. Acta Neuropathol. 2010 Jan;119(1):7-35.

Sogabe T, Matsumae M, Sato O, Miura I. Change in glucose metabolism with time in hydrocephalic rats. Biochem Int. 1989 Sep;19(3):513-8.

Solomon RA, Antunes JL, Chen RY, Bland L, Chien S. Decrease in cerebral blood flow in rats after experimental subarachnoid hemorrhage: a new animal model. Stroke. 1985 Jan-Feb;16(1):58-64.

Speake T, Whitwell C, Kajita H, Majid A, Brown PD. Mechanisms of CSF secretion by the choroid plexus. Microsc Res Tech. 2001 Jan 1;52(1):49-59.

Strahle J, Garton H, Maher C, Muraszko K, Keep R, Xi G. Mechanisms of Hydrocephalus After Neonatal and Adult Intraventricular Hemorrhage. Translational Stroke Research. 2012:1-14.

Stramer BM, Mori R, Martin P. The inflammation-fibrosis link? A Jekyll and Hyde role for blood cells during wound repair. J Invest Dermatol. 2007 May;127(5):1009-17.

Strazielle N, Ghersi-Egea JF. Choroid plexus in the central nervous system: biology and physiopathology. J Neuropathol Exp Neurol. 2000 Jul;59(7):561-74.

Su WH, Cheng MH, Lee WL, Tsou TS, Chang WH, Chen CS, et al. Nonsteroidal anti-inflammatory drugs for wounds: pain relief or excessive scar formation? Mediators of inflammation. 2010;2010:413238.

Suzuki H, Ayer R, Sugawara T, Chen W, Sozen T, Hasegawa Y, et al. Protective effects of recombinant osteopontin on early brain injury after subarachnoid hemorrhage in rats. Crit Care Med. 2010 Feb;38(2):612-8.

Suzuki S, Ishii M, Ottomo M, Iwabuchi T. Changes in the subarachnoid space after experimental subarachnoid haemorrhage in the dog: scanning electron microscopic observation. Acta Neurochir (Wien). 1977;39(1-2):1-14.

Szabo A, Kalman M. Disappearance of the post-lesional laminin immunopositivity of brain vessels is parallel with the formation of gliovascular junctions and common basal lamina. A double-labelling immunohistochemical study. Neuropathol Appl Neurobiol. 2004 Apr;30(2):169-77.

Szmydynger-Chodobska J, Chodobski A, Johanson CE. Postnatal developmental changes in blood flow to choroid plexuses and cerebral cortex of the rat. Am J Physiol. 1994 May;266(5 Pt 2):R1488-92.

Tada T, Kanaji M, Kobayashi S. Induction of communicating hydrocephalus in mice by intrathecal injection of human recombinant transforming growth factor-beta 1. J Neuroimmunol. 1994 Mar;50(2):153-8.

Tada T, Zhan H, Tanaka Y, Hongo K, Matsumoto K, Nakamura T. Intraventricular administration of hepatocyte growth factor treats mouse communicating hydrocephalus induced by transforming growth factor beta1. Neurobiol Dis. 2006 Mar;21(3):576-86.

Tait MJ, Saadoun S, Bell BA, Verkman AS, Papadopoulos MC. Increased brain edema in aqp4-null mice in an experimental model of subarachnoid hemorrhage. Neuroscience. 2010 Apr 28;167(1):60-7.

Takata K, Sheng H, Borel CO, Laskowitz DT, Warner DS, Lombard FW. Long-term cognitive dysfunction following experimental subarachnoid hemorrhage: new perspectives. Exp Neurol. 2008 Oct;213(2):336-44.

Takeuchi Y, Kodama Y, Matsumoto T. Bone matrix decorin binds transforming growth factor-beta and enhances its bioactivity. J Biol Chem. 1994 Dec 23;269(51):32634-8.

Tashiro Y, Chakrabortty S, Drake JM, Hattori T. Progressive loss of glutamic acid decarboxylase, parvalbumin, and calbindin D28K immunoreactive neurons in the cerebral cortex and hippocampus of adult rat with experimental hydrocephalus. J Neurosurg. 1997a Feb;86(2):263-71.

Tashiro Y, Drake JM. Reversibility of functionally injured neurotransmitter systems with shunt placement in hydrocephalic rats: implications for intellectual impairment in hydrocephalus. J Neurosurg. 1998 Apr;88(4):709-17.

Tashiro Y, Drake JM, Chakrabortty S, Hattori T. Functional injury of cholinergic, GABAergic and dopaminergic systems in the basal ganglia of adult rat with kaolin-induced hydrocephalus. Brain Res. 1997b Oct 3;770(1-2):45-52.

Taylor AW. Review of the activation of TGF-beta in immunity. J Leukoc Biol. 2009 Jan;85(1):29-33.

Tourdias T, Dragonu I, Fushimi Y, Deloire MS, Boiziau C, Brochet B, et al. Aquaporin 4 correlates with apparent diffusion coefficient and hydrocephalus severity in the rat brain: a combined MRI-histological study. Neuroimage. 2009 Aug 15;47(2):659-66.
Unsicker K, Flanders KC, Cissel DS, Lafyatis R, Sporn MB. Transforming growth factor beta isoforms in the adult rat central and peripheral nervous system. Neuroscience. [doi: 10.1016/0306-4522(91)90082-Y]. 1991;44(3):613-25.
Upton ML, Weller RO. The morphology of cerebrospinal fluid drainage pathways in human arachnoid granulations. J Neurosurg. 1985 Dec;63(6):867-75.
Vale FL, Bradley EL, Fisher WS, 3rd. The relationship of subarachnoid hemorrhage and the need for postoperative shunting. J Neurosurg. 1997 Mar;86(3):462-6.
Vandenabeele F, Creemers J, Lambrichts I. Ultrastructure of the human spinal arachnoid mater and dura mater. J Anat. 1996 Oct;189 (Pt 2):417-30.
Verrecchia F, Mauviel A. Transforming growth factor-beta signaling through the Smad pathway: role in extracellular matrix gene expression and regulation. J Invest Dermatol. 2002 Feb;118(2):211-5.
Vinukonda G, Csiszar A, Hu F, Dummula K, Pandey NK, Zia MT, et al. Neuroprotection in a rabbit model of intraventricular haemorrhage by cyclooxygenase-2, prostanoid receptor-1 or tumour necrosis factor-alpha inhibition. Brain. 2010 Aug;133(Pt 8):2264-80.
Voelz K, Kondziella D, von Rautenfeld DB, Brinker T, Ludemann W. A ferritin tracer study of compensatory spinal CSF outflow pathways in kaolin-induced hydrocephalus. Acta Neuropathol. 2007 May;113(5):569-75.
Wagshul ME, McAllister JP, Rashid S, Li J, Egnor MR, Walker ML, et al. Ventricular dilation and elevated aqueductal pulsations in a new experimental model of communicating hydrocephalus. Exp Neurol. 2009 Jul;218(1):33-40.
Wahl SM, Hunt DA, Wakefield LM, McCartney-Francis N, Wahl LM, Roberts AB, et al. Transforming growth factor type beta induces monocyte chemotaxis and growth factor production. Proc Natl Acad Sci U S A. 1987 Aug;84(16):5788-92.
Wahl SM, McCartney-Francis N, Mergenhagen SE. Inflammatory and immunomodulatory roles of TGF-beta. Immunol Today. 1989 Aug;10(8):258-61.

Walter BA, Valera VA, Takahashi S, Ushiki T. The olfactory route for cerebrospinal fluid drainage into the peripheral lymphatic system. Neuropathol Appl Neurobiol. 2006 Aug;32(4):388-96.

Wang YM, Lin YJ, Chuang MJ, Lee TH, Tsai NW, Cheng BC, et al. Predictors and outcomes of shunt-dependent hydrocephalus in patients with aneurysmal sub-arachnoid hemorrhage. BMC Surg. 2012;12:12.

Wells RG. Fibrogenesis. V. TGF-beta signaling pathways. Am J Physiol Gastrointest Liver Physiol. 2000 Nov;279(5):G845-50.

Westergren-Thorsson G, Hernnas J, Sarnstrand B, Oldberg A, Heinegard D, Malmstrom A. Altered expression of small proteoglycans, collagen, and transforming growth factor-beta 1 in developing bleomycin-induced pulmonary fibrosis in rats. J Clin Invest. 1993 Aug;92(2):632-7.

Whinna HC, Choi HU, Rosenberg LC, Church FC. Interaction of heparin cofactor II with biglycan and decorin. Journal of Biological Chemistry. 1993 February 25, 1993;268(6):3920-4.

Whitelaw A, Christie S, Pople I. Transforming growth factor-beta1: a possible signal molecule for posthemorrhagic hydrocephalus? Pediatr Res. 1999 Nov;46(5):576-80.

Whitelaw A, Evans D, Carter M, Thoresen M, Wroblewska J, Mandera M, et al. Randomized clinical trial of prevention of hydrocephalus after intraventricular hemorrhage in preterm infants: brain-washing versus tapping fluid. Pediatrics. 2007 May;119(5):e1071-8.

Whitelaw A, Odd DE. Intraventricular streptokinase after intraventricular hemorrhage in newborn infants. Cochrane Database Syst Rev. 2007(4):CD000498.

Wiig H, Rubin K, Reed RK. New and active role of the interstitium in control of interstitial fluid pressure: potential therapeutic consequences. Acta Anaesthesiologica Scandinavica. 2003;47(2):111-21.

Winnemoller M, Schon P, Vischer P, Kresse H. Interactions between thrombospondin and the small proteoglycan decorin: interference with cell attachment. Eur J Cell Biol. 1992 Oct;59(1):47-55.

Wu F, Yao H, Bader A, Dong F, Zhu F, Wu N, et al. Decorin gene transfer inhibited the expression of TGFbeta1 and ECM in rat mesangial cells. Eur J Med Res. 2007 Aug 16;12(8):360-8.

Wynn TA. Cellular and molecular mechanisms of fibrosis. J Pathol. 2008 Jan;214(2):199-210.

Wynn TA, Barron L. Macrophages: master regulators of inflammation and fibrosis. Semin Liver Dis. 2010 Aug;30(3):245-57.

Wynn TA, Ramalingam TR. Mechanisms of fibrosis: therapeutic translation for fibrotic disease. Nat Med. 2012 Jul;18(7):1028-40.

Wyss-Coray T, Feng L, Masliah E, Ruppe MD, Lee HS, Toggas SM, et al. Increased central nervous system production of extracellular matrix components and development of hydrocephalus in transgenic mice overexpressing transforming growth factor-beta 1. Am J Pathol. 1995 Jul;147(1):53-67.

Xaus J, Comalada M, Cardo M, Valledor AF, Celada A. Decorin inhibits macrophage colony-stimulating factor proliferation of macrophages and enhances cell survival through induction of p27(Kip1) and p21(Waf1). Blood. 2001 Oct 1;98(7):2124-33.

Xu H, Zhang SL, Tan GW, Zhu HW, Huang CQ, Zhang FF, et al. Reactive gliosis and neuroinflammation in rats with communicating hydrocephalus. Neuroscience. 2012 Aug 30;218:317-25.

Yamada H, Yokota A, Furuta A, Horie A. Reconstitution of shunted mantle in experimental hydrocephalus. J Neurosurg. 1992 May;76(5):856-62.

Yamaguchi Y, Mann DM, Ruoslahti E. Negative regulation of transforming growth factor-beta by the proteoglycan decorin. Nature. 1990 Jul 19;346(6281):281-4.

Yan W, Wang P, Zhao CX, Tang J, Xiao X, Wang DW. Decorin gene delivery inhibits cardiac fibrosis in spontaneously hypertensive rats by modulation of transforming growth factor-beta/Smad and p38 mitogen-activated protein kinase signaling pathways. Hum Gene Ther. 2009 Oct;20(10):1190-200.

Yang L, Pang Y, Moses HL. TGF-beta and immune cells: an important regulatory axis in the tumor microenvironment and progression. Trends Immunol. 2010 Jun;31(6):220-7.

Yu L, Hebert MC, Zhang YE. TGF-beta receptor-activated p38 MAP kinase mediates Smad-independent TGF-beta responses. EMBO J. 2002 Jul 15;21(14):3749-59.

Zafiropoulos A, Nikitovic D, Katonis P, Tsatsakis A, Karamanos NK, Tzanakakis GN. Decorin-induced growth inhibition is overcome through protracted expression and

activation of epidermal growth factor receptors in osteosarcoma cells. Mol Cancer Res. 2008 May;6(5):785-94.

Zhang YE. Non-Smad pathways in TGF-beta signaling. Cell Res. 2009 Jan;19(1):128-39.

Zhang Z, Li XJ, Liu Y, Zhang X, Li YY, Xu WS. Recombinant human decorin inhibits cell proliferation and downregulates TGF-beta1 production in hypertrophic scar fibroblasts. Burns. 2007 Aug;33(5):634-41.

Zhu JX, Goldoni S, Bix G, Owens RT, McQuillan DJ, Reed CC, et al. Decorin evokes protracted internalization and degradation of the epidermal growth factor receptor via caveolar endocytosis. J Biol Chem. 2005 Sep 16;280(37):32468-79.

Zonta M, Carmignoto G. Calcium oscillations encoding neuron-to-astrocyte communication. J Physiol Paris. 2002 Apr-Jun;96(3-4):193-8.